Interfacial properties using classical density functional theory: curved interfaces and surfactants

A thesis accepted by the Faculty of Energy-, Process- and Bio-Engineering of the University of Stuttgart and the Stuttgart Center for Simulation Science in partial fulfilment of the requirements for the degree of Doctor of Engineering Sciences (Dr.-Ing.)

by

Philipp Rehner

born in Sindelfingen

Committee chair:	Prof. Dr.-Ing. Joachim Groß
Committee member:	Prof. Dr. George Jackson
Date of defence:	13.10.2021

Institute of Thermodynamics and Thermal Process Engineering
University of Stuttgart

2021

Contents

Abstract

Interfaces play an important role in natural and industrial processes. Classical density functional theory (DFT) has been established as a tool capable of predicting interfacial properties, but also of providing insight in the structure of fluids at interfaces. Compared to other statistical mechanical methods, particularly molecular simulation, an efficient implementation of DFT offers a significant reduction in computation time. This advantage comes with the cost of an increased modeling effort. In this work, the calculation of interfacial properties using DFT is discussed and applied to different aspects of interfaces. First, the properties of highly curved interfaces, as they appear in nucleation processes, are studied. This is done first by directly calculating the properties of nanodroplets using DFT in spherical coordinates and afterwards in an expansion around a flat interface. Because for some applications, the calculation time of DFT is a limiting factor, a new method to predict surface tensions from equation of state parameters is introduced. This is achieved by using a Taylor expansion of the full DFT Helmholtz energy functional around a local density. The resulting functional is identical to that used in density gradient theory except for an explicit, temperature and density dependent expression for the influence matrix. The method is subsequently used to examine in detail the parametrization of associating components, particularly water and alcohols, that pose difficulties with respect to the simultaneous description of bulk phase equilibria and interfacial properties. A multiobjective optimization approach is used to assess different models and to quantify their capabilities and limitations. The so obtained water model presents the foundation for the last segment of this work, that studies the interfacial properties of water/surfactant and water/alkane/surfactant systems. The amphiphilic surfactant molecules are modeled using a heteronuclear DFT approach that resolves the distributions of individual segments. The parameters of this group contribution method are obtained by fitting to properties of small surfactant molecules and can then be used to predict properties of larger molecules for which less or no experimental data is available. The model is used to study the adsorption and orientation of surfactant molecules at interfaces and the corresponding reduction in interfacial tension.

Zusammenfassung

Grenzflächen spielen eine wichtige Rolle in natürlichen und industriellen Prozessen. Die klassische Dichtefunktionaltheorie (DFT) hat sich als ein Werkzeug etabliert, das in der Lage ist, Grenzflächeneigenschaften vorherzusagen, aber auch Einblicke in die Struktur von Fluiden an Grenzflächen zu geben. Im Vergleich zu anderen Methoden der statistischen Mechanik, insbesondere der Molekularsimulation, bietet eine effiziente Implementierung der DFT eine signifikante Reduktion der Rechenzeit. Dieser Vorteil geht jedoch mit einem erhöhten Modellierungsaufwand einher. In dieser Arbeit wird die Berechnung von Grenzflächeneigenschaften mittels DFT diskutiert und auf verschiedene Aspekte von Grenzflächen angewendet. Zunächst werden die Eigenschaften von stark gekrümmten Grenzflächen, wie sie bei Nukleationsprozessen auftreten, untersucht. Dies geschieht erst durch direkte Berechnung der Eigenschaften von Nanotropfen mittels DFT in sphärischen Koordinaten und anschließend in einer Reihenentwicklung um eine ebene Grenzfläche. Da für einige Anwendungen die Rechenzeit der DFT ein limitierender Faktor ist, wird eine neue Methode zur Vorhersage von Oberflächenspannungen aus Zustandsgleichungsparametern eingeführt. Diese beruht auf einer Taylorentwicklung des vollständigen DFT-Helmholtzenergiefunktionals um eine lokale Dichte. Das resultierende Funktional ist identisch mit dem in der Dichtegradiententheorie verwendeten, mit Ausnahme eines expliziten, temperatur- und dichteabhängigen Ausdrucks für die Einflussmatrix. Die Methode wird anschließend verwendet, um die Parametrisierung assoziierender Komponenten, insbesondere Wasser und Alkohole, die Schwierigkeiten bei der gleichzeitigen Beschreibung von Bulk-Phasengleichgewichten und Grenzflächeneigenschaften bereiten, im Detail zu untersuchen. Ein multikriterieller Optimierungsansatz wird verwendet, um verschiedene Modelle zu bewerten und ihre Fähigkeiten und Grenzen zu quantifizieren. Das so erhaltene Wassermodell stellt die Grundlage für den letzten Abschnitt dieser Arbeit dar, in dem die Grenzflächeneigenschaften von Wasser/Tensid- und Wasser/Alkan/Tensid-Systemen untersucht werden. Die amphiphilen Tensidmoleküle werden mit einem heteronuklearen DFT-Ansatz modelliert, der die Verteilungen der einzelnen Segmente auflöst. Die Parameter dieser Gruppenbeitragsmethode werden durch Anpassung an Stoffdaten kleiner Tensidmoleküle bestimmt und können dann zur Vorhersage von Eigenschaften größerer Moleküle, für die weniger oder keine experimentellen Daten verfügbar sind, verwendet werden. Das Modell wird benutzt, um die Adsorption und Orientierung von Tensidmolekülen an Grenzflächen und die entsprechende Reduzierung der Grenzflächenspannung zu untersuchen.

Journal Publications

This thesis is based on the following publications:

- Chapter 3: P. Rehner and J. Gross. Surface tension of droplets and Tolman lengths of real substances and mixtures from density functional theory. *The Journal of Chemical Physics*, **148.16**:164703, 2018. doi:10.1063/1.5020421
- Chapter 4: P. Rehner, A. Aasen, and Ø. Wilhelmsen. Tolman lengths and rigidity constants from free-energy functionals—General expressions and comparison of theories. *The Journal of Chemical Physics*, **151.24**:244710, 2019. doi:10.1063/1.5135288
- Chapter 5: P. Rehner and J. Gross. Predictive density gradient theory based on nonlocal density functional theory. *Physical Review E*, **98.6**:063312, 2018. doi:10.1103/PhysRevE.98.063312
- Chapter 6: P. Rehner and J. Gross. Multiobjective Optimization of PCP-SAFT Parameters for Water and Alcohols Using Surface Tension Data. *Journal of Chemical & Engineering Data*, **65.12**:5698-5707, 2020. doi:10.1021/acs.jced.0c00684
- Chapter 7: P. Rehner, B. Bursik and J. Gross. Surfactant Modelling Using Classical Density Functional Theory and a Group Contribution PC-SAFT Approach. *Industrial & Engineering Chemistry Research*, **60.19**:7111-7123, 2021. doi:10.1021/acs.iecr.1c00169

The chapters 3 to 7 present literal quotes of the published work. Any addition with respect to the published work is marked. Any deletion is indicated with square brackets as "[...]". Cross-references between chapters of this thesis are added to the published version of the text to increase readability. The supporting information to the published work is presented in the appendix of this thesis.

1 Interfaces from a molecular perspective

Whenever two or more phases coexist, they are separated by an interface, that is characterized by a jump in properties like the density, composition, or, in the case of a curved interface, pressure. From a macroscopic point of view, the transition appears sharp, however, on a microscopic scale, all properties change continuously from one phase to the other. The quantitative framework for the thermodynamic of interfaces was predominantly developed by J. W. Gibbs[1], decades before experimental evidence for the thickness of interfaces was obtained using optical reflectivity measurements[2].

The presence of an interface is associated with an interfacial tension, that can be understood as a net force acting on the interface in a direction parallel to it. The concept of an interfacial tension can be used to explain the shape of droplets and bubbles, the rise or fall of liquids in a capillary tube, or the wetting of a solid surface. While the macroscopic theory of capillarity is well understood and validated, a strict thermodynamic description leads to subtleties, that are discussed in the subsequent chapter.

Observing interfaces from a molecular perspective gives insight into phenomena like the enrichment of light-boiling components in the interface[3], the structure and orientation of molecules in confined media[4], and the properties of highly curved interfaces appearing during nucleation processes[5,6]. However, with sufficiently powerful models, it is possible to not only describe these phenomena qualitatively, but also predict macroscopic properties. All methods to describe interfaces on a molecular level stem from statistical mechanics, which studies the behavior of many-body systems, and provides strict relations between (microscopic) ensemble averages and (macroscopic) thermodynamic properties[7]. A well-established method to calculate ensemble averages purely based on interactions of the molecules in the system, is molecular simulation[8]. However, despite advances in the effectiveness of statistical methods and in computational power, they are still computationally expensive.

Instead of finding methods to efficiently sample configurations of molecules, the relations between averaged properties can be used directly to calculate properties of the system. Classical density functional theory[5,7] (DFT) can be understood as a generalization of bulk thermodynamics to microscopically inhomogeneous systems. Since the properties studied in DFT are already ensemble averages, no sampling is required and therefore no statistical uncertainty is present in the results and the computational effort is reduced. It is also

much more straightforward to reduce the dimensionality of the system when symmetry can be exploited. The advantage in computation time comes at the cost of a higher modeling requirement, because instead of a force field, that describes the interactions of atoms or groups of atoms, a Helmholtz energy functional is required, that describes all effective interactions in the fluid phase, analogously to an equation of state for bulk phases.

The key ideas, the major model developments, and the application to interfaces of DFT are described in chapter 2. The theory is applied to study the interfacial properties of strongly curved interfaces in chapter 3. In chapter 4, properties of curved interfaces are predicted based only on properties of the planar interface. Chapter 5 introduces a fast method for predicting interfacial tensions purely from equation of state parameters. This approach is used in chapter 6 to improve the parametrization of water and alcohols using experimental surface tension data as an additional input to the parameter regression. Finally, in chapter 7, the model is extended to calculate interfacial properties of water/surfactant systems, that are characterized by a significant enrichment of the amphiphilic surfactant molecules in the interface and by drastically altered interfacial properties as a result.

References

[1] J. Gibbs. *The Collected Works of J. Willard Gibbs, Volume I: Thermodynamics*. Longmans, Green and Co., 1928.

[2] G. H. Gilmer, W. Gilmore, J. Huang, and W. W. Webb. Diffuse Interface in a Critical Fluid Mixture. *Physical Review Letters*, **14**:491–494, 1965. doi:10.1103/PhysRevLett.14.491.

[3] S. Stephan and H. Hasse. Enrichment at vapour–liquid interfaces of mixtures: establishing a link between nanoscopic and macroscopic properties. *International Reviews in Physical Chemistry*, **39**(3):319–349, 2020. doi:10.1080/0144235X.2020.1777705.

[4] B. Smit. Molecular Simulations of Zeolites: Adsorption, Diffusion, and Shape Selectivity. *Chemical Reviews*, **108**(10):4125–4184, 2008. doi:10.1021/cr8002642. PMID: 18817356.

[5] V. Kalikmanov. *Statistical physics of fluids: basic concepts and applications*. Springer Science & Business Media, 2013.

[6] V. Kalikmanov. *Nucleation theory*, volume 860. Springer, 2012.

[7] J. P. Hansen and I. R. McDonald. *Theory of simple liquids*. Elsevier [u.a.], Amsterdam, 3rd edition, 2006. ISBN 0-12-370535-5.

[8] D. Frenkel and B. Smit. *Understanding molecular simulation: from algorithms to applications*, volume 1. Elsevier, 2001.

2 Thermodynamics of inhomogeneous systems

Interfaces between different phases, including the adsorption of fluid phases on walls and in porous media, and microstructures like colloids or micelles differ in their thermodynamic properties from bulk phases due to their microscopic inhomogeneity. On a molecular level, the isotropy of a bulk system is broken by the addition of an external field $\boldsymbol{V}^{\mathrm{ext}}(\mathbf{r})$ that acts on all or some molecules and can be due to the presence of body forces like gravity or an electric field. Solid matter that interacts with the fluid molecules but is considered with fixed positions can also be approximated well by a constant external potential. The grand potential functional Ω of an inhomogeneous system is

$$\Omega = \mathscr{F} - \int \boldsymbol{\rho}(\mathbf{r}) \cdot (\boldsymbol{\mu} - \boldsymbol{V}^{\mathrm{ext}}(\mathbf{r}))\, \mathrm{d}\mathbf{r} \tag{2.1}$$

with the intrinsic Helmholtz energy $\mathscr{F}$, the density profiles $\boldsymbol{\rho}(\mathbf{r})$ and the chemical potentials $\boldsymbol{\mu}$. In this chapter bold symbols refer to arrays over all different species in the system. It can be shown rigorously, that the intrinsic Helmholtz energy $\mathscr{F} = \mathscr{F}(T, [\boldsymbol{\rho}(\mathbf{r})])$ is a unique functional of the density profiles and a function of temperature T. Further, it can be shown, that the density profile, that minimizes the grand potential functional defined in eq. (2.1) is indeed the equilibrium density profile of the system and the corresponding value of Ω its grand canonical energy. These two important findings are known together as Hohenberg-Kohn-Mermin theorems and were initially developed for quantum systems[1,2]. Later, the concept was transferred to statistical mechanics[3–5] to form the foundation of methods to describe inhomogeneous systems known as (classical) density functional theory. The intrinsic Helmholtz energy functional describes fluid-fluid interactions independent of the external potential and is therefore key to modeling inhomogeneous systems. For an ideal gas, the intrinsic Helmholtz energy functional is known exactly from statistical mechanics[5], as

$$\beta \mathscr{F}^{\mathrm{ig}} = \int \boldsymbol{\rho}(\mathbf{r}) \cdot \left(\ln\left(\boldsymbol{\rho}(\mathbf{r}) \boldsymbol{\Lambda}^3\right) - \mathbf{1} \right) \mathrm{d}\mathbf{r} \tag{2.2}$$

with the overall molecular de Broglie wavelength $\boldsymbol{\Lambda}$, that includes the contributions from intramolecular degrees of freedom and the inverse temperature $\beta = \frac{1}{k_B T}$. The multiplication of two array (bold) properties without the explicit dot product is assumed elementwise and so

is the logarithm. The bold face **1** is a vector of unities. For a real fluid, the Helmholtz energy can be split into an ideal gas contribution at the same temperature and density distribution and a residual contribution $\mathscr{F}^{\mathrm{res}}$. An overview over different models is given in section 2.4. The total Helmholtz energy

$$F = \mathscr{F} + \int \boldsymbol{\rho}(\mathbf{r}) \cdot \boldsymbol{V}^{\mathrm{ext}}(\mathbf{r})\,\mathrm{d}\mathbf{r} \tag{2.3}$$

is the sum of the intrinsic contribution $\mathscr{F}$ and the contribution due to the external field $\boldsymbol{V}^{\mathrm{ext}}$ acting on the fluid. In the absence of an external potential, the total Helmholtz energy is identical to the intrinsic Helmholtz energy. Therefore, no distinction between the two is made in chapters 3–7.

2.1 Density functional theory

To find the equilibrium density profile of an inhomogeneous system, it is necessary to minimize the grand potential functional as described above. Mathematically, this is done by solving for the roots of the functional derivative of the grand potential, as

$$\left(\frac{\delta\Omega}{\delta\boldsymbol{\rho}(\mathbf{r})}\right)_{T,\boldsymbol{\mu}} = 0. \tag{2.4}$$

Using eq. (2.1), the equation, often referred to as Euler-Lagrange equation, can be written as

$$\left(\frac{\delta\mathscr{F}}{\delta\boldsymbol{\rho}(\mathbf{r})}\right)_{T} = \boldsymbol{\mu} - \boldsymbol{V}^{\mathrm{ext}}(\mathbf{r}). \tag{2.5}$$

Aside from the Helmholtz energy and the grand potential, additional thermodynamic properties are available from DFT. The relations from bulk thermodynamics apply with the exception, that inhomogeneous systems are not Euler-homogeneous, and thus fundamental thermodynamic relations for various potentials can not be simply integrated. By comparing the total differential of $F(T,[\boldsymbol{\rho}(\mathbf{r})])$ at equilibrium for fixed external potentials

$$\mathrm{d}F = \left(\frac{\partial\mathscr{F}}{\partial T}\right)_{\boldsymbol{\rho}(\mathbf{r})}\mathrm{d}T + \int \underbrace{\left(\frac{\delta\mathscr{F}}{\delta\boldsymbol{\rho}(\mathbf{r})}\right)_{T}}_{\boldsymbol{\mu}-\boldsymbol{V}^{\mathrm{ext}}(\mathbf{r})} \cdot\delta\boldsymbol{\rho}(\mathbf{r})\,\mathrm{d}\mathbf{r} + \int \boldsymbol{V}^{\mathrm{ext}}(\mathbf{r})\cdot\delta\boldsymbol{\rho}(\mathbf{r})\,\mathrm{d}\mathbf{r} \tag{2.6}$$

$$= \left(\frac{\partial\mathscr{F}}{\partial T}\right)_{\boldsymbol{\rho}(\mathbf{r})}\mathrm{d}T + \boldsymbol{\mu}\cdot\,\mathrm{d}\boldsymbol{N} \tag{2.7}$$

with its fundamental equation at constant volume $\mathrm{d}F = -S\,\mathrm{d}T + \boldsymbol{\mu}\cdot\,\mathrm{d}\boldsymbol{N}$, the entropy S can be identified as

$$S = -\left(\frac{\partial \mathscr{F}}{\partial T}\right)_{\boldsymbol{\rho}(\mathbf{r})}. \tag{2.8}$$

It is not a function of the external potential and can be evaluated at constant density. With the entropy, the internal energy U of the system is also known as

$$U = F + TS = \mathscr{F} - T\left(\frac{\partial \mathscr{F}}{\partial T}\right)_{\boldsymbol{\rho}(\mathbf{r})} + \int \boldsymbol{\rho}(\mathbf{r})\cdot\boldsymbol{V}^{\mathrm{ext}}(\mathbf{r})\,\mathrm{d}\mathbf{r} \tag{2.9}$$

or in the style of the Gibbs-Helmholtz equation as

$$U = \left(\frac{\partial \beta\mathscr{F}}{\partial \beta}\right)_{\boldsymbol{\rho}(\mathbf{r})} + \int \boldsymbol{\rho}(\mathbf{r})\cdot\boldsymbol{V}^{\mathrm{ext}}(\mathbf{r})\,\mathrm{d}\mathbf{r}. \tag{2.10}$$

From the total differential of $\Omega(T,\boldsymbol{\mu},[\boldsymbol{\rho}(\mathbf{r})])$ at equilibrium for fixed external potentials

$$\mathrm{d}\Omega = \left(\frac{\partial \Omega}{\partial T}\right)_{\boldsymbol{\mu},\boldsymbol{\rho}(\mathbf{r})}\mathrm{d}T + \left(\frac{\partial \Omega}{\partial \boldsymbol{\mu}}\right)_{T,\boldsymbol{\rho}(\mathbf{r})}\cdot\,\mathrm{d}\boldsymbol{\mu} + \int \underbrace{\left(\frac{\delta\Omega}{\delta\boldsymbol{\rho}(\mathbf{r})}\right)_{T,\mu}}_{0}\cdot\delta\boldsymbol{\rho}(\mathbf{r})\,\mathrm{d}\mathbf{r} \tag{2.11}$$

$$= \left(\frac{\partial \mathscr{F}}{\partial T}\right)_{\boldsymbol{\rho}(\mathbf{r})}\mathrm{d}T - \int \boldsymbol{\rho}(\mathbf{r})\,\mathrm{d}\mathbf{r}\cdot\,\mathrm{d}\boldsymbol{\mu} \tag{2.12}$$

and comparison with its fundamental equation at constant volume $\mathrm{d}\Omega = -S\,\mathrm{d}T - \boldsymbol{N}\cdot\,\mathrm{d}\boldsymbol{\mu}$, the relation

$$\boldsymbol{N} = \int \boldsymbol{\rho}(\mathbf{r})\,\mathrm{d}\mathbf{r} = -\left(\frac{\partial \Omega}{\partial \boldsymbol{\mu}}\right)_{T,\boldsymbol{\rho}(\mathbf{r})} \tag{2.13}$$

follows, which is again a useful generalization of the partial derivative of Ω with respect to the chemical potential to inhomogeneous systems.

The enthalpy and Gibbs energy are not properly defined for inhomogeneous systems, because pressure p and volume V do not appear as Legendre pair in the fundamental equations anymore. If the system is described using an external potential, the volume that is implicitly contained in the bounds for the integration over $\mathbf{r}$ can be replaced by an integration over the entire space with the external potential being infinite in non-accessible regions. In situations in which no external potential is present, there is no physical boundary in the system. To obtain meaningful results, it is therefore necessary to define domains in a way, that the fluid is in a bulk state (or close to one) all over their boundaries. This would limit the possible

systems to very few specific cases, however, it is possible to take advantage of the symmetry of the systems by exploiting translational invariance. The most common example is a planar interface, where the domain is set up in a way, that the axis perpendicular to the interface is cut off when the density is reasonably close to each bulk density and the directions parallel to the interface can be eliminated entirely due to the translational invariance of the system.

2.2 DFT with constraints

The nature of the open systems studied using density functional theory often poses problems with respect to the uniqueness of the solutions, particularly if no external potentials are present. A common case is a system that is at a bulk phase equilibrium for the given temperature and chemical potentials. Because the derivation of the Euler-Lagrange equation only takes equilibrium into account and not stability, both bulk phases and a planar interface are correct solutions. The bulk phases have the lower grand potential and thus are the stable solutions, but the more interesting solution is of course the interface. Further, due to the unboundedness of the system, the interface can be shifted in its normal direction to generate infinite solutions to the Euler-Lagrange equation. Similarly, for chemical potentials between the spinodal points, a stable bulk phase, a metastable bulk phase, and a spherical or cylindrical droplet can all be solutions to the Euler-Lagrange equation. In all these cases, it is useful to be able to specify the number of molecules in the system rather than the chemical potentials.

If the system is described using temperature, volume and molecule numbers, the appropriate thermodynamic potential is the Helmholtz energy F. Therefore, the equilibrium is described by

$$F[\boldsymbol{\rho}(\mathbf{r})] \stackrel{!}{=} \min \quad \text{s.t.} \quad \boldsymbol{N} = \int \boldsymbol{\rho}(\mathbf{r})\,\mathrm{d}\mathbf{r}. \tag{2.14}$$

This constrained minimization problem is transformed to an unconstrained minimization problem using the Lagrange multiplier $\boldsymbol{\lambda}$, as

$$\mathscr{L}([\boldsymbol{\rho}(\mathbf{r})], \boldsymbol{\lambda}) = F + \boldsymbol{\lambda} \cdot \left(\boldsymbol{N} - \int \boldsymbol{\rho}(\mathbf{r})\,\mathrm{d}\mathbf{r} \right) \stackrel{!}{=} \min \tag{2.15}$$

The derivatives of the Lagrangian $\mathscr{L}$ are expressed using eqs. (2.2) and (2.3) as

$$\frac{\delta \mathscr{L}}{\delta \boldsymbol{\rho}(\mathbf{r})} = \frac{\delta F}{\delta \boldsymbol{\rho}(\mathbf{r})} - \boldsymbol{\lambda} = \frac{1}{\beta} \ln\left(\boldsymbol{\rho}(\mathbf{r})\boldsymbol{\Lambda}^3\right) + \frac{\delta \mathscr{F}^{\mathrm{res}}}{\delta \boldsymbol{\rho}(\mathbf{r})} + \boldsymbol{V}^{\mathrm{ext}}(\mathbf{r}) - \boldsymbol{\lambda} \stackrel{!}{=} 0 \tag{2.16}$$

$$\frac{\partial \mathscr{L}}{\partial \boldsymbol{\lambda}} = \boldsymbol{N} - \int \boldsymbol{\rho}(\mathbf{r})\,\mathrm{d}\mathbf{r} \stackrel{!}{=} 0 \tag{2.17}$$

Equation (2.16) can be partially solved for the density profile and substituted into eq. (2.17), giving

$$\boldsymbol{N} = \boldsymbol{\Lambda}^{-3} e^{\beta\boldsymbol{\lambda}} \int e^{-\beta\left(\frac{\delta \mathscr{F}}{\delta \boldsymbol{\rho}(\mathbf{r})} + \boldsymbol{V}^{\mathrm{ext}}(\mathbf{r})\right)} \mathrm{d}\mathbf{r}. \tag{2.18}$$

Comparison with the Euler-Lagrange equation shows that at the solution of the constrained optimization $\boldsymbol{\lambda}$ is indeed the chemical potential of the system. Therefore, it is appropriate to refer to $\boldsymbol{z} = \boldsymbol{\Lambda}^{-3} e^{\beta\boldsymbol{\lambda}}$ as the fugacity* of the system[6]. From eqs. (2.16) and (2.18) the system of equations

$$\boldsymbol{\rho}(\mathbf{r}) = \boldsymbol{z} e^{-\beta\left(\frac{\delta \mathscr{F}}{\delta \boldsymbol{\rho}(\mathbf{r})} + \boldsymbol{V}^{\mathrm{ext}}(\mathbf{r})\right)} \tag{2.19}$$

$$\boldsymbol{z} = \frac{\boldsymbol{N}}{\int e^{-\beta\left(\frac{\delta \mathscr{F}}{\delta \boldsymbol{\rho}(\mathbf{r})} + \boldsymbol{V}^{\mathrm{ext}}(\mathbf{r})\right)} \mathrm{d}\mathbf{r}} \tag{2.20}$$

can be derived, that extends the Euler-Lagrange equation by an additional equation for the fugacities. Equations (2.19) and (2.20) can be combined to one single equation

$$\boldsymbol{\rho}(\mathbf{r}) = \frac{\boldsymbol{N} e^{-\beta\left(\frac{\delta \mathscr{F}}{\delta \boldsymbol{\rho}(\mathbf{r})} + \boldsymbol{V}^{\mathrm{ext}}(\mathbf{r})\right)}}{\int e^{-\beta\left(\frac{\delta \mathscr{F}}{\delta \boldsymbol{\rho}(\mathbf{r})} + \boldsymbol{V}^{\mathrm{ext}}(\mathbf{r})\right)} \mathrm{d}\mathbf{r}}, \tag{2.21}$$

however, it can be advantageous to the flexibility with respect to the implementation and the robustness of the numerical solution procedure to keep them separated.

For multi-component mixtures, the number of molecules of each species might not be the preferred specification. A better specification can be the total number of molecules N, as it can be used as an indicator of cluster or droplet sizes, in particular for vapor–liquid systems. The correct thermodynamic potential can be found by rewriting the fundamental equation for the Helmholtz energy as

$$\mathrm{d}F = -S\,\mathrm{d}T + \boldsymbol{\mu}\cdot\,\mathrm{d}\boldsymbol{N} = -S\,\mathrm{d}T + \boldsymbol{\mu}\cdot\,\mathrm{d}\boldsymbol{N} - \mu_1\,\mathrm{d}N + \mu_1\,\mathrm{d}N = -S\,\mathrm{d}T + \Delta\boldsymbol{\mu}\cdot\,\mathrm{d}\boldsymbol{N} + \mu_1\,\mathrm{d}N \tag{2.22}$$

*The fugacity $\boldsymbol{z}$ as used in a statistical mechanical context is related to the fugacity $\boldsymbol{f}$ used in classical thermodynamics by $\boldsymbol{z} = \beta\boldsymbol{f}$ and is also sometimes referred to as activity[5].

with μ_1 the chemical potential of component 1 (for the further development it is irrelevant which component is chosen as reference) and $\Delta\boldsymbol{\mu} = \boldsymbol{\mu} - \mu_1$. A Legendre transform with respect to the $\Delta\boldsymbol{\mu} - \boldsymbol{N}$ pair leads to the definition of the semi grand potential Ω^* with

$$\Omega^* = F - \Delta\boldsymbol{\mu} \cdot \boldsymbol{N} \quad \text{and} \quad \mathrm{d}\Omega^* = -S\,\mathrm{d}T + \boldsymbol{N} \cdot \mathrm{d}\Delta\boldsymbol{\mu} + \mu_1\,\mathrm{d}N. \tag{2.23}$$

The constrained minimization problem thus becomes

$$\Omega^*[\boldsymbol{\rho}(\mathbf{r})] \stackrel{!}{=} \min \quad \text{s.t.} \quad N = \int \boldsymbol{\rho}(\mathbf{r}) \cdot \mathbf{1}\,\mathrm{d}\mathbf{r} \tag{2.24}$$

and the unconstrained problem

$$\mathscr{L}^*([\boldsymbol{\rho}], \lambda) = \Omega^* + \lambda \left(N - \int \boldsymbol{\rho}(\mathbf{r}) \cdot \mathbf{1}\,\mathrm{d}\mathbf{r} \right) \stackrel{!}{=} \min \tag{2.25}$$

The gradients of the new Lagrangian $\mathscr{L}^*$ using eqs. (2.2), (2.3) and (2.23) are

$$\frac{\delta \mathscr{L}^*}{\delta \boldsymbol{\rho}(\mathbf{r})} = \frac{\delta \Omega^*}{\delta \boldsymbol{\rho}(\mathbf{r})} - \lambda = \frac{1}{\beta} \ln\left(\boldsymbol{\rho}(\mathbf{r}) \boldsymbol{\Lambda}^3\right) + \frac{\delta \mathscr{F}^{\mathrm{res}}}{\delta \boldsymbol{\rho}(\mathbf{r})} + \boldsymbol{V}^{\mathrm{ext}}(\mathbf{r}) - \Delta\boldsymbol{\mu} - \lambda \stackrel{!}{=} 0 \tag{2.26}$$

$$\frac{\partial \mathscr{L}^*}{\partial \lambda} = N - \int \boldsymbol{\rho}(\mathbf{r}) \cdot \mathbf{1}\,\mathrm{d}\mathbf{r} \stackrel{!}{=} 0. \tag{2.27}$$

Combining eqs. (2.26) and (2.27) leads to

$$N = e^{\beta\lambda} \boldsymbol{\Lambda}^{-3} e^{\beta\Delta\mu} \cdot \int e^{-\beta\left(\frac{\delta \mathscr{F}}{\delta \rho(\mathbf{r})} + \boldsymbol{V}^{\mathrm{ext}}(\mathbf{r})\right)} \mathrm{d}\mathbf{r}. \tag{2.28}$$

Similar to the canonical case before, the fugacity can be identified by comparing the Euler-Lagrange equation to the constrained minimization which in this case leads to $\boldsymbol{z} = e^{\beta\lambda} \boldsymbol{\Lambda}^{-3} e^{\beta\Delta\mu}$. The system of equations becomes

$$\boldsymbol{\rho}(\mathbf{r}) = \boldsymbol{z} e^{-\beta\left(\frac{\delta \mathscr{F}}{\delta \rho(\mathbf{r})} + \boldsymbol{V}^{\mathrm{ext}}(\mathbf{r})\right)} \tag{2.29}$$

$$\boldsymbol{z} = \frac{N \boldsymbol{\Lambda}^{-3} e^{\beta\Delta\mu}}{\boldsymbol{\Lambda}^{-3} e^{\beta\Delta\mu} \cdot \int e^{-\beta\left(\frac{\delta \mathscr{F}}{\delta \rho(\mathbf{r})} + \boldsymbol{V}^{\mathrm{ext}}(\mathbf{r})\right)} \mathrm{d}\mathbf{r}}. \tag{2.30}$$

It is important to keep in mind, that these expressions do not solve density profiles in a canonical or semi-grand ensemble. The underlying equation is still the Euler-Lagrange equation as derived in an open system. It is merely a mathematical modification of the equations to find the chemical potentials that will result in a system containing the desired number of molecules. A decomposition of density functional theory to obtain density profiles

in a canonical ensemble was presented by de las Heras and Schmidt[7].

It might seem unintuitive to iterate the chemical potential for systems like planar interfaces in which it can be easily determined from bulk phase equilibrium calculations. However, in the presence of a planar interface T and $\Delta\boldsymbol{\mu}$ already specify the phase equilibrium completely. The remaining degree of freedom N uniquely determines the position of the interface avoiding the multiplicity of the solutions discussed at the outset of this section. Assuming a solver that converges independent of initial conditions, a phase equilibrium calculation is not necessary to calculate the density profile of an interface using the constrained DFT. However, given the negligible computation time for determining the phase equilibrium compared to the DFT calculation, it is still advisable to use it to generate good initial values. Another reason for performing an initial phase equilibrium calculation is that for multi-component mixtures it is usually desired to specify the composition of one of the phases instead of $\Delta\boldsymbol{\mu}$.

2.3 Thermodynamics of interfaces

The systematic thermodynamic description of interfaces was pioneered by Gibbs[8]. The core element of the approach is the definition of an abstract model system, that is identical to the real system with respect to its thermodynamic potential and its characteristic variables. For macroscopic systems, the distinction between abstract and physical system can appear meaningless and is sometimes forgotten. However, it is crucial for describing microscopic systems.

In the Gibbsian approach the model (or Gibbs) system contains two or more bulk phases that are separated by interfaces. Extensive properties are then written as a sum over contributions from each phase plus the contribution due to the interfaces. For the simplest case, two bulk phases α and β and their interface σ, the grand potential Ω, entropy S, total number of molecules $\boldsymbol{N}$ and the volume V can be written as

$$\Omega = \Omega^\alpha + \Omega^\beta + \Omega^\sigma = -p^\alpha V^\alpha - p^\beta V^\beta + \gamma A \tag{2.31}$$

$$S = S^\alpha + S^\beta + S^\sigma = \hat{s}^\alpha V^\alpha + \hat{s}^\beta V^\beta + \Gamma_S A \tag{2.32}$$

$$\boldsymbol{N} = \boldsymbol{N}^\alpha + \boldsymbol{N}^\beta + N^\sigma = \boldsymbol{\rho}^\alpha V^\alpha + \boldsymbol{\rho}^\beta V^\beta + \boldsymbol{\Gamma} A \tag{2.33}$$

$$V = V^\alpha + V^\beta. \tag{2.34}$$

A is the interfacial area separating phases α and β. Equations (2.31)–(2.33) define the interfacial tension γ, entropy Γ_S, and adsorption $\boldsymbol{\Gamma}$, respectively. Further $\hat{s}$ indicates a bulk entropy density. The volume of the interface is by definition negligible, therefore no additional

term is required in eq. (2.34).

In the last section, it was illustrated, how, from a molecular modeling point of view, systems are characterized using the temperature, chemical potentials, and external potentials. In the absence of an external potential, the volume of the system is unbounded. Since the Gibbs system is equated with the physical system, the extensive properties, but also the bulk phase properties $p^{\alpha/\beta}$, $\hat{s}^{\alpha/\beta}$ and $\boldsymbol{\rho}^{\alpha/\beta}$ are fixed, if the physical system is fixed. Therefore, in eqs. (2.31)–(2.34) the geometry (V^α, V^β, A) and the interfacial properties can not be varied independently. Instead, the interfacial properties are only defined within the Gibbs system and depend on its chosen geometry.

2.3.1 Capillarity approximation

The observation, that interfacial properties depend on the chosen geometry of a reference system can seem unintuitive, as the interfacial tension can be reliably measured in experiments without considering the choice of dividing surface. They are also not in agreement with any of the commonly given thermodynamic expressions for the interfacial tension[5,6,9,10]

$$\gamma = \left(\frac{\partial U}{\partial A}\right)_{S,V,\boldsymbol{N}} = \left(\frac{\partial H}{\partial A}\right)_{S,p,\boldsymbol{N}} = \left(\frac{\partial F}{\partial A}\right)_{T,V,\boldsymbol{N}} = \left(\frac{\partial G}{\partial A}\right)_{T,p,\boldsymbol{N}} = \left(\frac{\partial \Omega}{\partial A}\right)_{T,V,\boldsymbol{\mu}}. \tag{2.35}$$

The reason for this discrepancy is that the effect of the curvature becomes only significant for nanoscale systems. "Large" systems (i.e. length scales above $\sim 1\,\mu$m) can be described without major losses in precision using the capillarity approximation, that assumes the interfacial tension is independent of the curvature of the interface. A work $\gamma\,\mathrm{d}A$ is associated with the change of the interfacial area, that must be included in the fundamental equation of the homogeneous grand potential, as

$$\mathrm{d}\Omega = -S\,\mathrm{d}T - p\,\mathrm{d}V - \boldsymbol{N}\cdot\mathrm{d}\boldsymbol{\mu} + \gamma\,\mathrm{d}A. \tag{2.36}$$

Since T, V and $\boldsymbol{\mu}$ are all independent of A for planar interfaces, standard Legendre transforms can be applied, that result in fundamental equations for all other thermodynamic potentials and the expressions in eq. (2.35). To devise a model system, in which the interfacial area is independent of the other fundamental variables requires some sort of movable confinements as proposed by Rowlinson and Widom[9] or Davis[10]. In the case of a fixed confinement geometry, and thus also for every point in time during a reversible movement of the confinement, the equilibrium state is characterized by a minimum in the thermodynamic potential at given fundamental variables and the interfacial area A becomes an internal degree of freedom like the density profiles in DFT. Equations (2.35) and (2.36) are thus not general and can only be

applied and defended for planar or only slightly curved interfaces.

2.3.2 Young-Laplace equation

Going back to the strict application of Gibbs' interfacial thermodynamics and with the restrictions for properly defined systems in mind, there are only three basic geometries, that a two-phase system in the absence of an external field can reach in equilibrium: a spherical droplet, a cylindrical tube, and a planar interface. If index α is assigned to the continuous phase and β is used for the disperse phase, we can define $\Delta p = p^\beta - p^\alpha$ and eliminate the volume from eq. (2.31) by writing

$$\Delta\Omega = \Omega + p^\alpha V = -\Delta p V^\beta + \gamma A \tag{2.37}$$

This definition of the property $\Delta\Omega$ is useful because it eliminates the diverging volume from all further considerations. Because Ω, p^α and V are unambiguously defined by the physical system, $\Delta\Omega$ does not depend on the geometry of the Gibbs system. Taking the derivative of eq. (2.37) with respect to V^β while keeping the physical system unaltered results in the general Young-Laplace equation

$$\Delta p = \gamma \left[\frac{\partial A}{\partial V^\beta}\right]_{T,\boldsymbol{\mu}} + A\left[\frac{\partial \gamma}{\partial V^\beta}\right]_{T,\boldsymbol{\mu}} = \frac{\gamma g}{R} + \left[\frac{\partial \gamma}{\partial R}\right]_{T,\boldsymbol{\mu}} \tag{2.38}$$

with the geometry factor g, which is 0 for a planar interface, 1 for a cylindrical interface and 2 for spherical interface, and the radius R. The derivatives with respect to properties defined in the Gibbs system are referred to as notional derivatives[9]. As a reminder, that these derivatives describe the change of defined properties while keeping the physical system unaltered, they are displayed using square brackets. Similar expressions can be derived from eqs. (2.32) and (2.33), as

$$\Delta\hat{s} = -\frac{\Gamma_S g}{R} - \left[\frac{\partial \Gamma_S}{\partial R}\right]_{T,\boldsymbol{\mu}} \quad \text{and} \quad \Delta\boldsymbol{\rho} = -\frac{\boldsymbol{\Gamma} g}{R} - \left[\frac{\partial \boldsymbol{\Gamma}}{\partial R}\right]_{T,\boldsymbol{\mu}}. \tag{2.39}$$

The interfacial tension has a unique value only after introducing a dividing surface. That is reflected in the Young-Laplace equation which contains an additional term for the dependence of the interfacial tension on this dividing surface. A pragmatic choice for the dividing surface is the surface of tension with radius R_s, that is defined by $\left[\frac{\partial \gamma}{\partial R}\right]_{T,\boldsymbol{\mu}} = 0$ and thus eliminates the notional derivative from (2.38). Although the resulting expression $\Delta p = \frac{\gamma g}{R_s}$ looks identical to the Young-Laplace equation based on the capillarity approximation, the interfacial tension in the Gibbs framework is still a function of the size of the droplet or bubble.

Other choices for the dividing surface are the Koenig surface[11] for which $\boldsymbol{\Gamma} \cdot \mathrm{d}\boldsymbol{\mu} = 0$, the total equimolar surface defined by $\boldsymbol{\Gamma} \cdot \mathbf{1} = 0$, or the equimolar surface of component i with $\Gamma_i = 0$. For a pure component all these surfaces are identical and just referred to as equimolar surface.

2.3.3 Gibbs adsorption equation

As stated above, the interfacial tension depends on the temperature and chemical potentials, as well as the choice of the dividing surface. To quantify this relationship, the fundamental equations of the physical system

$$\mathrm{d}\Omega = -S\,\mathrm{d}T - \boldsymbol{N} \cdot \mathrm{d}\boldsymbol{\mu} \tag{2.40}$$

and the bulk systems α and β

$$\mathrm{d}\Omega^{\alpha/\beta} = -S^{\alpha/\beta}\,\mathrm{d}T - p^{\alpha/\beta}\,\mathrm{d}V^{\alpha/\beta} - \boldsymbol{N}^{\alpha/\beta} \cdot \mathrm{d}\boldsymbol{\mu}^{\alpha/\beta} \tag{2.41}$$

are substituted in the derivative of eq. (2.31), namely

$$\mathrm{d}\Omega = \mathrm{d}\Omega^{\alpha} + \mathrm{d}\Omega^{\beta} + \gamma\,\mathrm{d}A + A\,\mathrm{d}\gamma. \tag{2.42}$$

The resulting expression

$$-A\Gamma_S\,\mathrm{d}T - A\boldsymbol{\Gamma} \cdot \boldsymbol{\mu} = -p^{\alpha}\,\mathrm{d}V^{\alpha} - p^{\beta}\,\mathrm{d}V^{\beta} + \gamma\,\mathrm{d}A + A\,\mathrm{d}\gamma \tag{2.43}$$

can be solved for $\mathrm{d}\gamma$, as

$$\mathrm{d}\gamma = -\Gamma_S\,\mathrm{d}T - \boldsymbol{\Gamma} \cdot \mathrm{d}\boldsymbol{\mu} + \frac{\Delta p}{A}\,\mathrm{d}V^{\beta} - \frac{\gamma}{A}\,\mathrm{d}A = -\Gamma_S\,\mathrm{d}T - \boldsymbol{\Gamma} \cdot \mathrm{d}\boldsymbol{\mu} + \Delta p\,\mathrm{d}R - \frac{\gamma g}{R}\,\mathrm{d}R \tag{2.44}$$

or using the general Young-Laplace equation (2.38), as

$$\mathrm{d}\gamma = -\Gamma_S\,\mathrm{d}T - \boldsymbol{\Gamma} \cdot \mathrm{d}\boldsymbol{\mu} + \left[\frac{\partial \gamma}{\partial R}\right]_{T,\boldsymbol{\mu}} \mathrm{d}R. \tag{2.45}$$

Equation (2.45) is known as Gibbs adsorption equation and can be interpreted as an extension of the Gibbs-Duhem equation to interfacial systems. For a given dividing surface, $\gamma = \gamma(T, \boldsymbol{\mu})$ and thus the interfacial tension becomes a function of the state variables. This relation is only well defined if two stable or metastable states α and β can be found at a given T and $\boldsymbol{\mu}$. In the case that $p^{\alpha}(T, \boldsymbol{\mu}) = p^{\beta}(T, \boldsymbol{\mu})$, the system is at a bulk phase equilibrium and the interface is planar. If not, the system contains a metastable continuous phase with a droplet

or a bubble. In this case, it is often more convenient to characterize the system using a bulk phase equilibrium as reference and a supersaturation, that can be in terms of the temperature, the pressure, or the the composition of one of the components. In chapter 3 density functional theory is used to calculate the interfacial tensions of nanodroplets. Thereby it is shown, that a convenient choice of variables is the temperature, the chemical potentials of a reference point on the coexistence curve and the curvature $\frac{1}{R}$ of the droplet. This observation is used in chapter 4 to develop a model, that allows a precise approximation of the surface tension of curved interfaces based on properties of the planar interface.

The Gibbs adsorption equation can be used to relate the change of the surface tension of planar interfaces with respect to the state variables. However, a planar interface only exists at a phase equilibrium, therefore the variables in eq. (2.45) are connected and one variable can be eliminated. For a pure component, the dependence of the surface tension on the temperature is

$$\mathrm{d}\gamma = \left(\Gamma \frac{\hat{s}^\alpha - \hat{s}^\beta}{\rho^\alpha - \rho^\beta} - \Gamma_S \right) \mathrm{d}T \tag{2.46}$$

and for a mixture one possible way is to eliminate the temperature to give

$$\mathrm{d}\gamma = \left(\Gamma_S \frac{\boldsymbol{\rho}^\alpha - \boldsymbol{\rho}^\beta}{\hat{s}^\alpha - \hat{s}^\beta} - \boldsymbol{\Gamma} \right) \cdot \mathrm{d}\boldsymbol{\mu}. \tag{2.47}$$

2.4 Non-local Helmholtz energy functionals

As described above, the key to modeling inhomogeneous systems using density functional theory is the knowledge about the intrinsic Helmholtz energy functional. Over the last decades, developing and improving models for the residual Helmholtz energy functional has been an important research topic in the field of density functional theory. The fluids, that have been studied range from simple model fluids like hard spheres to multi-component mixtures of real molecules.

Particularly non-local functionals have proved successful when it comes to modeling structural properties of fluid. In these approaches, the Helmholtz energy density f is itself a functional of the density profiles $\boldsymbol{\rho}(\mathbf{r})$. Often the non-locality can be fully included in the calculation of a set of weighted densities n_α with

$$\mathscr{F} = \int f(\{n_\alpha(\mathbf{r})\}) \, \mathrm{d}\mathbf{r} \quad \text{and} \quad n_\alpha(\mathbf{r}) = \int \boldsymbol{\rho}(\mathbf{r}') \cdot \boldsymbol{\omega}_\alpha(\mathbf{r} - \mathbf{r}') \, \mathrm{d}\mathbf{r}'. \tag{2.48}$$

The weighted densities are obtained as convolutions of the density profiles with weight functions $\boldsymbol{\omega}_\alpha$. The Helmholtz energy density is then only a local function of the weighted densities.

2.4.1 Short-range repulsion

At high densities, the short-range repulsion is largely responsible for the structure of the fluid. Therefore, many early efforts in DFT modeling were focussing on the description of hard-sphere systems. Based on the insights from scaled particle theory[12] and the Percus-Yevick integral theory[13,14] for bulk systems, Rosenfeld developed his fundamental measure theory (FMT)[15] to model inhomogeneous systems not only of hard spheres, but of hard sphere mixtures with a remarkable accuracy. As opposed to the weighted density approximation proposed earlier by Tarazona and Evans[16], Rosenfelds FMT uses a number of weighted densities associated with geometrical measures of the interacting particles. An FMT that avoids the use of vector weighted densities, but was shown to be equivalent to Rosenfelds version[17] was proposed by Kierlik and Rosinberg[18].

The disadvantage of Rosenfelds original FMT is, that for bulk systems it simplifies to the slightly imprecise Percus-Yevick result[19]. Therefore, a modification to the theory was proposed[20,21] that is based on the more precise Boublík-Mansoori-Carnahan-Starling-Leland[22,23] equation of state and is widely used as a reference in perturbation theories. In the meantime, a number of extensions to FMT were proposed to deal with freezing transitions[24–27] and non-spherical particles[28–30].

2.4.2 Van der Waals attraction

In order to model real fluids, van der Waals forces, like dispersive attraction and polar interactions, must be included in the Helmholtz energy functional. As perturbation theories have proven to be successful in the development of equations of state, it is straightforward to apply the same concept to Helmholtz energy functionals. The pair potential $\phi_{ij}(\mathbf{r}_{12})$ is split into a reference contribution $\phi_{ij}^{\mathrm{ref}}(\mathbf{r}_{12})$, usually containing mostly repulsive interactions, and a perturbation contribution $\phi_{ij}^{\mathrm{PT}}(\mathbf{r}_{12}) = \phi_{ij}(\mathbf{r}_{12}) - \phi_{ij}^{\mathrm{ref}}(\mathbf{r}_{12})$. In this general notation, the position vector $\mathbf{r}$ can also include orientational degrees of freedom of the molecules. With the introduction of a coupling parameter λ, a continuous transition from the reference fluid to the target fluid can be described, as

$$\phi_{\lambda,ij}(\mathbf{r}_{12}) = \phi_{ij}^{\mathrm{ref}}(\mathbf{r}_{12}) + \lambda\phi_{ij}^{\mathrm{PT}}(\mathbf{r}_{12}). \tag{2.49}$$

For pairwise additive potentials the Helmholtz energy functional is then known exactly, as[5,31]

$$\mathscr{F}^{\mathrm{PT}} = \frac{1}{2}\sum_i\sum_j \int_0^1 \iint \rho_i(\mathbf{r}_1)\rho_j(\mathbf{r}_2) g_{\lambda,ij}(\mathbf{r}_1,\mathbf{r}_2)\phi_{ij}^{\mathrm{PT}}(\mathbf{r}_{12})\,\mathrm{d}\mathbf{r}_1\,\mathrm{d}\mathbf{r}_2\,\mathrm{d}\lambda. \tag{2.50}$$

For inhomogeneous systems, the pair correlation function $g_{\lambda,ij}(\mathbf{r}_1,\mathbf{r}_2)$ is not only a function of the distance and relative orientation of two molecules, but also of their respective positions and orientations. Therefore, even a first order perturbation theory becomes difficult to formulate. A common approximation is the so-called mean-field approach (MFA) in which $g_{\lambda,ij}(\mathbf{r}_1,\mathbf{r}_2) \approx \Theta(|\mathbf{r}_{12}| - d_{ij})$ is assumed[32]. In this case, eq. (2.50) simplifies to

$$\mathscr{F}^{\mathrm{PT}} = \frac{1}{2}\sum_i\sum_j \iint_{|\mathbf{r}_{12}|>d_{ij}} \rho_i(\mathbf{r}_1)\rho_j(\mathbf{r}_2)\phi_{ij}^{\mathrm{PT}}(\mathbf{r}_{12})\,\mathrm{d}\mathbf{r}_1\,\mathrm{d}\mathbf{r}_2. \tag{2.51}$$

The approach extends the van der Waals equation to inhomogeneous systems. Similar to the equation of state, it covers important fluid features like phase equilibria, but can be seen as at most semiquantitive[33].

Instead of basing the expansion on the (long range) pair correlation function, the n-th order direct correlation function $\boldsymbol{c}^{(n)}(\mathbf{r}_1,\mathbf{r}_2)$ can be used. The direct correlation function shows up naturally as the functional derivatives of the residual Helmholtz energy functional

$$\boldsymbol{c}^{(1)}(\mathbf{r}) = -\frac{\delta\mathscr{F}^{\mathrm{res}}}{\delta\boldsymbol{\rho}(\mathbf{r})} \quad \text{and} \quad \boldsymbol{c}^{(2)}(\mathbf{r}_1,\mathbf{r}_2) = -\frac{\delta^2\mathscr{F}^{\mathrm{res}}}{\delta\boldsymbol{\rho}(\mathbf{r}_1)\delta\boldsymbol{\rho}(\mathbf{r}_2)}. \tag{2.52}$$

For the density profile $\boldsymbol{\rho}_0(\mathbf{r})$ and the first order direct correlation function $\boldsymbol{c}_0^{(1)}(\mathbf{r})$ of a reference system, a coupling parameter λ can be introduced, that transforms the system from the reference state to the target state as

$$\boldsymbol{\rho}_\lambda(\mathbf{r}) = \boldsymbol{\rho}_0(\mathbf{r}) + \lambda\Delta\boldsymbol{\rho}(\mathbf{r}) \quad \text{with} \quad \Delta\boldsymbol{\rho}(\mathbf{r}) = \boldsymbol{\rho}(\mathbf{r}) - \boldsymbol{\rho}_0(\mathbf{r}). \tag{2.53}$$

The functional derivatives in eq. (2.52) can be integrated to give[5]

$$\mathscr{F}^{\mathrm{res}}[\boldsymbol{\rho}] = \mathscr{F}^{\mathrm{res}}[\boldsymbol{\rho}_0] - \int \boldsymbol{c}_0^{(1)}(\mathbf{r})\cdot\Delta\boldsymbol{\rho}(\mathbf{r})\,\mathrm{d}\mathbf{r} - \int_0^1 (1-\lambda)\iint \Delta\boldsymbol{\rho}^{\intercal}(\mathbf{r}_1)\boldsymbol{c}_\lambda^{(2)}(\mathbf{r}_1,\mathbf{r}_2)\Delta\boldsymbol{\rho}(\mathbf{r}_2)\,\mathrm{d}\mathbf{r}_1\,\mathrm{d}\mathbf{r}_2\,\mathrm{d}\lambda. \tag{2.54}$$

If a homogeneous reference state is chosen one gets $\boldsymbol{c}_0^{(1)} = \boldsymbol{\mu}^{\mathrm{res}}$ and $\boldsymbol{c}_0^{(2)} = c_0^{(2)}(|\mathbf{r}_{12}|)$. Therefore,

the first order expansion of eq. (2.54) simplifies to

$$\mathscr{F}^{\mathrm{res}}[\boldsymbol{\rho}] = \mathscr{F}^{\mathrm{res}}[\boldsymbol{\rho}_0] - \boldsymbol{\mu}^{\mathrm{res}} \cdot \int \Delta\boldsymbol{\rho}(\mathbf{r})\,\mathrm{d}\mathbf{r} - \frac{1}{2}\iint \Delta\boldsymbol{\rho}^{\intercal}(\mathbf{r}_1)\mathbf{c}_0^{(2)}(|\mathbf{r}_{12}|)\Delta\boldsymbol{\rho}(\mathbf{r}_2)\,\mathrm{d}\mathbf{r}_1\,\mathrm{d}\mathbf{r}_2. \quad (2.55)$$

A density functional theory combining this perturbation theory with an analytic direct correlation function from first order mean spherical approximation[34] improved the results from MFA significantly[35].

The aforementioned Helmholtz energy functionals require either the pair correlation $g_{\lambda=0,ij}$ or the direct correlation $\mathbf{c}_0^{(2)}$ of the reference fluid as input. These quantities are rarely known, particularly for non-spherical molecules. Instead, it can be useful to build the Helmholtz energy functional based on a bulk equation of state. The most basic approach is a local density approximation (LDA)

$$\mathscr{F}^{\mathrm{LDA}} = \int \rho(\mathbf{r})\tilde{f}^{\mathrm{eos}}(\boldsymbol{\rho}(\mathbf{r}))\,\mathrm{d}\mathbf{r} \quad (2.56)$$

in which $\rho(\mathbf{r})$ is the total density and $\tilde{f}^{\mathrm{eos}}(\boldsymbol{\rho}(\mathbf{r}))$ is the Helmholtz energy per molecule from the equation of state evaluated locally at every point in the system. This functional contains no information about the structure of the system and can therefore only be applied in weakly inhomogeneous systems, like interfaces in proximity to critical points. It is entirely unapplicable in systems with strong adsorption where the local densities can be much larger than the liquid bulk densities and thus the evaluation of the equation of state for these densities is not possible.

A better description is obtained using a weighted density approximation (WDA)[5,31,36–39]

$$\mathscr{F}^{\mathrm{WDA}} = \int \rho(\mathbf{r})\tilde{f}^{\mathrm{eos}}(\bar{\rho}(\mathbf{r}))\,\mathrm{d}\mathbf{r} \quad (2.57)$$

in which the equation of state is evaluated for the set of weighted densities $\bar{\rho}(\mathbf{r})$ instead. The weighted densities are obtained by convolving the density profile with a specific normalized weight function according to eq. (2.48). The WDA can also be used in the form[40]

$$\mathscr{F}^{\mathrm{WDA}} = \int \bar{\rho}(\mathbf{r})\tilde{f}^{\mathrm{eos}}(\bar{\rho}(\mathbf{r}))\,\mathrm{d}\mathbf{r}. \quad (2.58)$$

that has the advantage, that the Helmholtz energy density only depends on the weighted density and not also directly on the density itself. Since the equation of state is usually known during the development of the WDA functional, the shape of the weight function is the critical ingredient. In the earlier publications, the weight function was dependent on

the density profiles[36,37]. Later it was shown, that precise results could also be obtained with simpler and faster models in which the weight function has the shape of the pair potential[40], a Gauss distribution[41] or a step function[42,43]. For a weighted density approximation in combination with the PCP-SAFT equation of state, a detailed comparison between eqs. (2.57) and (2.58) showed that the latter, combined with a simple step weight function with a fitted, but component-independent range describes both fluid-liquid interfaces and adsorption phenomena well[44].

2.4.3 Association and chain formation

Most theories for fluids with highly directional attractive forces are based on Wertheim's thermodynamic perturbation theory[45–49]. In the limit of complete association, the theory can be used to describe chain formation, which is the basis of the SAFT family of equations of state[50,51]. Even though it was an important breakthrough in the development of bulk equations of state, Wertheim's theory was initially derived for inhomogeneous systems[52]. Therefore, association functionals could be obtained directly from it[53,54]. The disadvantage of this approach is that calculating the fraction of non-bonded sites involves the solution of an integral equation. Faster methods were proposed, that make use of weighted densities from fundamental measure theory[55,56], Tarazona[16] weighting[57–59], or Gaussian weight functions[60].

Analogously to the development of equations of state for non-spherical molecules, Helmholtz energy functionals for chains were proposed based on Wertheim's theory by Kierlik and Rosinberg[52,61]. Similar to the functional based on fundamental measure theory by Yu and Wu[62], this formulation requires an involved solution procedure with additional degrees of freedom. An improvement was the development of the iSAFT functional by Tripathi and Chapman[63,64], that is based on the association functional of Segura et al.[54] and simplifies to the SAFT equation of state in the bulk limit. Since the approaches are based on Wertheim's theory, they essentially model tangentially bonded spheres and assume that the density profiles of all segments on one chain is equal. This approximation becomes poor if the molecules are heterogeneous, like alcohols or carboxylic acids. Therefore, the iSAFT approach was extended by Jain et al.[65] to model molecules by calculating the density profiles of individual segments. This framework combined with the group contribution PC-SAFT equation of state[66] is used in chapter 7 to model the interfacial properties of non-ionic surfactants.

2.5 Density gradient theory

Before the foundations of density functional theory were developed, van der Waals formulated a theory to describe interfaces with continuous density profiles[67]. The theory was later refined by Cahn and Hilliard[68] and is now often referred to as density gradient or square gradient theory (DGT). The Helmholtz energy functional can be written as

$$\mathscr{F} = \int \left(f^{\text{eos}} + \frac{1}{2} \nabla \boldsymbol{\rho}^{\intercal} \boldsymbol{C} \nabla \boldsymbol{\rho}) \right) \mathrm{d}\mathbf{r} \tag{2.59}$$

with the local Helmholtz energy density as calculated from a bulk equation of state f^{eos} and the influence matrix $\boldsymbol{C}$. Without the second term, the functional would simplify to a local density approximation. The influence of the interface on the Helmholtz energy is obtained through the density gradients $\nabla \boldsymbol{\rho}$.

In comparison to non-local density functional theory, DGT is not able to model the structure of fluids and is thus not suited for applications like adsorption in porous media. This restricts the usage primarily to vapor-liquid and liquid-liquid interfaces. Also, while non-local Helmholtz energy functionals have been proposed, that are consistent with bulk equations of state and require no additional parameters, the calculation of interfacial tension requires knowledge about the values of the influence matrix. For pure components, the influence parameter $C(T, \boldsymbol{\rho})$ is usually treated as a constant, which is fitted to experimental surface tension data or correlated with equation of state parameters[69–75]. For mixtures, a simple geometric combining rule has proven successful for many systems[76].

The simple mathematical form of eq. (2.59) also leads to shorter computation times compared to DFT. This advantage is particularly noticeable when planar interfaces of pure components are considered. In that case, the surface tension can be computed explicitly from

$$\gamma = \int_{\rho^V}^{\rho^L} \sqrt{2C \left(f^{\text{eos}} - \rho\mu + p \right)} \, \mathrm{d}\rho. \tag{2.60}$$

For mixtures, the density profile needs to be calculated iteratively and thus the performance advantage is diminished.

Chapter 5 introduces an expression for the influence matrix based on non-local density functional theory, that shares the parameters with the underlying equation of state and thus makes the DGT approach predictive. The predictiveness and the fast evaluation of eq. (2.60) makes it possible to include surface tension data in the parameter estimation of the equation

of state. This is carried out using the PCP-SAFT equation of state for water and alcohols in chapter 6.

References

[1] P. Hohenberg and W. Kohn. Inhomogeneous Electron Gas. *Physical Review*, **136**:B864–B871, 1964. doi:10.1103/PhysRev.136.B864.

[2] N. D. Mermin. Thermal Properties of the Inhomogeneous Electron Gas. *Physical Review*, **137**:A1441–A1443, 1965. doi:10.1103/PhysRev.137.A1441.

[3] C. Ebner, W. F. Saam, and D. Stroud. Density-functional theory of simple classical fluids. I. Surfaces. *Physical Review A*, **14**:2264–2273, 1976. doi:10.1103/PhysRevA.14.2264.

[4] R. Evans. The nature of the liquid-vapour interface and other topics in the statistical mechanics of non-uniform, classical fluids. *Advances in Physics*, **28**(2):143–200, 1979. doi:10.1080/00018737900101365.

[5] J. P. Hansen and I. R. McDonald. *Theory of simple liquids*. Elsevier [u.a.], Amsterdam, 3rd edition, 2006. ISBN 0-12-370535-5.

[6] V. Kalikmanov. *Statistical physics of fluids: basic concepts and applications*. Springer Science & Business Media, 2013.

[7] D. de las Heras and M. Schmidt. Full Canonical Information from Grand-Potential Density-Functional Theory. *Physical Review Letters*, **113**:238304, 2014. doi:10.1103/PhysRevLett.113.238304.

[8] J. Gibbs. *The Collected Works of J. Willard Gibbs, Volume I: Thermodynamics*. Longmans, Green and Co., 1928.

[9] J. S. Rowlinson and B. Widom. *Molecular Theory of Capillarity*. Oxford: Clarendon, 1982.

[10] H. Davis. *Statistical Mechanics of Phases, Interfaces and Thin Films*. Advances in interfacial engineering series. Wiley, 1996. ISBN 9780471185628.

[11] F. O. Koenig. On the Thermodynamic Relation between Surface Tension and Curvature. *The Journal of Chemical Physics*, **18**(4):449–459, 1950. doi:10.1063/1.1747660.

[12] H. Reiss, H. L. Frisch, E. Helfand, and J. L. Lebowitz. Aspects of the Statistical Thermodynamics of Real Fluids. *The Journal of Chemical Physics*, **32**(1):119–124, 1960. doi:10.1063/1.1700883.

[13] J. K. Percus and G. J. Yevick. Analysis of Classical Statistical Mechanics by Means of Collective Coordinates. *Physical Review*, **110**:1–13, 1958. doi:10.1103/PhysRev.110.1.

[14] J. L. Lebowitz. Exact Solution of Generalized Percus-Yevick Equation for a Mixture of Hard Spheres. *Physical Review*, **133**:A895–A899, 1964. doi:10.1103/PhysRev.133.A895.

[15] Y. Rosenfeld. Free-energy model for the inhomogeneous hard-sphere fluid mixture and density-functional theory of freezing. *Physical Review Letters*, **63**:980–983, 1989. doi:10.1103/PhysRevLett.63.980.

[16] P. Tarazona and R. Evans. A simple density functional theory for inhomogeneous liquids. *Molecular Physics*, **52**(4):847–857, 1984. doi:10.1080/00268978400101601.

[17] S. Phan, E. Kierlik, M. L. Rosinberg, B. Bildstein, and G. Kahl. Equivalence of two free-energy models for the inhomogeneous hard-sphere fluid. *Physical Review E*, **48**:618–620, 1993. doi:10.1103/PhysRevE.48.618.

[18] E. Kierlik and M. L. Rosinberg. Free-energy density functional for the inhomogeneous hard-sphere fluid: Application to interfacial adsorption. *Physical Review A*, **42**:3382–3387, 1990. doi:10.1103/PhysRevA.42.3382.

[19] M. S. Wertheim. Exact Solution of the Percus-Yevick Integral Equation for Hard Spheres. *Physical Review Letters*, **10**:321–323, 1963. doi:10.1103/PhysRevLett.10.321.

[20] R. Roth, R. Evans, A. Lang, and G. Kahl. Fundamental measure theory for hard-sphere mixtures revisited: the White Bear version. *Journal of Physics: Condensed Matter*, **14**(46):12063, 2002. doi:10.1088/0953-8984/14/46/313.

[21] Y.-X. Yu and J. Wu. Structures of hard-sphere fluids from a modified fundamental-measure theory. *The Journal of Chemical Physics*, **117**(22):10156–10164, 2002. doi:10.1063/1.1520530.

[22] T. Boublík. Hard-Sphere Equation of State. *The Journal of Chemical Physics*, **53**(1):471–472, 1970. doi:10.1063/1.1673824.

[23] G. A. Mansoori, N. F. Carnahan, K. E. Starling, and T. W. Leland. Equilibrium Thermodynamic Properties of the Mixture of Hard Spheres. *The Journal of Chemical Physics*, **54**(4):1523–1525, 1971. doi:10.1063/1.1675048.

[24] Y. Rosenfeld, M. Schmidt, H. Löwen, and P. Tarazona. Fundamental-measure free-energy density functional for hard spheres: Dimensional crossover and freezing. *Physical Review E*, **55**:4245–4263, 1997. doi:10.1103/PhysRevE.55.4245.

[25] P. Tarazona. Density Functional for Hard Sphere Crystals: A Fundamental Measure Approach. *Physical Review Letters*, **84**:694–697, 2000. doi:10.1103/PhysRevLett.84.694.

[26] H. Hansen-Goos, M. Mortazavifar, M. Oettel, and R. Roth. Fundamental measure theory for the inhomogeneous hard-sphere system based on Santos' consistent free energy. *Physical Review E*, **91**:052121, 2015. doi:10.1103/PhysRevE.91.052121.

[27] T. Bernet, E. A. Müller, and G. Jackson. A tensorial fundamental measure density functional theory for the description of adsorption in substrates of arbitrary three-dimensional geometry. *The Journal of Chemical Physics*, **152**(22):224701, 2020. doi:10.1063/5.0010974.

[28] H. Hansen-Goos and K. Mecke. Fundamental Measure Theory for Inhomogeneous Fluids of Nonspherical Hard Particles. *Physical Review Letters*, **102**:018302, 2009. doi:10.1103/PhysRevLett.102.018302.

[29] M. Marechal, H. H. Goetzke, A. Härtel, and H. Löwen. Inhomogeneous fluids of colloidal hard dumbbells: Fundamental measure theory and Monte Carlo simulations. *The Journal of Chemical Physics*, **135**(23):234510, 2011. doi:10.1063/1.3664742.

[30] R. Wittmann, M. Marechal, and K. Mecke. Fundamental measure theory for non-spherical hard particles: predicting liquid crystal properties from the particle shape. *Journal of Physics: Condensed Matter*, **28**(24):244003, 2016. doi:10.1088/0953-8984/28/24/244003.

[31] J. R. Solana. *Perturbation theories for the thermodynamic properties of fluids and solids*. CRC Press, 2013.

[32] Z. Tang, L. E. Scriven, and H. T. Davis. Density-functional perturbation theory of inhomogeneous simple fluids. *The Journal of Chemical Physics*, **95**(4):2659–2668, 1991. doi:10.1063/1.460918.

[33] J. Wu. Density functional theory for chemical engineering: From capillarity to soft materials. *AIChE Journal*, **52**(3):1169–1193, 2006. doi:10.1002/aic.10713.

[34] Y. Tang and B. C.-Y. Lu. On the mean spherical approximation for the Lennard–Jones fluid. *Fluid Phase Equilibria*, **190**(1):149 – 158, 2001. doi:https://doi.org/10.1016/S0378-3812(01)00600-8.

[35] Y. Tang and J. Wu. Modeling inhomogeneous van der Waals fluids using an analytical direct correlation function. *Physical Review E*, **70**:011201, 2004. doi:10.1103/PhysRevE.70.011201.

[36] W. A. Curtin and N. W. Ashcroft. Weighted-density-functional theory of inhomogeneous liquids and the freezing transition. *Physical Review A*, **32**:2909–2919, 1985. doi:10.1103/PhysRevA.32.2909.

[37] R. Leidl and H. Wagner. Hybrid WDA: A weighted-density approximation for inhomogeneous fluids. *The Journal of Chemical Physics*, **98**(5):4142–4148, 1993. doi:10.1063/1.465022.

[38] M. Müller and L. G. MacDowell. Interface and Surface Properties of Short Polymers in Solution: Monte Carlo Simulations and Self-Consistent Field Theory. *Macromolecules*, **33**(10):3902–3923, 2000. doi:10.1021/ma991796t.

[39] M. Müller, L. G. MacDowell, and A. Yethiraj. Short chains at surfaces and interfaces: A quantitative comparison between density-functional theories and Monte Carlo simulations. *The Journal of Chemical Physics*, **118**(6):2929–2940, 2003. doi:10.1063/1.1535893.

[40] B. Peng and Y.-X. Yu. A Density Functional Theory with a Mean-field Weight Function: Applications to Surface Tension, Adsorption, and Phase Transition of a Lennard-Jones Fluid in a Slit-like Pore. *The Journal of Physical Chemistry B*, **112**(48):15407–15416, 2008. doi:10.1021/jp805697p. PMID: 19006278.

[41] J. Hughes, E. J. Krebs, and D. Roundy. A classical density-functional theory for describing water interfaces. *The Journal of Chemical Physics*, **138**(2):024509, 2013. doi:10.1063/1.4774155.

[42] Z. Ye, J. Cai, H. Liu, and Y. Hu. Density and chain conformation profiles of square-well chains confined in a slit by density-functional theory. *The Journal of Chemical Physics*, **123**(19):194902, 2005. doi:10.1063/1.2117009.

[43] G. Shen, X. Ji, and X. Lu. A hybrid perturbed-chain SAFT density functional theory for representing fluid behavior in nanopores. *The Journal of Chemical Physics*, **138**(22):224706, 2013. doi:10.1063/1.4808160.

[44] E. Sauer and J. Gross. Classical Density Functional Theory for Liquid–Fluid Interfaces and Confined Systems: A Functional for the Perturbed-Chain Polar Statistical Associating Fluid Theory Equation of State. *Industrial & Engineering Chemistry Research*, **56**(14):4119–4135, 2017. doi:10.1021/acs.iecr.6b04551.

[45] M. S. Wertheim. Fluids with highly directional attractive forces. I. Statistical thermodynamics. *Journal of Statistical Physics*, **35**(1):19–34, 1984. doi:10.1007/BF01017362.

[46] M. S. Wertheim. Fluids with highly directional attractive forces. II. Thermodynamic perturbation theory and integral equations. *Journal of Statistical Physics*, **35**(1):35–47, 1984. doi:10.1007/BF01017363.

[47] M. S. Wertheim. Fluids with highly directional attractive forces. III. Multiple attraction sites. *Journal of Statistical Physics*, **42**(3):459–476, 1986. doi:10.1007/BF01127721.

[48] M. S. Wertheim. Fluids with highly directional attractive forces. IV. Equilibrium polymerization. *Journal of Statistical Physics*, **42**(3):477–492, 1986. doi:10.1007/BF01127722.

[49] W. Zmpitas and J. Gross. Detailed pedagogical review and analysis of Wertheim's thermodynamic perturbation theory. *Fluid Phase Equilibria*, **428**:121 – 152, 2016. doi:http://dx.doi.org/10.1016/j.fluid.2016.07.033. Theo W. de Loos Festschrift.

[50] W. G. Chapman, K. E. Gubbins, G. Jackson, and M. Radosz. New reference equation of state for associating liquids. *Industrial & Engineering Chemistry Research*, **29**(8):1709–1721, 1990. doi:10.1021/ie00104a021.

[51] E. A. Müller and K. E. Gubbins. Molecular-Based Equations of State for Associating Fluids: A Review of SAFT and Related Approaches. *Industrial & Engineering Chemistry Research*, **40**(10):2193–2211, 2001. doi:10.1021/ie000773w.

[52] E. Kierlik and M. L. Rosinberg. A perturbation density-functional theory for polyatomic fluids. I. Rigid molecules. *The Journal of Chemical Physics*, **97**(12):9222–9239, 1992. doi:10.1063/1.463298.

[53] C. J. Segura and W. G. Chapman. Associating fluids with four bonding sites against solid surfaces: Monte Carlo simulations. *Molecular Physics*, **86**(3):415–442, 1995.

doi:10.1080/00268979509413622.

[54] B. C. J. Segura, W. G. Chapman, and K. P. Shukla. Associating fluids with four bonding sites against a hard wall: density functional theory. *Molecular Physics*, **90**(5):759–772, 1997. doi:10.1080/002689797172110.

[55] Y.-X. Yu and J. Wu. A fundamental-measure theory for inhomogeneous associating fluids. *The Journal of Chemical Physics*, **116**(16):7094–7103, 2002. doi:10.1063/1.1463435.

[56] D. Fu and J. Wu. Vapor–Liquid Equilibria and Interfacial Tensions of Associating Fluids within a Density Functional Theory. *Industrial & Engineering Chemistry Research*, **44**(5):1120–1128, 2005. doi:10.1021/ie049788a.

[57] O. Pizio, A. Patrykiejew, and S. Sokołowski. Evaluation of liquid–vapor density profiles for associating fluids in pores from density-functional theory. *The Journal of Chemical Physics*, **113**(23):10761–10767, 2000. doi:10.1063/1.1323747.

[58] C. J. Segura, J. Zhang, and W. G. Chapman. Binary associating fluid mixtures against a hard wall: density functional theory and simulation. *Molecular Physics*, **99**(1):1–12, 2001. doi:10.1080/00268970109483483.

[59] E. L. C. Vergara, G. M. Kontogeorgis, and X. Liang. A new study of associating inhomogeneous fluids with classical density functional theory. *Molecular Physics*, **0**(0):e1725668, 2020. doi:10.1080/00268976.2020.1725668.

[60] A. Patrykiejew, S. Sokolowski, and D. Henderson. The structure of associating fluids restricted by permeable walls: a density functional approach. *Molecular Physics*, **95**(2):211–218, 1998. doi:10.1080/00268979809483153.

[61] E. Kierlik and M. L. Rosinberg. A perturbation density functional theory for polyatomic fluids. II. Flexible molecules. *The Journal of Chemical Physics*, **99**(5):3950–3965, 1993. doi:10.1063/1.466142.

[62] Y.-X. Yu and J. Wu. Density functional theory for inhomogeneous mixtures of polymeric fluids. *The Journal of Chemical Physics*, **117**(5):2368–2376, 2002. doi:10.1063/1.1491240.

[63] S. Tripathi and W. G. Chapman. Microstructure of inhomogeneous polyatomic mixtures from a density functional formalism for atomic mixtures. *The Journal of Chemical Physics*, **122**(9):094506, 2005. doi:10.1063/1.1853371.

[64] S. Tripathi and W. G. Chapman. Microstructure and Thermodynamics of Inhomogeneous Polymer Blends and Solutions. *Physical Review Letters*, **94**:087801, 2005. doi:10.1103/PhysRevLett.94.087801.

[65] S. Jain, A. Dominik, and W. G. Chapman. Modified interfacial statistical associating fluid theory: A perturbation density functional theory for inhomogeneous complex fluids. *The Journal of Chemical Physics*, **127**(24):244904, 2007. doi:10.1063/1.2806932.

[66] E. Sauer, M. Stavrou, and J. Gross. Comparison between a Homo- and a Heterosegmented Group Contribution Approach Based on the Perturbed-Chain Polar Statistical Associating Fluid Theory Equation of State. *Industrial & Engineering Chemistry Research*, **53**(38):14854–14864, 2014. doi:10.1021/ie502203w.

[67] J. Van der Waals. Thermodynamische Theorie der Kapillarität unter voraussetzung stetiger Dichteänderung. *Zeitschrift für Physikalische Chemie*, **13**(1):657–725, 1894.

[68] J. W. Cahn and J. E. Hilliard. Free Energy of a Nonuniform System. I. Interfacial Free Energy. *The Journal of Chemical Physics*, **28**(2):258–267, 1958. doi:10.1063/1.1744102.

[69] P. M. W. Cornelisse, C. J. Peters, and J. de Swaan Arons. On the fundamentals of the gradient theory of van der Waals. *The Journal of Chemical Physics*, **106**(23):9820–9834, 1997. doi:10.1063/1.473872.

[70] H. Kahl and S. Enders. Calculation of surface properties of pure fluids using density gradient theory and SAFT-EOS. *Fluid Phase Equilibria*, **172**(1):27 – 42, 2000. doi:https://doi.org/10.1016/S0378-3812(00)00361-7.

[71] C. Miqueu, B. Mendiboure, A. Graciaa, and J. Lachaise. Modelling of the surface tension of pure components with the gradient theory of fluid interfaces: a simple and accurate expression for the influence parameters. *Fluid Phase Equilibria*, **207**(1):225 – 246, 2003. doi:https://doi.org/10.1016/S0378-3812(03)00028-1.

[72] H. Lin, Y.-Y. Duan, and Q. Min. Gradient theory modeling of surface tension for pure fluids and binary mixtures. *Fluid Phase Equilibria*, **254**(1):75 – 90, 2007. doi:https://doi.org/10.1016/j.fluid.2007.02.013.

[73] B. Breure and C. Peters. Modeling of the surface tension of pure components and mixtures using the density gradient theory combined with a theoretically derived influence parameter correlation. *Fluid Phase Equilibria*, **334**:189 – 196, 2012. doi:https://doi.org/10.1016/j.fluid.2012.08.010.

[74] X. Liang, M. L. Michelsen, and G. M. Kontogeorgis. A density gradient theory based method for surface tension calculations. *Fluid Phase Equilibria*, **428**:153 – 163, 2016. doi:https://doi.org/10.1016/j.fluid.2016.06.017. Theo W. de Loos Festschrift.

[75] J. M. Garrido, A. Mejía, M. M. Piñeiro, F. J. Blas, and E. A. Müller. Interfacial tensions of industrial fluids from a molecular-based square gradient theory. *AIChE Journal*, **62**(5):1781–1794, 2016. doi:10.1002/aic.15190.

[76] X. Liang, M. L. Michelsen, and G. M. Kontogeorgis. Pitfalls of using the geometric-mean combining rule in the density gradient theory. *Fluid Phase Equilibria*, **415**:75 – 83, 2016. doi:https://doi.org/10.1016/j.fluid.2016.01.047.

3 Surface tension of droplets and Tolman lenghts of real substances and mixtures from density functional theory

The content of this chapter is reproduced from

P. Rehner, J. Gross. The Journal of Chemical Physics 148.16 (2018): 164703,

with the permission of AIP Publishing. Additions or deletions compared to the published work are marked with angular brackets.

The curvature dependence of interfacial properties has been discussed extensively over the last decades. After Tolman published his work on the effect of droplet size on surface tension, where he introduced the interfacial property now known as Tolman length, several studies were performed with varying results. In recent years, however, some consensus has been reached about the sign and magnitude of the Tolman length of simple model fluids. In this work, we reexamine Tolman's equation and how it relates the Tolman length to the surface tension and we apply non-local classical density functional theory (DFT) based on the PC-SAFT equation of state to characterize the curvature dependence of the surface tension of real fluids, as well as mixtures. In order to obtain a simple expression for the surface tension, we use a first order expansion of the Tolman length as a function of droplet radius R_s, as $\delta(R_s) = \delta_0 + \delta_1/R_s$, and subsequently expand Tolman's integral equation for the surface tension, whereby a second order expansion is found to give excellent agreement with the DFT result. The radius-dependence of the surface tension of increasingly non-spherical substances is studied for n-alkanes, up to icosane. The infinite diameter Tolman length is approximately $\delta_0 = -0.38\text{Å}$ at low temperatures. For more strongly non-spherical substances and for temperatures approaching the critical point, however, the infinite diameter Tolman lengths δ_0 turn positive. For mixtures, even if they contain similar molecules, the extrapolated Tolman length behaves strongly non-ideal, implying a qualitative change of the curvature behavior of the surface tension of the mixture.

3.1 Introduction

In 1949 Tolman[1] studied the dependence of the surface tension on the size of a droplet. He related the surface tension to what is now known as Tolman length δ, the distance between the equimolar radius and the radius of the surface of tension. He predicted this distance δ to be a small positive value and assumed, that it is independent of droplet size. From this assumption, he predicted a radius-dependent surface tension $\gamma(R)$, that is monotonically decreasing from the surface tension of a planar interface γ_∞ with decreasing radius R, as

$$\gamma(R) = \frac{\gamma_\infty}{1 + \frac{2\delta}{R}}. \tag{3.1}$$

Since then many studies were performed on the issue with different results. For an in-depth review of different studies on the surface properties of droplets we refer to the study of Malijevský and Jackson[2].

It is important to note, however, that after a period of discourse about the magnitude and sign of the Tolman length, some form of consensus has been reached. Calculations of the Tolman length by means of molecular dynamics (MD) simulation tend to result in a small positive value[3–6]. However, with a closer look, the reported Tolman lengths decrease with the radius of the simulated droplets. Simulation studies that consider the radius-dependence of the Tolman length[6,7], find a Tolman length for a Lennard-Jones fluid, extrapolated to infinitely large drops, of about -0.1 in reduced variables. This behavior, a monotonic increase of the Tolman length with curvature, has now been the result of many different studies using molecular simulation[8–12], density functional theory (DFT)[13–18] or a combination thereof[19,20].

Experiments in nucleation processes, the most relevant application for the surface tension of nanodroplets, also show, that the Tolman equation in the form of eq. (3.1) is insufficient. Bruot and Caupin[21] propose a linear behavior of the Tolman length with curvature and give a slope and planar limit based on experimental data.

A very effective way of predicting the curvature dependence of surface tension follows the curvature expansion proposed by Helfrich[22]. In this framework, the surface tension is expanded in terms of the total curvature J and the Gaussian curvature K of the interface, as

$$\gamma(J,K) = \gamma_\infty - \delta\gamma_\infty J + \frac{k}{2}J^2 + \tilde{k}K + \ldots. \tag{3.2}$$

A method of calculating the rigidity constants k and $\tilde{k}$, as well as the Tolman length δ, has been proposed by Blokhuis and Bedeaux[23] and has since been used to predict these properties for the Lennard-Jones fluid[24,25].

The vast majority of studies about the size-dependence of the surface tension has been performed on simple model fluids like Lennard-Jones fluids. Recently, real fluids have become more of a focus with water being the most prominent, due to its ubiquity in technical applications[26,27]. To calculate the properties of small droplets of real fluids, an equation of state is required, that extrapolates well in the metastable region of the phase diagram. PC-SAFT[28] suits this requirement since it's based on molecular properties of the fluid. Furthermore, the non-local extension of PC-SAFT, that can be used in density functional theory, has already been applied successfully to predict surface tensions of planar interfaces[29–31] and confined fluids[32]

In this work, we want to examine the relation between the Tolman length and the surface tension of a spherical droplet, so that we can generalize it to mixtures. Thermodynamic properties of droplets are calculated using density functional theory based on the PC-SAFT equation of state, of which a short reference is given in section 3.3. In the study of nanodroplets, the size of the particles appears as an additional degree of freedom besides the temperature and the composition. To be able to calculate plenty of state points, convolution integrals are implemented in Fourier space and a quickly converging solver is used. We validate this method in a study on sphericle particles and extend the field to real fluids consisting of non-spherical particles as well as mixtures thereof.

3.2 Surface tension of curved interfaces

In this section we review the thermodynamic approach to the surface tension of droplets. Further, we reexamine the derivation of Tolman's equation, point out the important assumptions made therein, and reformulate it to describe mixtures.

3.2.1 Gibbs' dividing surface

We consider a volume V of an inhomogeneous fluid with defined chemical potentials $\boldsymbol{\mu} = \mu_1, ...\mu_K$ of all K components at temperature T. The system has a field of local densities $\boldsymbol{\rho}(\mathbf{r}) = \rho_1(\mathbf{r}), ...\rho_K(\mathbf{r})$ of all components and a total local density $\rho(\mathbf{r}) = \sum_i^K \rho_i(\mathbf{r})$. In the following we consider a liquid droplet in a surrounding vapor phase, but the principles are not limited to this case.

Following Gibbs' concept of a dividing surface[33] p. 219 ff, we construct a hypothetical system, that is equivalent in N, V and $\boldsymbol{\mu}$, containing a homogeneous liquid phase (index L) and a homogeneous vapor phase (index V) separated by an infinitely thin surface phase (index σ).

Any extensive property X of the system can then be described as the sum over the contributions of each phase, as

$$X = X^L + X^V + X^\sigma. \tag{3.3}$$

By definition the volume of the surface phase $V^\sigma = 0$. Writing eq. (3.3) for the total number of molecules

$$N = N^L + N^V + N^\sigma = \rho^L V^L + \rho^V V^V + N^\sigma \tag{3.4}$$

leads to the definition of the equimolar radius: a sphere with radius R_e for which, if used as dividing surface, the interfacial adsorption $N^\sigma = 0$. The densities $\rho^L(T, \boldsymbol{\mu})$ and $\rho^V(T, \boldsymbol{\mu})$ appearing in this equation are the bulk phase densities for defined conditions T and $\boldsymbol{\mu}$. One can furthermore define

$$\Delta N = N - \rho^V V = \Delta\rho \; V^L(R_e) = \Delta\rho \; \frac{4}{3}\pi R_e^3 \tag{3.5}$$

or

$$R_e = \left(\frac{3\Delta N}{4\pi\Delta\rho}\right)^{\frac{1}{3}} \tag{3.6}$$

with $\Delta\rho = \rho^L - \rho^V$ as the difference between the densities of the bulk phases. Writing eq. (3.3) for the grand potential of the system leads to

$$\Omega = \Omega^L + \Omega^V + \Omega^\sigma = -p^L V^L - p^V V^V + \Omega^\sigma. \tag{3.7}$$

Analogous to ΔN we can define an excess of grand potential due to the presence of the liquid phase, as

$$\Delta\Omega = \Omega + p^V V = -\Delta p V^L + \Omega^\sigma. \tag{3.8}$$

For given chemical potentials $\boldsymbol{\mu}$ and temperature T, the droplet contribution to the grand potential $\Delta\Omega$ and the pressure difference $\Delta p = p^L - p^V$ are determined (for a given topology and assuming the volume is large enough to contain the entire droplet). By defining the radius of the surface of tension R_s and the corresponding surface tension γ with the set of equations

$$\Delta p = \frac{2\gamma}{R_s} \qquad \text{and} \qquad \Omega^\sigma = \gamma 4\pi R_s^2, \tag{3.9}$$

one can eliminate Ω^σ and $V^L = \frac{4}{3}\pi R_s^3$ in eq. (3.8) and the system of equations can be solved for the surface tension

$$\gamma = \left(\frac{3\Delta\Omega\Delta p^2}{16\pi}\right)^{\frac{1}{3}} \tag{3.10}$$

and the surface of tension

$$R_s = \left(\frac{3\Delta\Omega}{2\pi\Delta p}\right)^{\frac{1}{3}}. \tag{3.11}$$

Therefore, with the definition of the surface of tension R_s, the surface tension γ is also uniquely determined for given $\boldsymbol{\mu}$ and T and so is the Tolman length, that is defined as $\delta = R_e - R_s$. The same concept can be applied to cylindrical interfaces. The surface tension and radius of surface of tension in this case are

$$\gamma_{\text{cyl}} = \left(\frac{\Delta\Omega\Delta p}{\pi z}\right)^{\frac{1}{2}} \qquad \text{and} \qquad R_{s,\text{cyl}} = \left(\frac{\Delta\Omega}{\pi z\Delta p}\right)^{\frac{1}{2}} \tag{3.12}$$

with z as the axial dimension of the cylindrical interface.

3.2.2 Derivation of Tolman's equation

We show a derivation of Tolman's equation, that is solely based on the definition of the radius of the surface of tension and the corresponding surface tension and in this context extend the derivation to describe mixtures. We start by rewriting eq. (3.7) as

$$\Delta\Omega = -\Delta p\frac{4}{3}\pi R_s^3 + \gamma 4\pi R_s^2 \tag{3.13}$$

and taking the derivative

$$\mathrm{d}\Delta\Omega = -\frac{4}{3}\pi R_s^3\,\mathrm{d}\Delta p - \Delta p 4\pi R_s^2\,\mathrm{d}R_s + \gamma 8\pi R_s\,\mathrm{d}R_s + 4\pi R_s^2\,\mathrm{d}\gamma. \tag{3.14}$$

The two terms in $\mathrm{d}R_s$ cancel due to eq. (3.9). The left hand side can be replaced by the total differential of $\Delta\Omega$. Note that, as opposed to the total grand potential of the system Ω, this expression does not depend on the volume of the system, provided the system is large enough

to contain the entire droplet. Therefore we find

$$\begin{aligned}(\mathrm{d}\Delta\Omega)_T &= \sum_i \left(\frac{\partial \Delta\Omega}{\partial \mu_i}\right)_{T,\mu_{j\neq i}} \mathrm{d}\mu_i = \sum_i \left(\frac{\partial \left(\Omega + p^V V\right)}{\partial \mu_i}\right)_{T,V,\mu_{j\neq i}} \mathrm{d}\mu_i \\ &= \sum_i \left(-N_i + \rho_i^V V\right) \mathrm{d}\mu_i = -\Delta \boldsymbol{N} \cdot \mathrm{d}\boldsymbol{\mu}. \end{aligned} \tag{3.15}$$

It is common to examine the size dependence of properties of the droplet at constant temperature. For mixtures, additional constraints are required. Intuitively it may be reasonable to require a constant composition of the vapor phase. However, in order to obtain equations for mixtures in close analogy to pure components, we rewrite eq. (3.15), such that it contains the total molecule number ΔN of the droplet by adding $0 = \sum_i \Delta N_i \,\mathrm{d}\mu_n - \Delta N \,\mathrm{d}\mu_n$ to the right hand side, to give

$$(\mathrm{d}\Delta\Omega)_T = -\sum_i \Delta N_i \,\mathrm{d}\mu_i + \sum_i \Delta N_i \,\mathrm{d}\mu_n - \Delta N \,\mathrm{d}\mu_n = -\sum_i \Delta N_i \,\mathrm{d}\underbrace{(\mu_i - \mu_n)}_{\equiv \Delta\mu_i} - \Delta N \,\mathrm{d}\mu_n. \tag{3.16}$$

With the same concept, we express the Gibbs-Duhem relations of the two bulk phases for constant temperature as

$$\sum_i \Delta\rho_i \,\mathrm{d}\Delta\mu_i + \Delta\rho \,\mathrm{d}\mu_n = \mathrm{d}\Delta p. \tag{3.17}$$

We thus study the curvature dependence of surface tensions of mixtures in a semi grand ensemble where the temperature T and the difference between the chemical potentials $\Delta\boldsymbol{\mu}$ (with respect to the n-th component) are kept constant. Since by definition $N^\sigma(R_e) = 0$, we also find that

$$\sum_i N_i^\sigma(R_e) \,\mathrm{d}\mu_i = \sum_i N_i^\sigma(R_e) \,\mathrm{d}\Delta\mu_i + N^\sigma(R_e) \,\mathrm{d}\mu_n = 0. \tag{3.18}$$

The condition $\sum_i N_i^\sigma(R_k) \,\mathrm{d}\mu_i = 0$ defines the Koenig surface R_k for a given choice of path through the metastable region[34]. We thus identify the equimolar surface of the total particle number as the Koenig surface corresponding to a path with constant $\Delta\boldsymbol{\mu}$. Using eqs. (3.16) and (3.17) in eq. (3.14) and replacing ΔN with eq. (3.5) leads to

$$-\frac{1}{3}\left(R_e^3 - R_s^3\right) \mathrm{d}\Delta p = R_s^2 \,\mathrm{d}\gamma \tag{3.19}$$

or, in terms of the Tolman length $\delta = R_e - R_s$,

$$-\delta\left(1+\frac{\delta}{R_s}+\frac{\delta^2}{3R_s^2}\right)\mathrm{d}\Delta p = \mathrm{d}\gamma. \tag{3.20}$$

The pressure difference can be replaced with the derivative of the Young-Laplace equation (3.9)

$$\mathrm{d}\Delta p = \frac{2}{R_s}\mathrm{d}\gamma - \frac{2\gamma}{R_s^2}\mathrm{d}R_s \tag{3.21}$$

and the result can be integrated from infinite radius to get the equation derived by Tolman[1], as

$$\ln\frac{\gamma}{\gamma_\infty} = \int_\infty^{R_s} \frac{\frac{2\delta}{R_s^2}\left(1+\frac{\delta}{R_s}+\frac{\delta^2}{3R_s^2}\right)}{1+\frac{2\delta}{R_s}\left(1+\frac{\delta}{R_s}+\frac{\delta^2}{3R_s^2}\right)}\mathrm{d}R_s. \tag{3.22}$$

For completeness, we also present the result for a cylindrical interface, that can be derived analogously, as

$$\ln\frac{\gamma_{\mathrm{cyl}}}{\gamma_\infty} = \int_\infty^{R_s} \frac{\frac{\delta}{R_s^2}\left(1+\frac{\delta}{2R_s}\right)}{1+\frac{\delta}{R_s}\left(1+\frac{\delta}{2R_s}\right)}\mathrm{d}R_s. \tag{3.23}$$

In both expressions, γ_∞ is the surface tension of a planar interface. So far, no additional statement about the curvature dependence of the surface tension has been made. Without profound knowledge of the Tolman length, eq. (3.22) is of no more use than eq. (3.10). Tolman assumed that δ is small and doesn't change significantly with the size of the droplet. By neglecting the terms $\frac{\delta}{R_s}$ and $\frac{\delta^2}{3R_s^2}$ in the brackets and treating δ as constant, the integral can be solved leading to

$$\frac{\gamma}{\gamma_\infty} = \frac{1}{1+\frac{2\delta}{R_s}} \tag{3.24}$$

what is now commonly referred to as Tolman's equation. Often, due to the approximations used in its derivation, the equation is instead given as a series in $\frac{1}{R_s}$ neglecting terms above the linear one, as

$$\frac{\gamma}{\gamma_\infty} = 1 - \frac{2\delta}{R_s} + \mathcal{O}\left(\left(\frac{1}{R_s}\right)^2\right). \tag{3.25}$$

While all subsequent studies suggest that the Tolman length δ is in fact small, Tolman's second assumption that δ does not depend on the size of the droplet, isn't supported by recent simulation results nor DFT predictions[13,19]. We use DFT to evaluate the Tolman length over a wide range of radii and from there reassess whether the integral form of Tolman's equation (3.22) can still be used for describing the curvature dependence of surface tension.

3.3 Density Functional Theory

In an open, isothermal and isochoric system, a stable equilibrium state is characterized by a minimum in the grand potential Ω with respect to all allowable variations. For an inhomogeneous system, with density profiles of all components $\boldsymbol{\rho}(\mathbf{r})$ as internal degrees of freedom, this equilibrium condition results in vanishing functional derivatives of the grand potential, according to

$$\left(\frac{\delta\Omega}{\delta\rho_i(\mathbf{r})}\right)_{T,V,\boldsymbol{\mu}} = 0. \tag{3.26}$$

The grand potential can be expressed as a Legendre transform of the Helmholtz energy $F[\boldsymbol{\rho}(\mathbf{r})]$, as

$$\Omega = F[\boldsymbol{\rho}(\mathbf{r})] - \boldsymbol{\mu}\cdot\boldsymbol{N} = F[\boldsymbol{\rho}(\mathbf{r})] - \int \boldsymbol{\mu}\cdot\boldsymbol{\rho}(\mathbf{r})\,\mathrm{d}\mathbf{r}. \tag{3.27}$$

Using eq. (3.26), the density profile at equilibrium can thus be obtained by solving

$$\frac{\delta F[\boldsymbol{\rho}(\mathbf{r})]}{\delta\rho_i(\mathbf{r})} = \mu_i. \tag{3.28}$$

The Helmholtz energy functional can be split into an ideal gas contribution, which is known from statistical mechanics, and a residual part, that accounts for intermolecular potentials, as

$$F[\boldsymbol{\rho}(\mathbf{r})] = F^{\mathrm{ig}}[\boldsymbol{\rho}(\mathbf{r})] + F^{\mathrm{res}}[\boldsymbol{\rho}(\mathbf{r})] \tag{3.29}$$

with

$$\beta F^{\mathrm{ig}}[\boldsymbol{\rho}(\mathbf{r})] = \int \sum_i \rho_i(\mathbf{r})\left(\ln\left(\rho_i\Lambda_i^3\right) - 1\right)\mathrm{d}\mathbf{r} \tag{3.30}$$

where $\beta = \frac{1}{kT}$ is the inverse temperature. The thermal wavelength Λ_i contains density-independent intramolecular degrees of freedom. It is only a function of temperature and

therefore has no influence on the equilibrium density profile. For the residual contribution $F^{\text{res}}[\boldsymbol{\rho}(\mathbf{r})]$ we use functionals based on the PC-SAFT equation of state[28,32]. Therefore, the Helmholtz energy functional is split into contributions of specific interactions, as

$$F^{\text{res}}[\boldsymbol{\rho}(\mathbf{r})] = F^{\text{hs}}[\boldsymbol{\rho}(\mathbf{r})] + F^{\text{disp}}[\boldsymbol{\rho}(\mathbf{r})] + F^{\text{chain}}[\boldsymbol{\rho}(\mathbf{r})]. \tag{3.31}$$

In our case we are interested in modeling non-polar but non-spherical molecules, so the three contributions to the residual Helmholtz energy are hard-spheres (hs), dispersive attraction (disp) and chain formation (chain). The pure component parameters of the PC-SAFT model characterizing substance i, are the segment size parameter σ_{ii}, the depth of the potential well ε_{ii}, and the number of spherical segments per molecule m_i.

Hard-sphere contribution

Fundamental Measure Theory (FMT) goes back to Rosenfeld[35] and provides a description of inhomogeneous hard-sphere mixtures. In FMT the Helmholtz energy

$$\beta F^{\text{hs}}[\boldsymbol{\rho}(\mathbf{r})] = \int \Phi(\{n_\alpha\})\,\mathrm{d}\mathbf{r} \tag{3.32}$$

is given as the integral over a reduced Helmholtz energy density $\Phi(\{n_\alpha\})$, that is a function of the weighted densities n_α. The weighted densities are obtained by convolving the density profile with a weight function ω_α^i, as

$$n_\alpha = \sum_i m_i \int \rho_i(\mathbf{r}')\omega_\alpha^i(\mathbf{r}-\mathbf{r}')\,\mathrm{d}\mathbf{r}'. \tag{3.33}$$

Here the segment length m_i is included to extend the theory, originally derived for spherical fluids, to homosegmented chains. The original FMT by Rosenfeld[35] uses four scalar weight functions $\omega_3^i(\mathbf{r}) = \Theta(d_i/2-|\mathbf{r}|)$, $\omega_2^i(\mathbf{r}) = \delta(d_i/2-|\mathbf{r}|)$, $\omega_1^i(\mathbf{r}) = \omega_2^i(\mathbf{r})/2\pi d_i$ and $\omega_0^i(\mathbf{r}) = \omega_2^i(\mathbf{r})/\pi d_i^2$, as well as two vector weight functions $\vec{\omega}_2^i(\mathbf{r}) = \frac{\mathbf{r}}{|\mathbf{r}|}\delta(d_i/2-|\mathbf{r}|)$ and $\vec{\omega}_1^i(\mathbf{r}) = \vec{\omega}_2^i(\mathbf{r})/2\pi d_i$. The temperature-dependent effective hard-sphere diameter d_i accounts for the steep but non-infinite repulsion of van der Waals intermolecular potentials[28]. The weight functions ω_α^i thus limit the range of the integrals in eq. (3.33) to rather short range. For a homogeneous fluid the original FMT functional simplifies to the Percus-Yevick compressibility equation of state[36], which is known to overestimate the pressure of hard-sphere systems at higher densities. To alleviate this problem, Roth et al.[37] and Yu and Wu[38] independently derived a modified version of FMT that simplifies to the more accurate MCSL[39] equation of state, consistent with the hard-sphere term used in PC-SAFT[28]. The functional form of the reduced

Helmholtz energy density in this version is

$$\Phi = -n_0 \ln(1-n_3) + \frac{n_1 n_2 - \vec{n}_1 \cdot \vec{n}_2}{1-n_3} + (n_2^3 - 3n_2 \vec{n}_2 \cdot \vec{n}_2) \frac{n_3 + (1-n_3)^2 \ln(1-n_3)}{36\pi n_3^2 (1-n_3)^2}. \tag{3.34}$$

To calculate the hard-sphere contribution to the functional derivative of the Helmholtz energy, the partial derivatives (see ref.[29]) are convolved with their respective weight function

$$\frac{\delta \beta F^{\mathrm{hs}}}{\delta \rho_i(\mathbf{r})} = m_i \sum_{\alpha=0}^{3} \int \frac{\partial \Phi}{\partial n_\alpha}(\mathbf{r}') \omega_\alpha^i(\mathbf{r}-\mathbf{r}')\,\mathrm{d}\mathbf{r}' - m_i \sum_{\alpha=1}^{2} \int \frac{\partial \Phi}{\partial \vec{n}_\alpha}(\mathbf{r}') \cdot \vec{\omega}_\alpha^i(\mathbf{r}-\mathbf{r}')\,\mathrm{d}\mathbf{r}'. \tag{3.35}$$

The negative sign in front of the partial derivatives with respect to the vector weighted densities arises from the odd parity of the vector weight functions[40].

Chain contribution

A functional for chain formation in the framework of SAFT equations of state was developed by Tripathi and Chapman[41,42]. It is based on Wertheim's first order perturbation theory and reads

$$\begin{aligned}\beta F^{\mathrm{chain}}[\boldsymbol{\rho}(\mathbf{r})] = \sum_i (m_i - 1) \int \rho_i(\mathbf{r}) \left(\ln\left(\rho_i \Lambda_i^3\right) - 1\right) \mathrm{d}\mathbf{r} \\ - \sum_i (m_i - 1) \int \rho_i(\mathbf{r}) \left(\ln\left(y_{ii}^{dd}(\{\bar{\rho}_k\}) \lambda_i(\mathbf{r})\right) - 1\right) \mathrm{d}\mathbf{r}.\end{aligned} \tag{3.36}$$

The perturbation theory of Wertheim uses an ideal gas fluid of unconnected spherical segments as reference. This form of the chain term is rewritten such that it can be combined with the ideal gas term for molecules, according to eq. (3.30). The first part of eq. (3.36) thus describes an ideal gas, where each component is split into its m_i segments. The second term then adds the Helmholtz energy contribution of chain formation for each of the $m_i - 1$ bonds on the component. The cavity correlation function at contact $y_{ii}^{dd}(\bar{\boldsymbol{\rho}})$ is approximated by the bulk radial distribution function evaluated for weighted densities $\bar{\boldsymbol{\rho}}$[41,43]. The BMCSL theory results in

$$y_{ii}^{dd}(\bar{\boldsymbol{\rho}}) = \frac{1}{1-\zeta_3} + \frac{1.5 d_i \zeta_2}{(1-\zeta_3)^2} + \frac{0.5 (d_i \zeta_2)^2}{(1-\zeta_3)^3} \tag{3.37}$$

with the mixture segment densities

$$\zeta_n = \frac{\pi}{6} \sum_i \bar{\rho}_i m_i d_i^n, \quad n = 2, 3. \tag{3.38}$$

As weighted densities $\bar{\boldsymbol{\rho}}$, the average density in the interpenetration volume of two segments is used. Similar to the weighted densities in FMT the weighted density of component i can be written as a convolution integral

$$\bar{\rho}_i(\mathbf{r}) = \int \rho_i(\mathbf{r}')\omega^i_{\text{chain}}(\mathbf{r}-\mathbf{r}')\,\mathrm{d}\mathbf{r}' \tag{3.39}$$

with the weight function $\omega^i_{\text{chain}}(\mathbf{r}) = \frac{3}{4\pi d_i^3}\Theta(d_i - |\mathbf{r}|)$. In eq. (3.36), the cavity correlation function y^{dd}_{ii} is weighted with the contact density λ_i, that is defined, similarly to $\bar{\rho}_i$, as the average density in a spherical surface

$$\lambda_i(\mathbf{r}) = \int \rho_i(\mathbf{r}')\omega^i_{\text{contact}}(\mathbf{r}-\mathbf{r}')\,\mathrm{d}\mathbf{r}' \tag{3.40}$$

with $\omega^i_{\text{contact}}(\mathbf{r}) = \frac{1}{4\pi d_i^2}\delta(d_i - |\mathbf{r}|)$. The chain contribution to the functional derivative of the Helmholtz energy is[30]

$$\begin{aligned}\frac{\delta\beta F^{\text{chain}}}{\delta\rho_i(\mathbf{r})} = (m_i-1)\left(\ln\left(\frac{\rho_i(\mathbf{r})}{y^{dd}_{ii}(\mathbf{r})\lambda_i(\mathbf{r})}\right) + 1 - \int \frac{\rho_i(\mathbf{r}')}{\lambda_i(\mathbf{r}')}\omega^i_{\text{contact}}(\mathbf{r}-\mathbf{r}')\,\mathrm{d}\mathbf{r}'\right) \\ - \int\left(\sum_j (m_j-1)\rho_j(\mathbf{r}')\frac{\partial \ln(y^{dd}_{jj})}{\partial\bar{\rho}_i}(\mathbf{r}')\right)\omega^i_{\text{chain}}(\mathbf{r}-\mathbf{r}')\,\mathrm{d}\mathbf{r}'.\end{aligned} \tag{3.41}$$

Dispersive attraction

Recently Sauer and Gross[32] proposed a functional for dispersive attraction based on the PC-SAFT equation of state, with equivalent quantitative results compared to earlier models[29,30], but with significantly lower computational cost. It is based on the weighted density approximation similar to the ones used in FMT or the chain term. The Helmholtz energy functional is

$$\beta F^{\text{disp}}[\boldsymbol{\rho}(\mathbf{r})] = \int \hat{\rho}(\mathbf{r})\tilde{a}^{\text{disp}}(\hat{\boldsymbol{\rho}})\,\mathrm{d}\mathbf{r} \tag{3.42}$$

with the weighted density

$$\hat{\rho}(\mathbf{r}) = \sum_i \hat{\rho}_i(\mathbf{r}) = \sum_i \int \rho_i(\mathbf{r}')\omega^i_{\text{disp}}(\mathbf{r}-\mathbf{r}')\,\mathrm{d}\mathbf{r}' \tag{3.43}$$

and $\omega^i_{\text{disp}}(\mathbf{r}) = \frac{\Theta(\psi d_i - |\mathbf{r}|)}{\frac{4}{3}\pi(\psi d_i)^3}$. The functional derivative of the Helmholtz energy contribution simplifies to a convolution of the chemical potential, as

$$\frac{\delta \beta F^{\text{disp}}}{\delta \rho_i(\mathbf{r})} = \int \beta \mu_i^{\text{disp}}(\mathbf{r}') \omega^i_{\text{disp}}(\mathbf{r} - \mathbf{r}') \, \mathrm{d}\mathbf{r}'. \tag{3.44}$$

For detailed expressions of the reduced Helmholtz energy $\tilde{a}^{\text{disp}}$ and the chemical potential μ_i^{disp} of the PC-SAFT model, we refer to the primary literature[28].

3.4 Implementation

A stability analysis of a nanoscopic droplet reveals, that while being in equilibrium according to eq. (3.26), the droplet is not stable in an open system. Instead, it appears as a maximum or a saddle point on a free energy surface[44–46]. The stable equilbrium state, that the system would move towards should be a homogeneous liquid phase. To obtain a stable solution, the density profiles of droplets are solved in a canonical ensemble[2,47]. For mixtures, we also prefer to specify the total number of molecules N in the system, because N is a good measure for the size of the droplet and we derived Tolman's equation for mixtures by introducing a path along which the differences in chemical potentials $\Delta\mu_i = \mu_i - \mu_n$ are fixed. To find the appropriate thermodynamic potential, the total differential of the grand potential is rewritten as

$$\mathrm{d}\Omega = -S \, \mathrm{d}T - p \, \mathrm{d}V - \boldsymbol{N} \cdot \mathrm{d}\boldsymbol{\mu} + \sum_{i=1}^{n} N_i \, \mathrm{d}\mu_n - N \, \mathrm{d}\mu_n \tag{3.45}$$

$$= -S \, \mathrm{d}T - p \, \mathrm{d}V - \boldsymbol{N} \cdot \mathrm{d}(\underbrace{\boldsymbol{\mu} - \mu_n}_{\equiv \Delta\boldsymbol{\mu}}) - N \, \mathrm{d}\mu_n \tag{3.46}$$

and a Legendre transform

$$\Omega^*(T, V, N, \Delta\boldsymbol{\mu}) = \Omega + \mu_n N = F - \Delta\boldsymbol{\mu} \cdot \boldsymbol{N} \tag{3.47}$$

on the variable μ_n is applied. The equilibrium condition in this semi grand potential is

$$\left. \frac{\delta \Omega^*}{\delta \rho_i} \right|_{T,V,N,\Delta\boldsymbol{\mu}} = 0 \quad \text{s.t.} \quad N = \sum_i \int \rho_i \, \mathrm{d}\mathbf{r}. \tag{3.48}$$

This condition leads to a set of equations that can be solved to determine the density profiles $\boldsymbol{\rho}(\mathbf{r})$ of all species in the mixture, as

$$\beta\mu_i = \ln\left(N e^{\beta\Delta\mu_i} \left(\sum_i e^{\beta\Delta\mu_i} \int e^{-\frac{\delta\beta F^{\mathrm{res}}}{\delta\rho_i}} d\mathbf{r} \right)^{-1} \right) \tag{3.49}$$

and

$$\rho_i = e^{\beta\mu_i - \frac{\delta\beta F^{\mathrm{res}}}{\delta\rho_i}}. \tag{3.50}$$

These equations use N and $\Delta\mu_i$ as input parameters. To be able to specify the equimolar radius R_e, instead of the molecule number, the total liquid and vapor densities $\rho^L(T,\boldsymbol{\mu})$ and $\rho^V(T,\boldsymbol{\mu})$ are calculated in every iteration from the corresponding bulk equation of state. Then from eq. (3.5) the total number of molecules is available via

$$N = \left(\rho^L - \rho^V\right)\frac{4}{3}\pi R_e^3 + \rho^V V. \tag{3.51}$$

The equations are solved using an Anderson-mixing scheme[48,49]. The convolution integrals appearing in non-local Helmholtz energy functionals are solved using the Fourier transform. The 3D Fourier transform can be simplified to a sine transform (see section 3.B.1) allowing for an efficient and robust solution procedure. In this work we target a wide range of droplet sizes. For rather large droplets the center of the droplet reaches flat (bulk-like) density profiles. We then solve the DFT only in the range $R_e - \frac{L}{2} \leq r \leq R_e + \frac{L}{2}$. The liquid in the interior of the droplet is well described by a bulk liquid at the defined temperature and chemical potentials. This approach increases the numerical efficiency and allows to calculate arbitrarily large droplets. For the convolution integrals we make use of the projection-slice theorem as described in section 3.B.2.

3.5 Results and discussion

3.5.1 Pure fluids

We start with studying the Tolman length of a fluid consisting of spherical particles ($m_i = 1$). The PC-SAFT model is not exactly a model for Lennard-Jones fluids, but approximates the properties of Lennard-Jones fluids rather well[32]. We use the same dimensionless variables, that are commonly used in the study of Lennard-Jones systems $r^* = r/\sigma_{ii}$, $T^* = kT/\varepsilon_{ii}$, $\gamma^* = \gamma\sigma_{ii}^2/\varepsilon_{ii}$ and $\delta^* = \delta/\sigma_{ii}$.

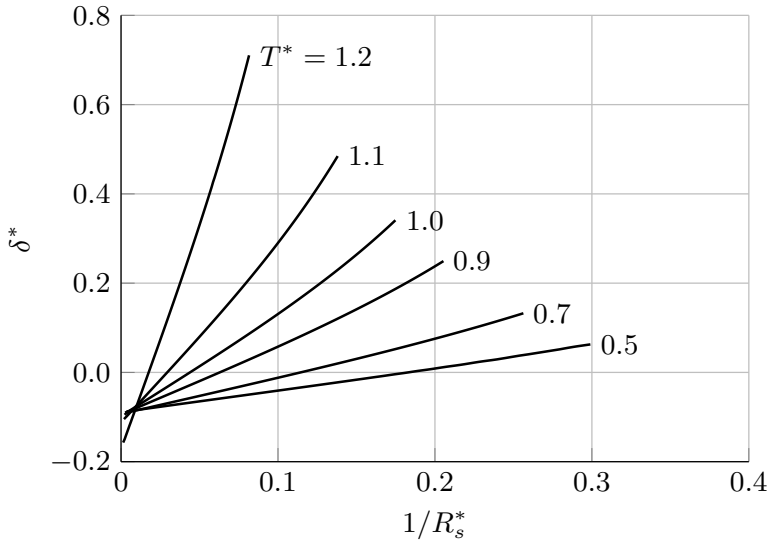

Figure 3.1: The radius dependent dimensionless Tolman length δ^* as a function of the inverse radius $1/R_s^*$ for different temperatures ($m = 1$).

After calculating the density profile according to section 3.4, the surface tension and Tolman length are directly available from eqs. (3.10) and (3.11). Figure 3.1 shows the Tolman length δ^* as a function of the inverse radius of surface of tension $1/R_s^*$. Different temperatures are considered, ranging from the temperature at the triple point $T_{Tr}^* \approx 0.48$ to close to the critical temperature $T_c^* \approx 1.28$.

For all temperatures, the Tolman length increases significantly with the curvature of the droplet. The curve can be described as almost linear with a slightly positive curvature for very small droplets. These findings are similar to the results from van der Waals capillarity theory obtained by Baidakov and Boltachev[50]. The slope of the curves depends strongly on temperature, whereas the limit for infinitely large drops is fairly constant at $\lim_{R_s\to\infty} \delta^*(R_s) \approx -0.1$. The results show, that Tolman's approximation of a constant δ is not applicable. Using the ansatz $\delta(R_s) = \delta_0 + \frac{\delta_1}{R_s}$ instead of a constant δ in eq. (3.22) leads to an extended version of the Tolman equation. In section 3.A we present an exact solution to the integral (eq. (3.A.8)) as well as a series approximation (eq. (3.A.11)) thereof.

Calculating the Tolman length is usually motivated by the question how the surface tension is curvature dependent. In figure 3.2 we therefore analyze the DFT results at one specific temperature and compare the results with other model predictions. The parameters δ_0 and δ_1 are obtained by adjusting eq. (3.A.8) to the DFT results. Let's go from left to right in figure 3.2. The diagram shows that beyond a certain curvature, the second order term in the expansion of the surface tension becomes dominant. The surface tension no longer increases, as is predicted by the common version of Tolman's equations, but it even decreases for small

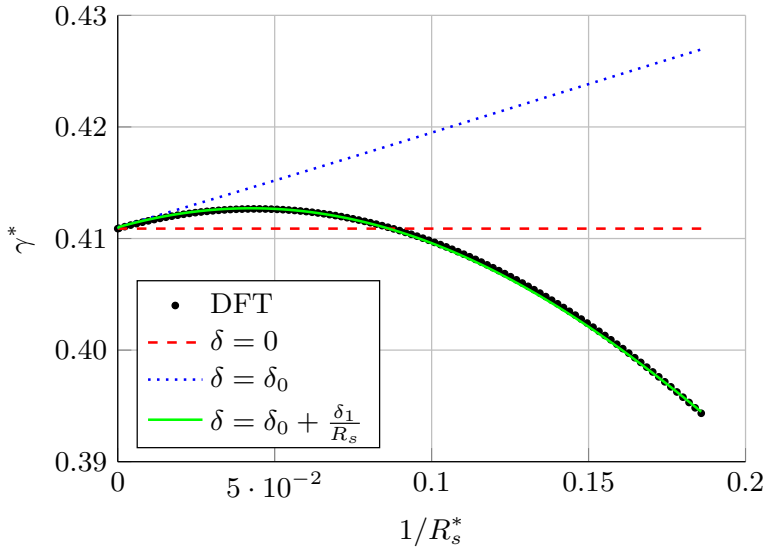

Figure 3.2: The dimensionless surface tension γ^* as a function of the inverse radius $1/R_s^*$ ($T^* = 1$, $m = 1$). Comparison between DFT results and different models. $\delta = 0$: no curvature dependence, $\delta = \delta_0$: Tolman equation (3.24), $\delta = \delta_0 + \frac{\delta_1}{R_s}$: extended Tolman equation (3.A.8).

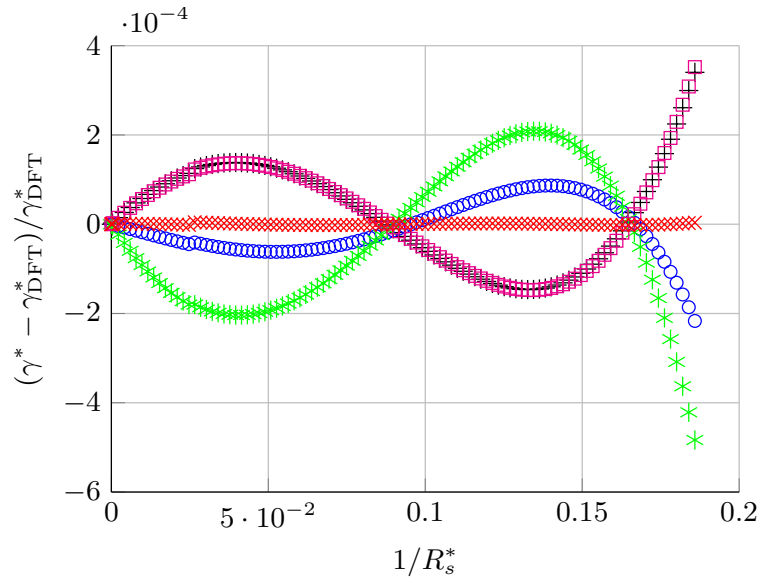

Figure 3.3: The relative error between different models for the curvature dependence of surface tension and DFT results ($T^* = 1$, $m = 1$). Full extended Tolman equation (3.A.8) (black pluses), series approximation (3.A.11) truncated after second (blue circles), third (green stars) and fourth (magenta boxes) order term, generic fourth order polynomial with four parameters (red crosses).

droplets. This course of $\delta(R_s)$ is the reason why early simulation studies seemed contradictory to the theory, showing a monotonous decrease in surface tension instead of the increase that was expected at the time.

In figure 3.2 we used the full analytical solution of the Tolman integral. This equation requires the roots of a sixth order polynomial and is cumbersome in use. In figure 3.3 the relative errors between various simplifications to this expression and DFT calculations are compared. There are no detectable improvements gained by keeping terms above the quadratic in the series expansion. A way to reduce the error drastically, is to use a fourth order polynomial with four instead of two parameters. However, the low relative error of less than 0.05% of all variants using two parameters does not justify the introduction of two additional parameters. We therefore propose the series expansion truncated after the quadratic term as a simple and surprisingly accurate model, as

$$\frac{\gamma}{\gamma_\infty} = 1 - \frac{2\delta_0}{R_s} + \frac{3\delta_0^2 - \delta_1}{R_s^2}. \tag{3.52}$$

This expression has a structure closely related to the curvature expansion of Helfrich[22] written for spherical surfaces

$$\gamma = \gamma_\infty - \frac{2\delta_0\gamma_\infty}{R_s} + \frac{2k + \tilde{k}}{R_s^2} + \mathcal{O}\left(\left(\frac{1}{R_s}\right)^3\right) \tag{3.53}$$

with the bending rigidity k and the rigidity constant associated with Gaussian curvature $\tilde{k}$. The work of Helfrich provides some physical interpretation to our parameter δ_1. Comparing eq. (3.52) to eq. (3.53), we obtain the parameter $\hat{k} = \gamma_\infty(3\delta_0^2 - \delta_1) = 2k + \tilde{k}$ allowing us to compare the results with previous work of Blokhuis and van Giessen[6,8,24] and of Wilhelmsen et al.[25] who used curvature expansion to directly calculate the Tolman length and rigidity constants of Lennard-Jones fluids. Instead of directly calculating these properties we have to estimate them by calculating the surface tension for different drop sizes and adjusting eq. (3.52) to the results. The Tolman length and rigidity constant for a Lennard-Jones like fluid are compared in figure 3.4. The assessment made in figure 3.4 requires awareness of the fact that, first, the PC-SAFT equation of state gives rather good results for non-truncated LJ fluids[28], but is not specifically a model for heterogeneous LJ fluids. Secondly, data of Wilhelmsen et al.[25] and Blokhuis and van Giessen[24] are for LJ fluids with shifted and truncated potentials. With these remarks, we consider our predictions in rather good agreement to the results of the previous studies.

The Helmholtz energy functionals for the PC-SAFT model allow to extend the study to non-spherical molecules. Following the same concepts used for Lennard-Jones like fluids, we calculate the Tolman length and the rigidity constant for various alkanes. The results are shown in figure 3.5. The qualitative behavior of the rigidity constant is similar for all chain

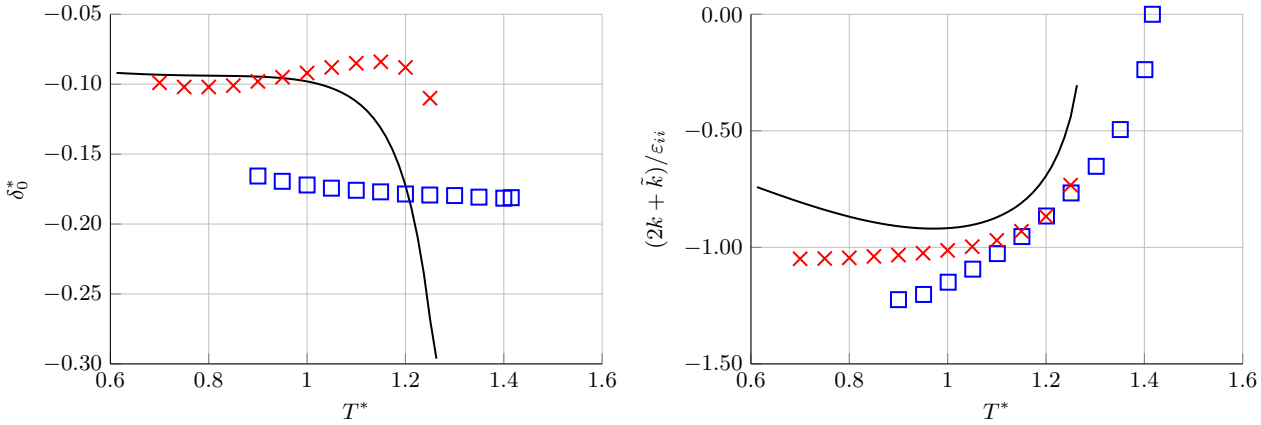

Figure 3.4: Tolman length and rigidity constant of a Lennard-Jones like fluid ($m = 1$) as a function of reduced temperature. Comparison between DFT results (line) and literature: Wilhelmsen et al.[25] (red crosses) and Blokhuis and van Giessen[24] (blue boxes).

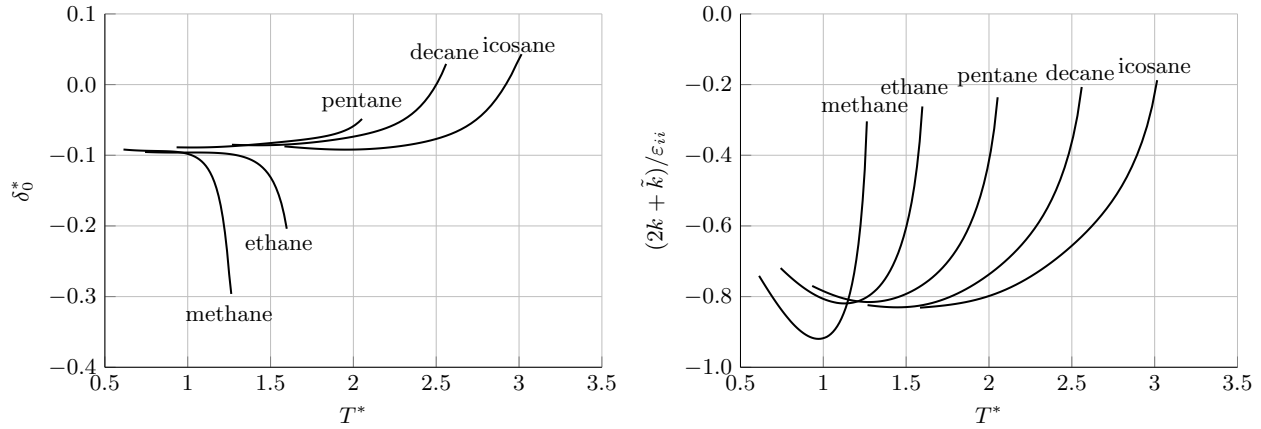

Figure 3.5: Tolman length and rigidity constant as a function of temperature for different alkanes.

lengths with a small decrease followed by an increase towards zero for temperatures close to the critical temperature. The infinite-radius Tolman length δ_0 on the other hand changes its behavior. For small molecules, it decreases close to the critical point, whereas for longer chains it increases. For lower temperatures, the Tolman length δ_0 is almost independent of chain length at a value of about −0.1 times a segment size parameter, which corresponds to a value of about −0.38 Å.

3.5.2 Mixtures

The concept of dimensionless variables becomes difficult to maintain for mixtures due to the number of parameters involved. We proceed with non-dimensionless quantities. The parameters are obtained by fitting the same model used for pure components to results for the

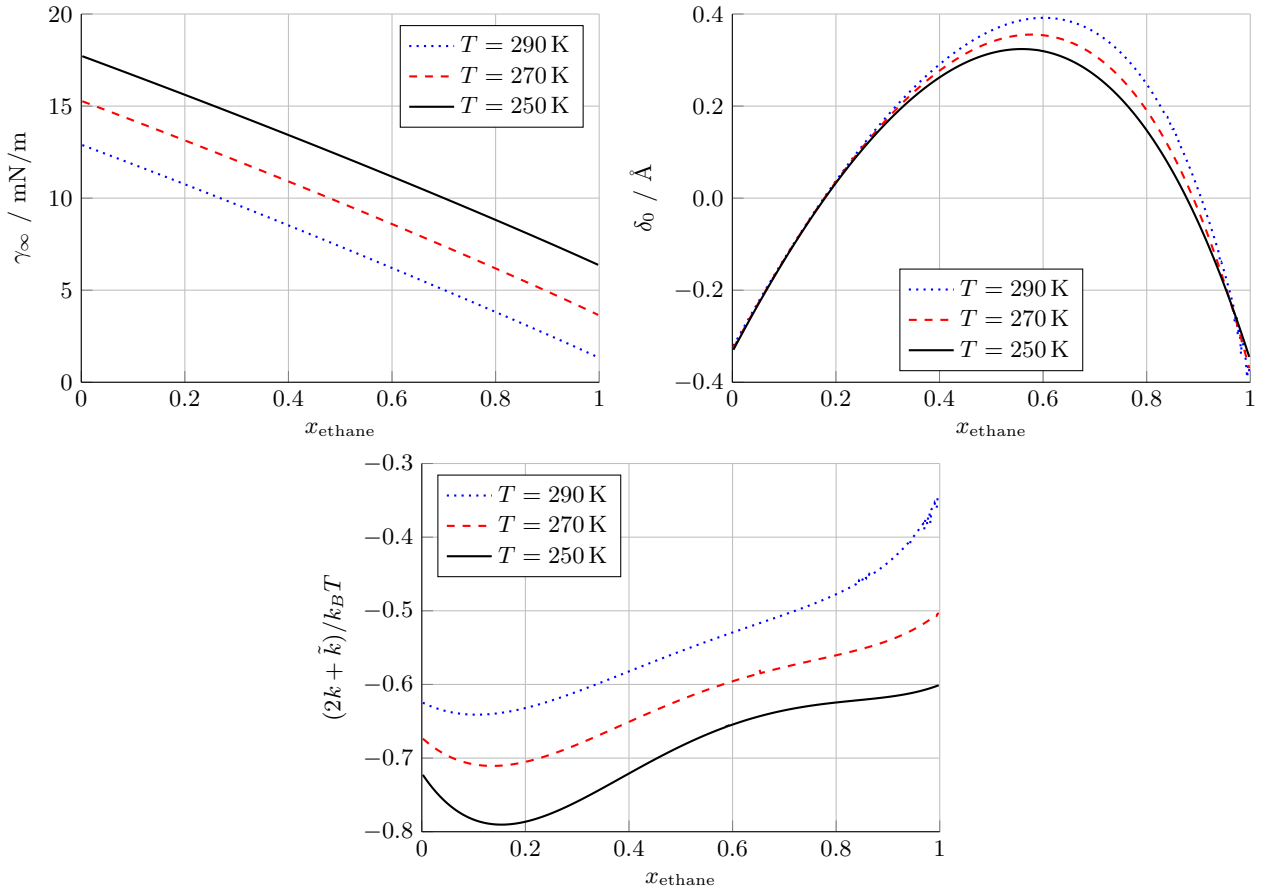

Figure 3.6: Surface tension of the planar interface, Tolman length and rigidity constant for a binary mixture of ethane and n-butane at different subcritical temperatures.

surface tension obtained from DFT along a line of constant $\Delta\mu_i$. Results for a binary mixture of ethane and butane for three different subcritical temperatures are shown in figure 3.6. As expected, the surface tension of a planar interface γ_∞ behaves almost ideally in this mixture. The Tolman length on the other hand has a peak close to the equimolar mixture in the liquid phase. The relative increase with respect to the value of the pure components is close to 200 % at this peak and the sign is positive on a large concentration interval. The positive sign of the Tolman length means, that for these concentrations, the surface tension drops monotonously with curvature, without an initial increase. A similar concentration dependence of the Tolman length was calculated in the framework of van der Waals gradient theory for an oxygen-nitrogen mixture by Baidakov and Anbaeva[51] and for a methane-nitrogen mixture by Baidakov and Khotienkova[52]. The rigidity constant shows a less non-ideal behavior and stays close to the values of the pure components. Our results suggest that a simple mixing rule based on pure substance values of the surface tension, can not be expected to be a successful approach to mixtures.

3.6 Conclusion

This study proposes a simple expansion for the Tolman length for calculating the curvature-dependence of the surface tension. We take Tolman's equation in integral form with the expansion $\delta = \delta_0 + \delta_1/R_s$ and subsequently expand the equation for the surface tension in curvature. A second order expansion is in excellent agreement with the DFT result and there is no substantial increase in quality obtained by including higher order terms. The model obtained is qualitatively identical to that of Helfrich[22,24,25] allowing to simply convert the model parameters.

We study the curvature dependence of a model fluid and of real pure substances, as well as mixtures using DFT based on the PC-SAFT equation of state. For a simple spherically symmetric model-fluid of Lennard-Jones type, we find a value for the Tolman length for infinite-radius droplets of about -0.1 times the molecular size parameter σ for low temperatures (which is in good agreement to previous studies[2]) and a steep decrease close to the critical point. The rigidity constant is negative and has a minimum close to a reduced temperature of $T^* = 1$. This leads to a non-monotonic surface tension with increasing curvature: With increasing curvature the surface tension first increases, reaches a maximum and decrease for high curvatures, i.e. for small droplets.

We regard n-alkanes from methane to icosane as non-spherical substances. For all alkanes, the infinite-radius Tolman length δ_0 has values of about -0.38Å for low temperatures. For more strongly non-spherical substances and for temperatures approaching the critical point, however, the values of δ_0 turn positive. The behavior of the rigidity parameter does not change qualitatively from methane to icosane.

Little work has previously been done for mixtures. We consider a binary mixture of mildly shape-asymmetric fluids. The binary mixture of ethane and n-butane shows strong non-linear behavior of the Tolman length with varying composition. For a range of composition, around an equimolar mixture, the Tolman length is substantially higher (and reaches a positive sign) compared to both pure substances. In that range of composition, the surface tension decreases monotonically with decreasing droplet size.

Appendix

3.A Derivation of the extended Tolman equation

Using the ansatz $\delta(R_s) = \delta_0 + \frac{\delta_1}{R_s}$ in eq. (3.22) simplifies to

$$\ln \frac{\gamma}{\gamma_\infty} = \int_\infty^{R_s} \left(\frac{1}{R_s} - \frac{R_s^5}{p(R_s)} \right) \mathrm{d}R_s \tag{3.A.1}$$

with the polynomial

$$p(R_s) = R_s^6 + 2\delta_0 R_s^5 + 2(\delta_0^2 + \delta_1) R_s^4 + \frac{2}{3}(\delta_0^3 + 6\delta_0\delta_1) R_s^3 + 2(\delta_0^2\delta_1 + \delta_1^2) R_s^2 + 2\delta_0\delta_1^2 R_s + \frac{2}{3}\delta_1^3 \tag{3.A.2}$$

in the denominator. This polynomial can be expressed using its complex roots R_i, as

$$p(R_s) = \prod_{i=1}^{6} (R_s - R_i) \quad \text{with} \quad p(R_i) = 0. \tag{3.A.3}$$

Next, we perform an expansion into partial fractions

$$\begin{aligned} \frac{R_s^5}{p(R_s)} &= \sum_{i=1}^{6} \frac{\kappa_i}{R_s - R_i} \\ \Rightarrow \quad R_s^5 &= \sum_{i=1}^{6} \kappa_i \prod_{j \neq i} (R_s - R_j). \end{aligned} \tag{3.A.4}$$

The coefficients κ_i are linked to the derivative of $p(R_s)$

$$\begin{aligned} p'(R_s) &= \sum_{i=1}^{6} \prod_{j \neq i} (R_s - R_j) \\ \Rightarrow \quad p'(R_i) &= \prod_{j \neq i} (R_i - R_j). \end{aligned} \tag{3.A.5}$$

Evaluating eq. (3.A.4) at the roots and using eq. (3.A.5) results in an expression for κ_i, as

$$\kappa_i = \frac{R_i^5}{p'(R_i)} \tag{3.A.6}$$

with

$$p'(R_i) = 6R_i^5 + 10\delta_0 R_i^4 + 8(\delta_0^2 + \delta_1)R_i^3 + 2(\delta_0^3 + 6\delta_0\delta_1)R_i^2 + 4(\delta_0^2\delta_1 + \delta_1^2)R_i + 2\delta_0\delta_1^2. \quad (3.A.7)$$

Using the expansion in partial fractions, the integral in eq. (3.A.1) can be evaluated, as

$$\ln\frac{\gamma}{\gamma_\infty} = \int_\infty^{R_s}\left(\frac{1}{R_s} - \sum_{i=1}^{6}\frac{\kappa_i}{R_s - R_i}\right)\mathrm{d}R_s \qquad \Rightarrow \qquad \gamma(R_s) = \frac{\gamma_\infty}{\prod_{i=1}^{6}(1-\frac{R_i}{R_s})^{\kappa_i}}. \quad (3.A.8)$$

Equation (3.A.8) is the exact solution of Tolman's integral equation assuming linear behavior of the Tolman length. However, the need to find the complex roots of a sixth order polynomial makes it unpractical to use. Instead we want to express the surface tension as a series expansion in $\frac{1}{R_s}$. We start with the expansion of the integral in eq. (3.A.1)

$$\ln\frac{\gamma}{\gamma_\infty} = -\frac{2\delta_0}{R_s} + \frac{\delta_0^2 - \delta_1}{R_s^2} - \frac{2\delta_0^3 - 12\delta_0\delta_1}{9R_s^3} - \frac{2\delta_0^4 + 3\delta_0^2\delta_1 - 3\delta_1^2}{6R_s^4} + \mathcal{O}\left(\left(\frac{1}{R_s}\right)^5\right) \quad (3.A.9)$$

and use this result in the series expansion of the exponential function

$$\frac{\gamma}{\gamma_\infty} = e^{\ln\frac{\gamma}{\gamma_\infty}} = \sum_{k=0}^{\infty}\frac{1}{k!}\left(\ln\frac{\gamma}{\gamma_\infty}\right)^k \quad (3.A.10)$$

to get to the solution

$$\frac{\gamma}{\gamma_\infty} = 1 - \frac{2\delta_0}{R_s} + \frac{3\delta_0^2 - \delta_1}{R_s^2} - \frac{32\delta_0^3 - 30\delta_0\delta_1}{9R_s^3} + \frac{59\delta_0^4 - 111\delta_0^2\delta_1 + 18\delta_1^2}{18R_s^4} + \mathcal{O}\left(\left(\frac{1}{R_s}\right)^5\right). \quad (3.A.11)$$

3.B DFT in Spherical Coordinates

In the framework of FMT and weighted density approximations, three kinds of convolution integrals have to be evaluated: The convolution of a scalar function f with a scalar weight function ω, as

$$f(\mathbf{r}) \otimes \omega(\mathbf{r}) = \int f(\mathbf{r}')\omega(\mathbf{r} - \mathbf{r}')\,\mathrm{d}\mathbf{r}', \quad (3.B.1)$$

the convolution of a scalar function f and a vector weight function $\vec{\omega}$, with

$$f(\mathbf{r}) \otimes \vec{\omega}(\mathbf{r}) = \int f(\mathbf{r}')\vec{\omega}(\mathbf{r} - \mathbf{r}')\,\mathrm{d}\mathbf{r}' \quad (3.B.2)$$

and the convolution of a vector function $\vec{f}$ and a vector weight function $\vec{\omega}$, as

$$\vec{f}(\mathbf{r}) \otimes \vec{\omega}(\mathbf{r}) = \int \vec{f}(\mathbf{r}') \cdot \vec{\omega}(\mathbf{r}-\mathbf{r}')\,\mathrm{d}\mathbf{r}'. \tag{3.B.3}$$

All of these convolution integrals can be solved efficiently using the convolution theorem of the Fourier transform

$$\int f(\mathbf{r}')\omega(\mathbf{r}-\mathbf{r})\,\mathrm{d}\mathbf{r}' = \mathscr{F}^{-1}(\mathscr{F}(f)\mathscr{F}(\omega)) \tag{3.B.4}$$

with the 3D Fourier transform $\mathscr{F}$ and its inverse, that are defined by

$$\mathscr{F}(f) = \int f(\mathbf{r}) e^{-2\pi i \mathbf{k}\cdot\mathbf{r}}\,\mathrm{d}\mathbf{r} \qquad \text{and} \qquad \mathscr{F}^{-1}(f) = \int f(\mathbf{k}) e^{2\pi i \mathbf{k}\cdot\mathbf{r}}\,\mathrm{d}\mathbf{k}. \tag{3.B.5}$$

The weight functions are generally spherically symmetric by nature and in case of a droplet all thermodynamic properties are also spherically symmetric. In this case $f(\mathbf{r}) = f(r)$ and $\vec{f}(\mathbf{r}) = f_r(r)\vec{e}_r$ with the unit vector in radial direction $\vec{e}_r$ and the calculation of the 3D Fourier transform and thus the convolution can be simplified.

3.B.1 Sine Transform

In the Fourier transform of a spherically symmetric function, the integration over the angles can be performed analytically and the transform simplifies based on the sine transform $\mathscr{S}(f)$, as

$$\mathscr{F}(f(r)) = \frac{2}{k_r}\int_{r=0}^{\infty} f(r) r \sin(2\pi k_r r)\,\mathrm{d}r = \frac{1}{k_r}\mathscr{S}(f(r)r). \tag{3.B.6}$$

The simplification of the inverse Fourier transform results in $\mathscr{F}^{-1}(f) = \frac{1}{r}\mathscr{S}^{-1}(f(k_r)k_r)$. With this result and the analytic Fourier transform of the weight function $\tilde{\omega}(k_r) = \mathscr{F}(\omega(r))$, the convolution can be written as

$$f(r) \otimes \omega(r) = \frac{1}{r}\mathscr{S}^{-1}\left(\mathscr{S}(f(r)r)\tilde{\omega}(k_r)\right). \tag{3.B.7}$$

The Fourier transform of a vector $\vec{f}(r) = f_r(r)\vec{e}_r$ results in a combination of sine and cosine transforms, with

$$\mathscr{F}(\vec{f}(r)) = \frac{i\vec{e}_{k_r}}{2\pi k_r^2}\left(2\pi k_r \mathscr{C}(f_r(r)r) - \mathscr{S}(f_r(r))\right) \tag{3.B.8}$$

and

$$\mathscr{F}^{-1}(\vec{f}(k_r)) = \frac{-i\vec{e}_r}{2\pi r^2}\left(2\pi r \mathscr{C}^{-1}(f_{k_r}(k_r)k_r) - \mathscr{S}^{-1}(f_{k_r}(k_r))\right). \tag{3.B.9}$$

To avoid the use of complex numbers in this context, the vector weight functions can be rewritten as $\vec{\omega}(r) = -\nabla\omega^*(r)$, the Fourier transform of which is $\tilde{\vec{\omega}}(k_r) = -2\pi i k_r \vec{e}_{k_r}\tilde{\omega}^*(k_r)$. Then, convolutions involving vector weight functions can also be simplified to

$$f(r) \otimes \vec{\omega}(r) = \vec{e}_r\left(\frac{1}{r^2}\mathscr{S}^{-1}(\mathscr{S}(f(r)r)\tilde{\omega}^*(k_r)) - \frac{1}{r}\mathscr{C}^{-1}(\mathscr{S}(f(r)r)2\pi k_r\tilde{\omega}^*(k_r))\right) \tag{3.B.10}$$

and

$$\vec{f}(r) \otimes \vec{\omega}(r) = \frac{1}{r}\mathscr{S}^{-1}\left(\mathscr{C}(f_r(r)r)2\pi k_r\tilde{\omega}^*(k_r) - \mathscr{S}(f_r(r))\tilde{\omega}^*(k_r)\right). \tag{3.B.11}$$

3.B.2 Projection on z-Axis

Roth[40] mentions that the convolution in spherical coordinates can be performed using a 1D Fourier transform. We want to generalize this concept and use it to calculate density profiles of spherical interfaces. With this method it is possible to use any interval on r as the system under observation. Thus, for larger droplets, only the density profile in the interfacial region of the droplet is calculated with DFT, while the interior of the drop is calculated using the corresponding bulk equation of state. This procedure allows to study arbitrarily large droplets.

The method is based on the projection-slice theorem which states, that a slice through a function in Fourier space is equal to the Fourier transform of a projection of the function in real space, as

$$\mathscr{F}(f)(k_x = 0, k_y = 0, k_z) = \mathscr{F}_z(\mathscr{P}(f))(k_z). \tag{3.B.12}$$

The projection of a spherically symmetric function $f(r)$ is

$$\mathscr{P}(f) = 2\pi\int_{|z|}^{\infty} f(r)r\,\mathrm{d}r \tag{3.B.13}$$

and for a vector function $\vec{f}(r) = f_r(r)\vec{e}_r$, it is

$$\mathscr{P}(\vec{f}) = 2\pi z \vec{e}_z \int_{|z|}^{\infty} f_r(r)\,\mathrm{d}r. \tag{3.B.14}$$

The respective inverse transforms of functions $F(z)$ and $\vec{F}(z) = F_z(z)\vec{e}_z$ are

$$\mathscr{P}^{-1}(F) = -\frac{1}{2\pi r}\left.\frac{\mathrm{d}F(z)}{\mathrm{d}z}\right|_{z=r} \quad \text{and} \quad \mathscr{P}^{-1}(\vec{F}) = -\frac{1}{2\pi}\left.\frac{\mathrm{d}\frac{F_z(z)}{z}}{\mathrm{d}z}\right|_{z=r}. \tag{3.B.15}$$

Using these transformations in conjunction with the convolution theorem (3.B.4) leads to the convolution, that Roth[40] mentions

$$f(r) \otimes \omega(r) = \frac{1}{r}\int f(|z'|)|z'|\mathscr{P}(\omega)(r - z')\,\mathrm{d}z' \tag{3.B.16}$$

and that can be expressed in Fourier space as

$$f(r) \otimes \omega(r) = \frac{1}{r}\mathscr{F}_z^{-1}(\mathscr{F}_z(f(|z|)z)\tilde{\omega}(|k_z|))|_{z=r}. \tag{3.B.17}$$

Using $\vec{\omega}(r) = -\nabla\omega^*(r)$ again leads to similar expressions involving vector weight functions, with

$$f(r) \otimes \vec{\omega}(r) = \vec{e}_r\left(\frac{1}{r^2}\mathscr{F}_z^{-1}(\mathscr{F}_z(f(|z|)z)\tilde{\omega}^*(|k_z|))|_{z=r} - \frac{1}{r}\mathscr{F}_z^{-1}(\mathscr{F}_z(f(|z|)z)2\pi i k_z\tilde{\omega}^*(|k_z|))|_{z=r}\right) \tag{3.B.18}$$

and

$$\vec{f}(r) \otimes \vec{\omega}(r) = -\frac{1}{r}\mathscr{F}_z^{-1}(\mathscr{F}_z(f_r(|z|)\mathrm{sign}(z))\tilde{\omega}^*(|k_z|) + \mathscr{F}_z(f_r(|z|)|z|)2\pi i k_z\tilde{\omega}^*(|k_z|))|_{z=r}. \tag{3.B.19}$$

References

[1] R. C. Tolman. The Effect of Droplet Size on Surface Tension. *The Journal of Chemical Physics*, **17**(3):333–337, 1949. doi:10.1063/1.1747247.

[2] A. Malijevský and G. Jackson. A perspective on the interfacial properties of nanoscopic liquid drops. *Journal of Physics: Condensed Matter*, **24**(46):464121, 2012. doi:10.1088/0953-

8984/24/46/464121.

[3] S. M. Thompson, K. E. Gubbins, J. P. R. B. Walton, R. A. R. Chantry, and J. S. Rowlinson. A molecular dynamics study of liquid drops. *The Journal of Chemical Physics*, **81**(1):530–542, 1984. doi:10.1063/1.447358.

[4] J. Vrabec, G. K. Kedia, G. Fuchs, and H. Hasse. Comprehensive study of the vapour-liquid coexistence of the truncated and shifted Lennard-Jones fluid including planar and spherical interface properties. *Molecular Physics*, **104**(9):1509–1527, 2006. doi:10.1080/00268970600556774.

[5] M. Horsch, H. Hasse, A. K. Shchekin, A. Agarwal, S. Eckelsbach, J. Vrabec, E. A. Müller, and G. Jackson. Excess equimolar radius of liquid drops. *Physical Review E*, **85**:031605, 2012. doi:10.1103/PhysRevE.85.031605.

[6] A. E. van Giessen and E. M. Blokhuis. Direct determination of the Tolman length from the bulk pressures of liquid drops via molecular dynamics simulations. *The Journal of Chemical Physics*, **131**(16):164705, 2009. doi:10.1063/1.3253685.

[7] A. Tröster, M. Oettel, B. Block, P. Virnau, and K. Binder. Numerical approaches to determine the interface tension of curved interfaces from free energy calculations. *The Journal of Chemical Physics*, **136**(6):064709, 2012. doi:10.1063/1.3685221.

[8] A. E. van Giessen and E. M. Blokhuis. Determination of curvature corrections to the surface tension of a liquid–vapor interface through molecular dynamics simulations. *The Journal of Chemical Physics*, **116**(1):302–310, 2002. doi:10.1063/1.1423617.

[9] J. G. Sampayo, A. Malijevský, E. A. Müller, E. de Miguel, and G. Jackson. Communications: Evidence for the role of fluctuations in the thermodynamics of nanoscale drops and the implications in computations of the surface tension. *The Journal of Chemical Physics*, **132**(14):141101, 2010. doi:10.1063/1.3376612.

[10] G. Kharlamov, A. Onischuk, S. Vosel, and P. Purtov. Molecular dynamics calculations of small drops surface tension. *Colloids and Surfaces A: Physicochemical and Engineering Aspects*, **379**(1-3):10 – 13, 2011. doi:10.1016/j.colsurfa.2010.12.002. 6th International Conference on Interfaces Against PollutionSelected papers from the International Conference.

[11] V. G. Baidakov and K. S. Bobrov. Spontaneous cavitation in a Lennard-Jones liquid at negative pressures. *The Journal of Chemical Physics*, **140**(18):184506, 2014. doi:10.1063/1.4874644.

[12] G. V. Lau, I. J. Ford, P. A. Hunt, E. A. Müller, and G. Jackson. Surface thermodynamics of planar, cylindrical, and spherical vapour-liquid interfaces of water. *The Journal of Chemical Physics*, **142**(11):114701, 2015. doi:10.1063/1.4913371.

[13] K. Koga, X. C. Zeng, and A. K. Shchekin. Validity of Tolman's equation: How large should a droplet be? *The Journal of Chemical Physics*, **109**(10):4063–4070, 1998. doi:10.1063/1.477006.

[14] T. V. Bykov and X. C. Zeng. Heterogeneous nucleation on mesoscopic wettable articles: A hybrid

thermodynamic/density-functional theory. *The Journal of Chemical Physics*, **117**(4):1851–1868, 2002. doi:10.1063/1.1485733.

[15] T. V. Bykov and X. C. Zeng. Homogeneous nucleation at high supersaturation and heterogeneous nucleation on microscopic wettable articles: A hybrid thermodynamic/density-functional theory. *The Journal of Chemical Physics*, **125**(14):144515, 2006. doi:10.1063/1.2357937.

[16] Z. Li and J. Wu. Toward a Quantitative Theory of Ultrasmall Liquid Droplets and Vapor–Liquid Nucleation. *Industrial & Engineering Chemistry Research*, **47**(15):4988–4995, 2007. doi:10.1021/ie070578i.

[17] D. S. Corti, K. J. Kerr, and K. Torabi. On the interfacial thermodynamics of nanoscale droplets and bubbles. *The Journal of Chemical Physics*, **135**(2):024701, 2011. doi:10.1063/1.3609274.

[18] S. Zong-Li and K. Yan-Shuang. Curvature Dependence of Interfacial Properties for Associating Lennard–Jones Fluids: A Density Functional Study. *Chinese Physics Letters*, **28**(2):026101, 2011. doi:10.1088/0256-307X/28/2/026101.

[19] J. Julin, I. Napari, J. Merikanto, and H. Vehkamäki. A thermodynamically consistent determination of surface tension of small Lennard-Jones clusters from simulation and theory. *The Journal of Chemical Physics*, **133**(4):044704, 2010. doi:10.1063/1.3456184.

[20] B. J. Block, S. K. Das, M. Oettel, P. Virnau, and K. Binder. Curvature dependence of surface free energy of liquid drops and bubbles: A simulation study. *The Journal of Chemical Physics*, **133**(15):154702, 2010. doi:10.1063/1.3493464.

[21] N. Bruot and F. Caupin. Curvature Dependence of the Liquid-Vapor Surface Tension beyond the Tolman Approximation. *Physical Review Letters*, **116**:056102, 2016. doi:10.1103/PhysRevLett.116.056102.

[22] W. Helfrich. Elastic Properties of Lipid Bilayers: Theory and Possible Experiments. *Zeitschrift für Naturforschung C*, **28**, 1973. doi:10.1515/znc-1973-11-1209.

[23] E. M. Blokhuis and D. Bedeaux. Van der Waals theory of curved surfaces. *Molecular Physics*, **80**(4):705–720, 1993. doi:10.1080/00268979300102581.

[24] E. M. Blokhuis and A. E. van Giessen. Density functional theory of a curved liquid-vapour interface: evaluation of the rigidity constants. *Journal of Physics: Condensed Matter*, **25**(22):225003, 2013. doi:10.1088/0953-8984/25/22/225003.

[25] Ø. Wilhelmsen, D. Bedeaux, and D. Reguera. Tolman length and rigidity constants of the Lennard-Jones fluid. *The Journal of Chemical Physics*, **142**(6):064706, 2015. doi:10.1063/1.4907588.

[26] Ø. Wilhelmsen, D. Bedeaux, and D. Reguera. Communication: Tolman length and rigidity constants of water and their role in nucleation. *The Journal of Chemical Physics*, **142**(17):171103, 2015. doi:10.1063/1.4919689.

[27] F. Sedlmeier and R. R. Netz. The spontaneous curvature of the water-hydrophobe interface. *The Journal of Chemical Physics*, **137**(13):135102, 2012. doi:10.1063/1.4755753.

[28] J. Gross and G. Sadowski. Perturbed-Chain SAFT: An Equation of State Based on a Perturbation Theory for Chain Molecules. *Industrial & Engineering Chemistry Research*, **40**(4):1244–1260, 2001. doi:10.1021/ie0003887.

[29] J. Gross. A density functional theory for vapor-liquid interfaces using the PCP-SAFT equation of state. *The Journal of Chemical Physics*, **131**(20):204705, 2009. doi:10.1063/1.3263124.

[30] C. Klink and J. Gross. A Density Functional Theory for Vapor-Liquid Interfaces of Mixtures Using the Perturbed-Chain Polar Statistical Associating Fluid Theory Equation of State. *Industrial & Engineering Chemistry Research*, **53**(14):6169–6178, 2014. doi:10.1021/ie4029895.

[31] C. Klink, B. Plankova, and J. Gross. Density Functional Theory for Liquid-Liquid Interfaces of Mixtures Using the Perturbed-Chain Polar Statistical Associating Fluid Theory Equation of State. *Industrial & Engineering Chemistry Research*, **54**(16):4633–4642, 2015. doi:10.1021/acs.iecr.5b00445.

[32] E. Sauer and J. Gross. Classical Density Functional Theory for Liquid–Fluid Interfaces and Confined Systems: A Functional for the Perturbed-Chain Polar Statistical Associating Fluid Theory Equation of State. *Industrial & Engineering Chemistry Research*, **56**(14):4119–4135, 2017. doi:10.1021/acs.iecr.6b04551.

[33] J. Gibbs. *The Collected Works of J. Willard Gibbs, Volume I: Thermodynamics*. Longmans, Green and Co., 1928.

[34] F. O. Koenig. On the Thermodynamic Relation between Surface Tension and Curvature. *The Journal of Chemical Physics*, **18**(4):449–459, 1950. doi:10.1063/1.1747660.

[35] Y. Rosenfeld. Free-energy model for the inhomogeneous hard-sphere fluid mixture and density-functional theory of freezing. *Physical Review Letters*, **63**:980–983, 1989. doi:10.1103/PhysRevLett.63.980.

[36] M. S. Wertheim. Analytic Solution of the Percus-Yevick Equation. *Journal of Mathematical Physics*, **5**(5):643–651, 1964. doi:10.1063/1.1704158.

[37] R. Roth, R. Evans, A. Lang, and G. Kahl. Fundamental measure theory for hard-sphere mixtures revisited: the White Bear version. *Journal of Physics: Condensed Matter*, **14**(46):12063, 2002. doi:10.1088/0953-8984/14/46/313.

[38] Y.-X. Yu and J. Wu. Structures of hard-sphere fluids from a modified fundamental-measure theory. *The Journal of Chemical Physics*, **117**(22):10156–10164, 2002. doi:10.1063/1.1520530.

[39] G. A. Mansoori, N. F. Carnahan, K. E. Starling, and T. W. Leland. Equilibrium Thermodynamic Properties of the Mixture of Hard Spheres. *The Journal of Chemical Physics*, **54**(4):1523–1525, 1971. doi:10.1063/1.1675048.

[40] R. Roth. Fundamental measure theory for hard-sphere mixtures: a review. *Journal of Physics: Condensed Matter*, **22**(6):063102, 2010. doi:10.1088/0953-8984/22/6/063102.

[41] S. Tripathi and W. G. Chapman. Microstructure of inhomogeneous polyatomic mixtures from a density functional formalism for atomic mixtures. *The Journal of Chemical Physics*, **122**(9):094506, 2005. doi:10.1063/1.1853371.

[42] S. Tripathi and W. G. Chapman. Microstructure and Thermodynamics of Inhomogeneous Polymer Blends and Solutions. *Physical Review Letters*, **94**:087801, 2005. doi:10.1103/PhysRevLett.94.087801.

[43] E. Kierlik and M. L. Rosinberg. A perturbation density functional theory for polyatomic fluids. II. Flexible molecules. *The Journal of Chemical Physics*, **99**(5):3950–3965, 1993. doi:10.1063/1.466142.

[44] A. J. Yang. The thermodynamical stability of the heterogeneous system with a spherical interface. *The Journal of Chemical Physics*, **82**(4):2082–2085, 1985. doi:10.1063/1.448344.

[45] D. W. Oxtoby and R. Evans. Nonclassical nucleation theory for the gas–liquid transition. *The Journal of Chemical Physics*, **89**(12):7521–7530, 1988. doi:10.1063/1.455285.

[46] Ø. Wilhelmsen, D. Bedeaux, S. Kjelstrup, and D. Reguera. Thermodynamic stability of nanosized multicomponent bubbles/droplets: The square gradient theory and the capillary approach. *The Journal of Chemical Physics*, **140**(2):024704, 2014. doi:10.1063/1.4860495.

[47] D. J. Lee, M. M. T. da Gama, and K. E. Gubbins. A microscopic theory for spherical interfaces: Liquid drops in the canonical ensemble. *The Journal of Chemical Physics*, **85**(1):490–499, 1986. doi:10.1063/1.451627.

[48] D. G. Anderson. Iterative Procedures for Nonlinear Integral Equations. *Journal of the ACM*, **12**(4):547–560, 1965. doi:10.1145/321296.321305.

[49] J. Mairhofer and J. Gross. Numerical aspects of classical density functional theory for one-dimensional vapor-liquid interfaces. *Fluid Phase Equilibria*, **444**:1–12, 2017. doi:http://doi.org/10.1016/j.fluid.2017.03.023.

[50] V. G. Baidakov and G. S. Boltachev. Curvature dependence of the surface tension of liquid and vapor nuclei. *Physical Review E*, **59**:469–475, 1999. doi:10.1103/PhysRevE.59.469.

[51] V. Baidakov and V. Andbaeva. The liquid–gas interface of oxygen–nitrogen solutions 2: Description in the Framework of the van der Waals gradient theory. *Fluid Phase Equilibria*, **286**(2):175 – 181, 2009. doi:https://doi.org/10.1016/j.fluid.2009.09.001.

[52] V. Baidakov and M. Khotienkova. Surface tension of methane–nitrogen solutions: 2. Description in the framework of the van der Waals gradient theory. *Fluid Phase Equilibria*, **425**:402 – 410, 2016. doi:https://doi.org/10.1016/j.fluid.2016.06.038.

4 Tolman lengths and rigidity constants from free-energy functionals – General expressions and comparison of theories

The content of this chapter is reproduced from

> *P. Rehner, A. Aasen, and Ø. Wilhelmsen. The Journal of Chemical Physics 151.24 (2019): 244710,*

with the permission of AIP Publishing. Additions or deletions compared to the published work are marked with angular brackets.

The leading order terms in a curvature expansion of the surface tension, the Tolman length (first order), and rigidities (second order) have been shown to play an important role in the description of nucleation processes. This work presents general and rigorous expressions to compute these quantities for any non-local density functional theory (DFT). The expressions hold for pure fluids and mixtures, and reduce to the known expressions from density gradient theory (DGT). The framework is applied to a Helmholtz energy functional based on the perturbed chain polar statistical associating fluid theory (PCP-SAFT) and is used for an extensive investigation of curvature corrections for pure fluids and mixtures. Predictions from the full DFT are compared to two simpler theories: predictive density gradient theory (pDGT), that has a density and temperature dependent influence matrix derived from DFT, and DGT, where the influence parameter reproduces the surface tension as predicted from DFT. All models are based on the same equation of state and predict similar Tolman lengths and spherical rigidities for small molecules, but the deviations between DFT and DGT increase with chain length for the alkanes. For all components except water, we find that DGT underpredicts the value of the Tolman length, but overpredicts the value of the spherical rigidity. An important basis for the calculation is an accurate prediction of the planar surface tension. Therefore, further work is required to accurately extract Tolman lengths and rigidities of alkanols, because DFT with PCP-SAFT does not accurately predict surface tensions of these fluids.

4.1 Introduction

The dependence of the surface tension on the interfacial curvature has been discussed intensely over the last decades. One of the motivations for studying the subject was the discrepancies between experiments and theoretical predictions for nucleation rates in condensation and evaporation[1,2]. In classical nucleation theory, the nucleation rate depends exponentially on the formation energy of the nano-sized critical cluster. Therefore, it has been hypothesized that omitting the curvature dependence of the surface tension is the cause of the large discrepancies between theory and experiments[2–5]. The curvature dependence of the surface tension also has implications for other important examples such as the properties of biomembranes[6], and wetting at the nanoscale[7].

The first quantitative description was proposed by Tolman[8]. By introducing the distance between the equimolar radius R_e and the radius of the surface of tension R_s, referred to as $\delta_T(R_s)$, he proposed the expression

$$\sigma(R_s) = \frac{\sigma_0}{1 + \frac{2\delta_T(R_s)}{R_s}}, \tag{4.1}$$

for the curvature dependent surface tension $\sigma(R_s)$ in relation to the surface tension of a planar interface σ_0. In eq. (4.1), the curvature dependent Tolman length, $\delta_T(R_s)$ is often replaced by the Tolman length of the planar interface δ. In later works[4,9–11] [see also chapter 3], it was shown that with this approximation, eq. (4.1) is incapable of representing the surface tension of small droplets. Instead, the second-order expression by Helfrich[6] has been established as the preferred model to capture the curvature dependence of the surface tension. For an arbitrarily curved interface, it reads

$$\sigma(J,K) = \sigma_0 - \delta\sigma_0 J + \frac{k}{2}J^2 + \bar{k}K + \ldots, \tag{4.2}$$

where δ is the the Tolman length, k is the bending rigidity and $\bar{k}$ is the Gaussian rigidity. The interface is characterized locally by the total curvature $J = 1/R_1 + 1/R_2$ and the Gaussian curvature $K = 1/(R_1R_2)$, with R_1 and R_2 being the two principal radii. The expansion truncated at second order is known as the Helfrich expansion, and the coefficients σ_0, δ, k and $\bar{k}$ are referred to as Helfrich coefficients. For spherical (index s) and cylindrical (index c) geometries, eq. (4.2) simplifies to

$$\sigma^s(R) = \sigma_0 - \frac{2\delta\sigma_0}{R} + \frac{2k + \bar{k}}{R^2} + \ldots \tag{4.3}$$

and

$$\sigma^c(R) = \sigma_0 - \frac{\delta\sigma_0}{R} + \frac{k}{2R^2} + \dots \tag{4.4}$$

where R is an arbitrarily chosen dividing surface. The Tolman length for the vapor–liquid interface has been the subject of many discussions and controversies, in particular its sign, since different routes to obtain it have yielded different results. Due to its simplicity, most works in the literature have considered the truncated and shifted Lennard–Jones (LJ) fluid. Theoretical calculations based on free-energy functionals of the density profile, such as density gradient theory (DGT) and non-local density functional theory (DFT), have consistently given zero or negative values[12–15]. However, positive values have been reported from Monte Carlo and molecular dynamics (MD) simulations that compute the Tolman length from the pressure tensor (see[16–18] and references therein). MD simulations by van Giessen and Blokhuis, and also by Block et al. have only recently resulted in negative Tolman lengths around −0.1 in units of the LJ diameter[14,19,20]. Curvature corrections for water have also been investigated intensely[4,7,21–25], also with conflicting results on the sign of the Tolman length. Still, DGT and DFT have been shown to agree *quantitatively* with the predictions of recent simulation studies for both the LJ fluid[9,19,26] and water[4,22–24], giving credibility to DFT and DGT as methodologies to calculate curvature corrections.

Free-energy functionals allow direct calculation of the curvature dependence of the surface tension. [As shown in chapter 3], the unknown coefficients in eqs. (4.3) and (4.4) can be estimated by fitting a second order polynomial of the surface tension as a function of the curvature, $1/R$. Since the surface tension of large droplets and bubbles is very similar to σ_0, coefficients computed in this manner have limited accuracy. A more accurate and rigorous route is to directly calculate the derivatives of the surface tension with respect to curvature from the free-energy functional[27]. This involves solving for the first-order curvature expansion of the density profiles. The methodology was first presented by Blokhuis and Bedeaux for pure fluids described by DGT[28], and later extended to mixtures described by DGT by Aasen et al[11]. Estimates of the Helfrich coefficients have also been computed from various other free-energy functionals[26,29,30]. Still, a robust method for calculating these coefficients rigorously from arbitrary free-energy functionals and a systematic comparison of the values derived from different functionals for a range of fluids is missing.

This work presents general expressions to compute the Tolman length and rigidity constants for arbitrary free-energy functionals, that hold for pure fluids and mixtures. These expressions are next applied to predict the Helfrich coefficients to state-of-the-art accuracy for a range of pure fluids and mixtures, using a non-local DFT based on the perturbed-chain polar statistical associating fluid theory (PCP-SAFT) equation of state. We present the first systematic

comparison of these coefficients to predictions from DGT and predictive density gradient theory (pDGT[, see chapter 5]). The comparison yields insight into the limits of using gradient theories for the description of curved interfaces. We will also shed light on the impact of the underlying equation of state in DGT and non-local DFT.

In section 4.2 we develop the general expressions for the Helfrich coefficients, valid for any free-energy functional. In sections 4.3.1 and 4.3.2, coefficients for a range of pure fluids and mixtures are compared. In section 4.4, we offer some concluding remarks.

4.2 Theory

In this section we first review the general model-independent relations appearing in the curvature expansion. Subsequently we present the new expressions for the Helfrich coefficients for non-local DFT and shed light on how to treat the density dependence of the influence parameter in predictive density gradient theory. In all expressions, we consider isothermal conditions and paths. Bold symbols denote vector properties with respect to the components in the system.

4.2.1 General relations for curvature expansion

The aim of a curvature expansion is to determine thermodynamic properties of a curved interface by Taylor expanding around the planar interface. Therefore, every property X that depends on the curvature is written as

$$X = X_0 + \frac{X_1}{R} + \frac{X_2}{R^2} + \ldots, \tag{4.5}$$

where the coefficients X_i do not depend on the curvature. To be able to describe an arbitrarily shaped interface using the Helfrich expansion, the curvature expansion has to be performed in spherical and cylindrical coordinates. In the following, we derive expressions that are valid for both geometries, captured by the geometry factor g, which is 0 for a planar interface, 1 for a cylindrical interface and 2 for a spherical interface. Before presenting model-specific expressions, we derive general relations between the different properties of curved interfaces.

Gibbs–Duhem equation

The bulk pressures in the liquid (L) and the vapor (V) phase are related to the chemical potential $\boldsymbol{\mu}$ and the density $\boldsymbol{\rho}$ of the system via the Gibbs-Duhem equation

$$\boldsymbol{\rho}^V \cdot \mathrm{d}\boldsymbol{\mu} = \mathrm{d}p^V \qquad \text{and} \qquad \boldsymbol{\rho}^L \cdot \mathrm{d}\boldsymbol{\mu} = \mathrm{d}p^L. \tag{4.6}$$

Thus, the pressure difference $\Delta p = p^L - p^V$ is linked to the difference in densities $\Delta\boldsymbol{\rho} = \boldsymbol{\rho}^L - \boldsymbol{\rho}^V$ via $\Delta\boldsymbol{\rho} \cdot \mathrm{d}\boldsymbol{\mu} = \mathrm{d}\Delta p$. Using eq. (4.5) for all properties leads to the expression

$$\left(\Delta\boldsymbol{\rho}_0 + \frac{\Delta\boldsymbol{\rho}_1}{R} + \dots\right) \cdot \left(\boldsymbol{\mu}_1 + \frac{2\boldsymbol{\mu}_2}{R} + \dots\right) \mathrm{d}\left(\frac{1}{R}\right) = \left(\Delta p_1 + \frac{2\Delta p_2}{R} + \dots\right) \mathrm{d}\left(\frac{1}{R}\right). \tag{4.7}$$

Collecting terms with the same power of R results in the relations

$$\Delta p_1 = \Delta\boldsymbol{\rho}_0 \cdot \boldsymbol{\mu}_1 \qquad \text{and} \qquad \Delta p_2 = \Delta\boldsymbol{\rho}_0 \cdot \boldsymbol{\mu}_2 + \frac{1}{2}\Delta\boldsymbol{\rho}_1 \cdot \boldsymbol{\mu}_1. \tag{4.8}$$

Adsorption

The adsorption, $\boldsymbol{\Gamma}$ refers to the amount of particles accumulated at the interface per surface area, and is defined as

$$\boldsymbol{\Gamma} = \int \boldsymbol{\rho}^E(r) \left(\frac{r}{R}\right)^g \mathrm{d}r, \tag{4.9}$$

where we introduce the excess density

$$\boldsymbol{\rho}^E(r) = \boldsymbol{\rho}(r) - \boldsymbol{\rho}^L \Theta(R - r) - \boldsymbol{\rho}^V \Theta(r - R), \tag{4.10}$$

with the Heaviside step function $\Theta(r)$. By changing the integration variable to $z = r - R$ and again collecting terms of the same order in curvature, the following expansion coefficients

$$\boldsymbol{\Gamma}_0 = \int \boldsymbol{\rho}_0^E(z)\,\mathrm{d}z \qquad \text{and} \qquad \boldsymbol{\Gamma}_1 = \int \left(\boldsymbol{\rho}_1^E(z) + gz\boldsymbol{\rho}_0^E(z)\right) \mathrm{d}z \tag{4.11}$$

are obtained.

Gibbs adsorption equation

The Gibbs adsorption equation

$$\mathrm{d}\sigma = -\boldsymbol{\Gamma} \cdot \mathrm{d}\boldsymbol{\mu} + \left[\frac{\partial \sigma}{\partial R}\right]_{T,\boldsymbol{\mu}} \mathrm{d}R \tag{4.12}$$

links the adsorption to the surface tension σ. As we have not yet made a choice of dividing surface, the notional derivative, $\left[\frac{\partial \sigma}{\partial R}\right]_{T,\boldsymbol{\mu}}$ appears in the equation. The notional derivative describes the change in surface tension due to a change in the dividing surface, while keeping the physical system unaltered. The notional derivative also enters the general form of the Young-Laplace equation, as

$$\Delta p = \frac{g\sigma}{R} + \left[\frac{\partial \sigma}{\partial R}\right]_{T,\boldsymbol{\mu}}. \tag{4.13}$$

Substituting the notional derivative from eq. (4.13) into eq. (4.12) and expanding the resulting expression gives a general relation between the coefficients of the pressure difference and the surface tension, as

$$\Delta p_0 = 0, \qquad \Delta p_1 = g\sigma_0 \qquad \text{and} \qquad \Delta p_2 = -\boldsymbol{\Gamma}_0 \cdot \boldsymbol{\mu}_1 + (g-1)\sigma_1. \tag{4.14}$$

Density profiles

The density profile of an open system is obtained as a stationary point of the grand potential functional Ω. Using a Legendre transform, the equilibrium condition can be formulated in terms of the functional derivative of the Helmholtz energy, F instead

$$\left.\frac{\delta \Omega}{\delta \boldsymbol{\rho}(\mathbf{r})}\right|_{T,V,\boldsymbol{\mu}} = 0 \quad \Leftrightarrow \quad \left.\frac{\delta F}{\delta \boldsymbol{\rho}(\mathbf{r})}\right|_{T,V} = \boldsymbol{\mu}. \tag{4.15}$$

A curvature expansion of eq. (4.15) gives

$$\boldsymbol{\mu}_0 = \left(\frac{\delta F}{\delta \boldsymbol{\rho}(\mathbf{r})}\right)_0 \qquad \text{and} \qquad \boldsymbol{\mu}_1 = \int \left(\frac{\delta^2 F}{\delta \boldsymbol{\rho}(\mathbf{r}) \delta \boldsymbol{\rho}(\mathbf{r}')}\right)_0 \boldsymbol{\rho}_1(\mathbf{r}')\, \mathrm{d}\mathbf{r}'. \tag{4.16}$$

The density profile of the planar interface and the first-order term in the curvature expansion of the density can be obtained by solving the above equations. It is not obvious from the general formulation how they should be solved. However, one important property can be

derived. For free-energy functionals F, the expression

$$\int \left(\frac{\delta^2 F}{\delta\boldsymbol{\rho}(\mathbf{r})\delta\boldsymbol{\rho}(\mathbf{r}')}\right)_0 \nabla\boldsymbol{\rho}_0(\mathbf{r}')\,\mathrm{d}\mathbf{r}' = \nabla\left(\frac{\delta F}{\delta\boldsymbol{\rho}(\mathbf{r})}\right)_0 = 0, \tag{4.17}$$

vanishes at equilibrium. It follows, that if $\boldsymbol{\rho}_1(\mathbf{r})$ is a solution of eq. (4.16), $\boldsymbol{\rho}_1(\mathbf{r}) + \varepsilon\nabla\boldsymbol{\rho}_0(\mathbf{r})$ is also a solution for any value of ε.

Surface tension

The surface tension is defined as the excess grand potential per surface area, $\sigma = \frac{\Omega^E}{A}$. Using the geometry factor g, it can be expressed as

$$\sigma = \int \left(f - \boldsymbol{\rho}\cdot\boldsymbol{\mu} + p^{LV}\right)\left(\frac{r}{R}\right)^g \mathrm{d}r \tag{4.18}$$

with the Helmholtz energy density, f and the pressure of the bulk phases, $p^{LV} = p^L\Theta(r-R) + p^V\Theta(R-r)$, which is related to the adsorption via the Gibbs-Duhem equation. After a few simplification steps and identifying the excess grand potential density of the planar interface, $\Delta\omega_0 = f_0 - \boldsymbol{\rho}_0\cdot\boldsymbol{\mu}_0 + p_0$, the resulting expressions for the coefficients are

$$\sigma_0 = \int \Delta\omega_0\,\mathrm{d}z \tag{4.19}$$

$$\sigma_1 = \int (f_1 - \boldsymbol{\rho}_1\cdot\boldsymbol{\mu}_0)\,\mathrm{d}z + g\int \Delta\omega_0 z\,\mathrm{d}z - \boldsymbol{\mu}_1\cdot\boldsymbol{\Gamma}_0 \tag{4.20}$$

$$\begin{aligned}\sigma_2 = \int \left(f_2 - \boldsymbol{\rho}_2\cdot\boldsymbol{\mu}_0 - \frac{1}{2}\boldsymbol{\rho}_1\cdot\boldsymbol{\mu}_1\right)\mathrm{d}z + g\int (f_1 - \boldsymbol{\rho}_1\cdot\boldsymbol{\mu}_0) z\,\mathrm{d}z + \frac{g(g-1)}{2}\int \Delta\omega_0 z^2\,\mathrm{d}z \\ - \frac{g}{2}\boldsymbol{\mu}_1\cdot\int \boldsymbol{\rho}_0^E z\,\mathrm{d}z - \boldsymbol{\mu}_2\cdot\boldsymbol{\Gamma}_0 - \frac{1}{2}\boldsymbol{\mu}_1\cdot\boldsymbol{\Gamma}_1\end{aligned} \tag{4.21}$$

It is tempting to neglect the first term in both the first and second order expressions for the surface tension as we find

$$\int (f_1 - \boldsymbol{\rho}_1\cdot\boldsymbol{\mu}_0)\,\mathrm{d}\mathbf{r} = \iint \left(\left(\frac{\delta f(\mathbf{r})}{\delta\boldsymbol{\rho}(\mathbf{r}')}\right)_0\cdot\boldsymbol{\rho}_1(\mathbf{r}') - \left(\frac{\delta f(\mathbf{r}')}{\delta\boldsymbol{\rho}(\mathbf{r})}\right)_0\cdot\boldsymbol{\rho}_1(\mathbf{r})\right)\mathrm{d}\mathbf{r}\,\mathrm{d}\mathbf{r}' \tag{4.22}$$

which is strictly zero. However, in eq. (4.20), the integration is over z. We have to take into account that the integration takes place in a curvilinear coordinate system, even if one is interested in the limit of zero curvature.

Path through the metastable region

Although the norms of the vectors $\boldsymbol{\mu}_1$ and $\boldsymbol{\mu}_2$ are fixed by eqs. (4.8) and (4.14), their directions represent degrees of freedom. Every point in the metastable region is defined by its temperature and chemical potentials. However, there is an infinite number of possible starting points on the phase envelope and paths towards the metastable point, which are each equipped with their own expansion coefficients. In a previous study[11], it was shown that a straight path (i.e. $\boldsymbol{\mu}_2 \propto \boldsymbol{\mu}_1$) where the composition of the liquid phase $\boldsymbol{x}^L$ is kept constant in the first order term gives low errors in the expansion. To obtain the coefficients of the chemical potential for this choice of path, the first order coefficient of the total liquid density is calculated as

$$\rho_1^L = \frac{g\sigma_0}{(\boldsymbol{x}^L)^T \left(\boldsymbol{\mu}_\rho^L\right)_0 \Delta\boldsymbol{\rho}_0}, \tag{4.23}$$

from which the chemical potential,

$$\boldsymbol{\mu}_1 = \rho_1^L \left(\boldsymbol{\mu}_\rho^L\right)_0 \boldsymbol{x}^L \tag{4.24}$$

and the vapor partial densities,

$$\boldsymbol{\rho}_1^V = \left(\boldsymbol{\mu}_\rho^V\right)_0^{-1} \boldsymbol{\mu}_1 \tag{4.25}$$

follow. The second order coefficient for the chemical potential can be derived from eqs. (4.8) and (4.14) as

$$\boldsymbol{\mu}_2 = \frac{(g-1)\sigma_1 - \left(\boldsymbol{\Gamma}_0 + \frac{1}{2}\Delta\boldsymbol{\rho}_1\right)\cdot\boldsymbol{\mu}_1}{g\sigma_0}\boldsymbol{\mu}_1. \tag{4.26}$$

Choice of dividing surface

The equations derived so far are valid for any choice of dividing surface. However, to be able to evaluate the expressions, a choice has to be made. The first option is the surface of tension R_s, for which the notional derivative of the surface tension vanishes. Thus, the usual form of the Young Laplace equation $\Delta p = \frac{g\sigma}{R_s}$ is valid and the Gibbs adsorption equation simplifies to

$$\sigma_1 = -\boldsymbol{\mu}_1 \cdot \boldsymbol{\Gamma}_0 \qquad \text{and} \qquad \sigma_2 = -\boldsymbol{\mu}_2 \cdot \boldsymbol{\Gamma}_0 - \frac{1}{2}\boldsymbol{\mu}_1 \cdot \boldsymbol{\Gamma}_1. \tag{4.27}$$

The second important option is the equimolar dividing surface or its generalization to multi-component mixtures, the Koenig surface[31] R_k, which is defined by $\mathbf{\Gamma} \cdot \mathrm{d}\boldsymbol{\mu} = 0$. As opposed to the surface of tension which is a state function, the Koenig surface is path dependent. For specific applications, one choice might be superior. However, it is important to keep in mind that neither the planar surface tension nor the Tolman length depend on the dividing surface and there are simple model-independent relations for the rigidity constants for different dividing surfaces[11].

In the density profile of the planar interface, the dividing surface is fixed by finding any density profile that solves the zeroth order Euler–Lagrange equation and then shifting the z-axis by the position of the Koenig surface z_{k0} or the surface of tension z_{s0}. The values for the two surfaces are given by

$$z_{k0} = \frac{\boldsymbol{\mu}_1 \cdot \mathbf{\Gamma}_0}{g\sigma_0} \qquad \text{and} \qquad z_{s0} = \frac{\sigma_1 + \boldsymbol{\mu}_1 \cdot \mathbf{\Gamma}_0}{g\sigma_0}. \tag{4.28}$$

From these relations, we obtain an expression for the Tolman length

$$z_{k0} - z_{s0} = \frac{-\sigma_1}{g\sigma_0} = \delta. \tag{4.29}$$

With a similar procedure, the correct solution of the first order Euler–Lagrange equation is found by first finding any solution $\tilde{\boldsymbol{\rho}}_1(z)$ and then obtaining the actual solution as $\boldsymbol{\rho}_1(z) = \tilde{\boldsymbol{\rho}}_1(z) + \varepsilon \boldsymbol{\rho}_0'(z)$ with

$$\varepsilon = \frac{2\boldsymbol{\mu}_2 \cdot \mathbf{\Gamma}_0 + \boldsymbol{\mu}_1 \cdot \tilde{\mathbf{\Gamma}}_1}{g\sigma_0} \tag{4.30}$$

for the Koenig surface and

$$\varepsilon = \frac{\sigma_2 + 2\boldsymbol{\mu}_2 \cdot \mathbf{\Gamma}_0 + \boldsymbol{\mu}_1 \cdot \tilde{\mathbf{\Gamma}}_1}{g\sigma_0} \tag{4.31}$$

for the surface of tension.

4.2.2 Non-local density functional theory

In non-local density functional theory (DFT), the Helmholtz energy $F[\boldsymbol{\rho}(\mathbf{r})] = \int f[\boldsymbol{\rho}(\mathbf{r})]\,\mathrm{d}\mathbf{r}$ and the Helmholtz energy density $f[\boldsymbol{\rho}(\mathbf{r})]$ are functionals of the density profiles $\boldsymbol{\rho}(\mathbf{r})$ of all components. In most DFT approaches, the Helmholtz energy density can be written as a function of any number of weighted densities n_α. This includes functionals based on

fundamental measure theory (FMT)[32], local and weighted density approximations[33] and mean-field theory[26]. The weighted densities are obtained by convolving the density profile with corresponding weight functions, $\boldsymbol{\omega}_\alpha$ in three dimensions

$$n_\alpha(\mathbf{r}) = \boldsymbol{\rho} \overset{3D}{\otimes} \boldsymbol{\omega}_\alpha = \int \boldsymbol{\rho}(\mathbf{r}-\mathbf{r}') \cdot \boldsymbol{\omega}_{\boldsymbol{\alpha}}(\mathbf{r}')\,\mathrm{d}\mathbf{r}', \tag{4.32}$$

where the sum in the inner product is over all components. To calculate the expansion coefficients, the curvature expansion of the convolution integral is required. This is straightforward for a spherical geometry, but significantly more tedious in cylindrical coordinates, as shown in section 4.A. The zeroth and first order expressions for the weighted densities can be written using one dimensional convolution integrals,

$$n_{\alpha 0} = \boldsymbol{\rho}_0 \otimes \boldsymbol{\omega}_\alpha \qquad \text{and} \qquad n_{\alpha 1} = \boldsymbol{\rho}_1 \otimes \boldsymbol{\omega}_\alpha - \frac{g}{2}\boldsymbol{\rho}_0 \otimes (z\boldsymbol{\omega}_\alpha). \tag{4.33}$$

For the curvature expansion, the first and second order coefficients of the Helmholtz energy density

$$f_1 = \sum_\alpha f_{\alpha 0} n_{\alpha 1} \qquad \text{and} \qquad f_2 = \frac{1}{2}\sum_\alpha f_{\alpha 1} n_{\alpha 1} + \sum_\alpha f_{\alpha 0} n_{\alpha 2} \tag{4.34}$$

are required. Here,

$$f_{\alpha 0} = \left(\frac{\partial f}{\partial n_\alpha}\right)_0 \qquad \text{and} \qquad f_{\alpha\beta 0} = \left(\frac{\partial^2 f}{\partial n_\alpha \partial n_\beta}\right)_0 \tag{4.35}$$

is shorthand for the zeroth order first and second partial derivatives of the Helmholtz energy density and $f_{\alpha 1} = \sum_\beta f_{\alpha\beta 0} n_{\beta 1}$ is the corresponding first order expression. The same concept as for the weighted densities is used to obtain the first and second order expressions for the Euler–Lagrange equation, giving

$$\boldsymbol{\mu}_0 = \left(\frac{\delta F}{\delta \boldsymbol{\rho}}\right)_0 = \sum_\alpha f_{\alpha 0} \otimes \boldsymbol{\omega}_\alpha \qquad \text{and} \tag{4.36}$$

$$\boldsymbol{\mu}_1 = \left(\frac{\delta F}{\delta \boldsymbol{\rho}}\right)_1 = \sum_\alpha \left(f_{\alpha 1} \otimes \boldsymbol{\omega}_\alpha - \frac{g}{2} f_{\alpha 0} \otimes (z\boldsymbol{\omega}_\alpha)\right). \tag{4.37}$$

Using eqs. (4.33), (4.34) and (4.36), the first term in the general expression (4.20) for σ_1 can be simplified as

$$\int (f_1 - \boldsymbol{\rho}_1 \cdot \boldsymbol{\mu}_0)\,\mathrm{d}z = \int \sum_\alpha \Big(f_{\alpha 0}(\boldsymbol{\rho}_1 \otimes \boldsymbol{\omega}_\alpha) - \frac{g}{2} f_{\alpha 0}(\boldsymbol{\rho}_0 \otimes (z\boldsymbol{\omega}_\alpha)) - \boldsymbol{\rho}_1 (f_{\alpha 0} \otimes \boldsymbol{\omega}_\alpha)\Big)\,\mathrm{d}z$$

$$= -\frac{g}{2} \int \sum_\alpha f_{\alpha 0} (\boldsymbol{\rho}_0 \otimes (z \boldsymbol{\omega}_\alpha)) \, \mathrm{d}z.$$

Through its definition $\sigma_1 = -g \delta \sigma_0$, the Tolman length follows as

$$\delta \sigma_0 = \frac{1}{2} \int \sum_\alpha f_{\alpha 0} (\boldsymbol{\rho}_0 \otimes (z \boldsymbol{\omega}_\alpha)) \, \mathrm{d}z - \int \Delta \omega_0 z \, \mathrm{d}z + \frac{1}{2} \boldsymbol{\mu}_1^s \cdot \boldsymbol{\Gamma}_0. \tag{4.38}$$

For different Helmholtz energy functionals, the Tolman length depends only on the planar density profile[26,28]. In a similar albeit more elaborate fashion, the rigidity constants are obtained as

$$k = -\frac{1}{4} \int \sum_\alpha f_{\alpha 0} (\boldsymbol{\rho}_0 \otimes \tilde{\boldsymbol{\omega}}_\alpha) \, \mathrm{d}z - \frac{1}{4} \int \sum_\alpha \left(\boldsymbol{\rho}_1^s \cdot (f_{\alpha 0} \otimes (z \boldsymbol{\omega}_\alpha)) + f_{\alpha 1}^s (\boldsymbol{\rho}_0 \otimes (z \boldsymbol{\omega}_\alpha)) \right) \mathrm{d}z \\ - \frac{1}{2} \boldsymbol{\mu}_1^s \cdot \int \boldsymbol{\rho}_0^E z \, \mathrm{d}z - 2 \boldsymbol{\mu}_2^c \cdot \boldsymbol{\Gamma}_0 - \frac{1}{4} \boldsymbol{\mu}_1^s \cdot \boldsymbol{\Gamma}_1^s \tag{4.39}$$

and

$$\bar{k} = \int \Delta \omega_0 z^2 \, \mathrm{d}z + \frac{1}{2} \int \sum_\alpha f_{\alpha 0} (\boldsymbol{\rho}_0 \otimes \tilde{\boldsymbol{\omega}}_\alpha) \, \mathrm{d}z - \int \sum_\alpha f_{\alpha 0} (\boldsymbol{\rho}_0 \otimes (z \boldsymbol{\omega}_\alpha)) z \, \mathrm{d}z + \left(4 \boldsymbol{\mu}_2^c - \boldsymbol{\mu}_2^s \right) \cdot \boldsymbol{\Gamma}_0. \tag{4.40}$$

The full derivation of these expressions is shown in [appendix A.3]. The gaussian rigidity, $\bar{k}$ also does not depend on $\boldsymbol{\rho}_1$, but the bending rigidity, k does. To calculate all Helfrich coefficients, it is therefore necessary to calculate $\boldsymbol{\rho}_0$ and $\boldsymbol{\rho}_1$ from the zeroth and first order expressions of the Euler–Lagrange equation. It is, however, only necessary to calculate ρ_1 for one geometry, as all first order expressions are proportional to the geometry factor g and therefore $\boldsymbol{\rho}_1^s = 2 \boldsymbol{\rho}_1^c$, i.e. the value for a spherical geometry is twice the value for a cylindrical geometry. Further, if $\boldsymbol{\rho}_1$ is a solution to eq. (4.37), $\boldsymbol{\rho}_1 + \varepsilon \boldsymbol{\rho}_0'$ is also a solution for any value of ε. A thorough investigation of eq. (4.39) reveals, however, that k does not depend on the value of ε. Therefore, it is sufficient to find any solution of eq. (4.37) to compute the Helfrich coefficients.

Although different numerical methods have been applied[34], the standard method in DFT is to solve for the density profiles by use of fixed point iteration. To calculate the planar density profile, the functional derivative in eq. (4.36) is split into an ideal gas contribution and a residual, resulting in the iteration

$$\boldsymbol{\rho}_0 = \exp\left(\frac{1}{k_B T} \left(\boldsymbol{\mu}_0 - \left(\frac{\delta F^{\mathrm{res}}}{\delta \boldsymbol{\rho}} \right)_0 \right) \right). \tag{4.41}$$

The same concept can be used to solve for the curvature correction, giving

$$\boldsymbol{\rho}_1 = \frac{\boldsymbol{\rho}_0}{k_B T}\left(\boldsymbol{\mu}_1 - \left(\frac{\delta F^{\mathrm{res}}}{\delta \boldsymbol{\rho}}\right)_1\right). \tag{4.42}$$

The convergence of the iteration can be sped up significantly by using an Anderson mixing scheme[34,35].

4.2.3 Predictive density gradient theory

In predictive density gradient theory (pDGT[, see chapter 5]), the Helmholtz energy functional has the form

$$F[\boldsymbol{\rho}(\mathbf{r})] = \int \left(f^{\mathrm{eos}}(\boldsymbol{\rho}) + \frac{1}{2}\nabla\boldsymbol{\rho}^T \boldsymbol{C}(\boldsymbol{\rho})\nabla\boldsymbol{\rho}\right). \tag{4.43}$$

The difference compared to standard density or square gradient theory comes from the density and temperature dependence of the influence matrix, $\boldsymbol{C}$. Both the influence matrix and the bulk Helmholtz energy density, f^{eos} can be related to the Helmholtz energy density in non-local DFT as

$$f^{\mathrm{eos}}(\boldsymbol{\rho}) = f(\{n_\alpha^b\}) \qquad \text{and} \qquad \mathbf{C}(\boldsymbol{\rho}) = -\sum_{\alpha\beta} f_{\alpha\beta}(\{n_\alpha^b\})\left(\boldsymbol{\omega}_\alpha^0 \boldsymbol{\omega}_\beta^{2\,T} + \boldsymbol{\omega}_\alpha^2 \boldsymbol{\omega}_\beta^{0\,T}\right) \tag{4.44}$$

with the moments of the weight functions

$$\boldsymbol{\omega}_\alpha^0 = 4\pi \int_0^\infty \boldsymbol{\omega}_\alpha(r) r^2 \,\mathrm{d}r \qquad \text{and} \qquad \boldsymbol{\omega}_\alpha^2 = \frac{2\pi}{3}\int_0^\infty \boldsymbol{\omega}_\alpha(r) r^4 \,\mathrm{d}r.$$

and the weighted densities evaluated for local bulk conditions $n_\alpha^b = \boldsymbol{\rho}\cdot\boldsymbol{\omega}_\alpha^0$. The expressions for the Helfrich coefficients are the same as for standard DGT[11,28].

$$\sigma_0 = \int \boldsymbol{\rho}_0'^{\,T} \boldsymbol{C}_0 \boldsymbol{\rho}_0' \,\mathrm{d}z \tag{4.45}$$

$$\delta\sigma_0 = -\int \boldsymbol{\rho}_0'^{\,T} \boldsymbol{C}_0 \boldsymbol{\rho}_0' z \,\mathrm{d}z + \frac{1}{2}\boldsymbol{\mu}_1^s \cdot \boldsymbol{\Gamma}_0 \tag{4.46}$$

$$k = -\frac{1}{2}\int \boldsymbol{\rho}_0'^{\,T} \boldsymbol{C}_0 \boldsymbol{\rho}_1^s \,\mathrm{d}z - \frac{1}{2}\boldsymbol{\mu}_1^s \cdot \int \boldsymbol{\rho}_0^E z \,\mathrm{d}z - 2\boldsymbol{\mu}_2^c \cdot \boldsymbol{\Gamma}_0 - \frac{1}{4}\boldsymbol{\mu}_1^s \cdot \boldsymbol{\Gamma}_1^s \tag{4.47}$$

$$\bar{k} = \int \boldsymbol{\rho}_0'^{\,T} \boldsymbol{C}_0 \boldsymbol{\rho}_0' z^2 \,\mathrm{d}z + \left(4\boldsymbol{\mu}_2^c - \boldsymbol{\mu}_2^s\right)\cdot \boldsymbol{\Gamma}_0 \tag{4.48}$$

For pDGT, the density dependence of the influence matrix has to be taken into account when calculating the density profile from the Euler–Lagrange equation. Therefore, we propose a slight modification to the approach previously suggested for a constant influence matrix[11]. Similar to the method for planar interfaces [(see chapter 5)], we use the geometric combining rule $\boldsymbol{C} = \boldsymbol{c}\boldsymbol{c}^T$. The vector $\boldsymbol{c}$ contains the square root of the diagonal elements of the influence matrix. The advantage of this approach is that it leads to a separation of the Euler–Lagrange equation into a system of algebraic equations

$$f_{\boldsymbol{\rho}}^{\mathrm{eos}} - \boldsymbol{\mu} = \alpha \boldsymbol{c} \tag{4.49}$$

with the unknown α and one differential equation. To obtain it, we introduce $u = \boldsymbol{c} \cdot \boldsymbol{\rho}'$ and use it in the integrated form of the Euler–Lagrange equation

$$\left(f^{\mathrm{eos}} - \boldsymbol{\rho} \cdot \boldsymbol{\mu} - \frac{1}{2} \boldsymbol{\rho}'^T \boldsymbol{C} \boldsymbol{\rho}' \right)' - \frac{g}{r} \boldsymbol{\rho}'^T \boldsymbol{C} \boldsymbol{\rho}' = 0. \tag{4.50}$$

The above equation is applicable to planar ($g = 0$), cylindrical ($g = 1$) and spherical ($g = 2$) geometries. By identifying $\boldsymbol{\rho}'^T \boldsymbol{C} \boldsymbol{\rho}' = u^2$ and $(f^{\mathrm{eos}} - \boldsymbol{\rho} \cdot \boldsymbol{\mu})' = \alpha u$, eq. (4.50) can be written compactly as

$$\left(f^{\mathrm{eos}} - \boldsymbol{\rho} \cdot \boldsymbol{\mu} - \frac{1}{2} u^2 \right)' - \frac{g}{r} u^2 = 0. \tag{4.51}$$

or after evaluating the gradient and dividing by u as

$$u' = \alpha - \frac{g}{r} u. \tag{4.52}$$

To find the planar density profile $\boldsymbol{\rho}_0$, the system is discretized along a path function s, which has to be monotonous in the interface. Different choices for this path function have been proposed, including the density of the least volatile component[36–38], the so-called weighted molecular density $\frac{\boldsymbol{c}^T \boldsymbol{\rho}_0}{\sqrt{\boldsymbol{c}^T \boldsymbol{c}}}$ by Kou et al.[39], or the unscaled version $\boldsymbol{c}^T \boldsymbol{\rho}_0$ of Liang et al.[40]. At every discretization point, the zeroth order expansion of eq. (4.49)

$$f_{\boldsymbol{\rho}0}^{\mathrm{eos}} - \boldsymbol{\mu}_0 = \alpha_0 \boldsymbol{c}_0 \tag{4.53}$$

has to be solved. For the planar interface, eq. (4.51) can be integrated analytically to give u_0 as

$$u_0 = \sqrt{2 \left(f_0^{\mathrm{eos}} - \boldsymbol{\rho}_0 \cdot \boldsymbol{\mu}_0 + p_0 \right)} = \sqrt{2 \Delta \omega_0^{\mathrm{eos}}} \tag{4.54}$$

where the pressure p_0 appears as a constant of the integration. Finally, using the zeroth order term of the definition of u, the z-axis is obtained as

$$u_0 = \boldsymbol{c}_0 \cdot \boldsymbol{\rho}_0' = \boldsymbol{c}_0 \cdot \frac{\mathrm{d}\boldsymbol{\rho}_0}{\mathrm{d}s}\frac{\mathrm{d}s}{\mathrm{d}z} \quad \Rightarrow \quad z = \int \frac{\boldsymbol{c}_0 \cdot \frac{\mathrm{d}\boldsymbol{\rho}_0}{\mathrm{d}s}}{\sqrt{2\Delta\omega_0^{\mathrm{eos}}}}\,\mathrm{d}s \tag{4.55}$$

The integration constant is determined by the choice of dividing surface, analogous to section 4.2.2.

For the curvature correction, the first order expression of eq. (4.49), which is the linear algebraic equation

$$\left(f_{\boldsymbol{\rho}\boldsymbol{\rho}0}^{\mathrm{eos}} - \alpha_0 \boldsymbol{c}_{\boldsymbol{\rho}0}\right)\boldsymbol{\rho}_1 = \boldsymbol{\mu}_1 + \alpha_1 \boldsymbol{c}_0, \tag{4.56}$$

has to be solved simultaneously with the linear differential equation

$$u_1' = \boldsymbol{c}_0\boldsymbol{\rho}_1'' + \boldsymbol{c}_0'\boldsymbol{\rho}_1' + \boldsymbol{c}_1\boldsymbol{\rho}_0'' + \boldsymbol{c}_1'\boldsymbol{\rho}_0' = \alpha_1 - g u_0 \tag{4.57}$$

for the density profile $\boldsymbol{\rho}_1$ and α_1. Again, the solution corresponding to a specific dividing surface can be found using eq. (4.30) or eq. (4.31).

4.2.4 The PCP-SAFT equation of state

The expressions shown in section 4.2.2 are valid for any Helmholtz energy functional that can be written in terms of weighted densities. To calculate Helfrich coefficients for a variety of pure components and mixtures, we apply it to the Helmholtz energy functional based on the perturbed-chain polar statistical associating fluid theory (PCP-SAFT) equation of state[41–43]. Similar to the equation of state, the residual Helmholtz energy functional is split into different contributions, each modeling different intermolecular interactions, as

$$F^{\mathrm{res}}[\boldsymbol{\rho}(\mathbf{r})] = F^{\mathrm{hs}}[\boldsymbol{\rho}(\mathbf{r})] + F^{\mathrm{chain}}[\boldsymbol{\rho}(\mathbf{r})] + F^{\mathrm{assoc}}[\boldsymbol{\rho}(\mathbf{r})] + F^{\mathrm{att}}[\boldsymbol{\rho}(\mathbf{r})]. \tag{4.58}$$

For the hard-sphere (hs) contribution, fundamental measure theory[32,44] has been well established. We used the version proposed by Roth[45] and Yu and Wu[46] that uses vector weight functions. If those are to be avoided, the version by Kierlik and Rosinberg[47], that also simplifies to the Boublík-Mansoori-Carnahan-Starling-Leland equation of state[48–50] used in PCP-SAFT, can be used instead. The difference between the two models can be regarded as negligible compared to other model errors for the calculation of surface tensions. The chain contribution $F^{\mathrm{chain}}[\boldsymbol{\rho}(\mathbf{r})]$, is a modified version of the functional by Tripathi and Chapman[51,52] for the

PCP-SAFT equation of state. For the association contribution $F^{\text{assoc}}[\boldsymbol{\rho}(\mathbf{r})]$, we use the model by Yu and Wu[53] and dispersive and polar interactions are combined in an attractive functional $F^{\text{att}}[\boldsymbol{\rho}(\mathbf{r})]$, which uses a weighted density approach to account for the range of the interactions[54]. For the vector weight functions appearing in the FMT and association functionals, the expressions in section 4.2.2 have to be amended according to section 4.D. In previous works, the functional has already been applied to calculate the properties of adsorbed[55] and free droplets [see chapter 3] as well as adsorption isotherms of pure components and mixtures[56]. With the exception of water, all components are described using parameters that have previously been published[41–43,57].

4.3 Results and discussion

We first compare Helfrich coefficients obtained by use of different methodologies for pure components: the full non-local density functional theory as presented in this work, the predictive density gradient theory and standard density gradient theory (section 4.3.1). All theories reduce to the PCP-SAFT equation of state in bulk systems. While DFT and pDGT are predictive in nature, an influence parameter is required for DGT. There are various ways to obtain an appropriate influence parameter. However, since one of the objectives is to evaluate the influence of the Helmholtz energy functional on the Tolman lengths and rigidity constants, we set the DGT influence parameter to reproduce the surface tension of a planar interface predicted by the full DFT at each temperature.

Little is known about the Helfrich coefficients of mixtures. Because all derivations shown in section 4.2 are valid for multicomponent systems, we use the DFT expressions together with the PCP-SAFT equation of state to examine the behavior of Helfrich coefficients in ideal and non-ideal mixtures in section 4.3.2.

All coefficients presented in the following are calculated using the surface of tension as dividing surface.

4.3.1 Pure components

To confirm the validity of the calculated Helfrich coefficients and confirm the correctness of the implementation, we first compare the surface tension of droplets (positive curvature) and bubbles (negative curvatures) to results from the curvature expansion. For pDGT and DGT, the surface tensions are obtained by solving eq. (4.50) directly. For DFT we use the approach presented in [chapter 3].

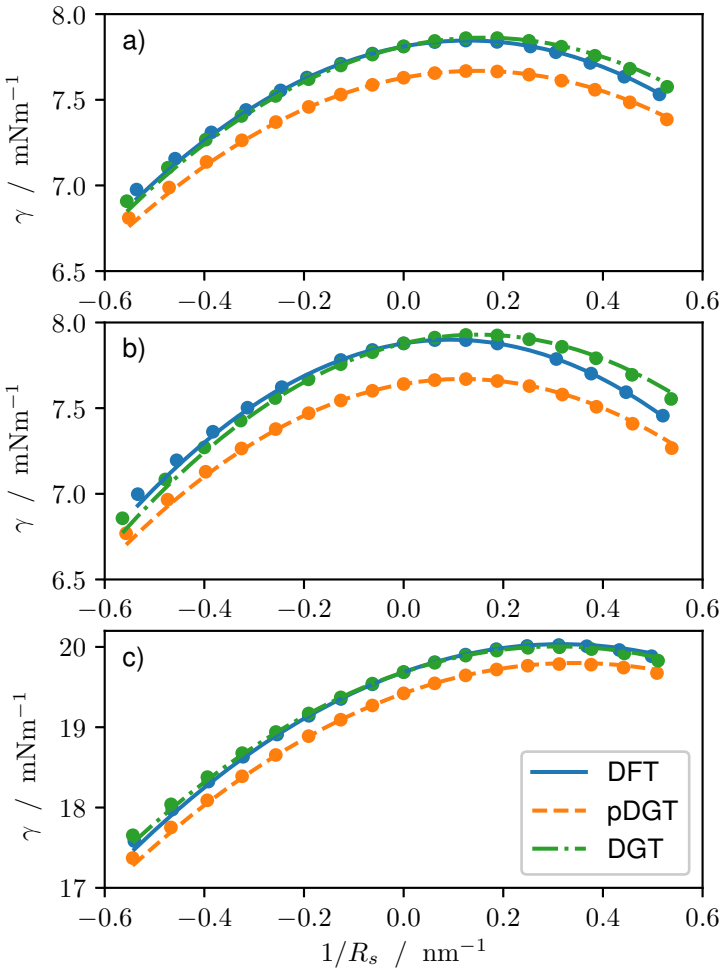

Figure 4.1: Comparison of the surface tension of droplets ($R_s > 0$) and bubbles ($R_s < 0$) (symbols) with the Helfrich expansion (lines) for pDGT, DFT and DGT. The influence parameter in DGT is found by fixing the value of the planar surface tension to the corresponding result from DFT. a) methane at $T = 140\,\mathrm{K}$ b) n-hexane at $T = 400\,\mathrm{K}$, c) water at $T = 550\,\mathrm{K}$

In figure 4.1, results from this comparison are shown for three different components and temperatures. In all cases, the surface tension of the droplets and bubbles is well approximated by the Helfrich expansion in the whole range of curvatures. In general, the different models also yield similar results, with the pDGT predicting slightly lower values for the surface tension for all curvatures. The planar surface tension from DGT is by construction equal to DFT. By increasing the curvature, the results start to differ with the effect being especially pronounced for n-hexane, the most elongated component considered.

To obtain further insight about the chain length dependence of the Helfrich coefficients, we calculated them for n-alkanes of different lengths. Figure 4.2 presents the results for methane, n-pentane and n-dodecane. Two observations made in [chapter 3] can be confirmed here. The Tolman length of alkanes is over a wide temperature range very close to −0.1 times the

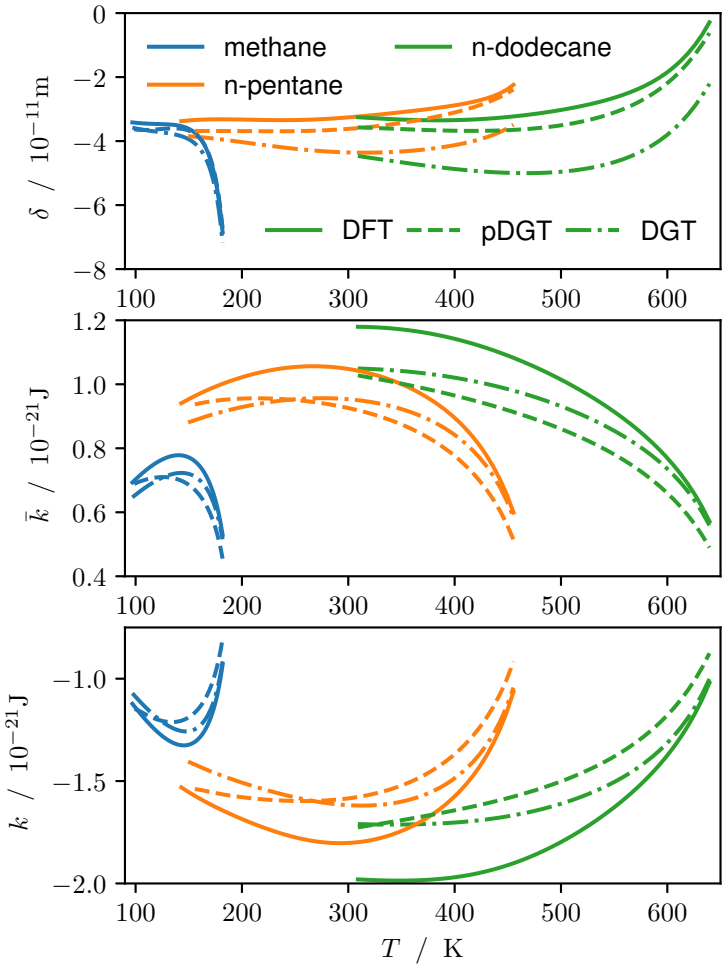

Figure 4.2: Tolman length and rigidities of n-alkanes. Comparison between DFT, pDGT and DGT predictions.

segment diameter. In vicinity of the critical temperature however, the Tolman length deviates from this value. For small alkanes, the Tolman length decreases, whereas for longer alkanes the Tolman length increases. For methane, the different theories give similar results for the Tolman length. This conformity deteriorates for longer chains, with the magnitude of the DGT results being up to 50 % larger than the DFT results for n-dodecane.

A similar trend can be observed for the rigidity constants. The qualitative behavior is similar for all of the theories, but for longer chain lengths the difference between them increases. While the Tolman lengths from pDGT are close to the DFT results, both gradient based methods display comparable deviations from DFT for the rigidities, being up to 15 % for n-dodecane. Because bulk properties are described by the same equation of state for all considered theories, it is likely a difference in the description of structural properties that leads to the difference in predicted Helfrich coefficients. However, the way the different

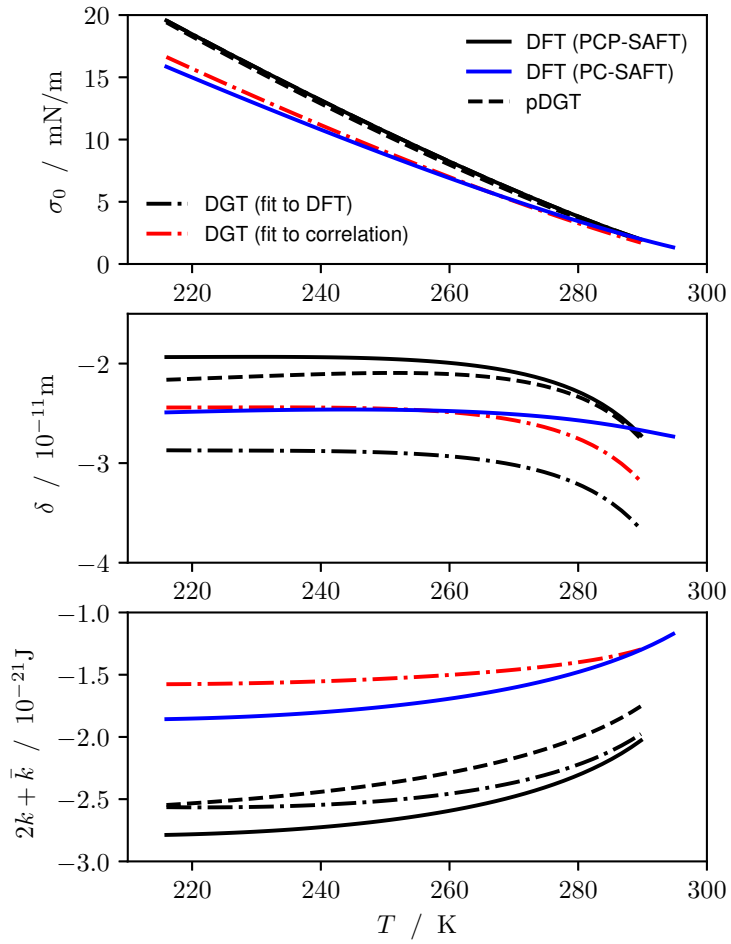

Figure 4.3: Planar surface tension, Tolman length and spherical rigidity of CO_2. Comparison between DFT, pDGT and DGT predictions. Except for the blue line all results are obtained using the PCP-SAFT equation of state. For DGT, the results are obtained by fitting to the surface tension from DFT (black) and to an empirical correlation[58] (red).

PCP-SAFT contributions affect the surface tension and the Helfrich coefficients is convoluted and not a simple linear combination. Hence, the role of the chain contribution in the different theories is not easily isolated. A more thorough investigation into the structure of interfaces of chain molecules, e.g. by molecular simulation, is advised to gain further insight about structural anisotropies at the interface.

To expand the study to polar components, the Helfrich coefficients of CO_2 are presented in figure 4.3. For homogeneous nucleation, the primary application of this framework, only spherical droplets are relevant. We find that the behavior of the two rigidities is very similar for all studied components. Therefore, from here on we only show the spherical rigidity $k_s = 2k + \bar{k}$, which appears as the second order coefficient in a curvature expansion of the surface tension for a spherical geometry. The quantitative behavior of the different theories

m	σ	ε/k_B	μ	$\kappa^{A_iB_i}$	ε/k_B
1.0	3.0084 Å	165.53 K	1.6341 D	.094273	2660.9 K

Table 4.1: PCP-SAFT parameters for the 2B water model used in this work.

are similar for CO_2 and the alkanes. The predictions of the Tolman length from pDGT lie slightly below the DFT results with the difference decreasing with temperature. The DGT results on the other hand are significantly lower. For the rigidities, both pDGT and DGT predict larger values than DFT. We find that these are general trends for non-associating fluids, where results for other substances such as nitrogen and argon are included in [appendix A.1].

Figure 4.3-top shows that PC-SAFT predicts the surface tension of CO_2 to a reasonable accuracy, since DFT with PC-SAFT (blue solid line) agrees well with DGT for which the influence parameter was fitted to an empirical correlation[58] for the surface tension (red dash-dot line). The surface tension from PCP-SAFT, however, lies above the experimental values. The values for the Tolman length and rigidities reflect this, where the Tolman length and rigidities from PC-SAFT and PCP-SAFT are significantly different. The prediction of the surface tension with the PC-SAFT equation of state is better than with PCP-SAFT, despite the latter describing the phase equilibrium and the critical point of CO_2 more accurately[43]. The same trend can be seen for DGT, where there is a large difference between the Helfrich coefficients when the influence parameter has been fitted to DFT values (black dash-dot line) and an empirical correlation (red dash-dot line). This effect is especially pronounced for the rigidity, which decreases about 40 % in magnitude by fitting to the empirical surface tension rather than to DFT. Hence, an important basis for reliable estimates of the curvature dependence of the surface tension is accurate prediction of the planar surface tension.

We next discuss the Helfrich coefficients for water, as this has been a popular example in the literature[4,7,21,23,25]. Since the numerous PCP-SAFT water parameter sets that have been published predict vastly different planar surface tensions[60], new parameters have been obtained that use quasi experimental surface tension data[61] as additional input in the estimation. These parameters are for the 2B association scheme[62] and include a fitted dipole moment. They are shown in table 4.1.

For the Tolman length, we find the same behavior for pDGT and DFT as for non-associating fluids. The Tolman length obtained from DGT however, is larger than the DFT result. The spherical rigidity shows a remarkable resemblance for the three different approaches. We further compare the spherical rigidity to previous results[4] that were calculated using DGT combined with the cubic plus association (CPA)[63] equation of state. The Tolman length has a comparable magnitude and the temperature dependence is the same for DGT with PCP-SAFT. For the rigidity at higher temperatures, we again observe good agreement. For

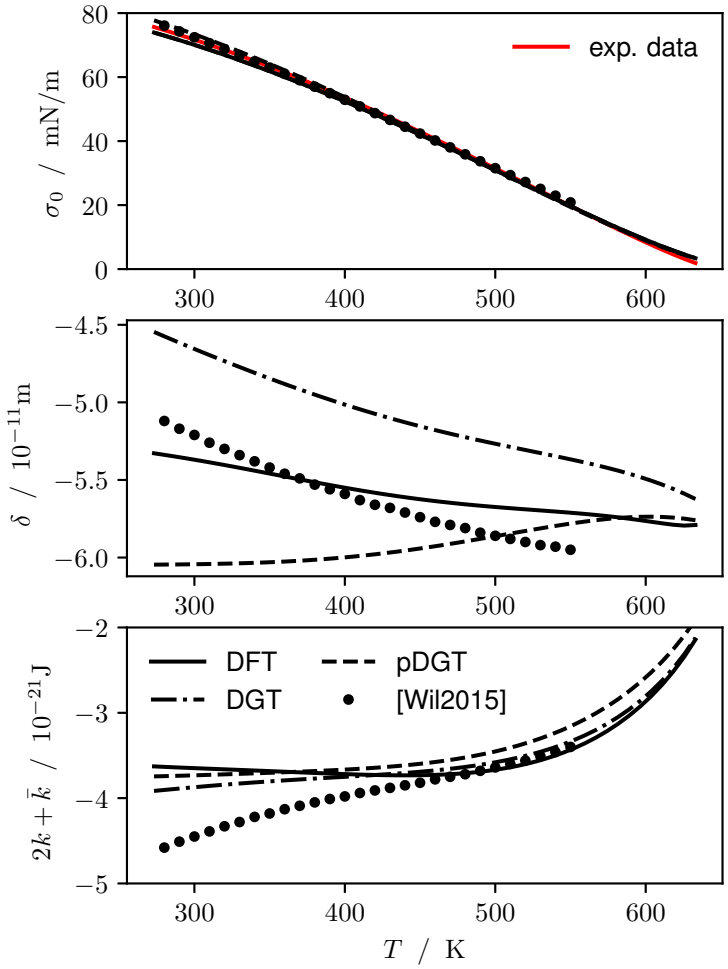

Figure 4.4: Planar surface tension, Tolman length and spherical rigidity of water. Comparison between DFT, pDGT and DGT predictions for the PCP-SAFT equation of state, as well as DGT results using CPA from previous work[4]. The planar surface tension is also compared to experimental data[59].

lower temperatures, the results deviate by up to 25 %. Since the influence parameters do not differ significantly between the different approaches, this deviation can be attributed to the difference in equation of state. Hence, the equation of state has an important role in the prediction of the Helfrich coefficients.

In conclusion, we find that the different descriptions of the considered Helmholtz energy functionals give relatively similar results. However, for strongly polar or elongated molecules, deviations between DFT and DGT should be expected, in particular for the Tolman length. Prerequisites for accurate prediction of the Helfrich coefficients are: a bulk equation of state that is able to describe the phase equilibrium well and a Helmholtz energy functional that is able to reproduce the planar surface tension accurately. As shown in [appendix A.1], for alcohols, that are frequently used in nucleation experiments, the surface tension predictions

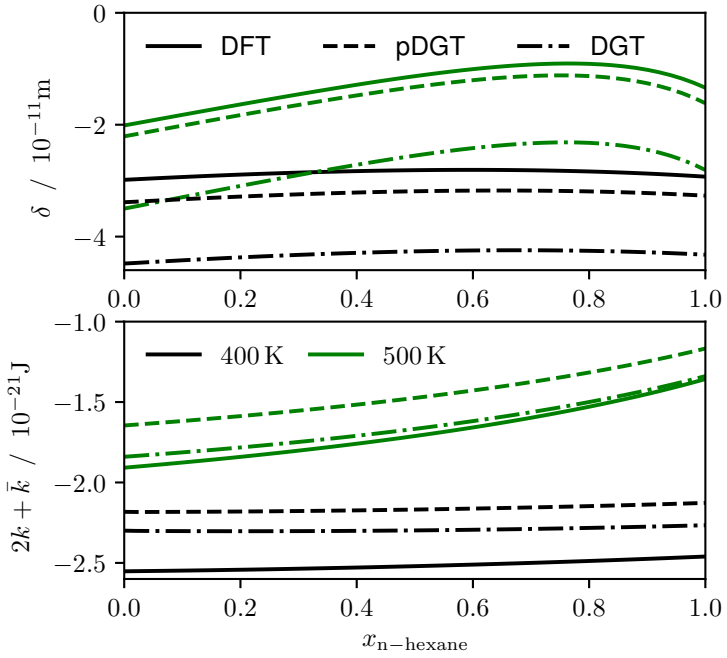

Figure 4.5: Composition dependence of the Tolman length and spherical rigidity for the binary mixture of n-hexane and n-heptane at different temperatures. Comparison between DFT, pDGT and DGT results.

using DFT and PCP-SAFT deviate significantly from experimental data. Therefore, further work has to be done to improve the parametrization of these components, before the influence of the curvature corrections on nucleation rates can be studied rigorously.

4.3.2 Mixtures

In a previous work[11], it was shown that the values of the Helfrich coefficients for mixtures are significantly influenced by the choice of path through the metastable region. We emphasize that already for pure components, a deliberate choice has been made by choosing the isothermal path. An isentropic path is another possible choice.

The value of the surface tension of a droplet is only a function of the thermodynamic state and the choice of dividing surface, and does not depend on the path. A different path, however, leads to a different quality of the prediction using the Helfrich expansion and a different composition dependence of the coefficients. Following the recommendations in a previous study by Aasen et al.[11], we choose a straight path through the metastable region that keeps the liquid composition constant to first order.

We first study the behavior of a close to ideal mixture. To that end, we examine the n-hexane/n-heptane mixture at different temperatures with the binary interaction parameter

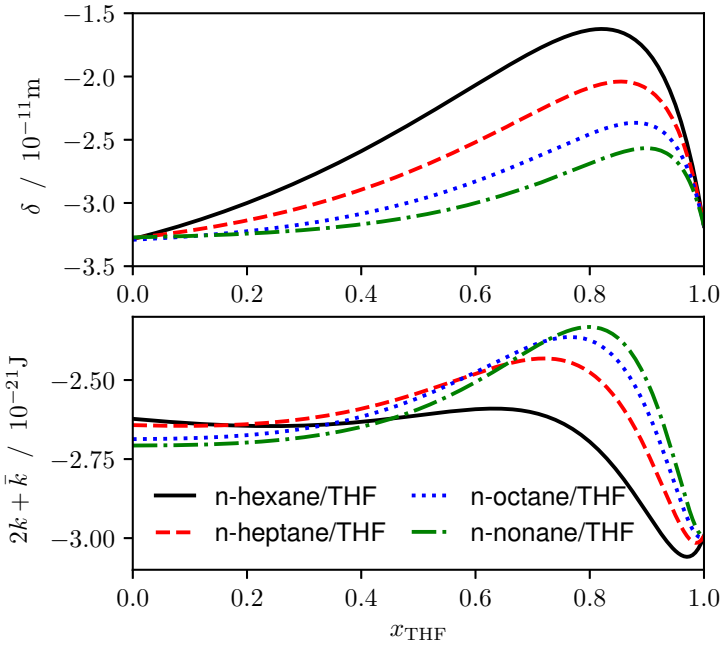

Figure 4.6: DFT result for the composition dependence of the Tolman length and spherical rigidity for the binary mixture of various n-alkanes with the polar component tetrahydrofuran (THF) at 298.15 K.

k_{ij} equal to 0. In figure 4.5, the Tolman length and the spherical rigidity are displayed as functions of the liquid mole fraction of n-hexane in the system. At lower temperatures, the pure component values of both coefficients are similar and there is almost no composition dependence. For temperatures close to the critical point, however, the Tolman length displays a non-linear dependence on the composition. The spherical rigidity is higher for n-hexane than for n-heptane closer to the critical point, but the composition dependence is still close to linear. Comparing the different theories, an almost constant difference in predicted values can be observed over the whole composition range for both temperatures. Therefore, if a good agreement is obtained for the pure components, it can be expected that DGT using the geometric combining rule will also predict similar values as DFT and pDGT for this mixture.

We extend the study to the more non ideal binary mixtures of n-alkanes with the polar solvent tetrahydrofuran (THF). Parameters for this system, including the binary interaction parameter k_{ij} were obtained by Klink and Gross[57] and the DFT results using them were shown to concur well with experimental data[54]. In figure 4.6, the Tolman length and spherical rigidity are shown for the binary mixture of THF with n-hexane, n-heptane, n-octane and n-nonane at $T = 298.15\,\mathrm{K}$. Although all of the pure components have almost the same Tolman length at this temperature, the Tolman lengths of the mixtures are significantly different, with a peak near $x_{\mathrm{THF}} = 0.8$. This effect is most pronounced at higher concentrations of THF and for

smaller alkanes, with the Tolman length of the n-hexane/THF mixture being up to 50 % higher than both pure component values. Contrary to that, the spherical rigidity of the same system is constant in a large composition range until the value drops towards the pure component value of THF. For longer alkanes, a peak in the spherical rigidity is observed, similar to the Tolman length. A comparison to the gradient theories can be seen in [appendix A.1]. Also for the non-ideal mixtures, DGT predicts a similar composition dependence as DFT for the Helfrich coefficients, with the main difference being a nearly constant difference in predicted values, which is determined by the deviation between the pure component values.

4.4 Conclusion

The curvature dependence of the surface tension can be described by the Helfrich expansion, where the first and second order expansion coefficients are called the Tolman length and the rigidities. They are also referred to as the Helfrich coefficients.

In this work, we have derived general expressions that can be used for calculating Helfrich coefficients from any non-local Helmholtz energy functional based on weighted densities. The curvature expansion can be used to calculate the surface energy of arbitrarily shaped interfaces for pure component and mixtures.

We used the framework to compare predictions from non-local density functional theory (DFT) with results from density gradient theory (DGT) and predictive density gradient theory (pDGT). Good agreement between the different theories was observed for small, approximately spherical molecules. An increase in chain length led to larger differences in the predictions. We found that the values of the Helfrich coefficients are sensitive to the choice of influence parameter in DGT and to the prediction of the surface tension in DFT and pDGT. We showed that to obtain a good agreement between the different functional theories, a model is required that gives a good description of the phase equilibrium (including liquid densities) *and* the surface tension.

For non ideal mixtures, the composition dependence of the Helfrich coefficients was found to be nonlinear. All three functionals studied gave very similar composition dependencies for the Helfrich coefficients, where the difference comes mainly from different predictions of the pure component values.

Further work is needed to describe the Helfrich coefficients of alcohols, since PC-SAFT and PCP-SAFT are currently unable to accurately predict their surface tensions. Because alcohols are frequently used in nucleation experiments, their Helfrich coefficients are of much interest.

Appendix

4.A Curvature expansion of convolution integrals

In non-local DFT using weighted densities, the density profile and the partial derivatives of the Helmholtz energy density are convolved with a weight function ω. To reduce the amount of different symbols, we use the same symbol for the different representations of ω and use the independent variable as an indicator for which representation to use. The different representations are the weight function in real space $\omega(\mathbf{r}) = \omega(r)$, the projection on the z-axis

$$\omega(z) = 2\pi \int_{|z|}^{\infty} \omega(r) r \, \mathrm{d}r \tag{4.A.1}$$

and the Fourier transform

$$\omega(k) = \int_{-\infty}^{\infty} \omega(z) e^{-2\pi i k z} \, \mathrm{d}z = \int_{0}^{\infty} \omega(r) \frac{2r}{k} \sin(2\pi k r) \, \mathrm{d}r. \tag{4.A.2}$$

The convolution of a spherically symmetric function $f(r)$ and a scalar weight function $\omega(r)$ can be expressed as[44]

$$\begin{aligned} f \overset{3D}{\otimes} \omega &= \frac{1}{r} \int f(r - z')(r - z') \omega(z') \, \mathrm{d}z' \\ &= f \otimes \omega - \frac{1}{r} f \otimes (z\omega) \\ &= f \otimes \omega - f \otimes (z\omega) \frac{1}{R} + z \left(f \otimes (z\omega) \right) \frac{1}{R^2} + \dots \end{aligned} \tag{4.A.3}$$

The convolution of a cylindrically symmetric function with a scalar weight function is more intricate. The projection-slice theorem of the Fourier transform states, that the 3D Fourier transform can be replaced by a projection on one of the axes followed by the one-dimensional Fourier transform along the given axis. In a cylindrical geometry, the projection is known as the Abel transform. To our knowledge, no concise expression is available like in the spherical case. However, the curvature coefficients can still be derived by performing the curvature expansion on the general convolution integral itself. The expression we obtain is

$$f \overset{3D}{\otimes} \omega = f \otimes \omega - \frac{1}{2} f \otimes (z\omega) \frac{1}{R} + \left(\frac{1}{2} z \left(f \otimes (z\omega) \right) - \frac{1}{8} f \otimes \tilde{\omega} \right) \frac{1}{R^2} + \dots \tag{4.A.4}$$

The full derivation is shown in [appendix A.2]. The weight function, $\tilde{\omega}$ appearing in the last convolution is

$$\tilde{\omega} = z^2\omega - \int_z^\infty \omega(z')z'\,\mathrm{d}z' = z^2\omega - (z\omega) \otimes \Theta(-z) \tag{4.A.5}$$

with the Heaviside step function $\Theta(z)$. The two geometries can be combined in a general expression involving the geometry factor g, as

$$f \overset{3D}{\otimes} \omega = f \otimes \omega - \frac{g}{2} f \otimes (z\omega)\frac{1}{R} + \left(\frac{g}{2} z\,(f \otimes (z\omega)) + \frac{g(g-2)}{8} f \otimes \tilde{\omega}\right)\frac{1}{R^2} + \ldots \tag{4.A.6}$$

4.B Convolutions in Fourier space

Aside from the convergence speed of the solver, the computation time of DFT is limited by the evaluation of the numerous convolution integrals. The calculation can be sped up using the convolution theorem of the Fourier transform. It states that the Fourier transform of a convolution is equal to the product of the Fourier transform of the functions that are being convolved. The Fourier transform of the density profiles and the partial derivatives can be calculated in $\mathcal{O}(N \log N)$ using the fast Fourier transform. The Fourier transform of the weight functions can be obtained analytically from eq. (4.A.2). The other weight functions needed to calculate the Helfrich coefficients can be obtained from the derivatives of the weight functions in Fourier space, as

$$\mathscr{F}(z\omega) = \frac{i}{2\pi}\omega'(k) \tag{4.B.1}$$

and

$$\begin{aligned}\mathscr{F}(\tilde{\omega}) &= \mathscr{F}\left(z^2\omega\right) - \mathscr{F}(z\omega)\,\mathscr{F}(\Theta(-z)) \\ &= -\frac{1}{4\pi^2}\omega''(k) - \frac{i}{2\pi}\omega'(k)\left(\frac{1}{2}\delta(k) + \frac{i}{2\pi k}\right) \\ &= \frac{1}{4\pi^2}\left(\frac{\omega'(k)}{k} - \omega''(k)\right).\end{aligned} \tag{4.B.2}$$

We focus on spherically symmetric weight functions, $\omega(r)$, $\omega(z)$ and $\omega(k)$ that are all even functions by construction. Therefore, $\omega'(k=0) = 0$ and the term involving the dirac distribution $\delta(k)$ cancels. Further, using L'Hôpital's rule we find that $\mathscr{F}(\tilde{\omega})(k=0) = 0$.

4.C Hyper-dual numbers

With the only exception being the derivative $\mathbf{c}_{\rho 0}$, all properties in the framework we discuss are related to at most second order partial derivatives of the Helmholtz energy density. Hyper-dual numbers[64] can be used to calculate the exact second partial derivatives and thus all related properties. The approach has recently been used in the context of equations of state[65]. Here, we propose its use to calculate the first and second partial derivatives of the non-local Helmholtz energy density in DFT and to calculate the different weight functions in Fourier space needed to calculate all convolution integrals for the curvature expansion. Therefore, the only properties that need to be implemented are the Helmholtz energy functional and the weight functions. All other properties, including derivatives of the underlying equation of state and the weight constants in pDGT are available through the hyper-dual numbers, making it simpler and less error-prone to include new functionals. This improvement in usability comes with increased computation time, since every operator and intrinsic function has to be evaluated for hyper-dual numbers. In particular for functions of many variables, there is significant redundancy when calculating derivatives. Therefore, in cases with many variables and simple derivatives like the FMT and chain functionals, it is advisable to override the hyper-dual differentiation with analytic derivatives to speed up the computation.

4.D Vector weighted densities

Some FMT[32,45,46] and association functionals[53] use vector weighted densities. To include those in the framework presented in this work, the expressions have to be amended accordingly. As we are still only considering spherically symmetric weight functions, we can write vector weight functions as $\vec{\omega}(\mathbf{r}) = \omega_r(r)\vec{e}_r$ with the radial unit vector $\vec{e}_r$. The projection on the z-axis then becomes

$$\vec{\omega}(z) = \omega_z(z)\vec{e}_z = 2\pi z\vec{e}_z \int_{|z|}^{\infty} \omega_r(r)\,\mathrm{d}r \tag{4.D.1}$$

and the representation in Fourier space is

$$\vec{\omega}(\mathbf{k}) = \omega_k(k)\vec{e}_k = \vec{e}_k \int_{-\infty}^{\infty} \omega_z(z)e^{-2\pi ikz}\,\mathrm{d}z$$

scalar expression	vector expression	equations
$\boldsymbol{\rho}_{0\|1} \otimes \boldsymbol{\omega}_\alpha$	$\boldsymbol{\rho}_{0\|1} \otimes \boldsymbol{\omega}_{\alpha z}$	(4.33)
$f_{\alpha 0\|1} \otimes \boldsymbol{\omega}_\alpha$	$-f_{\alpha 0\|1} \otimes \boldsymbol{\omega}_{\alpha z}$	(4.36), (4.37)
$\boldsymbol{\rho}_0 \otimes (z\boldsymbol{\omega}_\alpha)$	$\boldsymbol{\rho}_0 \otimes (z\boldsymbol{\omega}_{\alpha z} - \hat{\boldsymbol{\omega}}_{\alpha z})$	(4.38) - (4.40), (4.33)
$f_{\alpha 0} \otimes (z\boldsymbol{\omega}_\alpha)$	$-f_{\alpha 0} \otimes (z\boldsymbol{\omega}_{\alpha z} + \hat{\boldsymbol{\omega}}_{\alpha z})$	(4.39), (4.37)
$\boldsymbol{\rho}_0 \otimes \tilde{\boldsymbol{\omega}}_\alpha$	$\boldsymbol{\rho}_0 \otimes \left(z^2\boldsymbol{\omega}_{\alpha z} + z\hat{\boldsymbol{\omega}}_{\alpha z}\right)$	(4.39)
$\boldsymbol{\rho}_0 \otimes \tilde{\boldsymbol{\omega}}_\alpha$	$\boldsymbol{\rho}_0 \otimes \left(z^2\boldsymbol{\omega}_{\alpha z} - z\hat{\boldsymbol{\omega}}_{\alpha z}\right)$	(4.40)

Table 4.2: Replacement for convolution integrals for vector weighted densities.

$$= \vec{e}_k \int_0^\infty \omega_r(r) \frac{i}{\pi k^2} \left(2\pi k r \cos(2\pi k r) - \sin(2\pi k r)\right) \mathrm{d}r. \tag{4.D.2}$$

The convolution integrals involving vector weight functions are different from scalar weight functions. A detailed derivation of the handling of these convolutions is given in [appendix A.2]. To include vector weighted densities in the framework presented in this work, the convolution integrals in section 4.2.2 have to be changed according to table 4.2 for every vector weight function. The newly introduced weight function $\hat{\boldsymbol{\omega}}_{\alpha z}$ is defined as

$$\hat{\boldsymbol{\omega}}_{\alpha z} = \int_z^\infty \boldsymbol{\omega}_{\alpha z}(z')\,\mathrm{d}z' \tag{4.D.3}$$

and all combinations of weight functions are again easily obtained in Fourier space as

$$\mathscr{F}(z\omega_z \pm \hat{\omega}_z) = \frac{i}{2\pi}\left(\omega_k'(k) \pm \frac{\omega_k(k)}{k}\right) \tag{4.D.4}$$

$$\mathscr{F}(z^2\omega_z \pm z\hat{\omega}_z) = \frac{-1}{4\pi^2}\left(\omega_k''(k) \pm \left(\frac{\omega_k'(k)}{k} - \frac{\omega_k(k)}{k^2}\right)\right). \tag{4.D.5}$$

References

[1] K. Iland, J. Wölk, R. Strey, and D. Kashchiev. Argon Nucleation in a Cryogenic Pulse Chamber. *Journal of Chemical Physics*, **127**:154506, 2007.

[2] H. Vehkamäki. *Classical nucleation theory in multicomponent systems*. Springer Science & Business Media, 2006.

[3] P. R. ten Wolde and D. Frenkel. Computer simulation study of gas-liquid nucleation in a Lennard-Jones system. *The Journal of Chemical Physics*, **109**:9901, 1998. doi:10.1063/1.477658.

[4] Ø. Wilhelmsen, D. Bedeaux, and D. Reguera. Communication: Tolman length and rigidity

constants of water and their role in nucleation. *The Journal of Chemical Physics*, **142**(17):171103, 2015. doi:10.1063/1.4919689.

[5] V. D. Nguyen, F. C. Schoemaker, E. M. Blokhuis, and P. Schall. Measurement of the Curvature-Dependent Surface Tension in Nucleating Colloidal Liquids. *Physical Review Letters*, **121**(24):246102, 2018. doi:10.1103/PhysRevLett.121.246102.

[6] W. Helfrich. Elastic Properties of Lipid Bilayers: Theory and Possible Experiments. *Zeitschrift für Naturforschung C*, **28**, 1973. doi:10.1515/znc-1973-11-1209.

[7] S. Kim, D. Kim, J. Kim, S. An, and W. Jhe. Direct Evidence for Curvature-Dependent Surface Tension in Capillary Condensation: Kelvin Equation at Molecular Scale. *Physical Review X*, **8**, 2018. doi:10.1103/PhysRevX.8.041046.

[8] R. C. Tolman. The Effect of Droplet Size on Surface Tension. *The Journal of Chemical Physics*, **17**(3):333–337, 1949. doi:10.1063/1.1747247.

[9] Ø. Wilhelmsen, D. Bedeaux, and D. Reguera. Tolman length and rigidity constants of the Lennard-Jones fluid. *The Journal of Chemical Physics*, **142**(6):064706, 2015. doi:10.1063/1.4907588.

[10] N. Bruot and F. Caupin. Curvature Dependence of the Liquid-Vapor Surface Tension beyond the Tolman Approximation. *Physical Review Letters*, **116**:056102, 2016. doi:10.1103/PhysRevLett.116.056102.

[11] A. Aasen, E. M. Blokhuis, and Ø. Wilhelmsen. Tolman lengths and rigidity constants of multicomponent fluids: Fundamental theory and numerical examples. *The Journal of Chemical Physics*, **148**(20):204702, 2018. doi:10.1063/1.5026747.

[12] E. M. Blokhuis and J. Kuipers. Thermodynamic expressions for the Tolman length. *Journal of Chemical Physics*, **124**(7):74701–74701, 2006. doi:10.1063/1.2167642.

[13] Z. Li and J. Wu. Toward a Quantitative Theory of Ultrasmall Liquid Droplets and Vapor–Liquid Nucleation. *Industrial & Engineering Chemistry Research*, **47**(15):4988–4995, 2007. doi:10.1021/ie070578i.

[14] B. J. Block, S. K. Das, M. Oettel, P. Virnau, and K. Binder. Curvature dependence of surface free energy of liquid drops and bubbles: A simulation study. *The Journal of Chemical Physics*, **133**(15):154702, 2010. doi:10.1063/1.3493464.

[15] A. Tröster, M. Oettel, B. Block, P. Virnau, and K. Binder. Numerical approaches to determine the interface tension of curved interfaces from free energy calculations. *The Journal of Chemical Physics*, **136**(6):064709, 2012. doi:10.1063/1.3685221.

[16] A. E. van Giessen and E. M. Blokhuis. Determination of curvature corrections to the surface tension of a liquid–vapor interface through molecular dynamics simulations. *The Journal of Chemical Physics*, **116**(1):302–310, 2002. doi:10.1063/1.1423617.

[17] Y. A. Lei, T. Bykov, S. Yoo, and X. C. Zeng. The Tolman Length: Is it Positive or Negative? *J. Am. Chem. Soc.*, **127**:15346, 2005.

[18] M. Horsch, H. Hasse, A. K. Shchekin, A. Agarwal, S. Eckelsbach, J. Vrabec, E. A. Müller, and G. Jackson. Excess equimolar radius of liquid drops. *Physical Review E*, **85**:031605, 2012. doi:10.1103/PhysRevE.85.031605.

[19] A. E. van Giessen and E. M. Blokhuis. Direct determination of the Tolman length from the bulk pressures of liquid drops via molecular dynamics simulations. *The Journal of Chemical Physics*, **131**(16):164705, 2009. doi:10.1063/1.3253685.

[20] J. G. Sampayo, A. Malijevský, E. A. Müller, E. de Miguel, and G. Jackson. Communications: Evidence for the role of fluctuations in the thermodynamics of nanoscale drops and the implications in computations of the surface tension. *The Journal of Chemical Physics*, **132**(14):141101, 2010. doi:10.1063/1.3376612.

[21] G. Menzl, M. A. Gonzalez, P. Geiger, F. Caupin, J. L. F. Abascal, C. Valeriani, and C. Dellago. Molecular mechanism for cavitation in water under tension. *Proceedings of the National Academy of Sciences*, **113**(48):13582–13587, 2016. doi:10.1073/pnas.1608421113.

[22] M. N. Joswiak, N. Duff, M. F. Doherty, and B. Peters. Size-Dependent Surface Free Energy and Tolman-Corrected Droplet Nucleation of TIP4P/2005 Water. *The Journal of Physical Chemistry Letters*, **4**(24):4267–4272, 2013. doi:10.1021/jz402226p. PMID: 26296177.

[23] M. N. Joswiak, R. Do, M. F. Doherty, and B. Peters. Energetic and entropic components of the Tolman length for mW and TIP4P/2005 water nanodroplets. *Journal of Chemical Physics*, **145**(20):204703, 2016. doi:10.1063/1.4967875.

[24] M. Kanduč. Going beyond the standard line tension: Size-dependent contact angles of water nanodroplets. *The Journal of Chemical Physics*, **147**(17):174701, 2017. doi:10.1063/1.4990741.

[25] K.-Y. Leong and F. Wang. A molecular dynamics investigation of the surface tension of water nanodroplets and a new technique for local pressure determination through density correlation. *The Journal of Chemical Physics*, **148**(14):144503, 2018. doi:10.1063/1.5004985.

[26] E. M. Blokhuis and A. E. van Giessen. Density functional theory of a curved liquid-vapour interface: evaluation of the rigidity constants. *Journal of Physics: Condensed Matter*, **25**(22):225003, 2013. doi:10.1088/0953-8984/25/22/225003.

[27] M. P. A. Fisher and M. Wortis. Curvature corrections to the surface tension of fluid drops: Landau theory and a scaling hypothesis. *Physical Review B*, **29**:6252–6260, 1984. doi:10.1103/PhysRevB.29.6252.

[28] E. M. Blokhuis and D. Bedeaux. Van der Waals theory of curved surfaces. *Molecular Physics*, **80**(4):705–720, 1993. doi:10.1080/00268979300102581.

[29] A. E. van Giessen, E. M. Blokhuis, and D. J. Bukman. Mean field curvature corrections to the sur-

face tension. *The Journal of Chemical Physics*, **108**(3):1148–1156, 1998. doi:10.1063/1.475477.

[30] J. C. Barrett. On the thermodynamic expansion of the nucleation free-energy barrier. *The Journal of Chemical Physics*, **131**(8):084711, 2009. doi:10.1063/1.3173196.

[31] F. O. Koenig. On the Thermodynamic Relation between Surface Tension and Curvature. *The Journal of Chemical Physics*, **18**(4):449–459, 1950. doi:10.1063/1.1747660.

[32] Y. Rosenfeld. Free-energy model for the inhomogeneous hard-sphere fluid mixture and density-functional theory of freezing. *Physical Review Letters*, **63**:980–983, 1989. doi:10.1103/PhysRevLett.63.980.

[33] P. Tarazona. Free-energy density functional for hard spheres. *Physical Review A*, **31**:2672–2679, 1985. doi:10.1103/PhysRevA.31.2672.

[34] J. Mairhofer and J. Gross. Numerical aspects of classical density functional theory for one-dimensional vapor-liquid interfaces. *Fluid Phase Equilibria*, **444**:1–12, 2017. doi:http://doi.org/10.1016/j.fluid.2017.03.023.

[35] D. G. Anderson. Iterative Procedures for Nonlinear Integral Equations. *Journal of the ACM*, **12**(4):547–560, 1965. doi:10.1145/321296.321305.

[36] C. Miqueu, B. Mendiboure, C. Graciaa, and J. Lachaise. Modelling of the surface tension of binary and ternary mixtures with the gradient theory of fluid interfaces. *Fluid Phase Equilibria*, **218**(2):189 – 203, 2004. doi:https://doi.org/10.1016/j.fluid.2003.12.008.

[37] C. Miqueu, B. Mendiboure, A. Graciaa, and J. Lachaise. Modeling of the Surface Tension of Multicomponent Mixtures with the Gradient Theory of Fluid Interfaces. *Industrial & Engineering Chemistry Research*, **44**(9):3321–3329, 2005. doi:10.1021/ie049086l.

[38] J. Mairhofer and J. Gross. Modeling of interfacial properties of multicomponent systems using density gradient theory and PCP-SAFT. *Fluid Phase Equilibria*, **439**:31–42, 2017. doi:10.1016/j.fluid.2017.02.009.

[39] J. Kou, S. Sun, and X. Wang. Efficient numerical methods for simulating surface tension of multicomponent mixtures with the gradient theory of fluid interfaces. *Computer Methods in Applied Mechanics and Engineering*, **292**:92 – 106, 2015. doi:https://doi.org/10.1016/j.cma.2014.10.023. Special Issue on Advances in Simulations of Subsurface Flow and Transport (Honoring Professor Mary F. Wheeler).

[40] X. Liang, M. L. Michelsen, and G. M. Kontogeorgis. A density gradient theory based method for surface tension calculations. *Fluid Phase Equilibria*, **428**:153 – 163, 2016. doi:https://doi.org/10.1016/j.fluid.2016.06.017. Theo W. de Loos Festschrift.

[41] J. Gross and G. Sadowski. Perturbed-Chain SAFT: An Equation of State Based on a Perturbation Theory for Chain Molecules. *Industrial & Engineering Chemistry Research*, **40**(4):1244–1260, 2001. doi:10.1021/ie0003887.

[42] J. Gross. An equation-of-state contribution for polar components: Quadrupolar molecules. *AIChE Journal*, **51**(9):2556–2568, 2005. doi:10.1002/aic.10502.

[43] J. Gross and J. Vrabec. An equation-of-state contribution for polar components: Dipolar molecules. *AIChE Journal*, **52**(3):1194–1204, 2006. doi:10.1002/aic.10683.

[44] R. Roth. Fundamental measure theory for hard-sphere mixtures: a review. *Journal of Physics: Condensed Matter*, **22**(6):063102, 2010. doi:10.1088/0953-8984/22/6/063102.

[45] R. Roth, R. Evans, A. Lang, and G. Kahl. Fundamental measure theory for hard-sphere mixtures revisited: the White Bear version. *Journal of Physics: Condensed Matter*, **14**(46):12063, 2002. doi:10.1088/0953-8984/14/46/313.

[46] Y.-X. Yu and J. Wu. Structures of hard-sphere fluids from a modified fundamental-measure theory. *The Journal of Chemical Physics*, **117**(22):10156–10164, 2002. doi:10.1063/1.1520530.

[47] E. Kierlik and M. L. Rosinberg. Free-energy density functional for the inhomogeneous hard-sphere fluid: Application to interfacial adsorption. *Physical Review A*, **42**:3382–3387, 1990. doi:10.1103/PhysRevA.42.3382.

[48] T. Boublík. Hard-Sphere Equation of State. *The Journal of Chemical Physics*, **53**(1):471–472, 1970. doi:10.1063/1.1673824.

[49] G. A. Mansoori, N. F. Carnahan, K. E. Starling, and T. W. Leland. Equilibrium Thermodynamic Properties of the Mixture of Hard Spheres. *The Journal of Chemical Physics*, **54**(4):1523–1525, 1971. doi:10.1063/1.1675048.

[50] N. F. Carnahan and K. E. Starling. Equation of State for Nonattracting Rigid Spheres. *The Journal of Chemical Physics*, **51**(2):635–636, 1969. doi:10.1063/1.1672048.

[51] S. Tripathi and W. G. Chapman. Microstructure of inhomogeneous polyatomic mixtures from a density functional formalism for atomic mixtures. *The Journal of Chemical Physics*, **122**(9):094506, 2005. doi:10.1063/1.1853371.

[52] S. Tripathi and W. G. Chapman. Microstructure and Thermodynamics of Inhomogeneous Polymer Blends and Solutions. *Physical Review Letters*, **94**:087801, 2005. doi:10.1103/PhysRevLett.94.087801.

[53] Y.-X. Yu and J. Wu. A fundamental-measure theory for inhomogeneous associating fluids. *The Journal of Chemical Physics*, **116**(16):7094–7103, 2002. doi:10.1063/1.1463435.

[54] E. Sauer and J. Gross. Classical Density Functional Theory for Liquid–Fluid Interfaces and Confined Systems: A Functional for the Perturbed-Chain Polar Statistical Associating Fluid Theory Equation of State. *Industrial & Engineering Chemistry Research*, **56**(14):4119–4135, 2017. doi:10.1021/acs.iecr.6b04551.

[55] E. Sauer, A. Terzis, M. Theiss, B. Weigand, and J. Gross. Prediction of Contact Angles and Density

Profiles of Sessile Droplets Using Classical Density Functional Theory Based on the PCP-SAFT Equation of State. *Langmuir*, **34**(42):12519–12531, 2018. doi:10.1021/acs.langmuir.8b01985. PMID: 30247038.

[56] E. Sauer and J. Gross. Prediction of Adsorption Isotherms and Selectivities: Comparison between Classical Density Functional Theory Based on the Perturbed-Chain Statistical Associating Fluid Theory Equation of State and Ideal Adsorbed Solution Theory. *Langmuir*, **35**(36):11690–11701, 2019. doi:10.1021/acs.langmuir.9b02378. PMID: 31403314.

[57] C. Klink and J. Gross. A Density Functional Theory for Vapor-Liquid Interfaces of Mixtures Using the Perturbed-Chain Polar Statistical Associating Fluid Theory Equation of State. *Industrial & Engineering Chemistry Research*, **53**(14):6169–6178, 2014. doi:10.1021/ie4029895.

[58] A. Mulero, I. Cachadiña, and M. I. Parra. Recommended Correlations for the Surface Tension of Common Fluids. *Journal of Physical and Chemical Reference Data*, **41**(4):043105, 2012. doi:10.1063/1.4768782.

[59] I. A. for the Properties of Water and Steam. IAPWS R1-76(2014), revised release on surface tension of ordinary water substance. 2014.

[60] J. Mairhofer and J. Gross. Modeling properties of the one-dimensional vapor-liquid interface: Application of classical density functional and density gradient theory. *Fluid Phase Equilibria*, **458**:243 – 252, 2018. doi:https://doi.org/10.1016/j.fluid.2017.11.032.

[61] E. W. Lemmon, M. O. McLinden, and D. G. Friend. *NIST Chemistry WebBook, NIST Standard Reference Database Number 69*, chapter Thermophysical Properties of Fluid Systems. National Institute of Standards and Technology, Gaithersburg MD, 20899, ???? , http://webbook.nist.gov, (retrieved July 15, 2016).

[62] S. H. Huang and M. Radosz. Equation of state for small, large, polydisperse, and associating molecules. *Industrial & Engineering Chemistry Research*, **29**(11):2284–2294, 1990. doi:10.1021/ie00107a014.

[63] G. M. Kontogeorgis, E. C. Voutsas, I. V. Yakoumis, and D. P. Tassios. An Equation of State for Associating Fluids. *Ind. Eng. Chem. Res.*, **35**:4310, 1996.

[64] J. Fike and J. Alonso. *The Development of Hyper-Dual Numbers for Exact Second-Derivative Calculations*. 2011. doi:10.2514/6.2011-886.

[65] F. Diewald, M. Heier, M. Horsch, C. Kuhn, K. Langenbach, H. Hasse, and R. Müller. Three-dimensional phase field modeling of inhomogeneous gas-liquid systems using the PeTS equation of state. *The Journal of Chemical Physics*, **149**(6):064701, 2018. doi:10.1063/1.5035495.

5 Predictive density gradient theory based on non-local density functional theory

The content of this chapter is reproduced with permission from

P. Rehner, J. Gross. Physical Review E 98.6 (2018): 063312.

Density gradient theory has become an important tool for calculating the surface tension of pure components as well as mixtures. The calculation requires knowledge about the so-called influence parameter. Since in most applications this parameter is obtained by fitting results of the density gradient theory to experimental data for surface tensions, the approach lacks predictive power. We propose a predictive density gradient theory based on non-local density functional theory (DFT) using the perturbed chain polar statistical associating fluid theory (PCP-SAFT) as equation of state. The formalism can also be applied to other Helmholtz energy functionals based on weighted densities. The predictive density gradient theory (pDGT) is obtained by applying a gradient expansion to the weighted densities of the PCP-SAFT Helmholtz energy functional to second order and expanding the Helmholtz energy density to first order. The resulting model approximates the DFT and can be cast into the form of a density gradient theory. The resulting influence parameter depends on local densities and on temperature. We assess the predictive power of the proposed pDGT to calculate surface tensions of vapor-liquid interfaces of pure components as well as mixtures. The results show that pDGT reduces the computational complexity compared to non-local DFT calculations, while largely preserving its accuracy as well as its predictive capability.

5.1 Introduction

The design of process equipment, where multiple phases occur, requires knowledge of interfacial properties such as surface tension. Examples include distillation columns[1], general multiphase flow phenomena[2] and nucleation processes[3]. For pure materials, the surface tension is only a function of temperature and thus simple correlations have been used to describe this property reasonably well. Examples are the theory of Eötvös and variations thereof[4,5], the parachor method of Macleod[6] or Guggenheim's principle of corresponding states[7]. However, predictions of surface tension of pure substances and of mixtures requires a physically-based approach.

Classical density functional theory (DFT)[8,9] is well suited to calculate thermodynamic equilibrium properties of inhomogeneous systems, such as fluid-liquid or fluid-solid interfaces. The theory shares the abbreviation and the underlying approach with the electronic density functional theory by Hohenberg, Kohn, Mermin and Sham[10–12]. In classical DFT, the (one-body) density profile of an inhomogeneous fluid is calculated by minimizing the grand potential functional of the system. It requires a model for the Helmholtz energy functional of the mixture under consideration. Non-local classical density functional theory based on fundamental measure theory by Rosenfeld[13] or the weighted density approach of Tarazona[14] is able to express structural properties of the fluid, such as correlation functions and is thus an important basis for the development of Helmholtz energy functionals for real fluids. In our study, we use a Helmholtz energy functional based on the perturbed chain polar statistical associating fluid theory (PCP-SAFT)[15–18], that has already been used to predict properties of liquid-fluid interfaces and confined media[19], as well as nanodroplets [(see chapters 3 and 4)].

However, variational methods have been used to describe inhomogeneous fluids long before the advent of classical density functional theory by van der Waals[20]. The approach that uses the square of the gradient of the density to describe the inhomogeneity of the fluid was later refined by Cahn and Hilliard[21] and is referred to as density gradient theory (DGT). The approach requires knowledge of the so-called influence parameter c_{ij} and requires an equation of state that is able to accurately describe both bulk phases. Although the influence parameter can be determined from the direct correlation function of the fluid[22], this approach is rarely chosen either due to subpar results or due to a lack of knowledge of the direct correlation function. Therefore, the influence parameter is either fitted to experimental data of surface tensions[23], thus conceding the predictive ability of the theory, or is estimated by some form of correlation[24–28].

The DGT, as opposed to non-local density functional theory, is not able to reproduce the fluctuating density profiles appearing in highly structured systems. Therefore the prevalent

application of DGT are fluid-liquid interfaces, whereas interfaces to solid phases require DFT approaches. The advantage of DGT over DFT comes from the mathematical simplicity and numerical efficiency in solving density profiles. For cases where computational performance is essential, the solution of the convolution integrals appearing in DFT may be too expensive. Further, the structure allows a straightforward generalization to spherical and cylindrical geometries, that can be used for the characterization of the surface properties of curved interfaces[29–32].

In this work we present a predictive density gradient theory, that is derived from non-local density functional theory and (for fluid-liquid interfaces) maintains its accuracy and predictive power while attaining the simpler mathematical form of DGT. The derivation in section 5.2 is independent of the choice of Helmholtz energy functional model. In the subsequent sections, we apply the theory to a functional based on the PCP-SAFT equation of state and show results for this choice of model.

5.2 A density and temperature dependent influence parameter based on weighted densities

In non-local density functional theory, the Helmholtz energy $F[\boldsymbol{\rho}(\mathbf{r})]$ is a functional of the density profiles $\boldsymbol{\rho}(\mathbf{r}) = \rho_1(\mathbf{r}), \ldots, \rho_K(\mathbf{r})$ of all K components. It can be separated in an ideal gas part and a residual contribution that accounts for interaction potentials, as

$$\beta F[\boldsymbol{\rho}(\mathbf{r})] = \beta F^{\mathrm{ig}}[\boldsymbol{\rho}(\mathbf{r})] + \beta F^{\mathrm{res}}[\boldsymbol{\rho}(\mathbf{r})] = \int \sum_i \rho_i \left(\ln(\rho_i \Lambda_i^3) - 1\right) \mathrm{d}\mathbf{r} + \int \Phi(\{n_\alpha\}) \, \mathrm{d}\mathbf{r} \quad (5.1)$$

Here, $\beta = \frac{1}{k_B T}$ is the inverse temperature and Λ_i the thermal wavelength including the single molecule partition sum, that is only a function of temperature. The reduced residual Helmholtz energy density Φ is itself a functional of the density profiles, however, it can be approximated by a function of a number of weighted densities n_α. The weighted densities are obtained by convolving the density profiles $\rho_i(\mathbf{r})$ with corresponding weight functions ω_α^i and a summation over all components i, according to

$$n_\alpha(\mathbf{r}) = \sum_i n_\alpha^i(\mathbf{r}) = \sum_i \int \rho_i(\mathbf{r} - \mathbf{r}') \omega_\alpha^i(\mathbf{r}') \, \mathrm{d}\mathbf{r}'. \quad (5.2)$$

By replacing the density $\rho_i(\mathbf{r} - \mathbf{r}')$ with a Taylor expansion around $\mathbf{r}$

$$\rho_i(\mathbf{r} - \mathbf{r}') = \rho_i(\mathbf{r}) - \nabla \rho_i(\mathbf{r}) \cdot \mathbf{r}' + \frac{1}{2} \nabla \nabla \rho(\mathbf{r}) : \mathbf{r}' \mathbf{r}' + \ldots \quad (5.3)$$

the convolution integrals simplify to a series of integrations over the weight functions. For spherically symmetric weight functions $\omega_\alpha^i(\mathbf{r}) = \omega_\alpha^i(r)$, the integration over the angles can be performed analytically and the expression simplifies to

$$n_\alpha^i(\mathbf{r}) = \rho_i(\mathbf{r}) \underbrace{4\pi \int_0^\infty \omega_\alpha^i(r) r^2 \,\mathrm{d}r}_{\omega_\alpha^{i0}} + \nabla^2\rho_i(\mathbf{r}) \underbrace{\frac{2}{3}\pi \int_0^\infty \omega_\alpha^i(r) r^4 \,\mathrm{d}r}_{\omega_\alpha^{i2}} + \dots \tag{5.4}$$

The first term in eq. (5.4) corresponds to the weighted density of a bulk fluid with density $\rho_i(\mathbf{r})$. Therefore, we split the weighted densities in a local part n_α^0 and an excess part Δn_α, as

$$n_\alpha(\mathbf{r}) = \underbrace{\sum_i \rho_i(\mathbf{r}) \omega_\alpha^{i0}}_{n_\alpha^0} + \underbrace{\sum_i \nabla^2\rho_i(\mathbf{r}) \omega_\alpha^{i2} + \dots .}_{\Delta n_\alpha} \tag{5.5}$$

Further, we expand the reduced residual Helmholtz energy density around a local density approximation, as

$$\Phi(\{n_\alpha\}) = \Phi(\{n_\alpha^0\}) + \sum_i \sum_\alpha \frac{\partial \Phi}{\partial n_\alpha} \omega_\alpha^{i2} \nabla^2\rho_i + \dots . \tag{5.6}$$

Using this expression, truncated after the second term, in the general form of the Helmholtz energy functional eq. (5.1) leads to

$$\beta F[\boldsymbol{\rho}(\mathbf{r})] = \int \left(\beta f(\boldsymbol{\rho}) + \sum_i \sum_\alpha \frac{\partial \Phi}{\partial n_\alpha} \omega_\alpha^{i2} \nabla^2\rho_i \right) \mathrm{d}\mathbf{r}. \tag{5.7}$$

Here we introduce the local Helmholtz energy density

$$\beta f(\boldsymbol{\rho}) = \sum_i \rho_i \left(\ln(\rho_i \Lambda_i^3) - 1 \right) + \Phi(\{n_\alpha^0\}), \tag{5.8}$$

that can be calculated from the corresponding bulk equation of state (such as PCP-SAFT). After integrating the second term by parts, using $\nabla\Phi = \sum_j \sum_\beta \frac{\partial \Phi}{\partial n_\beta} \omega_\beta^{j0} \nabla\rho_j$ and reordering the sum over i and j so that the resulting influence matrix c_{ij} is symmetric, eq. (5.7) can be brought in the form known from density gradient theory

$$F[\boldsymbol{\rho}(\mathbf{r})] = \int \left(f(\boldsymbol{\rho}) + \sum_{ij} \frac{c_{ij}}{2} \nabla\rho_i \cdot \nabla\rho_j \right) \mathrm{d}\mathbf{r} \tag{5.9}$$

with the explicit expression for the density dependent influence parameter

$$\beta c_{ij} = -\sum_{\alpha\beta} \frac{\partial^2 \Phi}{\partial n_\alpha \partial n_\beta} \left(\omega_\alpha^{i2} \omega_\beta^{j0} + \omega_\alpha^{i0} \omega_\beta^{j2} \right). \tag{5.10}$$

If vector weighted densities are used, the derivation has to be extended according to section 5.A. Equation (5.10) can also be derived invoking the direct correlation function of the fluid as shown in section 5.B.

In order to simplify the implementation of the proposed formalism, we express thermodynamic properties, such as chemical potentials μ_i or derivatives of chemical potentials with respect to densities, in terms of partial derivatives of Φ with respect to weighted densities n_α only. Using $n_\alpha = \sum_i \rho_i \omega_\alpha^{i0}$ we get

$$\beta \mu_i = \left(\frac{\partial \beta f}{\partial \rho_i} \right)_{\rho_{j\neq i}, T} = \ln(\rho_i \Lambda_i^3) + \sum_\alpha \frac{\partial \Phi}{\partial n_\alpha} \omega_\alpha^{i0} \tag{5.11}$$

and the partial derivatives of chemical potential at constant temperature can be written as

$$\left(\frac{\partial \beta \mu_i}{\partial \rho_j} \right)_{\rho_{k\neq j}, T} = \frac{\delta_{ij}}{\rho_i} + \sum_{\alpha\beta} \frac{\partial^2 \Phi}{\partial n_\alpha \partial n_\beta} \omega_\alpha^{i0} \omega_\beta^{j0} \tag{5.12}$$

with the Kronecker delta δ_{ij}.

5.3 Surface tension

The grand potential functional Ω of a system with given temperature T, volume V, and chemical potentials $\boldsymbol{\mu} = \mu_1, \dots \mu_K$ of all K components is minimal at equilibrium. For an inhomogeneous system, with density profiles $\boldsymbol{\rho} = \rho_1, \dots \rho_K$ of all components, this condition results in

$$\left(\frac{\delta \Omega}{\delta \rho_i(\mathbf{r})} \right)_{T,V,\boldsymbol{\mu}} = 0. \tag{5.13}$$

The grand potential at this state can be expressed as a Legendre transform of the Helmholtz energy $F[\boldsymbol{\rho}(\mathbf{r})]$,

$$\Omega = F[\boldsymbol{\rho}(\mathbf{r})] - \int \boldsymbol{\mu} \cdot \boldsymbol{\rho}(\mathbf{r}) \, \mathrm{d}\mathbf{r}, \tag{5.14}$$

which leads to the equilibrium condition in terms of the Helmholtz energy functional, as

$$\frac{\delta F[\boldsymbol{\rho}(\mathbf{r})]}{\delta \rho_k} = \mu_k. \tag{5.15}$$

Due to the density dependence of the influence parameter, the Euler-Lagrange equation has to include an additional term compared to the form usually encountered in density gradient theory. It reads

$$\frac{\partial f}{\partial \rho_k} - \sum_i \sum_j \hat{c}_{ijk} \nabla \rho_i \cdot \nabla \rho_j - \sum_i c_{ik} \nabla^2 \rho_i = \mu_k \tag{5.16}$$

with

$$\hat{c}_{ijk} = \frac{1}{2}\left(\frac{\partial c_{ik}}{\partial \rho_j} + \frac{\partial c_{jk}}{\partial \rho_i} - \frac{\partial c_{ij}}{\partial \rho_k} \right) \tag{5.17}$$

or

$$\beta \hat{c}_{ijk} = \sum_{\alpha\beta\gamma} \frac{\partial^3 \Phi}{\partial n_\alpha \partial n_\beta \partial n_\gamma} \omega_\alpha^{i0} \omega_\beta^{j0} \omega_\gamma^{k2}. \tag{5.18}$$

Analogously to standard density gradient theory, eq. (5.16) can be integrated for a one-dimensional density profile by multiplying with $\frac{\mathrm{d}\rho_k}{\mathrm{d}z}$ and summing over k, as

$$\frac{\mathrm{d}}{\mathrm{d}z}\left(f - \frac{1}{2} \sum_i \sum_j c_{ij} \frac{\mathrm{d}\rho_i}{\mathrm{d}z} \frac{\mathrm{d}\rho_j}{\mathrm{d}z} - \sum_i \rho_i \mu_i \right) = 0. \tag{5.19}$$

In each of the bulk phases, the density gradients vanish and $f - \sum_i \rho_i \mu_i = -p$ with the bulk pressure p. With this boundary condition and the introduction of the local excess grand potential density $\Delta\omega = f - \sum_i \rho_i \mu_i + p$, it follows

$$\frac{1}{2} \sum_i \sum_j c_{ij} \frac{\mathrm{d}\rho_i}{\mathrm{d}z} \frac{\mathrm{d}\rho_j}{\mathrm{d}z} = \Delta\omega. \tag{5.20}$$

The surface tension can be calculated as the surface excess grand potential per area, as

$$\gamma = \frac{F - \sum_i \mu_i N_i + pV}{A} = 2 \int_{-\infty}^{\infty} \Delta\omega \, \mathrm{d}z. \tag{5.21}$$

The procedure for the calculation of surface tensions is thus: the solution of the differential equation (5.16) for the density profiles, the calculation of $\Delta\omega$ and the integration according

to eq. (5.21). A stable solution algorithm for classical density gradient theory, that could also be expanded to deal with the density dependent influence parameter, has been proposed by Mu et al.[33]. For an overview over solution methods for DGT, we refer to another publication from our group[34] and for an in-depth analysis we refer to Liang and Michelsen[35]. However, we see the advantage of density gradient theory in the decrease in calculation time that comes through spatial decoupling. Without this, the full solution of the boundary value problem is of the same order of complexity as the solution of the integral equations appearing in non-local density functional theory.

To eliminate the gradients from eq. (5.16), we have to presume the relations $\sqrt{c_{11}}c_{ik} = \sqrt{c_{kk}}c_{i1}$ and $\sqrt{c_{11}}\hat{c}_{ijk} = \sqrt{c_{kk}}\hat{c}_{ij1}$. Then the system of differential equations can be rewritten as a system of algebraic equations

$$\sqrt{c_{11}}\left(\frac{\partial f}{\partial \rho_k} - \mu_k\right) = \sqrt{c_{kk}}\left(\frac{\partial f}{\partial \rho_1} - \mu_1\right). \tag{5.22}$$

We provide rationale for this approximation with the fact, that for most fluids the dominant contribution to the influence parameter comes from dispersive attraction. Since the segment size parameters tend to not vary much for many components, the behavior of the mixture is mainly controlled by the energy parameter. If the conventional Berthelot-Lorentz combinig rule

$$\varepsilon_{ij} = \sqrt{\varepsilon_{ii}\varepsilon_{jj}}(1 - k_{ij}) \tag{5.23}$$

is employed, we deduce that for ideal mixtures, we can use the approximation $c_{ij} \approx \sqrt{c_{ii}c_{jj}}$ and hence the relation above. The assumption can be expected to worsen for mixtures, that are only well described with a binary interaction parameter $k_{ij} \neq 0$ or contain large contributions from other intermolecular interactions. Since the pDGT allows the calculation of the full influence matrix, we can assess this approximation when we study the surface tension of binary systems in section 5.5.2. The assumption of a geometric combination rule for the influence parameter also allows us to follow the approach proposed by Kou et al.[36] with slight variations to incorporate the density dependence of the influence parameter. We change the integration variable from z to the path function

$$u = \frac{1}{\sqrt{\lambda}} \sum_i \sqrt{c_{ii}}\rho_i \tag{5.24}$$

with the only non-zero eigenvalue $\lambda = \sum_i c_{ii}$ of the simplified influence matrix. The variable change is only possible if the path function is monotonous in the interfacial region, which was shown by Kou et al. to be always the case for a constant influence matrix[36]. The same cannot

strictly be said for the case of a density dependent influence matrix, however, we found the approach to be more reliable than using a reference component as integration variable.

To solve the density profile, the path function u is discretized between its bulk limits and at every node eq. (5.22) is solved together with eq. (5.24) for the densities of all components. For the surface tension, the mixture influence parameter c_{mix} is introduced in eq. (5.20), as

$$\underbrace{\frac{1}{2}\sum_i\sum_j c_{ij}\frac{\mathrm{d}\rho_i}{\mathrm{d}u}\frac{\mathrm{d}\rho_j}{\mathrm{d}u}}_{c_{\text{mix}}}\left(\frac{\mathrm{d}u}{\mathrm{d}z}\right)^2 = \Delta\omega. \tag{5.25}$$

Finally, the integration over z in eq. (5.21) can be replaced by an integration over u, as

$$\gamma = \int_{u^V}^{u^L} \sqrt{2c_{\text{mix}}\Delta\omega}\,\mathrm{d}u \tag{5.26}$$

In summary the formalism is based on three approximations: the density is expanded to second order (eq. (5.3)), the reduced Helmholtz energy density is expanded to first order (eq. (5.6)), and we presume the geometric mean $c_{ij} = \sqrt{c_{ii}c_{jj}}$, as well as the relation $\sqrt{c_{11}}\hat{c}_{ijk} = \sqrt{c_{kk}}\hat{c}_{ij1}$.

5.4 PCP-SAFT

The predictive density gradient theory presented in the last section can be used with any model for the residual Helmholtz energy functional as input. In the following, we use a functional based on the PCP-SAFT equation of state[15–18], that has successfully been applied to calculate surface tensions of pure components and mixtures, as well as adsorption isotherms in confined media[19]. As usual in SAFT based equations of state, the residual Helmholtz energy functional $F^{\text{res}}[\boldsymbol{\rho}]$ is decomposed into contributions corresponding to specific intermolecular interactions, as

$$F^{\text{res}}[\boldsymbol{\rho}(\mathbf{r})] = F^{\text{hs}}[\boldsymbol{\rho}(\mathbf{r})] + F^{\text{chain}}[\boldsymbol{\rho}(\mathbf{r})] + F^{\text{disp}}[\boldsymbol{\rho}(\mathbf{r})] + F^{\text{polar}}[\boldsymbol{\rho}(\mathbf{r})]. \tag{5.27}$$

The contributions considered here are hard-spheres (hs), chain formation (chain), dispersive attraction (disp) and a term combining dipolar and quadrupolar interaction (polar). In eq. (5.8), the reduced Helmholtz energy density $\Phi(\{n_\alpha^0\})$ is equivalent to $\tilde{a}^{\text{res}}\rho = \frac{\beta A^{\text{res}}}{N}\rho$ in the notation of reference[15]. By construction, the density dependent influence parameter can also

be written as a sum of contributions corresponding to all type of interactions, as

$$c_{ij} = c_{ij}^{\text{hs}} + c_{ij}^{\text{chain}} + c_{ij}^{\text{disp}} + c_{ij}^{\text{polar}}. \tag{5.28}$$

Pure component parameters of the PCP-SAFT equation are the segment size parameter σ_{ii}, the energy parameter ε_{ii} and the number of segments m_i per molecule of species i. Dipole and quadrupole moments can be used from literature[17].

Hard sphere contribution

PCP-SAFT uses the Boublík-Mansoori-Carnahan-Starling-Leland[37,38] equation of state for the hard-sphere reference system. There are two different versions of fundamental measure theory (FMT)[39], that are consistent with this bulk equation of state. The White-Bear or modified FMT[40,41], that use the same weight functions as Rosenfeld in his original theory[13], and a version by Kierlik and Rosinberg[42], that avoids using vector weighted densities. For a pure component, the hard-sphere contribution to the influence parameter only depends on the packing fraction $\eta = \frac{4}{3}\pi m R^3 \rho$. Equations (5.A.6) and (5.10) respectively simplify to

$$\frac{\beta c^{\text{KR}}}{m^2 R^5} = -\frac{4}{15}\pi \frac{16 - 11\eta - 2\eta^2 + 3\eta^3}{(1-\eta)^4} \tag{5.29}$$

and

$$\frac{\beta c^{\text{WB}}}{m^2 R^5} = -\frac{8}{45}\pi \left(\frac{29 - 34\eta + 17\eta^2 - 3\eta^3}{(1-\eta)^4} + \frac{5}{\eta}\ln(1-\eta) \right). \tag{5.30}$$

In figure 5.1 both versions are compared. The small deviation between the models justifies choosing the Kierlik-Rosinberg model going forward and thus avoiding the additional partial derivatives with respect to vector weighted densities appearing in the White-Bear version. Nonetheless, we provide expressions for the vector weighted densities in section 5.A.

The reduced Helmholtz energy density as function of weighted densities in this version is

$$\Phi^{HS}(\{n_\alpha\}) = -n_0 \ln(1-n_3) + \frac{n_1 n_2}{1-n_3} + \frac{n_2^3}{36\pi}\left(\frac{1}{(1-n_3)^2 n_3} + \frac{1}{n_3^2}\ln(1-n_3) \right). \tag{5.31}$$

First and second partial derivatives of this expression can be found in literature[43]. The weight functions are $\omega_3^i = \Theta(R_i - |\mathbf{r}|)$, $\omega_2^i = \delta(R_i - |\mathbf{r}|)$, $\omega_1^i = \frac{1}{8\pi}\delta'(R_i - |\mathbf{r}|)$ and $\omega_0^i = -\frac{1}{8\pi}\delta''(R_i - |\mathbf{r}|) +$

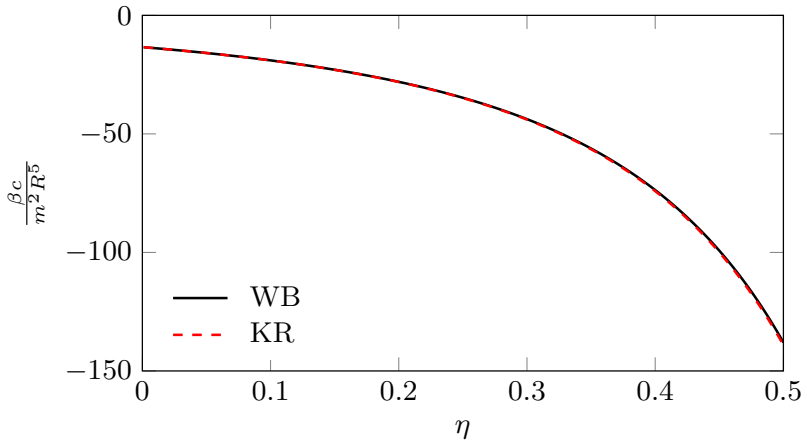

Figure 5.1: The dimensionless hard-sphere contribution to the influence parameter based on the White-Bear (WB) and Kierlik Rosinberg (KR) version of FMT.

$\frac{1}{2\pi|\mathbf{r}|}\delta'(R_i-|\mathbf{r}|)$. Thus, from eq. (5.4), the weight constants follow as

$$\omega_3^{i0} = \frac{4}{3}\pi m_i R_i^3 \qquad \omega_3^{i2} = \frac{2}{15}\pi m_i R_i^5$$
$$\omega_2^{i0} = 4\pi m_i R_i^2 \qquad \omega_2^{i2} = \frac{2}{3}\pi m_i R_i^4$$
$$\omega_1^{i0} = m_i R_i \qquad \omega_1^{i2} = \frac{1}{3} m_i R_i^3$$
$$\omega_0^{i0} = m_i \qquad \omega_0^{i2} = 0.$$

For a pure hard-sphere system, the radius R_i is half the constant hard sphere diameter $R_i = 0.5\,\sigma_{ii}$. In PCP-SAFT, the temperature dependent effective size parameter $R_i = 0.5\,d_i$ is used[15].

Contribution from chain formation

A functional description for the chain term used in SAFT-like equations of state was developped by Tripathi and Chapman[44,45]. The reduced Helmholtz energy density is given as

$$\Phi^{\text{chain}} = \sum_i (m_i - 1)\rho_i \ln(\rho_i) - \sum_i (m_i - 1)\rho_i \ln\left(y_{ii}^{dd}\lambda_i\right), \tag{5.32}$$

with the cavity correlation function

$$y_{ii}^{dd} = \frac{1}{1-\zeta_3} + \frac{3R_i\zeta_2}{(1-\zeta_3)^2} + \frac{2(R_i\zeta_2)^2}{(1-\zeta_3)^3}. \tag{5.33}$$

Several weighted densities are used in eqs. (5.32) and (5.33). The average density at contact λ_i has the weight function

$$\omega^i_{\lambda_j} = \delta_{ij}\frac{\delta(2R_j - |\mathbf{r}|)}{16\pi R_j^2} \tag{5.34}$$

and ζ_2 and ζ_3 have weight functions

$$\omega^i_{\zeta_2} = \frac{m_i}{16R_i}\Theta(2R_i - |\mathbf{r}|) \qquad \omega^i_{\zeta_3} = \frac{m_i}{8}\Theta(2R_i - |\mathbf{r}|). \tag{5.35}$$

To be consistent with the theory developed in this work, we also interpret the local density ρ_i, that appears in the chain term as a weighted density with weight function

$$\omega^i_{\rho_j} = \delta_{ij}\delta(\mathbf{r}). \tag{5.36}$$

Therefore, all weight constants can be calculated from eq. (5.4), as

$$\begin{aligned}
\omega^{i0}_{\rho_j} &= \delta_{ij} & \omega^{i2}_{\rho_j} &= 0\\
\omega^{i0}_{\lambda_j} &= \delta_{ij} & \omega^{i2}_{\lambda_j} &= \frac{2}{3}R_i^2\delta_{ij}\\
\omega^{i0}_{\zeta_2} &= \frac{2}{3}\pi m_i R_i^2 & \omega^{i2}_{\zeta_2} &= \frac{4}{15}\pi m_i R_i^4\\
\omega^{i0}_{\zeta_3} &= \frac{4}{3}\pi m_i R_i^3 & \omega^{i2}_{\zeta_3} &= \frac{8}{15}\pi m_i R_i^5.
\end{aligned}$$

Together with the partial derivatives given in section 5.C, the chain contribution to the influence parameter can be calculated.

Contribution from van-der-Waals attraction

Following Sauer and Gross[19], we use the PCP-SAFT bulk equation of state in a weighted density approximation. Then, the dispersive contribution to the reduced Helmholtz energy density Φ^{disp} is written as the total weighted density $\bar{\rho} = \sum_i \bar{\rho}_i$ times the reduced Helmholtz energy $\tilde{a}^{\text{disp}} = \frac{\beta A^{\text{disp}}}{N}$ evaluated for the same weighted densities $\bar{\boldsymbol{\rho}} = \bar{\rho}_1, \dots \bar{\rho}_K$, as

$$\Phi^{\text{disp}} = \bar{\rho}\,\tilde{a}^{\text{disp}}(\bar{\boldsymbol{\rho}}). \tag{5.37}$$

The weight function $\omega^i_{\bar{\rho}_j} = \frac{\delta_{ij}\Theta(2\psi R_i - |\mathbf{r}|)}{\frac{32}{3}\pi\psi^3 R_i^3}$ corresponding to the weighted density $\bar{\rho}_i$ contains a parameter ψ, that measures the effective range of the attractive van-der-Waals interactions. The functional was previously found to give excellent results using the substance independent

constant value[19] $\psi = 1.3862$. In section 5.5.1 we find, that in this study we can still use ψ as a universal constant, but agreement to experimental data is improved when changing its value. The weight constants are

$$\omega^{i0}_{\bar{\rho}_j} = \delta_{ij} \qquad \omega^{i2}_{\bar{\rho}_j} = \delta_{ij}\frac{2}{5}\psi^2 R_i^2. \tag{5.38}$$

Due to the structure of the weighted density approximation, the second partial derivatives with respect to the weighted densities simplify to the partial derivatives of the bulk chemical potential with respect to the densities evaluated for the weighted densities. For expressions of the chemical potential in PC-SAFT we refer to primary literature[15].

Contribution from polar interactions

Assuming the range of polar interactions is of the same magnitude as the range of dispersive attraction, we follow previous work in using the same weight function in a weighted density approximation for the contribution of polar interactions, as[19]

$$\Phi^{\text{polar}} = \bar{\rho}\tilde{a}^{\text{DD}}(\bar{\boldsymbol{\rho}}) + \bar{\rho}\tilde{a}^{\text{DQ}}(\bar{\boldsymbol{\rho}}) + \bar{\rho}\tilde{a}^{\text{QQ}}(\bar{\boldsymbol{\rho}}) \tag{5.39}$$

with the dipol-dipol contribution to the reduced Helmholtz energy $\tilde{a}^{\text{DD}}$[17], the dipol-quadrupol contribtion $\tilde{a}^{\text{DQ}}$[18] and the quadrupol-quadrupol contribution $\tilde{a}^{\text{QQ}}$[16].

5.5 Results and discussion

In the following sections, we use the predictive density gradient theory to calculate the surface tension of various pure components as well as mixtures and compare the values to results from non-local density functional theory and to experiments.

5.5.1 Pure components: vapor-liquid interfacial properties

Similar to the procedure used by Sauer and Gross[19] during the development of the dispersive contribution in DFT, we use the alkane series to fit the results of the predictive density gradient theory to experimental data and thus obtain the only (substance-independent) model parameter ψ. The parameter is subsequently used to predict the surface tension of all other pure substances and mixtures we examine. Minimizing the root-mean-square deviation between calculated surface tensions from all data points of the DIPPR database[46]

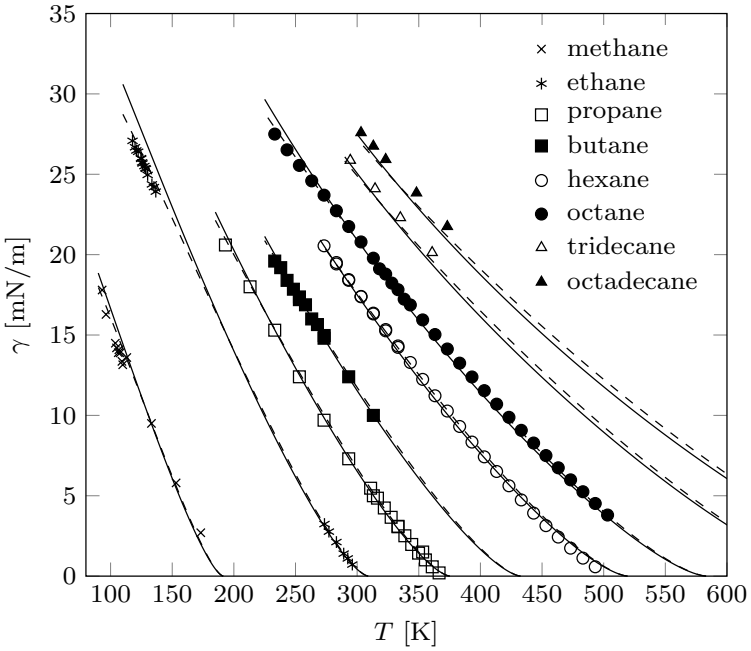

Figure 5.2: Surface tension of several n-alkanes. Comparison of results from predictive density gradient theory (solid lines) and from density functional theory (dashed lines) to experimental data[46] (symbols).

for n-alkanes gives a value of $\psi = 1.3286$. Figure 5.2 compares results of the pDGT for most of the alkanes used in the fit to measurements. We also include results of the full PCP-SAFT DFT. Over a wide range of temperatures for n-alkanes from methane to n-octadecane, the predictive density gradient theory is able to reproduce the results from density functional theory well. Some deviations are seen at low temperatures, which is expected because the two truncated gradient expansions introduced in our approach lose accuracy for increasingly sharp interfaces.

To verify the predictive capability of the model, we examine surface tensions of various polar or aromatic components in figure 5.3. The deviations of the predictive density gradient results from DFT-results and from experimental data at low temperatures is apparent, but the low-temperature behavior does not further deteriorate, compared with the results previously seen for n-alkanes.

5.5.2 Mixtures: vapor-liquid interfacial properties

Predictive density gradient theory can be applied to calculate the surface tension of mixtures without adjustable parameters. In the following, we apply the (optional) approximation mentioned in section 5.3 that implies the geometric mixing rule $c_{ij} = \sqrt{c_{ii}c_{jj}}$. After calculating the density profiles in the interface using the path function u, as described in section 5.3,

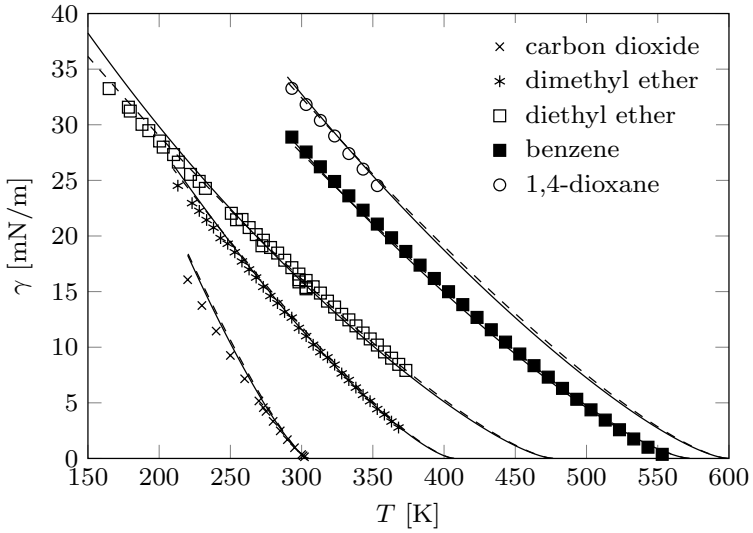

Figure 5.3: Surface tension of various polar or aromatic components. Comparison of results from predictive density gradient theory (solid lines) and from density functional theory (dashed lines) to experimental data (symbols) for carbon dioxide[47], dimethyl ether[48], diethyl ether[49,50], benzene[51] and 1,4-dioxane[52].

we can validate the approximation by comparing it directly to the off-diagonal values of the influence matrix. The results for the binary mixtures hexane/heptane and 1,4-dioxane/octane are shown in figure 5.4. For the essentially ideal mixture of the two alkanes, the geometric mean is indistinguishable from the off-diagonal element. In case of the more non-ideal mixture with the weakly polar component 1,4-dioxane, there is a small deviation that decreases with density.

We study the mixture of 1,4-dioxane with n-alkanes from n-hexane to n-decane. Due to the similarity of the alkanes, one binary interaction parameter k_{ij} was adjusted to experimental data of the vapor liquid equilibrium and that parameter was applied to all mixtures. No further parameter went into the calculation of the surface tension, so that we can indeed refer to it as a prediction. In figure 5.5, the results from predictive density gradient theory are compared to DFT results as well as to experimental data[53]. The agreement to experimental data is very satisfying. For this work it is most important, however, to observe that results from the predictive density gradient theory are in very good agreement to predictions from DFT, because that confirms the approximations made in the derivation of the proposed theory are sufficiently justified.

To further evaluate the capability of predictive density gradient theory, we calculate the surface tension of the eight-component mixture *wet gas* + CO_2, that was measured by Ng et al.[54]. In figure 5.6 the surface tension is shown as a function of pressure for four different temperatures. The results from predictive density gradient theory and density functional

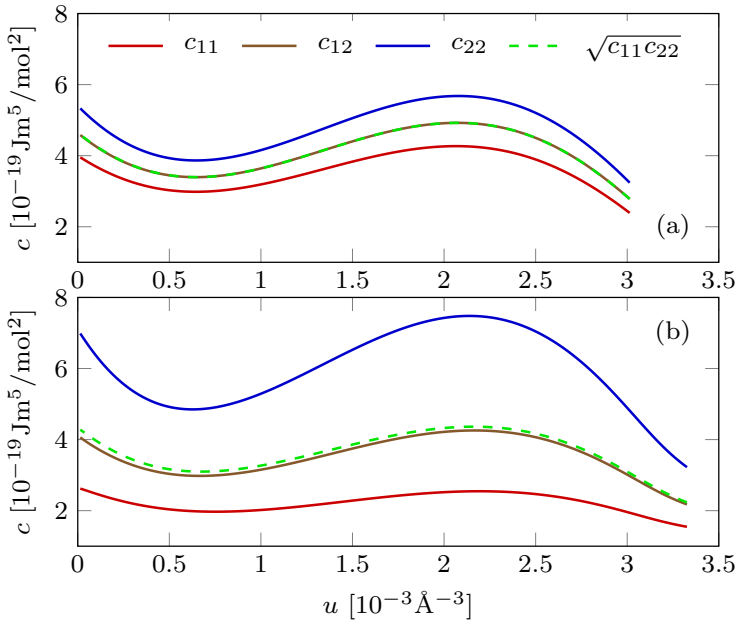

Figure 5.4: Elements of the influence matrix c_{ij}, as well as the geometrical mean approximation $c_{ij} = \sqrt{c_{ii}c_{jj}}$ over path function u. Binary mixtures of hexane/heptane (a) and 1,4-dioxane/octane (b) at $T = 298.15\,\mathrm{K}$ and equimolar liquid composition.

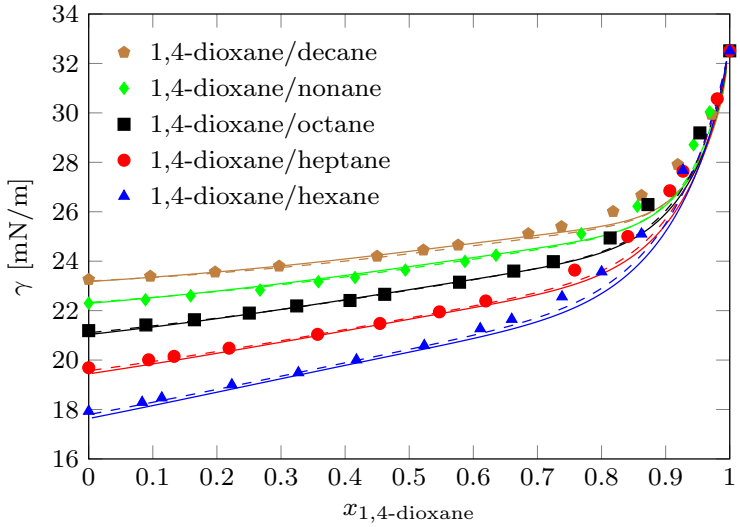

Figure 5.5: Surface tension of the binary mixture of 1,4-dioxane and various n-alkanes. Comparison of results from predictive density gradient theory (–) and from density functional theory (- -) to experimental data[53].

theory are in good accordance for a multicomponent mixture. The deviation of predicted results from experimental data at $T = 283.15\,\mathrm{K}$ is explained by Mairhofer and Gross[55] by a deviation of the bulk densities from the PCP-SAFT model, which uses no binary interaction parameters to describe this specific mixture.

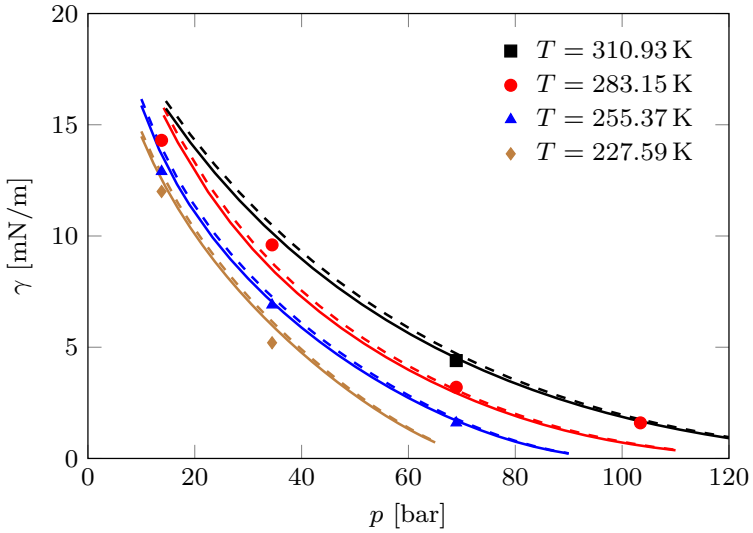

Figure 5.6: Surface tension of the eight-component mixture *wet gas* + CO_2 at different temperatures and pressures. Comparison of results from predictive density gradient theory (–) and from density functional theory (- -) to experimental data[54].

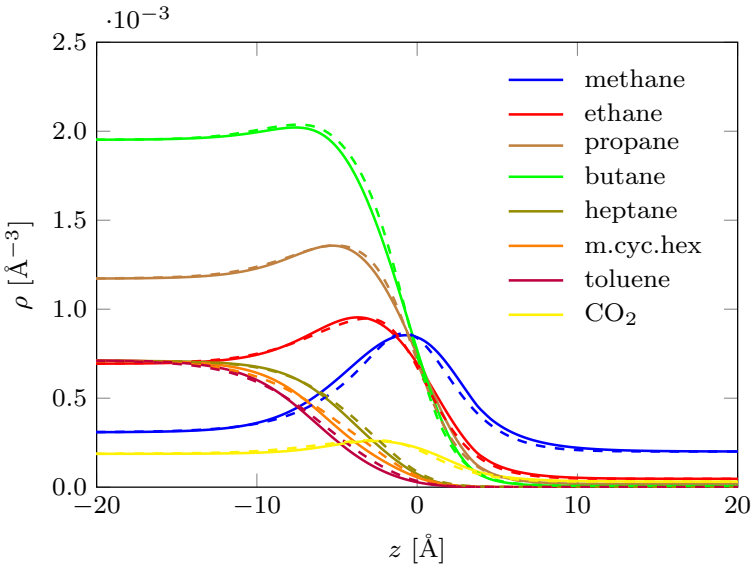

Figure 5.7: Interfacial density profiles of the eight-component mixture *wet gas* + CO_2 at $T = 255.37\,\mathrm{K}$ and $p = 10\,\mathrm{bar}$. Comparison of results from predictive density gradient theory (–) and from density functional theory (- -).

We further find it reassuring to confirm that density profiles across a vapor-liquid interface of various substances in a mixture are well described by predictive density gradient theory. Figure 5.7 indeed shows similar results from predictive density gradient theory and from DFT for the density profiles of all species in the interface and both models are able to predict the local enrichment (often referred to as 'adsorption') of the smaller alkanes (methane, ethane and propane) in the interface.

5.6 Conclusion

A predictive density gradient theory is developed, based on density functional theory expressed in terms of weighted densities. The formalism is illustrated with a PCP-SAFT Helmholtz energy functional. Two assumptions were introduced in order to cast the DFT approach in the form of a density gradient theory: (1) the weighted densities were gradient expanded to second order, and (2) the reduced Helmholtz energy functional was expanded to first order.

Despite being able to calculate the full influence matrix as a function of temperature and local densities in the interface, we apply the geometric mean $c_{ij} = \sqrt{c_{ii}c_{jj}}$ as third assumption. This enables simple numerical solution approaches which increase the solution speed significantly compared to the underlying non-local DFT. We argue, that this approximation is excellent for mixtures that are close to ideal and still applicable for more non-ideal mixtures.

The predictive density gradient theory implies no adjustable parameter for interfacial properties of pure components and mixtures. Results from the proposed theory are in very good agreement to results of the underlying DFT model, both for pure substances and for mixtures. The reduction in computational cost for predictive density gradient theory as opposed to DFT can be meaningful in applications such as the simultaneous optimization of solvents and processes[56–58].

Appendix

5.A Treatment of vector weighted densities

If vector weighted densities from fundamental measure theory, of the form

$$\vec{n}_\alpha(\mathbf{r}) = \sum_i \vec{n}^i_\alpha(\mathbf{r}) = \sum_i \int \rho_i(\mathbf{r}-\mathbf{r}')\vec{\omega}^i_\alpha(\mathbf{r}')\,\mathrm{d}\mathbf{r}', \tag{5.A.1}$$

shall be included in the Helmholtz energy functional, the formalism of section 5.2 has to be extended. Using a Taylor expansion of the density profile and integrating over the angles in this case leads to

$$\vec{n}^i_\alpha(\mathbf{r}) = -\nabla\rho_i(\mathbf{r}) \underbrace{\frac{4}{3}\pi \int_0^\infty \vec{\omega}^i_{\alpha r}(r) r^3\,\mathrm{d}r}_{\vec{\omega}^{i1}_\alpha} + \ldots. \tag{5.A.2}$$

The Taylor expansion of the reduced Helmholtz energy density has to include additional terms, as

$$\Phi(\{n_\alpha\},\{\vec{n}_\alpha\}) = \Phi(\{n_\alpha^0\}) + \sum_i \sum_\alpha^{\text{scal}} \frac{\partial \Phi}{\partial n_\alpha} \omega_\alpha^{i2} \nabla^2 \rho_i - \sum_i \sum_\alpha^{\text{vec}} \frac{\partial \Phi}{\partial \vec{n}_\alpha} \cdot \left(\vec{\omega}_\alpha^{i1} \nabla \rho_i\right)$$
$$+ \frac{1}{2} \sum_{ij} \sum_{\alpha\beta}^{\text{scal}} \frac{\partial^2 \Phi}{\partial n_\alpha \partial n_\beta} \omega_\alpha^{i2} \omega_\beta^{j2} \nabla^2 \rho_i \nabla^2 \rho_j - \sum_{ij} \sum_\alpha^{\text{scal}} \sum_\beta^{\text{vec}} \frac{\partial^2 \Phi}{\partial n_\alpha \partial \vec{n}_\beta} \cdot \left(\omega_\alpha^{i2} \vec{\omega}_\beta^{j1} \nabla^2 \rho_i \nabla \rho_j\right)$$
$$+ \frac{1}{2} \sum_{ij} \sum_{\alpha\beta}^{\text{vec}} \frac{\partial^2 \Phi}{\partial \vec{n}_\alpha \partial \vec{n}_\beta} : \left(\vec{\omega}_\alpha^{i1} \vec{\omega}_\beta^{j1} \nabla \rho_i \nabla \rho_j\right) + \ldots. \quad \text{(5.A.3)}$$

In the original Rosenfeld version, as well as in modified FMT, the second partial derivatives with respect to the vector weighted densities can be simplified as

$$\frac{\partial^2 \Phi}{\partial \vec{n}_\alpha \partial \vec{n}_\beta} = -\frac{\partial^2 \Phi}{\partial n_\alpha \partial n_\beta} \mathbf{I} \quad \text{(5.A.4)}$$

with the unit tensor $\mathbf{I}$. Thus, after dropping all terms higher than second order in spatial derivaitves and the first derivatives with respect to vector densities, that vanish in bulk phases, eq. (5.A.3) can be simplified to

$$\Phi(\{n_\alpha\},\{\vec{n}_\alpha\}) = \Phi(\{n_\alpha^0\}) + \sum_i \sum_\alpha^{\text{scal}} \frac{\partial \Phi}{\partial n_\alpha} \omega_\alpha^{i2} \nabla^2 \rho_i - \frac{1}{2} \sum_{ij} \sum_{\alpha\beta}^{\text{vec}} \frac{\partial^2 \Phi}{\partial n_\alpha \partial n_\beta} \vec{\omega}_\alpha^{i1} \vec{\omega}_\beta^{j1} \nabla \rho_i \cdot \nabla \rho_j. \quad \text{(5.A.5)}$$

The density dependent influence parameter becomes

$$\beta c_{ij} = -\sum_{\alpha\beta}^{\text{scal}} \frac{\partial^2 \Phi}{\partial n_\alpha \partial n_\beta} (\omega_\alpha^{i2} \omega_\beta^{j0} + \omega_\alpha^{i0} \omega_\beta^{j2}) - \sum_{\alpha\beta}^{\text{vec}} \frac{\partial^2 \Phi}{\partial n_\alpha \partial n_\beta} \vec{\omega}_\alpha^{i1} \vec{\omega}_\beta^{j1}. \quad \text{(5.A.6)}$$

5.B Derivation of the temperature-dependent and density-dependent influence parameter using the direct correlation function

This appendix presents an alternative derivation of the influence parameter $c_{ij}(\boldsymbol{\rho}(\mathbf{r}), T)$ of the predictive density gradient theory (eqs. (5.A.6) and (5.10)). The direct correlation function is defined as

$$c_{ij}^{(2)}(\mathbf{r}_1, \mathbf{r}_2) = -\frac{\delta^2 \beta F^{\text{res}}}{\delta \rho_i(\mathbf{r}_1) \delta \rho_j(\mathbf{r}_2)}. \quad \text{(5.B.1)}$$

Using the general Helmholtz energy functional used in non-local DFT and including vector weighted densities, this expression can be written as

$$\begin{aligned} c_{ij}^{(2)}(\mathbf{r}_1,\mathbf{r}_2) = &- \int \sum_{\alpha\beta}^{\text{scal}} \frac{\partial^2\Phi}{\partial n_\alpha \partial n_\beta} \omega_\alpha^i(\mathbf{r}-\mathbf{r}_1)\omega_\beta^j(\mathbf{r}-\mathbf{r}_2)\,\mathrm{d}\mathbf{r} \\ &- 2\int \sum_{\alpha}^{\text{scal}}\sum_{\beta}^{\text{vec}} \frac{\partial^2\Phi}{\partial n_\alpha \partial \vec{n}_\beta} \cdot \left(\omega_\alpha^i(\mathbf{r}-\mathbf{r}_1)\vec{\omega}_\beta^j(\mathbf{r}-\mathbf{r}_2)\right)\mathrm{d}\mathbf{r} \\ &- \int \sum_{\alpha\beta}^{\text{vec}} \frac{\partial^2\Phi}{\partial \vec{n}_\alpha \partial \vec{n}_\beta} : \left(\vec{\omega}_\alpha^i(\mathbf{r}-\mathbf{r}_1)\vec{\omega}_\beta^j(\mathbf{r}-\mathbf{r}_2)\right)\mathrm{d}\mathbf{r}. \end{aligned} \tag{5.B.2}$$

With the same properties of the vector weight functions as in section 5.A, the expression can be simplified for a local bulk approximation, as

$$c_{ij}^{(2)}(\mathbf{r}_{12}) = -\sum_{\alpha\beta}^{\text{scal}} \frac{\partial^2\Phi}{\partial n_\alpha \partial n_\beta} \int \omega_\alpha^i(\mathbf{r}')\omega_\beta^j(\mathbf{r}_{12}-\mathbf{r}')\,\mathrm{d}\mathbf{r}' - \sum_{\alpha\beta}^{\text{vec}} \frac{\partial^2\Phi}{\partial n_\alpha \partial n_\beta} \int \vec{\omega}_\alpha^i(\mathbf{r}')\cdot\vec{\omega}_\beta^j(\mathbf{r}_{12}-\mathbf{r}')\,\mathrm{d}\mathbf{r}'. \tag{5.B.3}$$

The convolution integrals appearing in this expression can be simplified for two spherically symmetric functions.

$$\int \omega_\alpha^i(\mathbf{r}')\omega_\beta^i(\mathbf{r}-\mathbf{r}')\,\mathrm{d}\mathbf{r}' = \frac{2\pi}{r}\int_0^\infty \int_{|r-r'|}^{r+r'} \omega_\alpha^i(r')\omega_\beta^j(r'')r'r''\,\mathrm{d}r''\,\mathrm{d}r' \tag{5.B.4}$$

$$\int \vec{\omega}_\alpha^i(\mathbf{r}')\cdot\vec{\omega}_\beta^i(\mathbf{r}-\mathbf{r}')\,\mathrm{d}\mathbf{r}' = \frac{\pi}{r}\int_0^\infty \int_{|r-r'|}^{r+r'} \vec{\omega}_{\alpha r}^i(r')\vec{\omega}_{\beta r}^j(r'')(r^2-r'^2-r''^2)\,\mathrm{d}r''\,\mathrm{d}r' \tag{5.B.5}$$

From the local approximation of the direct correlation function, we can calculate the local influence parameter using the relation[22]

$$\beta c_{ij} = \frac{2\pi}{3}\int_0^\infty c_{ij}^{(2)}(r)r^4\,\mathrm{d}r. \tag{5.B.6}$$

The integral over r can be solved analytically and the influence parameter can be brought into the form

$$\beta c_{ij} = -\sum_{\alpha\beta}^{\text{scal}} \frac{\partial^2\Phi}{\partial n_\alpha \partial n_\beta} \omega_{\alpha\beta}^{ij} - \sum_{\alpha\beta}^{\text{vec}} \frac{\partial^2\Phi}{\partial n_\alpha \partial n_\beta} \vec{\omega}_{\alpha\beta}^{ij} \tag{5.B.7}$$

with

$$\begin{aligned}
\omega_{\alpha\beta}^{ij} &= \frac{4\pi^2}{3} \int_0^\infty \int_0^\infty \omega_\alpha^i(r') \omega_\beta^j(r'') r' r'' \int_{|r'-r''|}^{r'+r''} r^3 \,\mathrm{d}r \,\mathrm{d}r' \,\mathrm{d}r'' \\
&= \frac{8\pi^2}{3} \int_0^\infty \int_0^\infty \omega_\alpha^i(r') \omega_\beta^j(r'') r'^2 r''^2 (r'^2 + r''^2) \,\mathrm{d}r' \,\mathrm{d}r'' \\
&= \omega_\alpha^{i0} \omega_\beta^{j2} + \omega_\alpha^{i2} \omega_\beta^{j0}
\end{aligned} \tag{5.B.8}$$

and

$$\begin{aligned}
\vec{\omega}_{\alpha\beta}^{ij} &= \frac{2\pi^2}{3} \int_0^\infty \int_0^\infty \vec{\omega}_\alpha^i(r') \vec{\omega}_\beta^j(r'') \int_{|r'-r''|}^{r'+r''} (r^5 - r^3(r'^2 + r''^2)) \,\mathrm{d}r \,\mathrm{d}r' \,\mathrm{d}r'' \\
&= \frac{16\pi^2}{9} \int_0^\infty \int_0^\infty \vec{\omega}_\alpha^i(r') \vec{\omega}_\beta^j(r'') r'^3 r''^3 \,\mathrm{d}r' \,\mathrm{d}r'' \\
&= \vec{\omega}_\alpha^{i1} \vec{\omega}_\beta^{j1}.
\end{aligned} \tag{5.B.9}$$

5.C Partial derivatives of chain term

The theory described in this paper requires the calculation of the second partial derivatives of the reduced Helmholtz energy density Φ with respect to all weighted densities. For the chain contribution the first partial derivatives are ($\alpha, \beta \in \{2, 3\}$)

$$\begin{aligned}
\frac{\partial \Phi^{\text{chain}}}{\partial \rho_i} &= (m_i - 1)\left(\ln(\rho_i) + 1 - \ln\left(y_{ii}^{dd} \lambda_i\right)\right) \\
\frac{\partial \Phi^{\text{chain}}}{\partial \lambda_i} &= -(m_i - 1)\frac{\rho_i}{\lambda_i} \\
\frac{\partial \Phi^{\text{chain}}}{\partial \zeta_\alpha} &= -\sum_i (m_i - 1)\frac{\rho_i}{y_{ii}^{dd}} \frac{\partial y_{ii}^{dd}}{\partial \zeta_\alpha}
\end{aligned}$$

and the second derivatives

$$\begin{aligned}
\frac{\partial^2\Phi^{\text{chain}}}{\partial\rho_i\partial\rho_j} &= \delta_{ij}\frac{(m_i-1)}{\rho_i}\\
\frac{\partial^2\Phi^{\text{chain}}}{\partial\rho_i\partial\lambda_j} &= -\delta_{ij}\frac{(m_i-1)}{\lambda_i}\\
\frac{\partial^2\Phi^{\text{chain}}}{\partial\rho_i\partial\zeta_\alpha} &= -(m_i-1)\frac{1}{y_{ii}^{dd}}\frac{\partial y_{ii}^{dd}}{\partial\zeta_\alpha}\\
\frac{\partial^2\Phi^{\text{chain}}}{\partial\lambda_i\partial\lambda_j} &= \delta_{ij}(m_i-1)\frac{\rho_i}{\lambda_i^2}\\
\frac{\partial^2\Phi^{\text{chain}}}{\partial\zeta_\alpha\partial\zeta_\beta} &= \sum_i(m_i-1)\frac{\rho_i}{y_{ii}^{dd}}\left(\frac{1}{y_{ii}^{dd}}\frac{\partial y_{ii}^{dd}}{\partial\zeta_\alpha}\frac{\partial y_{ii}^{dd}}{\partial\zeta_\beta}-\frac{\partial^2 y_{ii}^{dd}}{\partial\zeta_\alpha\partial\zeta_\beta}\right).
\end{aligned}$$

The partial derivatives not in this list vanish. The partial derivatives of the cavity correlation function are

$$\begin{aligned}
\frac{\partial y_{ii}^{dd}}{\partial\zeta_2} &= \frac{3R_i}{(1-\zeta_3)^2}+\frac{4R_i^2\zeta_2}{(1-\zeta_3)^3}\\
\frac{\partial y_{ii}^{dd}}{\partial\zeta_3} &= \frac{1}{(1-\zeta_3)^2}+\frac{6R_i\zeta_2}{(1-\zeta_3)^3}+\frac{6(R_i\zeta_2)^2}{(1-\zeta_3)^4}\\
\frac{\partial^2 y_{ii}^{dd}}{\partial\zeta_2^2} &= \frac{4R_i^2}{(1-\zeta_3)^3}\\
\frac{\partial^2 y_{ii}^{dd}}{\partial\zeta_2\partial\zeta_3} &= \frac{6R_i}{(1-\zeta_3)^3}+\frac{12R_i^2\zeta_2}{(1-\zeta_3)^4}\\
\frac{\partial^2 y_{ii}^{dd}}{\partial\zeta_3^2} &= \frac{2}{(1-\zeta_3)^3}+\frac{18R_i\zeta_2}{(1-\zeta_3)^4}+\frac{24(R_i\zeta_2)^2}{(1-\zeta_3)^5}.
\end{aligned}$$

References

[1] F. Zuiderweg and A. Harmens. The influence of surface phenomena on the performance of distillation columns. *Chemical Engineering Science*, **9**(2):89 – 103, 1958. doi:https://doi.org/10.1016/0009-2509(58)80001-9.

[2] J. P. Morris. Simulating surface tension with smoothed particle hydrodynamics. *International Journal for Numerical Methods in Fluids*, **33**(3):333–353, 2000. doi:10.1002/1097-0363(20000615)33:3<333::AID-FLD11>3.0.CO;2-7.

[3] V. Kalikmanov. *Nucleation theory*, volume 860. Springer, 2012.

[4] R. Eötvös. Ueber den Zusammenhang der Oberflächenspannung der Flüssigkeiten mit ihrem Molecularvolumen. *Annalen der Physik*, **263**(3):448–459, 1886. doi:10.1002/andp.18862630309.

[5] W. Ramsay and J. Shields. The Variation of Molecular Surface-Energy with Temperature. *Philosophical Transactions of the Royal Society of London. A*, **184**:647–673, 1893.

[6] D. B. Macleod. On a relation between surface tension and density. *Trans. Faraday Soc.*, **19**:38–41, 1923. doi:10.1039/TF9231900038.

[7] E. A. Guggenheim. The Principle of Corresponding States. *The Journal of Chemical Physics*, **13**(7):253–261, 1945. doi:10.1063/1.1724033.

[8] R. Evans. The nature of the liquid-vapour interface and other topics in the statistical mechanics of non-uniform, classical fluids. *Advances in Physics*, **28**(2):143–200, 1979. doi:10.1080/00018737900101365.

[9] R. Evans, M. Oettel, R. Roth, and G. Kahl. New developments in classical density functional theory. *Journal of Physics: Condensed Matter*, **28**(24):240401, 2016. doi:10.1088/0953-8984/28/24/240401.

[10] P. Hohenberg and W. Kohn. Inhomogeneous Electron Gas. *Physical Review*, **136**:B864–B871, 1964. doi:10.1103/PhysRev.136.B864.

[11] N. D. Mermin. Thermal Properties of the Inhomogeneous Electron Gas. *Physical Review*, **137**:A1441–A1443, 1965. doi:10.1103/PhysRev.137.A1441.

[12] W. Kohn and L. J. Sham. Self-Consistent Equations Including Exchange and Correlation Effects. *Physical Review*, **140**:A1133–A1138, 1965. doi:10.1103/PhysRev.140.A1133.

[13] Y. Rosenfeld. Free-energy model for the inhomogeneous hard-sphere fluid mixture and density-functional theory of freezing. *Physical Review Letters*, **63**:980–983, 1989. doi:10.1103/PhysRevLett.63.980.

[14] P. Tarazona. Free-energy density functional for hard spheres. *Physical Review A*, **31**:2672–2679, 1985. doi:10.1103/PhysRevA.31.2672.

[15] J. Gross and G. Sadowski. Perturbed-Chain SAFT: An Equation of State Based on a Perturbation Theory for Chain Molecules. *Industrial & Engineering Chemistry Research*, **40**(4):1244–1260, 2001. doi:10.1021/ie0003887.

[16] J. Gross. An equation-of-state contribution for polar components: Quadrupolar molecules. *AIChE Journal*, **51**(9):2556–2568, 2005. doi:10.1002/aic.10502.

[17] J. Gross and J. Vrabec. An equation-of-state contribution for polar components: Dipolar molecules. *AIChE Journal*, **52**(3):1194–1204, 2006. doi:10.1002/aic.10683.

[18] J. Vrabec and J. Gross. Vapor–Liquid Equilibria Simulation and an Equation of State Contribution

for Dipole–Quadrupole Interactions. *The Journal of Physical Chemistry B*, **112**(1):51–60, 2008. doi:10.1021/jp072619u. PMID: 18072758.

[19] E. Sauer and J. Gross. Classical Density Functional Theory for Liquid–Fluid Interfaces and Confined Systems: A Functional for the Perturbed-Chain Polar Statistical Associating Fluid Theory Equation of State. *Industrial & Engineering Chemistry Research*, **56**(14):4119–4135, 2017. doi:10.1021/acs.iecr.6b04551.

[20] J. Van der Waals. Thermodynamische Theorie der Kapillarität unter voraussetzung stetiger Dichteänderung. *Zeitschrift für Physikalische Chemie*, **13**(1):657–725, 1894.

[21] J. W. Cahn and J. E. Hilliard. Free Energy of a Nonuniform System. I. Interfacial Free Energy. *The Journal of Chemical Physics*, **28**(2):258–267, 1958. doi:10.1063/1.1744102.

[22] V. Bongiorno, L. Scriven, and H. Davis. Molecular theory of fluid interfaces. *Journal of Colloid and Interface Science*, **57**(3):462 – 475, 1976. doi:https://doi.org/10.1016/0021-9797(76)90225-3.

[23] H. Kahl and S. Enders. Calculation of surface properties of pure fluids using density gradient theory and SAFT-EOS. *Fluid Phase Equilibria*, **172**(1):27 – 42, 2000. doi:https://doi.org/10.1016/S0378-3812(00)00361-7.

[24] P. M. W. Cornelisse, C. J. Peters, and J. de Swaan Arons. On the fundamentals of the gradient theory of van der Waals. *The Journal of Chemical Physics*, **106**(23):9820–9834, 1997. doi:10.1063/1.473872.

[25] C. Miqueu, B. Mendiboure, A. Graciaa, and J. Lachaise. Modelling of the surface tension of pure components with the gradient theory of fluid interfaces: a simple and accurate expression for the influence parameters. *Fluid Phase Equilibria*, **207**(1):225 – 246, 2003. doi:https://doi.org/10.1016/S0378-3812(03)00028-1.

[26] H. Lin, Y.-Y. Duan, and Q. Min. Gradient theory modeling of surface tension for pure fluids and binary mixtures. *Fluid Phase Equilibria*, **254**(1):75 – 90, 2007. doi:https://doi.org/10.1016/j.fluid.2007.02.013.

[27] B. Breure and C. Peters. Modeling of the surface tension of pure components and mixtures using the density gradient theory combined with a theoretically derived influence parameter correlation. *Fluid Phase Equilibria*, **334**:189 – 196, 2012. doi:https://doi.org/10.1016/j.fluid.2012.08.010.

[28] J. M. Garrido, A. Mejía, M. M. Piñeiro, F. J. Blas, and E. A. Müller. Interfacial tensions of industrial fluids from a molecular-based square gradient theory. *AIChE Journal*, **62**(5):1781–1794, 2016. doi:10.1002/aic.15190.

[29] E. M. Blokhuis and D. Bedeaux. Van der Waals theory of curved surfaces. *Molecular Physics*, **80**(4):705–720, 1993. doi:10.1080/00268979300102581.

[30] V. G. Baidakov and G. S. Boltachev. Curvature dependence of the surface tension of liquid and vapor nuclei. *Physical Review E*, **59**:469–475, 1999. doi:10.1103/PhysRevE.59.469.

[31] E. M. Blokhuis and A. E. van Giessen. Density functional theory of a curved liquid-vapour interface: evaluation of the rigidity constants. *Journal of Physics: Condensed Matter*, **25**(22):225003, 2013. doi:10.1088/0953-8984/25/22/225003.

[32] A. Aasen, E. M. Blokhuis, and Ø. Wilhelmsen. Tolman lengths and rigidity constants of multicomponent fluids: Fundamental theory and numerical examples. *The Journal of Chemical Physics*, **148**(20):204702, 2018. doi:10.1063/1.5026747.

[33] X. Mu, F. Frank, F. O. Alpak, and W. G. Chapman. Stabilized density gradient theory algorithm for modeling interfacial properties of pure and mixed systems. *Fluid Phase Equilibria*, **435**:118 – 130, 2017. doi:https://doi.org/10.1016/j.fluid.2016.11.024.

[34] J. Mairhofer and J. Gross. Modeling properties of the one-dimensional vapor-liquid interface: Application of classical density functional and density gradient theory. *Fluid Phase Equilibria*, **458**:243 – 252, 2018. doi:https://doi.org/10.1016/j.fluid.2017.11.032.

[35] X. Liang and M. L. Michelsen. General approach for solving the density gradient theory in the interfacial tension calculations. *Fluid Phase Equilibria*, **451**:79 – 90, 2017. doi:https://doi.org/10.1016/j.fluid.2017.07.021.

[36] J. Kou, S. Sun, and X. Wang. Efficient numerical methods for simulating surface tension of multicomponent mixtures with the gradient theory of fluid interfaces. *Computer Methods in Applied Mechanics and Engineering*, **292**:92 – 106, 2015. doi:https://doi.org/10.1016/j.cma.2014.10.023. Special Issue on Advances in Simulations of Subsurface Flow and Transport (Honoring Professor Mary F. Wheeler).

[37] T. Boublík. Hard-Sphere Equation of State. *The Journal of Chemical Physics*, **53**(1):471–472, 1970. doi:10.1063/1.1673824.

[38] G. A. Mansoori, N. F. Carnahan, K. E. Starling, and T. W. Leland. Equilibrium Thermodynamic Properties of the Mixture of Hard Spheres. *The Journal of Chemical Physics*, **54**(4):1523–1525, 1971. doi:10.1063/1.1675048.

[39] R. Roth. Fundamental measure theory for hard-sphere mixtures: a review. *Journal of Physics: Condensed Matter*, **22**(6):063102, 2010. doi:10.1088/0953-8984/22/6/063102.

[40] R. Roth, R. Evans, A. Lang, and G. Kahl. Fundamental measure theory for hard-sphere mixtures revisited: the White Bear version. *Journal of Physics: Condensed Matter*, **14**(46):12063, 2002. doi:10.1088/0953-8984/14/46/313.

[41] Y.-X. Yu and J. Wu. Structures of hard-sphere fluids from a modified fundamental-measure theory. *The Journal of Chemical Physics*, **117**(22):10156–10164, 2002. doi:10.1063/1.1520530.

[42] E. Kierlik and M. L. Rosinberg. Free-energy density functional for the inhomogeneous hard-sphere fluid: Application to interfacial adsorption. *Physical Review A*, **42**:3382–3387, 1990. doi:10.1103/PhysRevA.42.3382.

[43] M. Levesque, R. Vuilleumier, and D. Borgis. Scalar fundamental measure theory for hard spheres in three dimensions: Application to hydrophobic solvation. *The Journal of Chemical Physics*, **137**(3):034115, 2012. doi:10.1063/1.4734009.

[44] S. Tripathi and W. G. Chapman. Microstructure of inhomogeneous polyatomic mixtures from a density functional formalism for atomic mixtures. *The Journal of Chemical Physics*, **122**(9):094506, 2005. doi:10.1063/1.1853371.

[45] S. Tripathi and W. G. Chapman. Microstructure and Thermodynamics of Inhomogeneous Polymer Blends and Solutions. *Physical Review Letters*, **94**:087801, 2005. doi:10.1103/PhysRevLett.94.087801.

[46] R. L. Rowley, W. V. Wilding, J. L. Oscarson, Y. Yang, N. A. Zundel, T. E. Daubert, and R. P. Danner. *DIPPR Data Compilation of Pure Chemical Properties*. Design Institute for Physical Properties, 2009.

[47] G. N. Muratov and V. Skripov. Poverxnostnoe natyazhenie dvuokisi ugleroda. *Teplofiz Vys. Temp.*, **20**:596–598, 1982.

[48] J. Wu, Z. Liu, F. Wang, and C. Ren. Surface Tension of Dimethyl Ether from (213 to 368) K. *Journal of Chemical & Engineering Data*, **48**(6):1571–1573, 2003. doi:10.1021/je034097r.

[49] T. Tonomura. Measurements of some physical constants of organic compounds at low temperatures. *Sci. Rep. Tohoku Imperial Univ*, **22**:104–130, 1933.

[50] S. Bi, G. Zhao, and J. Wu. Surface Tension of Diethyl Ether, Diisopropyl Ether, and Dibutyl Ether. *Journal of Chemical & Engineering Data*, **55**(4):1523–1526, 2010. doi:10.1021/je900665a.

[51] G. Muratov. Surface-tension of benzene and ethyl-alcohol. *Zhurnal Fizicheskoi Khimii*, **54**(8):2088–2089, 1980.

[52] A. N. Gaivoronskii, V. A. Granzhan, and Y. L. Vysotski. *Oniitekhim*, **Code 225 KHP - D83**:1–14, 1983.

[53] A. Penas, E. Calvo, M. Pintos, A. Amigo, and R. Bravo. Refractive Indices and Surface Tensions of Binary Mixtures of 1,4-Dioxane + n-Alkanes at 298.15 K. *Journal of Chemical & Engineering Data*, **45**(4):682–685, 2000. doi:10.1021/je000038r.

[54] H. Ng, S. Taylor, H. Schroeder, and D. Sieben. *GPA Research Report, Rep. No. PR-193*, pages 1–50, 2008.

[55] J. Mairhofer and J. Gross. Modeling of interfacial properties of multicomponent systems using density gradient theory and PCP-SAFT. *Fluid Phase Equilibria*, **439**:31–42, 2017. doi:10.1016/j.fluid.2017.02.009.

[56] A. Bardow, K. Steur, and J. Gross. Continuous-Molecular Targeting for Integrated Solvent and Process Design. *Industrial & Engineering Chemistry Research*, **49**(6):2834–2840, 2010.

doi:10.1021/ie901281w.

[57] M. Stavrou, M. Lampe, A. Bardow, and J. Gross. Continuous Molecular Targeting–Computer-Aided Molecular Design (CoMT–CAMD) for Simultaneous Process and Solvent Design for CO2 Capture. *Industrial & Engineering Chemistry Research*, **53**(46):18029–18041, 2014. doi:10.1021/ie502924h.

[58] J. Schilling, M. Lampe, J. Gross, and A. Bardow. 1-stage CoMT-CAMD: An approach for integrated design of ORC process and working fluid using PC-SAFT. *Chemical Engineering Science*, **159**:217 – 230, 2017. doi:https://doi.org/10.1016/j.ces.2016.04.048. ICAMD – Integrating Computer-Aided Molecular Design into Product and Process Design.

6 Multiobjective optimization of PCP-SAFT parameters for water and alcohols using surface tension data

With predictive methods, such as classical density functional theory and predictive density gradient theory (pDGT), it is possible to model bulk phase properties and interfacial tensions using the same model. For non-associating fluids, these models can be used to predict interfacial properties for systems that lack experimental data. For associating components, however, predictions often show large deviations to experiments, which is at least partially rooted in highly correlated pure component parameters. Therefore, we use interfacial properties for discriminating pure component parameters by amending the PCP-SAFT parameter estimation for water and alcohols by including surface tension data in the objective function. To obtain a comprehensive comparison between different association models, a multiobjective optimization is performed. By analyzing the resulting pareto fronts, it is shown, that including a fitted dipole moment improves the results for water but not for alcohols. The result of the multiobjective optimization is inconclusive about the optimal choice of association scheme for water as the preferred model changes along the pareto front. For small alcohols, in contrast to chemical intuition, the 4C association scheme gives the best results. For longer alcohols, the pareto analysis shows the limits of the homosegmented modeling approach.

6.1 Introduction

Molecular-based equations of state like the statistical associating fluid theory (SAFT) family[1–8] have become commonly used in industrial applications[9–12]. Because the models are based on a molecular model, few, physically meaningful parameters suffice to describe the thermodynamic behavior of pure fluids and mixtures accurately over a wide range of conditions. This robustness allows reliable predictions of properties for systems, with scarce or without experimental data. However, the optimal strategy for obtaining the parameters of the equation state is not clear and may depend on the envisaged application. In most cases, the parameters are obtained by fitting pure component properties to experimental data. With the prediction of phase behavior being an important application of SAFT type equations of state, the standard input for the fits is the vapor pressure and liquid densities along the saturation line. Other properties have been used, with the result that different sets of properties used in the fit lead to different parameters. This effect is particularly noticeable for fluids, that have strong associating interactions, like water[13,14] and alcohols[15]. For these components, there is also an ongoing discussion about the underlying association model that is shared between the different SAFT versions and is usually described in the nomenclature of Huang and Radosz[4]. Especially for water, both the chemical understanding and the results from parameter estimation are inconclusive about the choice of association scheme, with the most commonly chosen ones being 2B, 3B and 4C[13,14].

A method to compare different association schemes more comprehensively than by fitting single sets of parameters to given experimental data, was proposed by Forte et al.[16]. In their multiobjective optimization approach, the residuals in vapor pressures and saturated liquid densities are treated as separate objectives. The resulting pareto fronts, that contain optimal parameter sets for varying weights of the two objectives, can be compared for different association models. The comparison helps identifying weaknesses in models and allows the assessment of additional constraints or degrees of freedoms, such as a fitted dipole moment.

A reason for the problems associated with fitting parameters for associating components is the high number of parameters. Especially if only vapor pressures and saturated liquid densities are considered, both monovariate functions of temperature, the parameters are strongly correlated. The problem can be alleviated by calculating a subset of the parameters (usually the association parameters) with ab initio methods and regressing the remaining parameters[17,18]. Another possibility is the inclusion of additional properties in the objective function. Popular choices are enthalpy of vaporization, speed of sound[19] and compressibility factor[20] as they are properties that can be directly calculated from a residual equation of state like the SAFT variants and are also experimentally available.

One property that is seldomly used as input for a parameter regression is the surface tension. The obvious reason is, that a surface tension characterizes an inhomogeneous interface, that can not be described by a simple bulk equation of state. There are empirical models, that link the surface tension to bulk properties, often based on the expression by Macleod[21] but their predictive capabilities are limited. To be consistent with the equation of state, a molecular based approach is required. Notable studies in which equation of state parameters of associating components are fitted to vapor pressures, liquid densities, and surface tensions have been presented by Fu and Wu[22], by Gloor at al.[23], and more recently by Camacho Vergara et al[24] for a number of associating components including water and linear alcohols.

In this study, we will present the most prevalent methods for calculating surface tensions based on a molecular model in the following sections. In section 6.4 we present the relevant expressions of the PCP-SAFT model we used in this work and then show in section 6.5 how we can use surface tension data as an input for a multiobjective optimization of PCP-SAFT parameters. In section 6.6, we present the resulting pareto curves for water and alcohols and discuss, how we can utilize them to discriminate between different models and how we determine the optimal parameter set along the pareto front.

6.2 Density functional theory

Density functional theory[25] (DFT) extends classical equilibrium thermodynamics to model nanoscale inhomogeneous systems. Common applications are fluid-fluid interfaces and confinement effects in porous media[26–28]. In place of an equation of state, the fluid is modeled using a Helmholtz energy $F(T,[\boldsymbol{\rho}(\mathbf{r})])$ that is a function of the temperature T and a functional of the density profiles $\boldsymbol{\rho}(\mathbf{r})$ of all components. In an open system, specified with the temperature and chemical potentials $\boldsymbol{\mu}$, the grand potential $\Omega = F - \boldsymbol{\mu}\cdot\boldsymbol{N}$ attains a minimum when the system is in equilibrium. With the density profiles as internal degree of freedom, this equilibrium condition can be written as a functional derivative, as

$$\left(\frac{\delta\Omega}{\delta\boldsymbol{\rho}(\mathbf{r})}\right)_{T,\boldsymbol{\mu}} = 0 \;\Rightarrow\; \left(\frac{\delta F}{\delta\boldsymbol{\rho}(\mathbf{r})}\right)_{T} = \boldsymbol{\mu}. \tag{6.1}$$

By using a Helmholtz energy density $f(T,[\boldsymbol{\rho}(\mathbf{r})])$, that itself is a functional of the density profiles, structuring effects, such as adsorption layers, can be modelled with DFT. The Helmholtz energy is obtained as $F(T,[\boldsymbol{\rho}(\mathbf{r})]) = \int f(T,[\boldsymbol{\rho}(\mathbf{r})])d\mathbf{r}$. A powerful class of Helmholtz energy functionals use a weighted density approach to account for these non-localities. This includes functionals for hard spheres[29–32], hard chains[33,34] and also association[35,36] and dispersive attraction[37,38]. Mean field theories[39,40] can also be written in this form. In these approaches,

the Helmholtz energy density is written as a function of weighted densities $f(\{n_\alpha\})$, that are obtained by convolving the density profiles with corresponding weight functions $\boldsymbol{\omega}_\alpha$, as

$$n_\alpha(\mathbf{r}) = \int \boldsymbol{\rho}(\mathbf{r}') \cdot \boldsymbol{\omega}_\alpha(\mathbf{r}-\mathbf{r}')d\mathbf{r}'. \tag{6.2}$$

The equilibrium condition, eq. (6.1), can thus be written as

$$\int \sum_\alpha \frac{\partial f}{\partial n_\alpha}(\mathbf{r}')\boldsymbol{\omega}_\alpha(\mathbf{r}'-\mathbf{r})d\mathbf{r}' = \boldsymbol{\mu}. \tag{6.3}$$

For the calculation of the surface tension, the planar geometry of the interface can be exploited to reduce the dimensionality of the equations. A one-dimensional density profile $\boldsymbol{\rho}(z)$ is calculated from eq. (6.3). The surface tension γ then follows from

$$\gamma = \int \left(f(T,[\boldsymbol{\rho}(z)]) - \boldsymbol{\rho}(z)\cdot\boldsymbol{\mu} + p\right) dz \tag{6.4}$$

with the pressure p in both bulk phases. With an efficient implementation of the convolution integrals[41] and a fast solver[42], the surface tension of simple systems can be calculated on todays hardware in fractions of a second. A typical computation time for the surface tension of a pure substance is 0.1 s. This considerable speed is an advantage over molecular simulations, especially in cases, where symmetry can be exploited. For applications, that require a high number of surface tension calculations, DFT can, however, still be too slow. Possible applications where this applies are simultaneous process and solvent design[43], and also the multiobjective parameter estimations, that we are concerned with in this work.

6.3 Predictive density gradient theory

As a simple function of temperature, the surface tension can be modeled using a variety of models. To be able to make a prediction, however, it is necessary to have a description consistent with the bulk equation of state. A step towards this direction presents density gradient theory (DGT), often also referred to as square gradient theory. The concept was already published by Van der Waals[44] and later refined by Cahn and Hilliard[45]. Later, the approach was coupled with molecular and cubic equations of state to attain a reliable model to extrapolate surface tensions for pure components[46–49] and mixtures[50–55]. In DGT, the Helmholtz energy consists of a contribution from the local Helmholtz energy density $f(\boldsymbol{\rho})$, that is only a function (not a functional) of the local density profile $\boldsymbol{\rho}(\mathbf{r})$, and a correction for inhomogeneous systems, that contains the gradient of the density profiles $\nabla\boldsymbol{\rho}$ and the

so-called influence matrix $\boldsymbol{C}$, as

$$F = \int \left(f(\boldsymbol{\rho}) + \nabla \boldsymbol{\rho}^{\intercal} \boldsymbol{C} \nabla \boldsymbol{\rho} \right) d\mathbf{r}. \tag{6.5}$$

In the standard approach, the pure component entries of the influence matrix $\boldsymbol{c} = \mathrm{diag}(\boldsymbol{C})$ are either fitted to experimental surface tension data or correlated with parameters of the equation of state. The remaining matrix elements are often approximated using the geometric combining rule $\boldsymbol{C} = \sqrt{\boldsymbol{c}\boldsymbol{c}^{\intercal}}$.

The necessity to determine an additional parameter for each component is eliminated in predictive density gradient theory (pDGT[, see chapter 5]). Starting from a non-local Helmholtz energy functional, as used in DFT, an expression for the influence matrix is derived as

$$\boldsymbol{C} = -\sum_{\alpha\beta} \left(\frac{\partial^2 f}{\partial n_\alpha \partial n_\beta} \right)^{(0)} \left(\boldsymbol{\omega}_\alpha^{(2)} \boldsymbol{\omega}_\beta^{(0)\intercal} + \boldsymbol{\omega}_\alpha^{(0)} \boldsymbol{\omega}_\beta^{(2)\intercal} \right). \tag{6.6}$$

The weights

$$\boldsymbol{\omega}_\alpha^{(0)} = 4\pi \int_0^\infty \boldsymbol{\omega}_\alpha(r) r^2 dr \tag{6.7}$$

and

$$\boldsymbol{\omega}_\alpha^{(2)} = \frac{2}{3}\pi \int_0^\infty \boldsymbol{\omega}_\alpha(r) r^4 dr \tag{6.8}$$

only depend on temperature and the second partial derivatives of the Helmholtz energy density are evaluated using local bulk weighted densities $n_\alpha^{(0)} = \boldsymbol{\rho} \cdot \boldsymbol{\omega}_\alpha^{(0)}$. Therefore, the influence matrix can be evaluated locally as a simple function of temperature and density. Since pDGT yields all elements of the influence matrix, no combining rule is necessary to model interfacial tensions of mixtures. However, [in chapter 5] it was shown that to avoid the solution of a boundary value problem, the off-diagonal elements of the influence matrix can be approximated using the geometric combining rule, thus transforming the problem into the solution of an algebraic equation. If the geometric combining rule is used, the surface tension in DGT and pDGT can be calculated by applying a coordinate transform from the physical axis to a path function s[56,57]. The path function has to be monotonous in the interfacial region; in the simplest case it can be the density of a reference component. The surface tension follows as the integral over the path function from its value in the vapor phase s^V to its value in the

liquid phase s^L, as

$$\gamma = \int_{s^V}^{s^L} \sqrt{2(f - \boldsymbol{\rho} \cdot \boldsymbol{\mu} + p)} \left(\sqrt{\boldsymbol{c}} \cdot \frac{d\boldsymbol{\rho}}{ds} \right) ds. \tag{6.9}$$

To be able to solve this integral, the densities of all components have to be calculated iteratively for every value of the path function. This calculation slows the computation and particularly for pDGT, which requires expensive evaluations of the second partial derivatives of the Helmholtz energy density, the speed advantage compared to DFT dwindles. This disadvantage is absent in the one component case, where the density of the single component can be chosen as path function. In this case, no iteration is necessary and the surface tension can be calculated directly from

$$\gamma = \int_{\rho^V}^{\rho^L} \sqrt{2c(f - \rho\mu + p)} d\rho. \tag{6.10}$$

With the explicit expression for the influence parameter from pDGT, surface tensions of pure components can be predicted swiftly (i.e. in the order of milliseconds) solely based on the pure component properties of the underlying equation of state.

6.4 PCP-SAFT

The Helmholtz energy functional used in this work is based on the PCP-SAFT equation state and was already described in previous work[38]. Since we are focused on the surface tension of pure components in this work, we present concise expressions for the properties needed in eq. (6.10) to calculate the surface tension of a pure component using pDGT with PCP-SAFT. The Helmholtz energy density is split in contributions from different interactions, as

$$f = f^{\mathrm{ig}} + f^{\mathrm{hs}} + f^{\mathrm{chain}} + f^{\mathrm{disp}} + f^{\mathrm{polar}} + f^{\mathrm{assoc}}. \tag{6.11}$$

Equation (6.6) is linear in the Helmholtz energy density. Therefore, the influence parameter can also be written as a sum over contributions,

$$c = c^{\mathrm{ig}} + c^{\mathrm{hs}} + c^{\mathrm{chain}} + c^{\mathrm{disp}} + c^{\mathrm{polar}} + c^{\mathrm{assoc}}. \tag{6.12}$$

Ideal gas

The ideal gas contribution to the Helmholtz energy density of a pure component is known from statistical mechanics as

$$\beta f^{\mathrm{ig}} = \rho\left(\ln\left(\rho\Lambda^3\right) - 1\right) \tag{6.13}$$

with the inverse temperature $\beta = \frac{1}{kT}$ and the overall molecular thermal de Broglie wavelength $\Lambda(T)$ which incorporates the entire single molecule partition sum. Since Λ also appears in the chemical potential in eq. (6.10), its value has no influence on the surface tension and can be ignored. The ideal gas contribution has no non-local parts, hence its contribution to the influence parameter vanishes; $c^{\mathrm{ig}} = 0$.

Hard spheres

The Helmholtz energy density contribution for the hard spheres is equal to the residual Helmholtz energy density of the Carnahan-Starling equation of state[58] times the segment number m,

$$\beta f^{\mathrm{hs}} = m\rho\frac{4\eta - 3\eta^2}{(1-\eta)^2} \tag{6.14}$$

with the packing fraction $\eta = \frac{1}{6}\pi m d^3\rho$ and the temperature dependent segment diameter[7]

$$d = \sigma\left(1 - 0.12\exp\left(-\frac{3\varepsilon}{kT}\right)\right). \tag{6.15}$$

The influence parameter depends on the choice of Helmholtz energy functional used. The most common ones are the White-Bear or modified fundamental measure theory[31,32], with

$$\beta c^{\mathrm{hs,WB}} = -\frac{\pi m^2 d^5}{180}\left(\frac{29 - 34\eta + 17\eta^2 - 3\eta^3}{(1-\eta)^4} + \frac{5}{\eta}\ln(1-\eta)\right) \tag{6.16}$$

and the Kierlik-Rosinberg version[59], with

$$\beta c^{\mathrm{hs,KR}} = -\frac{\pi m^2 d^5}{120}\frac{16 - 11\eta - 2\eta^2 + 3\eta^3}{(1-\eta)^4}. \tag{6.17}$$

[As shown in figure 5.1], the difference between the two models is negligible.

Hard chains

For a pure component, the hard chain contribution to the PCP-SAFT equation of state can be written compactly as

$$\beta f^{\text{chain}} = -(m-1)\rho \ln\left(\frac{1-\frac{\eta}{2}}{(1-\eta)^3}\right). \tag{6.18}$$

The corresponding expression for the influence parameter is

$$\beta c^{\text{chain}} = \frac{\pi}{30} d^5 m(m-1)\left(\frac{3}{(1-\eta)^2} - \frac{2}{(2-\eta)^2}\right). \tag{6.19}$$

Dispersive and polar attraction

Both dispersive and polar attraction is modeled using a weighted density approach with the same weight function[38]. The Helmholtz energy density follows directly from the PCP-SAFT equation of state[7,60,61], as

$$\beta f^{\text{disp}} + \beta f^{\text{polar}} = \rho\left(\tilde{a}^{\text{disp}} + \tilde{a}^{\text{polar}}\right) \tag{6.20}$$

where $\tilde{a} = \frac{A}{NkT}$ denotes a dimensionless Helmholtz energy[7]. The influence parameter requires the derivative of the chemical potential contributions with respect to the density, as

$$\beta c^{\text{disp}} + \beta c^{\text{polar}} = \frac{1}{5}\psi^2 d^2 \left(\frac{\partial\left(\beta\mu^{\text{disp}} + \beta\mu^{\text{polar}}\right)}{\partial\rho}\right)_T \tag{6.21}$$

The implementation of these second partial derivatives is tedious and error prone. It can be automated with an acceptable loss in performance and no loss in precision using automatic differentiation with hyperdual numbers[62]. The ψ parameter was introduced by Sauer et al.[38] as an effective range of attractive interactions. [In chapter 5], for pDGT its value was redetermined as $\psi_{pDGT} = 1.3286$.

Association

For the association contribution, that was not included in [chapter 5], we use the functional by Yu and Wu[35] adapted to the PCP-SAFT equation of state. For a pure component, the

Helmholtz energy density is

$$\beta f^{\text{assoc}} = \rho \sum_A N_A \left(\ln \chi^A - \frac{\chi^A}{2} + \frac{1}{2} \right) \tag{6.22}$$

with N_A the number of association sites of kind A and χ^A the corresponding fraction of unbounded sites. The model is generic with respect to the association scheme. The 2B model is attained with $N_A = N_B = 1$, the 3B model corresponds to $N_A = 2$, $N_B = 1$ and the 4C model means $N_A = N_B = 2$. If only two types of association sites are considered (as is the case for the 2B, 3B and 4C schemes), the fractions of unbounded sites can be calculated analytically, as

$$\chi^A = \frac{\sqrt{(1+\rho k y (N_A - N_B))^2 + 4\rho k y N_B} + \rho k y (N_A - N_B) - 1}{2\rho k y N_A} \tag{6.23}$$

and

$$\chi^B = 1 + \frac{N_A}{N_B}(\chi^A - 1) \tag{6.24}$$

with the effective association volume

$$k = \sigma^3 \kappa^{AB} \left(\exp\left(\frac{\varepsilon^{AB}}{kT} \right) - 1 \right) \tag{6.25}$$

and the cavity correlation function at contact

$$y = \frac{1 - \frac{\eta}{2}}{(1-\eta)^3}. \tag{6.26}$$

The influence parameter for this case can be calculated as

$$\beta c^{\text{assoc}} = N_A N_B \chi^A \chi^B d^2 k \left(f_1(\eta) - \frac{\chi^A + \chi^B}{\chi^A + \chi^B - \chi^A \chi^B} f_2(\eta) \right) - \frac{d^2}{18\rho} \left(N_A \ln \chi^A + N_B \ln \chi^B \right) \tag{6.27}$$

with

$$f_1(\eta) = \frac{16\eta^5 - 100\eta^4 + 227\eta^3 - 200\eta^2 + 30\eta}{180(2-\eta)(1-\eta)^5} \tag{6.28}$$

and

$$f_2(\eta) = \frac{2\eta^5 - 13\eta^4 + 20\eta^3 + 16\eta^2 - 32\eta - 20}{120(2-\eta)(1-\eta)^5}. \tag{6.29}$$

The derivation of this closed form expression for the influence parameter of the association contribution is an adventurous endeavor, that we exercise in [appendix B.1].

6.5 Pareto optimization

To obtain a comprehensive comparison between different association schemes, we follow the approach by Forte et al.[16] and perform a pareto analysis. In our case, the first objective function is the relative average absolute deviation (AAD) of bulk equilibrium properties (vapor pressures and saturated liquid densities)

$$\mathrm{AAD}_{\mathrm{vle}} = \frac{1}{n_p}\sum_i \frac{\left|p_i^{\mathrm{sat,calc}} - p_i^{\mathrm{sat,exp}}\right|}{p_i^{\mathrm{sat,exp}}} + \frac{1}{n_\rho}\sum_i \frac{\left|\rho_i^{\mathrm{l,sat,calc}} - \rho_i^{\mathrm{l,sat,exp}}\right|}{\rho_i^{\mathrm{l,exp}}}. \tag{6.30}$$

For water, since experimental data is abundant, we also include liquid and supercritical densities in the fit. Because the surface tension becomes zero at the critical point, relative errors can become divergingly large and thus bias the fit towards values close to the critical point. To avoid this bias, for surface tensions, we define the AAD

$$\mathrm{AAD}_{\mathrm{sft}} = \frac{1}{n_\gamma}\sum_i \left|\gamma_i^{\mathrm{calc}} - \gamma_i^{\mathrm{exp}}\right| \tag{6.31}$$

as the second objective function.

The pareto fronts were calculated using the pygmo optimization suite[63] and the MOEA/D algorithm provided within. The solver uses a derivative free, global optimization approach and is thus independent of initial values for the parameters. We recommend this approach for these kind of optimization problems, with particularly expensive function evaluations and the possibility of local minima due to small numerical uncertainties in the evaluation of the integral in eq. (6.10) and the degeneracy of the parameters. Further, we want to be able to search for minima in a large parameter space. This will always lead to parameter combinations for which the influence parameter becomes negative or no vapor-liquid equilibrium can be calculated. With a derivative free algorithm, these parameter combinations can be simply suppressed by returning a large residual. In comparison, Jacobian-based algorithms tend to have a faster convergence speed close to the solution, but generally require continuous optimization problems.

For water, pseudo-experimental data is available based on the IAPWS formulations through NIST[64]. For alcohols, data is less abundant. Using unfiltered or unweighted experimental data introduces a bias towards lower temperatures, for which more experimental data is

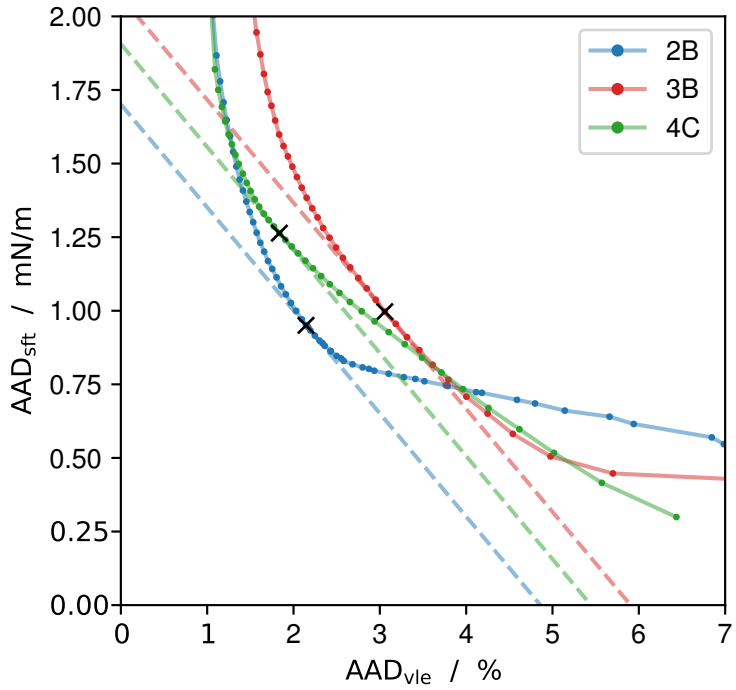

Figure 6.1: Pareto fronts for water and the PC-SAFT equation of state. The highlighted points represent the parameter sets, that are shown in table 6.1. They are picked by specifying the slope of the front, visualized by the tangents (dashed lines).

available. Therefore, we use the correlations recommended by Mulero et al.[65] for the surface tension and DIPPR correlations[66] for vapor pressures and saturated liquid densities. For water and 1-alcohols up to 1-decanol, data points are selected in equidistant steps in the range between the triple point and the critical point. For the other alcohols, the temperature range is reduced according to the availability of experimental data.

6.6 Results and discussion

6.6.1 Water

For water, pareto fronts for the three most prevalent association models 2B, 3B and 4C were calculated. The results are shown in figure 6.1, where the average absolute deviation (AAD) of the surface tension is shown versus the relative AAD of bulk phase properties, that contain vapor pressures and liquid densities at equilibrium and sub- and supercritical isotherms. Each point on the line represents the lower left corner of an area that it dominates. The union of these areas is bounded by the pareto front.

The analysis allows a comprehensive comparison between different models. In this case, we

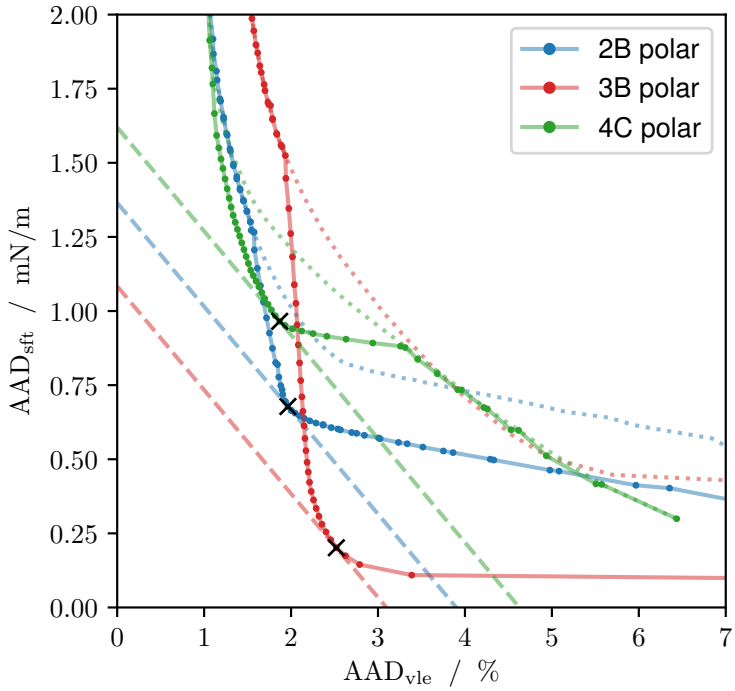

Figure 6.2: Pareto fronts for water and the PCP-SAFT equation of state with a fitted dipole moment. The results for PC-SAFT (dotted lines) are kept as reference. The highlighted points represent the parameter sets, that are shown in table 6.1. They are picked by specifying the slope of the front, visualized by the tangents (dashed lines).

observe, that in the most relevant part of the front, where a compromise between the two objectives is made, the 2B model performs best. We can also compare different equations of state or additional Helmholtz energy contributions. Therefore, in figure 6.2 the analysis is repeated using the PCP-SAFT equation of state with a fitted dipole moment. As reference, the pareto fronts of the PC-SAFT equation of state are kept as dotted lines. Due to the additional degree of freedom, the residuals can be decreased significantly; especially for the residual with respect to surface tensions.

An interesting observation can be made by examining figure 6.2: The question which association model to use is inconclusive for water. In fact, every one of the three models considered dominates the other two in some part of the diagram. The 4C model performs better than the others if the focus is on obtaining small residuals for the bulk properties, whereas the 3B model clearly reproduces the surface tensions best. Between these two ends, the 2C scheme is dominating in a small part of the curve. This behavior can not be observed by just performing a single objective optimization with fixed weights for the surface tension and bulk residuals respectively. Nevertheless, it is at one point necessary to choose a point on the front to work with. The choice can be made by finding the point with the smallest value of the weighted

equation of state	association scheme	M_i (g/mol)	m_i	σ_{ii} (Å)	ε_{ii}/k (K)	μ (D)	$\kappa^{A_iB_i}$	$\varepsilon^{A_iB_i}/k$ (K)
PC-SAFT	2B	18.015	1.0000	2.9375	272.03		0.044480	3125.3
	3B	18.015	1.6330	2.4570	238.32		0.037807	2749.0
	4C	18.015	1.8668	2.3950	169.78		0.133738	1772.0
PCP-SAFT	2B	18.015	1.0000	3.0054	166.61	1.6152	0.098194	2667.3
	3B	18.015	1.0488	2.9896	115.19	1.9374	0.038236	2377.9
	4C	18.015	1.2808	2.8129	117.78	1.5050	0.082907	1784.1

Table 6.1: Pure-component parameters for the PC(P)-SAFT equation of state for water.

equation of state	association scheme	$\mathrm{AAD}_{\mathrm{vle}}$ (%)	$\mathrm{AAD}_{\mathrm{pDGT}}$ ($\mathrm{mNm^{-1}}$)	$\mathrm{AAD}_{\mathrm{DFT}}$ ($\mathrm{mNm^{-1}}$)	T range (K)
PC-SAFT	2B	2.14	0.95	1.59	273 - 1073
	3B	3.06	1.00	1.14	273 - 1073
	4C	1.84	1.26	1.81	273 - 1073
PCP-SAFT	2B	1.96	0.68	1.27	273 - 1073
	3B	2.52	0.20	1.41	273 - 1073
	4C	1.87	0.97	2.12	273 - 1073

Table 6.2: AAD for the water parameters in table 6.1 and temperature range of experimental data.

AAD defined by

$$\mathrm{AAD}_w = \frac{\mathrm{AAD}_{\mathrm{sft}}}{\mathrm{ref}_{\mathrm{sft}}} + \frac{\mathrm{AAD}_{\mathrm{vle}}}{\mathrm{ref}_{\mathrm{vle}}}. \tag{6.32}$$

where values for $\mathrm{ref}_{\mathrm{sft}}$ and $\mathrm{ref}_{\mathrm{vle}}$ define weights for the two objectives. The choice of weights is somewhat arbitrary. For the water parameters, we use $\mathrm{ref}_{\mathrm{vle}} = 2\%$ and $\mathrm{ref}_{\mathrm{sft}} = 0.7\,\mathrm{mN\,m^{-1}}$ (2% of an average surface tension value of $35\,\mathrm{mN\,m^{-1}}$). Visually, we are looking for the tangent to the pareto front with the gradient $-\frac{\mathrm{ref}_{\mathrm{sft}}}{\mathrm{ref}_{\mathrm{vle}}}$. These tangents and the corresponding points on the pareto front are also shown as dashed lines in figures 6.1 and 6.2. The shape of the pareto front allows us now to evaluate whether the parameters we obtain are robust with respect to the choice of weights $\mathrm{ref}_{\mathrm{sft}}$ and $\mathrm{ref}_{\mathrm{vle}}$. If the curvature of the pareto fronts surrounding the chosen point is high, as is the case for the 2B polar model, a change of the weights will barely alter the parameters. Then the arbitrariness introduced with a choice for weights only weakly affects the proposed parameters.

The parameters corresponding to each of the three highlighted points in figures 6.1 and 6.2 are shown in table 6.1 with the corresponding AADs in table 6.2. For both equations of state, the 2B model reaches the lower bound of $m = 1$ in the vicinity of the optimum. This has the added value, that the parameter set can also be used effortlessly in a heterosegmented

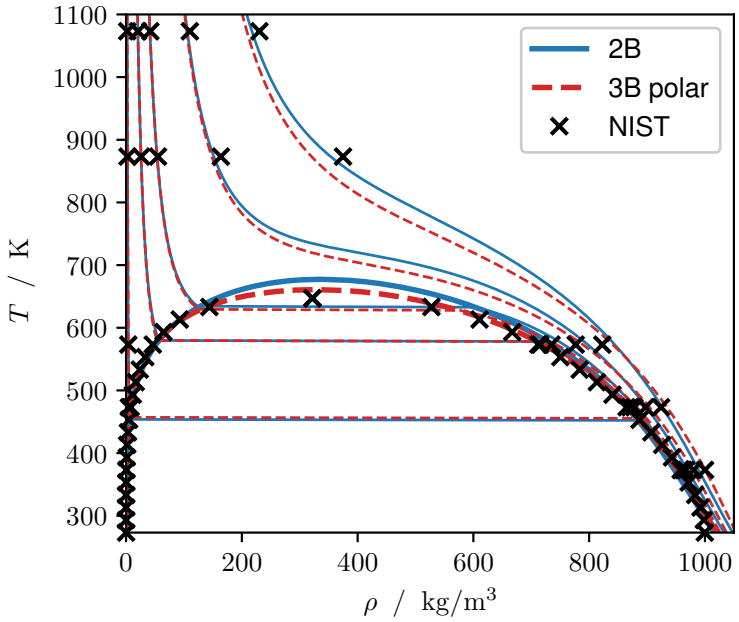

Figure 6.3: Phase diagram including isobars between 10 bar and 1000 bar for water. Comparison of PC(P)-SAFT results with reference data[64].

approach where chain formation is accounted for by actual segments and not a real valued chain length parameter m[67]. The fitted values of the dipole moment are close to the known ideal gas value for water of 1.8546 D. This suggests not optimizing the value and instead using the literature value instead. We decided against this approach for two reasons. First, due to its polarizability, the effective dipole moment of water is significantly higher in condensed phases[68] and we are mostly concerned with the properties of liquid water. Secondly, the association and dipole contribution in PCP-SAFT are modeled independently of each other, although, in fact, they are coupled. Most fluids are dominated by one of the two. We show in the subsequent section that this is the case for alcohols. Water once again is an exception, as we see that including a dipole moment improves the results. Due to these circumstances, we prefer to treat the effective dipole moment as adjustable, not defined as the ideal gas dipole moment known from quantum mechanics.

The phase diagram in figure 6.3 shows the phase envelope and a subset of the isobars used in the parameter estimation for two of the parameter sets in table 6.1: The 2B model for PC-SAFT and the 3B model for PCP-SAFT. Differences between the models are visible in the description of the critical point and the surrounding region. Both models compare well to the reference values obtained from NIST[64].

In figure 6.4, the corresponding surface tensions are shown. The 3B polar model reproduces the reference values better at temperatures close to the triple point and close to the critical

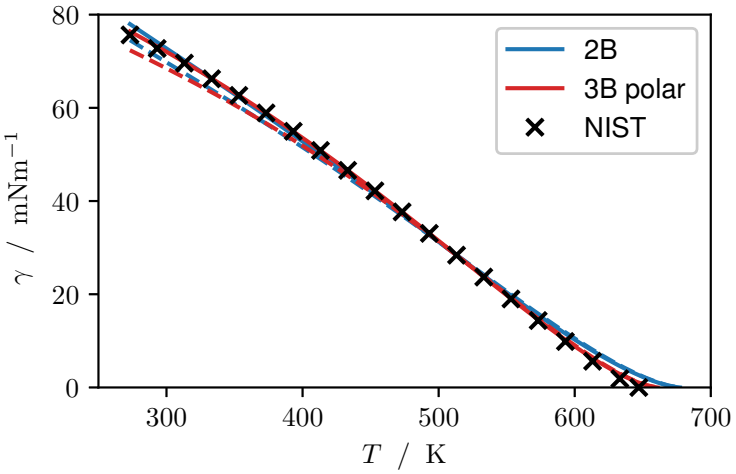

Figure 6.4: Surface tension of water. pDGT results (full lines) and DFT results (dashed lines) compared to reference data[64].

point. The figure also includes the results obtained from full density functional theory (DFT) in dashed lines. At low temperatures, pDGT tends to overpredict surface tensions compared to DFT, with the DFT results being closer to experimental data for non-associating components. This behavior now leads to an slight underprediction of the surface tension by DFT. Still, we can argue that the parameters obtained with pDGT can also be used with DFT to model interfacial phenomena like adsorption and water surfactant systems.

6.6.2 Alcohols

For linear alcohols up to 1-decanol, experimental data is available in the whole range from the triple point to the critical point. To obtain comparable data sets for all components, we use auxiliary models for the surface tension[65], the vapor pressure[66], and the liquid density[66] at equilibrium, that themselves are fitted to experimental data and discretize them along the temperature. The set of quasi-data compiled from these correlations is used to generate pareto fronts analogously to the study with water. The results for linear alcohols are shown in figure 6.5. The figures only include results for the non-polar PC-SAFT equation of state. The curves from calculations, where the dipole moment was included as adjustable parameter, are almost undistinguishable from the ones presented in figure 6.5. Therefore we do not consider using dipole moments to model alcohols. The full results are shown in [appendix B.2].

The pareto fronts in figure 6.5 show a clear progression moving along the homologous series. For small alcohols, the 4C model is clearly superior. At this point, we have to acknowledge that it is rather unusual to model primary alcohols using the 4C association scheme, because the scheme would indicate, that there are two hydrogen bond donor sites and two hydrogen bond

component	association scheme	M_i g/mol	m_i	σ_{ii} (Å)	ε_{ii}/k (K)	$\kappa^{A_iB_i}$	$\varepsilon^{A_iB_i}/k$ (K)
methanol	4C	32.042	2.4858	2.7309	101.08	0.119535	1834.8
ethanol	4C	46.069	3.0177	2.9146	124.58	0.100676	1810.4
1-propanol	4C	60.096	2.7558	3.3114	144.38	0.058107	1959.8
1-butanol	4C	74.123	3.3182	3.3476	163.66	0.072169	1862.1
1-pentanol	4C	88.150	3.2860	3.5783	179.75	0.076252	1824.6
1-hexanol	2B	102.177	3.3312	3.7483	270.86	0.002566	2778.9
1-heptanol	2B	116.203	4.2509	3.6209	252.76	0.003061	2700.9
1-octanol	2B	130.230	4.0012	3.8282	268.73	0.003110	2804.3
1-nonanol	2B	144.257	4.0471	3.9424	278.68	0.001491	3103.7
1-decanol	2B	158.284	4.1859	4.0421	281.29	0.002493	3023.6
1-dodecanol	2B	186.338	5.1403	3.9771	274.55	0.001267	3223.4
2-propanol	4C	60.096	3.7734	2.9580	136.16	0.097627	1718.8
2-butanol	4C	74.123	4.8327	2.9057	149.97	0.162615	1469.6
2-pentanol	4C	88.150	4.2950	3.2254	159.25	0.078709	1771.4
3-pentanol	4C	88.150	4.5094	3.1583	162.73	0.121993	1516.1
1,2-ethanediol	4C	62.068	2.2063	3.3447	211.90	0.041208	2550.3
1,2-propanediol	4C	76.095	3.4856	3.0837	183.10	0.084996	2268.8
glycerol	4C	92.095	2.2941	3.6607	299.78	0.019562	3069.7

Table 6.3: Pure-component parameters for the PC-SAFT equation of state for alcohols.

acceptor sites. Despite this not being the case for monohydric alcohols, the improvement in the fit based on the result in figure 6.5 is unquestionable, especially for methanol and ethanol. For the choice of parameters within the pareto front of the 4C model, the same approach as for water was used with different weights $\mathrm{ref}_{\mathrm{vle}} = 2\%$ and $\mathrm{ref}_{\mathrm{sft}} = 1.5\,\mathrm{mN\,m^{-1}}$. For longer alcohols, starting from 1-butanol, the results are less conclusive regarding the best association scheme and the advantage, that the 4C scheme has over the others dwindles. For chains larger than 1-pentanol, the aforementioned weights would lead to undesirably high residuals in the bulk equilibrium properties. In fact, in the optimizations a point emerges beyond which no further reduction in the residual of the surface tension is possible. In the vicinity of this point, the 2B model, which is also a popular choice for longer alcohols, has a slight edge. To obtain this point, we increase the surface tension weight to $\mathrm{ref}_{\mathrm{sft}} = 3\,\mathrm{mN\,m^{-1}}$. Due to the sharp bend in the profile, however, the exact value of this weight is not particularly important. The shape of the pareto fronts for large alcohols suggests, that the homosegmented approach is not well suited to describe these systems. Due to the amphiphilic character of the alcohols, a weak structuring at the interface can be expected. To model this structuring, an approach that captures the density of individual segments is required.[67,69]

The parameters belonging to the highlighted points in figure 6.5 are displayed in table 6.3 with the corresponding AADs and temperature ranges in table 6.4. Both tables also include

component	association scheme	AAD_{vle} (%)	AAD_{pDGT} mNm^{-1}	AAD_{DFT} mNm^{-1}	T range (K)
methanol	4C	4.00	0.89	0.68	176 - 509
ethanol	4C	2.51	1.38	1.07	180 - 503
1-propanol	4C	4.15	0.95	0.65	223 - 533
1-butanol	4C	4.94	1.14	0.88	245 - 558
1-pentanol	4C	3.64	0.80	0.51	273 - 573
1-hexanol	2B	0.76	4.16	3.90	243 - 603
1-heptanol	2B	1.85	3.16	1.93	258 - 623
1-octanol	2B	1.51	2.68	2.40	258 - 633
1-nonanol	2B	1.88	2.36	2.06	273 - 653
1-decanol	2B	1.63	1.85	1.54	283 - 683
1-dodecanol	2B	0.64	3.46	2.90	298 - 353
2-propanol	4C	3.23	0.97	0.94	273 - 353
2-butanol	4C	5.39	1.14	1.09	273 - 367
2-pentanol	4C	1.53	0.20	0.09	273 - 333
3-pentanol	4C	0.29	0.01	0.15	273 - 333
1,2-ethanediol	4C	3.61	1.39	1.76	264 - 471
1,2-propanediol	4C	1.75	1.56	1.21	293 - 453
glycerol	4C	2.33	0.69	2.58	293 - 475

Table 6.4: AAD for the alcohol parameters in table 6.3 and temperature range of experimental data.

results for those secondary and polyhydric alcohols for which experimental data is available. The full results for these components are shown [in appendix B.2]. Again, the 4C model is able to reproduce the quasi experimental data best. The remarkably small residuals for some components like 3-pentanol can be attributed to the smaller temperature range for which experimental data is present.

6.7 Conclusion

Predictive density gradient theory was used to perform a multiobjective optimization for PCP-SAFT parameters with the surface tension as one objective function and bulk phase equilibrium properties (vapor pressure and liquid densities) as the second objective. The method was used to quantitatively compare different models. For water, the model results can be improved significantly by including a dipole moment in the parameter optimization. The comparison between different association schemes is inconclusive, in the sense that the optimal association scheme changes along the pareto front. Residuals in bulk properties are lower for the 2B and 4C schemes, whereas the 3B scheme performs better if the focus is on

low residuals in surface tensions.

For small alcohols, we find that the 4C association scheme clearly delivers the best results, although a 4C scheme is not conform to our chemical intuition and experience. For longer alcohols, the analysis shows, that it is difficult to obtain a good compromise between bulk phase properties and surface tensions. The residual with respect to surface tensions can only be reduced at the expense of the description of bulk properties. This limitation points to a weakness of the model, that assumes a homosegmented chain molecule.

The calculation of the surface tension with predictive density gradient theory requires evaluations of the Helmholtz energy in the metastable and unstable regions of the phase diagram. Thus, we argue that the inclusion of experimental surface tension data increases the robustness of the PCP-SAFT parameters. Therefore, the parameters published are predestined but not restricted to usage in studies of interfacial phenomena. This includes the adsorption in porous media[70,71] and nucleation phenomena for which water and alcohols are prevalent components in studies[72].

References

[1] W. G. Chapman, G. Jackson, and K. E. Gubbins. Phase equilibria of associating fluids. *Molecular Physics*, **65**(5):1057–1079, 1988. doi:10.1080/00268978800101601.

[2] W. G. Chapman, K. E. Gubbins, G. Jackson, and M. Radosz. SAFT: Equation-of-state solution model for associating fluids. *Fluid Phase Equilibria*, **52**:31–38, 1989.

[3] W. G. Chapman, K. E. Gubbins, G. Jackson, and M. Radosz. New reference equation of state for associating liquids. *Industrial & Engineering Chemistry Research*, **29**(8):1709–1721, 1990. doi:10.1021/ie00104a021.

[4] S. H. Huang and M. Radosz. Equation of state for small, large, polydisperse, and associating molecules. *Industrial & Engineering Chemistry Research*, **29**(11):2284–2294, 1990. doi:10.1021/ie00107a014.

[5] A. Gil-Villegas, A. Galindo, P. J. Whitehead, S. J. Mills, G. Jackson, and A. N. Burgess. Statistical associating fluid theory for chain molecules with attractive potentials of variable range. *The Journal of Chemical Physics*, **106**(10):4168–4186, 1997. doi:10.1063/1.473101.

[6] F. J. Blas and L. F. Vega. Prediction of Binary and Ternary Diagrams Using the Statistical Associating Fluid Theory (SAFT) Equation of State. *Industrial & Engineering Chemistry Research*, **37**(2):660–674, 1998. doi:10.1021/ie970449+.

[7] J. Gross and G. Sadowski. Perturbed-Chain SAFT: An Equation of State Based on a Perturbation

Theory for Chain Molecules. *Industrial & Engineering Chemistry Research*, **40**(4):1244–1260, 2001. doi:10.1021/ie0003887.

[8] T. Lafitte, A. Apostolakou, C. Avendaño, A. Galindo, C. S. Adjiman, E. A. Müller, and G. Jackson. Accurate statistical associating fluid theory for chain molecules formed from Mie segments. *The Journal of Chemical Physics*, **139**(15):154504, 2013. doi:10.1063/1.4819786.

[9] E. A. Müller and K. E. Gubbins. Molecular-Based Equations of State for Associating Fluids: A Review of SAFT and Related Approaches. *Industrial & Engineering Chemistry Research*, **40**(10):2193–2211, 2001. doi:10.1021/ie000773w.

[10] I. G. Economou. Statistical Associating Fluid Theory: A Successful Model for the Calculation of Thermodynamic and Phase Equilibrium Properties of Complex Fluid Mixtures. *Industrial & Engineering Chemistry Research*, **41**(5):953–962, 2002. doi:10.1021/ie0102201.

[11] S. P. Tan, H. Adidharma, and M. Radosz. Recent Advances and Applications of Statistical Associating Fluid Theory. *Industrial & Engineering Chemistry Research*, **47**(21):8063–8082, 2008. doi:10.1021/ie8008764.

[12] C. McCabe and A. Galindo. *Applied thermodynmics of fluids*, chapter 8: SAFT associating fluids and fluid mixtures, pages 215–279. RSC, 2010.

[13] X. Liang, I. Tsivintzelis, and G. M. Kontogeorgis. Modeling Water Containing Systems with the Simplified PC-SAFT and CPA Equations of State. *Industrial & Engineering Chemistry Research*, **53**(37):14493–14507, 2014. doi:10.1021/ie501993y.

[14] L. Vega and F. Llovell. Review and new insights into the application of molecular-based equations of state to water and aqueous solutions. *Fluid Phase Equilibria*, **416**:150 – 173, 2016. doi:https://doi.org/10.1016/j.fluid.2016.01.024. Special Issue: SAFT 2015.

[15] A. de Villiers, C. Schwarz, A. Burger, and G. Kontogeorgis. Evaluation of the PC-SAFT, SAFT and CPA equations of state in predicting derivative properties of selected non-polar and hydrogen-bonding compounds. *Fluid Phase Equilibria*, **338**:1 – 15, 2013. doi:https://doi.org/10.1016/j.fluid.2012.09.035.

[16] E. Forte, J. Burger, K. Langenbach, H. Hasse, and M. Bortz. Multi-criteria optimization for parameterization of SAFT-type equations of state for water. *AIChE Journal*, **64**(1):226–237, 2018. doi:10.1002/aic.15857.

[17] K. Albers, M. Heilig, and G. Sadowski. Reducing the amount of PCP-SAFT fitting parameters. 2. Associating components. *Fluid Phase Equilibria*, **326**:31 – 44, 2012. doi:https://doi.org/10.1016/j.fluid.2012.04.014.

[18] M. Umer, K. Albers, G. Sadowski, and K. Leonhard. PC-SAFT parameters from ab initio calculations. *Fluid Phase Equilibria*, **362**:41 – 50, 2014. doi:https://doi.org/10.1016/j.fluid.2013.08.037. Special Issue on PPEPPD 2013.

[19] T. Lafitte, M. M. Piñeiro, J.-L. Daridon, and D. Bessières. A Comprehensive Description of Chemical Association Effects on Second Derivative Properties of Alcohols through a SAFT-VR Approach. *The Journal of Physical Chemistry B*, **111**(13):3447–3461, 2007. doi:10.1021/jp0682208. PMID: 17388508.

[20] P. C. Tybjerg, G. M. Kontogeorgis, M. L. Michelsen, and E. H. Stenby. Phase equilibria modeling of methanol-containing systems with the CPA and sPC-SAFT equations of state. *Fluid Phase Equilibria*, **288**(1):128 – 138, 2010. doi:https://doi.org/10.1016/j.fluid.2009.10.021.

[21] D. B. Macleod. On a relation between surface tension and density. *Trans. Faraday Soc.*, **19**:38–41, 1923. doi:10.1039/TF9231900038.

[22] D. Fu and J. Wu. Vapor–Liquid Equilibria and Interfacial Tensions of Associating Fluids within a Density Functional Theory. *Industrial & Engineering Chemistry Research*, **44**(5):1120–1128, 2005. doi:10.1021/ie049788a.

[23] G. J. Gloor, G. Jackson, F. J. Blas, E. M. del Río, and E. de Miguel. Prediction of the Vapor–Liquid Interfacial Tension of Nonassociating and Associating Fluids with the SAFT-VR Density Functional Theory. *The Journal of Physical Chemistry C*, **111**(43):15513–15522, 2007. doi:10.1021/jp072344i.

[24] E. L. Camacho Vergara, G. M. Kontogeorgis, and X. Liang. On the study of the vapor-liquid interface of associating fluids with classical density functional theory. *Fluid Phase Equilibria*, **522**:112744, 2020. doi:https://doi.org/10.1016/j.fluid.2020.112744.

[25] R. Evans. The nature of the liquid-vapour interface and other topics in the statistical mechanics of non-uniform, classical fluids. *Advances in Physics*, **28**(2):143–200, 1979. doi:10.1080/00018737900101365.

[26] H. Löwen. Density functional theory of inhomogeneous classical fluids: recent developments and new perspectives. *Journal of Physics: Condensed Matter*, **14**(46):11897, 2002. doi:10.1088/0953-8984/14/46/301.

[27] J. Wu. Density functional theory for chemical engineering: From capillarity to soft materials. *AIChE Journal*, **52**(3):1169–1193, 2006. doi:10.1002/aic.10713.

[28] E. Sauer and J. Gross. Prediction of Adsorption Isotherms and Selectivities: Comparison between Classical Density Functional Theory Based on the Perturbed-Chain Statistical Associating Fluid Theory Equation of State and Ideal Adsorbed Solution Theory. *Langmuir*, **35**(36):11690–11701, 2019. doi:10.1021/acs.langmuir.9b02378. PMID: 31403314.

[29] P. Tarazona. Free-energy density functional for hard spheres. *Physical Review A*, **31**:2672–2679, 1985. doi:10.1103/PhysRevA.31.2672.

[30] Y. Rosenfeld. Free-energy model for the inhomogeneous hard-sphere fluid mixture and density-functional theory of freezing. *Physical Review Letters*, **63**:980–983, 1989.

doi:10.1103/PhysRevLett.63.980.

[31] Y.-X. Yu and J. Wu. Structures of hard-sphere fluids from a modified fundamental-measure theory. *The Journal of Chemical Physics*, **117**(22):10156–10164, 2002. doi:10.1063/1.1520530.

[32] R. Roth, R. Evans, A. Lang, and G. Kahl. Fundamental measure theory for hard-sphere mixtures revisited: the White Bear version. *Journal of Physics: Condensed Matter*, **14**(46):12063, 2002. doi:10.1088/0953-8984/14/46/313.

[33] Y.-X. Yu and J. Wu. Density functional theory for inhomogeneous mixtures of polymeric fluids. *The Journal of Chemical Physics*, **117**(5):2368–2376, 2002. doi:10.1063/1.1491240.

[34] S. Tripathi and W. G. Chapman. Microstructure of inhomogeneous polyatomic mixtures from a density functional formalism for atomic mixtures. *The Journal of Chemical Physics*, **122**(9):094506, 2005. doi:10.1063/1.1853371.

[35] Y.-X. Yu and J. Wu. A fundamental-measure theory for inhomogeneous associating fluids. *The Journal of Chemical Physics*, **116**(16):7094–7103, 2002. doi:10.1063/1.1463435.

[36] E. L. C. Vergara, G. M. Kontogeorgis, and X. Liang. A new study of associating inhomogeneous fluids with classical density functional theory. *Molecular Physics*, **0**(0):e1725668, 2020. doi:10.1080/00268976.2020.1725668.

[37] M. Müller, L. G. MacDowell, and A. Yethiraj. Short chains at surfaces and interfaces: A quantitative comparison between density-functional theories and Monte Carlo simulations. *The Journal of Chemical Physics*, **118**(6):2929–2940, 2003. doi:10.1063/1.1535893.

[38] E. Sauer and J. Gross. Classical Density Functional Theory for Liquid–Fluid Interfaces and Confined Systems: A Functional for the Perturbed-Chain Polar Statistical Associating Fluid Theory Equation of State. *Industrial & Engineering Chemistry Research*, **56**(14):4119–4135, 2017. doi:10.1021/acs.iecr.6b04551.

[39] D. E. Sullivan. Van der Waals model of adsorption. *Physical Review B*, **20**:3991–4000, 1979. doi:10.1103/PhysRevB.20.3991.

[40] P. Tarazona and R. Evans. A simple density functional theory for inhomogeneous liquids. *Molecular Physics*, **52**(4):847–857, 1984. doi:10.1080/00268978400101601.

[41] R. Stierle, E. Sauer, J. Eller, M. Theiss, P. Rehner, P. Ackermann, and J. Gross. Guide to efficient solution of PC-SAFT classical density functional theory in various coordinate systems using fast fourier and similar transforms. *Fluid Phase Equilibria*, page 112306, 2019. doi:https://doi.org/10.1016/j.fluid.2019.112306.

[42] J. Mairhofer and J. Gross. Numerical aspects of classical density functional theory for one-dimensional vapor-liquid interfaces. *Fluid Phase Equilibria*, **444**:1–12, 2017. doi:http://doi.org/10.1016/j.fluid.2017.03.023.

[43] J. Schilling, M. Lampe, J. Gross, and A. Bardow. 1-stage CoMT-CAMD: An approach for integrated design of ORC process and working fluid using PC-SAFT. *Chemical Engineering Science*, **159**:217 – 230, 2017. doi:https://doi.org/10.1016/j.ces.2016.04.048. ICAMD – Integrating Computer-Aided Molecular Design into Product and Process Design.

[44] J. Van der Waals. Thermodynamische Theorie der Kapillarität unter voraussetzung stetiger Dichteänderung. *Zeitschrift für Physikalische Chemie*, **13**(1):657–725, 1894.

[45] J. W. Cahn and J. E. Hilliard. Free Energy of a Nonuniform System. I. Interfacial Free Energy. *The Journal of Chemical Physics*, **28**(2):258–267, 1958. doi:10.1063/1.1744102.

[46] B. S. Carey, L. E. Scriven, and H. T. Davis. Semiempirical theory of surface tensions of pure normal alkanes and alcohols. *AIChE Journal*, **24**(6):1076–1080, 1978. doi:10.1002/aic.690240620.

[47] P. Cornelisse, C. Peters, and J. de Swaan Arons. Application of the Peng-Robinson equation of state to calculate interfacial tensions and profiles at vapour-liquid interfaces. *Fluid Phase Equilibria*, **82**:119 – 129, 1993. doi:https://doi.org/10.1016/0378-3812(93)87135-N.

[48] H. Kahl and S. Enders. Calculation of surface properties of pure fluids using density gradient theory and SAFT-EOS. *Fluid Phase Equilibria*, **172**(1):27 – 42, 2000. doi:https://doi.org/10.1016/S0378-3812(00)00361-7.

[49] C. Miqueu, B. Mendiboure, A. Graciaa, and J. Lachaise. Modelling of the surface tension of pure components with the gradient theory of fluid interfaces: a simple and accurate expression for the influence parameters. *Fluid Phase Equilibria*, **207**(1):225 – 246, 2003. doi:https://doi.org/10.1016/S0378-3812(03)00028-1.

[50] H. Kahl and S. Enders. Interfacial properties of binary mixtures. *Physical Chemistry Chemical Physics*, **4**:931–936, 2002. doi:10.1039/B108535M.

[51] C. Miqueu, B. Mendiboure, C. Graciaa, and J. Lachaise. Modelling of the surface tension of binary and ternary mixtures with the gradient theory of fluid interfaces. *Fluid Phase Equilibria*, **218**(2):189 – 203, 2004. doi:https://doi.org/10.1016/j.fluid.2003.12.008.

[52] C. Miqueu, B. Mendiboure, A. Graciaa, and J. Lachaise. Modeling of the Surface Tension of Multicomponent Mixtures with the Gradient Theory of Fluid Interfaces. *Industrial & Engineering Chemistry Research*, **44**(9):3321–3329, 2005. doi:10.1021/ie049086l.

[53] A. Mejía, H. Segura, L. F. Vega, and J. Wisniak. Simultaneous prediction of interfacial tension and phase equilibria in binary mixtures: An approach based on cubic equations of state with improved mixing rules. *Fluid Phase Equilibria*, **227**(2):225 – 238, 2005. doi:https://doi.org/10.1016/j.fluid.2004.10.024.

[54] F. Llovell, O. Vilaseca, N. Jung, and L. Vega. Water+1-alkanol systems: Modeling the phase, interface and viscosity properties. *Fluid Phase Equilibria*, **360**:367 – 378, 2013. doi:https://doi.org/10.1016/j.fluid.2013.10.002.

[55] J. Mairhofer and J. Gross. Modeling of interfacial properties of multicomponent systems using density gradient theory and PCP-SAFT. *Fluid Phase Equilibria*, **439**:31–42, 2017. doi:10.1016/j.fluid.2017.02.009.

[56] J. Kou, S. Sun, and X. Wang. Efficient numerical methods for simulating surface tension of multicomponent mixtures with the gradient theory of fluid interfaces. *Computer Methods in Applied Mechanics and Engineering*, **292**:92 – 106, 2015. doi:https://doi.org/10.1016/j.cma.2014.10.023. Special Issue on Advances in Simulations of Subsurface Flow and Transport (Honoring Professor Mary F. Wheeler).

[57] X. Liang, M. L. Michelsen, and G. M. Kontogeorgis. A density gradient theory based method for surface tension calculations. *Fluid Phase Equilibria*, **428**:153 – 163, 2016. doi:https://doi.org/10.1016/j.fluid.2016.06.017. Theo W. de Loos Festschrift.

[58] N. F. Carnahan and K. E. Starling. Equation of State for Nonattracting Rigid Spheres. *The Journal of Chemical Physics*, **51**(2):635–636, 1969. doi:10.1063/1.1672048.

[59] E. Kierlik and M. L. Rosinberg. Free-energy density functional for the inhomogeneous hard-sphere fluid: Application to interfacial adsorption. *Physical Review A*, **42**:3382–3387, 1990. doi:10.1103/PhysRevA.42.3382.

[60] J. Gross. An equation-of-state contribution for polar components: Quadrupolar molecules. *AIChE Journal*, **51**(9):2556–2568, 2005. doi:10.1002/aic.10502.

[61] J. Gross and J. Vrabec. An equation-of-state contribution for polar components: Dipolar molecules. *AIChE Journal*, **52**(3):1194–1204, 2006. doi:10.1002/aic.10683.

[62] J. Fike and J. Alonso. *The Development of Hyper-Dual Numbers for Exact Second-Derivative Calculations*. 2011. doi:10.2514/6.2011-886.

[63] F. Biscani and D. Izzo. esa/pagmo2: pagmo 2.15.0. 2020. doi:10.5281/zenodo.3738182.

[64] E. W. Lemmon, M. O. McLinden, and D. G. Friend. *NIST Chemistry WebBook, NIST Standard Reference Database Number 69*, chapter Thermophysical Properties of Fluid Systems. National Institute of Standards and Technology, Gaithersburg MD, 20899, ???? , http://webbook.nist.gov, (retrieved July 15, 2016).

[65] A. Mulero, I. Cachadiña, and E. L. Sanjuán. Surface Tension of Alcohols. Data Selection and Recommended Correlations. *Journal of Physical and Chemical Reference Data*, **44**(3):033104, 2015. doi:10.1063/1.4927858.

[66] R. L. Rowley, W. V. Wilding, J. L. Oscarson, Y. Yang, N. A. Zundel, T. E. Daubert, and R. P. Danner. *DIPPR Data Compilation of Pure Chemical Properties*. Design Institute for Physical Properties, 2009.

[67] J. Mairhofer, B. Xiao, and J. Gross. A classical density functional theory for vapor-liquid interfaces consistent with the heterosegmented group-contribution perturbed-chain

polar statistical associating fluid theory. *Fluid Phase Equilibria*, **472**:117 – 127, 2018. doi:https://doi.org/10.1016/j.fluid.2018.05.016.

[68] A. V. Gubskaya and P. G. Kusalik. The total molecular dipole moment for liquid water. *The Journal of Chemical Physics*, **117**(11):5290–5302, 2002. doi:10.1063/1.1501122.

[69] S. Jain, A. Dominik, and W. G. Chapman. Modified interfacial statistical associating fluid theory: A perturbation density functional theory for inhomogeneous complex fluids. *The Journal of Chemical Physics*, **127**(24):244904, 2007. doi:10.1063/1.2806932.

[70] C. Malheiro, B. Mendiboure, J.-M. Míguez, M. M. Piñeiro, and C. Miqueu. Nonlocal Density Functional Theory and Grand Canonical Monte Carlo Molecular Simulations of Water Adsorption in Confined Media. *The Journal of Physical Chemistry C*, **118**(43):24905–24914, 2014. doi:10.1021/jp505239e.

[71] E. Sauer, A. Terzis, M. Theiss, B. Weigand, and J. Gross. Prediction of Contact Angles and Density Profiles of Sessile Droplets Using Classical Density Functional Theory Based on the PCP-SAFT Equation of State. *Langmuir*, **34**(42):12519–12531, 2018. doi:10.1021/acs.langmuir.8b01985. PMID: 30247038.

[72] A. Aasen, D. Reguera, and Ø. Wilhelmsen. Curvature Corrections Remove the Inconsistencies of Binary Classical Nucleation Theory. *Physical Review Letters*, **124**:045701, 2020. doi:10.1103/PhysRevLett.124.045701.

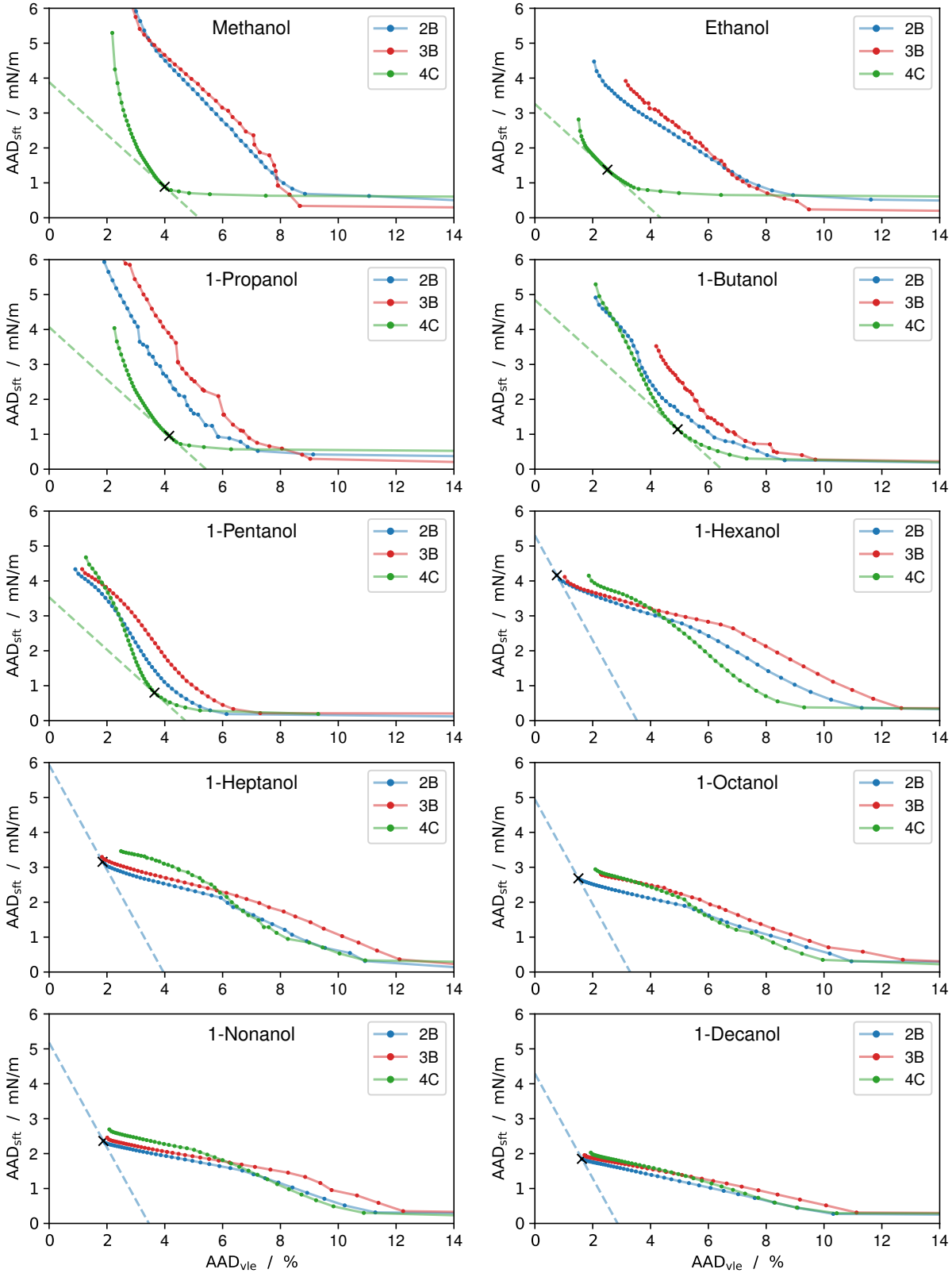

Figure 6.5: Pareto fronts for linear alcohols. Comparison between different association schemes for the PC-SAFT equation of state. The black crosses represent the parameter sets shown in table 6.3 and the dashed lines visualize the specified slope of the front.

7 Surfactant modeling using classical density functional theory and a group contribution PC-SAFT approach

The content of this chapter is reproduced with permission from

P. Rehner, B. Bursik, J. Gross. Industrial & Engineering Chemistry Research 60.19 (2021): 7111-7123.

 Additions or deletions compared to the published work are marked with angular brackets.

Models for surfactants need to incorporate the amphiphilic character of the molecules to describe key properties such as the adsorption at interfaces and the reduction of interfacial tensions. One possibility is to model the surfactant molecules as heteronuclear chains. Therefore, we revisit the heterosegmented density functional theory and present a theory consistent with the group contribution perturbed-chain statistical associating fluid theory equation of state. The model is used to study water/surfactant and water/surfactant/octane systems with surfactants from the group of polyethylene glycol alkyl ethers, a commonly used group of nonionic surfactants. The model parameters are obtained by fitting to pure component data of small surfactants. Binary interaction parameters are required to model the water/alkane subsystem and to account for the polarity of the head groups of the surfactant. The model is able to reproduce the significant enrichment of surfactant molecules at both vapor–liquid surfaces and liquid–liquid interfaces and the corresponding reduction of interfacial tensions. For liquid–liquid interfaces, the competing solubility of the surfactant in both phases has to be taken into account when searching for an optimal surfactant molecule.

7.1 Introduction

Surfactants, a blend of **surf**ace **act**ive **a**ge**nts**, constitute an important class of chemicals. They are used in a variety of industrial processes and household applications due to their significant influence on interfacial properties. The many important applications include emulsifiers in the food industry, detergents in cleaning products, soaps in personal care products, or solubilizers in the oil industry, for example, in enhanced oil recovery[1]. Surfactants generally consist of a hydrophilic head and a hydrophobic tail. Due to this amphiphilic character, surfactants adsorb at interfaces, which decreases the interfacial tension, or form complex mesostructures such as micelles or bilayers. The unfavorable interactions of hydrophilic head groups with a hydrophobic solvent (e.g., an alkane) or vice versa increase the free energy of a homogeneous solution of surfactant molecules. By adsorbing at an interface or by forming mesostructures unfavorable interactions are reduced, which lowers the free energy; although, a more ordered fluid structure entails an increase in entropy that opposes molecular order and local enrichment.

To reduce the substantial financial or temporal resources associated with the experimental studies of surfactant behavior[2,3], theoretical approaches are required. Models that are based on a molecular understanding of the surfactant molecules can improve the understanding of surfactant phenomena on a nanoscale and reduce the dependency on experimental techniques. Extensive surfactant research has been conducted using different surfactant models and theoretical frameworks. Early on, the theory of molecular thermodynamics was successfully applied to the study of surfactants[4–6] and has been improved and expanded since[7–9]. It models the free energy of quasi-isotropic micellar systems and is therefore able to predict properties such as the critical micelle concentration and surface tensions efficiently. To also obtain an understanding of the structure of micelles or surfactants adsorbed at interfaces, a statistical mechanical approach is required that is able to capture the local densities in microscopically inhomogeneous systems. In atomistic models, surfactant molecules consist of atoms or small groups of atoms. The interaction potentials between those atoms or groups explicitly include chemical bonds, bond angles, or electrostatic interactions[10]. The two main frameworks which are employed for atomistic surfactant models are molecular dynamics[11–13] and Monte Carlo[14] simulations. However, the length- and timescales for many practical systems are out of reach for atomistic simulations[15]. Coarse-grained models address this challenge by grouping together a larger number of atoms. These models can be classified based on whether the coarse-grained groups are located on a predefined lattice[10]. Both, more efficient lattice[16–18] and more realistic nonlattice[19,20] models, were applied to surfactant systems. Mesoscale approaches capture even larger time- and length scales[10]. Dissipative particle dynamics achieves this by modeling large groups of atoms and including dissipative

and random forces[21]. It was utilized to study the formation of smectic mesophases of surfactant molecules[22] and more recently to study the interfacial properties of water/octane/surfactant systems.[23] As a second mesoscale approach, lattice gas simulations are dynamic simulations on a lattice with a propagation and a collision step[24]. Self-assembling structures such as spherical or wormlike micelles and a sponge phase were obtained with this approach in a three-dimensional ternary system of water, oil, and surfactant.[25]

In contrast to the methods described so far, self-consistent field theory[26] and (classical) density functional theory (DFT),[27] which are based on statistical thermodynamics, predict density profiles of components or coarse-grained groups without simulating their trajectories[28]. Self-consistent field theory determines the free energy by evaluating the path integral of each molecule in a mean field[29]. It was applied, for example, to diblock copolymer surfactants in homopolymer blends to investigate micelle formation and interfacial tensions[30–32]. In self-consistent field theory, long-range attractions and compressibility are often neglected, which is a disadvantage compared to DFT[33]. DFT represents a mesoscopic modeling approach, which achieves high computational efficiency, while preserving a clear physical basis and high theoretical versatility[34]. A further advantage of DFT is the direct connection of model parameters to the underlying physics. This connection is often nontrivial for coarse-grained methods[35]. Applying the equilibrium conditions in DFT delivers density profiles of components in a system by minimizing the grand potential functional. This requires a suitable expression for a Helmholtz energy functional, which is not known exactly for real fluids[36].

The mean-field approach of da Gama and Gubbins[37] was one of the first DFT models, which was applied to surfactant systems. They studied a ternary mixture of water, oil, and surfactants and investigated the reduction of interfacial tension as results of surfactant adsorption to the liquid–liquid interface. All molecules were modeled as (single) hard spheres with mean-field attraction. An orientational vector was included in the surfactant molecule to account for its amphiphilic character. These model molecules are often referred to as Janus particles[38]. The approach was used to study the surfactant phase behavior and interfacial properties in planar and curved systems[39–41], in confinement or at a single wall[38,42–44], and using charged surfactants[45,46]. In some works, the surfactant molecule is treated as a dimer consisting of a hydrophobic and a hydrophilic hard sphere, connected either by an entropy term[47–49] or by a bonding potential[50]. Geometry-based DFT models with solely repulsive interactions were developed[51,52] based on the fundamental measure theory (FMT) of Rosenfeld for convex bodies[53]. The surfactant molecules, consisting of a hard sphere as the head and an infinitely thin needle as the tail, adsorb to the interface in binary surfactant-needle and ternary surfactant-needle-sphere systems. More detailed approaches model surfactants as chains of spheres, for example, as in the early work of Stillinger[54]. The combination of DFT

and self-consistent field theory using chain surfactants allowed for the study of interfaces in 1D systems[55] and of surfactant mesostructures in 3D systems[29,35].

A key in DFT is to construct accurate approximations for the Helmholtz energy functional[36]. One approach is to expand expressions for the Helmholtz energy from the bulk equations of state to inhomogeneous systems, which provides a unified framework for the treatment of homogeneous and inhomogeneous systems. Members of the family of statistical associating fluid theory (SAFT)[56,57] equations of state are often utilized in this context. SAFT is based on the first-order thermodynamic perturbation theory (TPT1) by Wertheim[58–62] and models molecules as chains of spherical segments. Tripathi and Chapman[63,64] developed a DFT based on SAFT for homosegmented chains and termed it interfacial SAFT (iSAFT). iSAFT was modified by Jain et al.[65] to make it applicable to heterosegmented chains. The model was applied to chain surfactants with hard sphere and hard chain contributions and a mean-field attraction. The interaction energy was set to zero for unlike interactions to model the amphiphilic character of surfactants[15]. With this model, the influence of the surfactant structure on interfacial tensions and density profiles at the oil–water interface were investigated. A more elaborate model with explicit association was employed to study the formation of micelles, inverse micelles, and surface tensions at the vapor–liquid interface[28]. The model was also extended to block copolymers[66] and reformulated in a density gradient theory[67].

Several variations of SAFT have been proposed since its development: soft-SAFT[68,69], SAFT with a variable range of the potential[70,71], SAFT-γ Mie,[72,73] and perturbed-chain SAFT (PC-SAFT)[74–79]. While in SAFT, the dispersion contribution of individual segments on a chain is equal to the contribution of nonbonded segments[57], PC-SAFT incorporates the chain structure in the dispersion term, which improves the description of the phase behavior for several systems[75]. PC-SAFT was applied to study bulk properties and phase equilibria in a variety of complex systems[76,80–82]. Subsequently, a Helmholtz energy functional based on PC-SAFT was developed[83,84] and applied to study vapor–liquid interfaces of pure components[85,86] and mixtures[87], liquid–liquid interfaces[88], adsorption in porous media[89,90], and interfacial properties of nanodroplets [see chapters 3 and 4]. Recently, a model that combines the modified iSAFT by Jain et al.[65] with the group contribution version of PC-SAFT[91] was developed in our group and applied to real systems[92].

In this work, the DFT approach based on the group contribution version of PC-SAFT is revised, and its capability to describe and predict surfactant phenomena is investigated. The model is applied to nonionic surfactants known as polyethylene glycol alkyl ethers. It is parametrized using experimental data for pure component properties of small surfactant molecules. The group contribution approach then allows a robust extrapolation to longer

surfactants. For both, binary surfactant/water systems in vapor–liquid equilibrium and ternary surfactant/octane/water systems in liquid–liquid equilibrium, the model is able to capture the key surfactant properties: the accumulation of surfactant molecules in the interface and a significant reduction of interfacial tensions.

7.2 Classical Density functional theory

In an open, inhomogeneous system at constant temperature T, chemical potentials μ_i of all species, and volume V, the grand potential Ω is minimal at equilibrium. With the density profiles $\rho_i(\mathbf{r})$ of all species i in the system as internal degrees of freedom, this minimization can be obtained by setting the functional derivative of Ω to zero, as

$$\frac{\delta\Omega}{\delta\rho_i(\mathbf{r})} = 0 \qquad \forall i. \tag{7.1}$$

The grand potential can be written in terms of the Helmholtz energy functional F, that only depends on interactions intrinsic to the fluid phase, as

$$\Omega = F - \sum_i \int \rho_i(\mathbf{r}) \left(\mu_i - V_i^{\text{ext}}(\mathbf{r})\right) \mathrm{d}\mathbf{r} \tag{7.2}$$

with the chemical potentials μ_i and the external potential $V_i^{\text{ext}}(\mathbf{r})$. The ideal gas contribution to the Helmholtz energy is known from statistical mechanics; therefore, it is convenient to split the Helmholtz energy into an ideal part and a residual part, as

$$\beta F = \int \sum_i \rho_i(\mathbf{r}) \left(\ln\left(\rho_i(\mathbf{r})\Lambda_i^3\right) - 1\right) \mathrm{d}\mathbf{r} + \beta F^{\text{res}} \tag{7.3}$$

with the inverse temperature $\beta = \frac{1}{k_B T}$ and the effective de Broglie wavelength Λ_i. Inserting eqs. (7.2) and (7.3) in (7.1) results in the expression, commonly referred to as Euler–Lagrange equation,

$$\ln\left(\rho_i(\mathbf{r})\Lambda_i^3\right) + \frac{\delta\beta F^{\text{res}}}{\delta\rho_i(\mathbf{r})} = \beta\left(\mu_i - V_i^{\text{ext}}(\mathbf{r})\right) \qquad \forall i. \tag{7.4}$$

With a model for the residual Helmholtz energy functional, eq. (7.4) can be used to determine the density profiles $\rho_i(\mathbf{r})$ of an inhomogeneous system.

A common application of DFT is the calculation of surface or interfacial tensions. To obtain these quantities, the density profile is solved for a one-dimensional cartesian grid in the

absence of an external potential using the coexistence densities as boundary values. The surface or interfacial tension γ can then be calculated from

$$\gamma = \frac{\Omega - \Omega^{\text{bulk}}}{A} = \int_{-\infty}^{\infty} \left(f(z) - \sum_i \rho_i(z)\mu_i + p \right) \mathrm{d}z \tag{7.5}$$

with p the bulk pressure, z as the coordinate in the normal direction of the interface, and A as the area perpendicular to the z-axis. The Helmholtz energy density f, with $F = \int f(\mathbf{r})\,\mathrm{d}\mathbf{r}$, is in general itself a functional of the density profiles of all species.

7.2.1 DFT for heterosegmented chains

The model for heterosegmented chains used in this work is based on the work by Jain et al.[65], which itself is based on Wertheim's thermodynamic perturbation theory[58,59]. Instead of calculating the density profiles of molecules in the system, the approach models the density profiles of the individual segments, from which the molecules are formed. The model is rewritten to be consistent with the gc-PC-SAFT equation of state in the bulk limit and to allow for a simpler and more generic implementation. The residual Helmholtz energy is split into different contributions, according to

$$F^{\text{res}} = F^{\text{bond}} + F^{\text{hs}} + F^{\text{disp}} + F^{\text{assoc}}. \tag{7.6}$$

While the contributions for hard spheres (hs), dispersive attraction (disp), and association (assoc) appear in a similar way in homosegmented DFT models, the contribution due to covalent bonds (bond) has to be included in the segment based approach. The starting point is the inhomogeneous version of Wertheim's perturbation theory[93], that describes the Helmholtz energy of systems of associating particles:

$$\beta F^{\text{bond}} = \int \sum_i \sum_\alpha \sum_{\alpha'} \rho_{i\alpha}(\mathbf{r}) \left(\ln \chi_{i\alpha\alpha'}(\mathbf{r}) - \frac{\chi_{i\alpha\alpha'}(\mathbf{r})}{2} + \frac{1}{2} \right) \mathrm{d}\mathbf{r} \tag{7.7}$$

Here, $\rho_{i\alpha}(\mathbf{r})$ is the density of segment α of component i, $\chi_{i\alpha\alpha'}$ is the fraction of non-bonded association sites for the bond between segment α and α', and α' is summed over all the segments that are bonded to segment α. The values for $\chi_{i\alpha\alpha'}$ are determined by the set of implicit integral equations

$$\chi_{i\alpha\alpha'}(\mathbf{r}) = \left(1 + \int \rho_{i\alpha'}(\mathbf{r}')\chi_{i\alpha'\alpha}(\mathbf{r}')\Delta_{i\alpha\alpha'}(\mathbf{r},\mathbf{r}')\,\mathrm{d}\mathbf{r}' \right)^{-1}. \tag{7.8}$$

For tangentially bonded segments with diameters $d_{i\alpha}$ and using the common approximation for the contact cavity correlation function of an inhomogeneous fluid

$$y_{i\alpha\alpha'}([\rho_i(\mathbf{r})],\mathbf{r},\mathbf{r}') \approx \sqrt{y_{i\alpha\alpha'}(\mathbf{r})y_{i\alpha\alpha'}(\mathbf{r}')}, \tag{7.9}$$

the association strength $\Delta_{i\alpha\alpha'}(\mathbf{r},\mathbf{r}')$ can be written as

$$\Delta_{i\alpha\alpha'}(\mathbf{r},\mathbf{r}') = K \underbrace{\frac{\delta(|\mathbf{r}-\mathbf{r}'|-d_{i\alpha\alpha'})}{4\pi d_{i\alpha\alpha'}^2}}_{\omega_{\text{chain}}^{i\alpha\alpha'}(\mathbf{r}-\mathbf{r}')} \sqrt{y_{i\alpha\alpha'}(\mathbf{r})y_{i\alpha\alpha'}(\mathbf{r}')} \tag{7.10}$$

with the constant K that contains the association energy and is going towards infinity, when covalent bonds are considered, the distance $d_{i\alpha\alpha'} = \frac{1}{2}(d_{i\alpha}+d_{i\alpha'})$ between the segments, and the bulk phase cavity correlation function at contact $y_{i\alpha\alpha'}(\mathbf{r})$ evaluated locally. To facilitate the derivation, we introduce the property $\hat{\chi}_{i\alpha\alpha'}$ as

$$\hat{\chi}_{i\alpha\alpha'}(\mathbf{r}) = \chi_{i\alpha\alpha'}(\mathbf{r})\sqrt{y_{i\alpha\alpha'}(\mathbf{r})} = \left(y_{i\alpha\alpha'}(\mathbf{r})^{-\frac{1}{2}} + K\int \rho_{i\alpha'}(\mathbf{r}')\hat{\chi}_{i\alpha'\alpha}(\mathbf{r}')\omega_{\text{chain}}^{i\alpha\alpha'}(\mathbf{r}-\mathbf{r}')\,\mathrm{d}\mathbf{r}' \right)^{-1}. \tag{7.11}$$

We further define a chain contribution $\hat{F}^{\text{chain}}$ that simplifies to the chain contribution in SAFT[57] when evaluated at bulk conditions, as

$$\beta\hat{F}^{\text{chain}} = -\frac{1}{2}\int \sum_i \sum_\alpha \sum_{\alpha'} \rho_{i\alpha}(\mathbf{r}) \ln y_{i\alpha\alpha'}(\mathbf{r})\,\mathrm{d}\mathbf{r}. \tag{7.12}$$

The residual Helmholtz energy functional, eq. (7.6), can then be re-summed as

$$F^{\text{res}} = \hat{F}^{\text{bond}} + \underbrace{\hat{F}^{\text{chain}} + F^{\text{hs}} + F^{\text{disp}} + F^{\text{assoc}}}_{\hat{F}^{\text{res}}} \tag{7.13}$$

with the modified contribution for covalent bonds

$$\beta\hat{F}^{\text{bond}} = \beta F^{\text{bond}} - \beta\hat{F}^{\text{chain}} = \int \sum_i \sum_\alpha \sum_{\alpha'} \rho_{i\alpha}(\mathbf{r}) \left(\ln \hat{\chi}_{i\alpha\alpha'}(\mathbf{r}) - \frac{\hat{\chi}_{i\alpha\alpha'}(\mathbf{r})}{2y_{i\alpha\alpha'}(\mathbf{r})} + \frac{1}{2} \right) \mathrm{d}\mathbf{r} \tag{7.14}$$

To calculate the functional derivative of $\hat{F}^{\text{bond}}$ with respect to the density profile, the approach by Michelsen and Hendriks[94] can be used. Therefore, the property

$$Q = \int \sum_i \sum_\alpha \sum_{\alpha'} \rho_{i\alpha}(\mathbf{r}) \left(\ln \hat{\chi}_{i\alpha\alpha'}(\mathbf{r}) - \frac{\hat{\chi}_{i\alpha\alpha'}(\mathbf{r})}{y_{i\alpha\alpha'}(\mathbf{r})} + 1 \right) \mathrm{d}\mathbf{r} - \frac{K}{2} \int \int \sum_i \sum_\alpha \sum_{\alpha'} \rho_{i\alpha}(\mathbf{r}) \rho_{i\alpha'}(\mathbf{r}') \hat{\chi}_{i\alpha\alpha'}(\mathbf{r}) \hat{\chi}_{i\alpha'\alpha}(\mathbf{r}') \omega_{\text{chain}}^{i\alpha\alpha'}(\mathbf{r}-\mathbf{r}') \, \mathrm{d}\mathbf{r} \, \mathrm{d}\mathbf{r}' \quad (7.15)$$

is defined. When evaluated at the solution of eq. (7.11), we find $Q = \beta \hat{F}^{\text{bond}}$ and $\frac{\delta Q}{\delta \hat{\chi}_{i\alpha\alpha'}} = 0$. As a result, the functional derivative of $\beta \hat{F}^{\text{bond}}$ can be calculated by evaluating the partial derivative of Q at constant $\chi_{i\alpha\alpha'}$, as

$$\frac{\delta \beta F^{\text{bond}}}{\delta \rho_{i\alpha}(\mathbf{r})} = \left(\frac{\delta Q}{\delta \rho_{i\alpha}(\mathbf{r})} \right)_{\hat{\chi}_{i\alpha\alpha'}} = \sum_{\alpha'} \left(\ln \hat{\chi}_{i\alpha\alpha'}(\mathbf{r}) - \frac{\hat{\chi}_{i\alpha\alpha'}(\mathbf{r})}{y_{i\alpha\alpha'}(\mathbf{r})} + 1 \right) + \int \sum_j \sum_\beta \sum_{\beta'} \rho_{j\beta}(\mathbf{r}') \frac{\hat{\chi}_{j\beta\beta'}(\mathbf{r}')}{y_{j\beta\beta'}(\mathbf{r}')^2} \frac{\delta y_{j\beta\beta'}(\mathbf{r}')}{\delta \rho_{i\alpha}(\mathbf{r})} \, \mathrm{d}\mathbf{r}' - \sum_{\alpha'} \hat{\chi}_{i\alpha\alpha'}(\mathbf{r}) K \int \rho_{i\alpha'}(\mathbf{r}') \hat{\chi}_{i\alpha'\alpha}(\mathbf{r}') \omega_{\text{chain}}^{i\alpha\alpha'}(\mathbf{r}-\mathbf{r}') \, \mathrm{d}\mathbf{r}'. \quad (7.16)$$

Using eq. (7.11) and evaluating the limit of complete association ($\hat{\chi}_{i\alpha\alpha'} \to 0$), the derivative simplifies to

$$\frac{\delta \beta F^{\text{bond}}}{\delta \rho_{i\alpha}(\mathbf{r})} = \sum_{\alpha'} \ln \hat{\chi}_{i\alpha\alpha'}(\mathbf{r}). \quad (7.17)$$

The functional derivative is inserted in the Euler–Lagrange equation, resulting in

$$\ln\left(\rho_{i\alpha}(\mathbf{r}) \Lambda_{i\alpha}^3\right) + \sum_{\alpha'} \ln \hat{\chi}_{i\alpha\alpha'}(\mathbf{r}) + \frac{\delta \beta \hat{F}^{\text{res}}}{\delta \rho_{i\alpha}(\mathbf{r})} = \beta \left(\mu_{i\alpha} - V_{i\alpha}^{\text{ext}}(\mathbf{r}) \right). \quad (7.18)$$

Equations (7.11) and (7.18) have to be solved simultaneously to obtain the density profiles. Analogous to Jain et al.[65], for linear molecules, the Euler–Lagrange equation is rewritten as

$$\rho_{i\alpha}(\mathbf{r}) = \Lambda_i^{-3} e^{\beta\left(\mu_i - \frac{\delta \hat{F}^{\text{res}}}{\delta \rho_{i\alpha}(\mathbf{r})} - V_{i\alpha}^{\text{ext}}(\mathbf{r})\right)} \hat{I}_{1,i\alpha} \hat{I}_{2,i\alpha} \quad (7.19)$$

with the effective de Broglie wavelength $\Lambda_i = \prod_\alpha \Lambda_{i\alpha}$ and the chemical potential $\mu_i = \sum_\alpha \mu_{i\alpha}$ of the chain. The integrals $\hat{I}_{1,i\alpha}$ and $\hat{I}_{2,i\alpha}$ are evaluated iteratively, as

$$\hat{I}_{1,i1}(\mathbf{r}) = 1 \tag{7.20}$$

$$\hat{I}_{1,i\alpha}(\mathbf{r}) = \int \hat{I}_{1,i\alpha-1}(\mathbf{r}') e^{-\beta\left(\frac{\delta \hat{F}^{\text{res}}}{\delta \rho_{i\alpha}(\mathbf{r}')} + V_{i\alpha}^{\text{ext}}(\mathbf{r}')\right)} \omega_{\text{chain}}^{i\alpha\alpha-1}(\mathbf{r}-\mathbf{r}')\,\mathrm{d}\mathbf{r}' \qquad \alpha > 1 \tag{7.21}$$

and

$$\hat{I}_{2,is_i}(\mathbf{r}) = 1 \tag{7.22}$$

$$\hat{I}_{2,i\alpha}(\mathbf{r}) = \int \hat{I}_{2,i\alpha+1}(\mathbf{r}') e^{-\beta\left(\frac{\delta \hat{F}^{\text{res}}}{\delta \rho_{i\alpha}(\mathbf{r}')} + V_{i\alpha}^{\text{ext}}(\mathbf{r}')\right)} \omega_{\text{chain}}^{i\alpha\alpha+1}(\mathbf{r}-\mathbf{r}')\,\mathrm{d}\mathbf{r}' \qquad \alpha < s_i \tag{7.23}$$

with s_i the number of segments on chain i. The formalism presented in this section is equivalent to the original version by Jain et al.[65] and can also be extended to branched molecules[95]. However, it has advantages with respect to its implementation. The model is strictly separated from the implementation and solution of the Euler–Lagrange equation. The only properties that are required to solve for the density profiles are the segment diameters $d_{i\alpha}$ and the residual Helmholtz energy functional $\hat{F}^{\text{res}}$. In addition, these equations are appealing and convenient because they resemble the expressions for weighted densities: the recurrence integrals $\hat{I}_{1,i\alpha}$ and $\hat{I}_{2,i\alpha}$ are written as convolutions that can be rapidly evaluated using a fast Fourier transform.

7.2.2 Calculation of functional derivatives

We focus on Helmholtz energy functionals, that can be expressed using weighted densities. This includes functionals based on fundamental measure theory[96], local and weighted density approximations[97], and also mean field theory[98,99]. In these approaches, the Helmholtz energy density f, which itself is a functional of the density profiles, can be written as a function of a set of weighted densities n_λ, as

$$F = \int f[\{\rho_{i\alpha}(\mathbf{r})\}]\,\mathrm{d}\mathbf{r} = \int f(\{n_\lambda(\mathbf{r})\})\,\mathrm{d}\mathbf{r}. \tag{7.24}$$

The weighted densities are obtained as a convolution of the density profiles with corresponding weight functions $\omega_\lambda^{i\alpha}$, as

$$n_\lambda(\mathbf{r}) = \sum_i \sum_\alpha n_\lambda^{i\alpha}(\mathbf{r}) = \sum_i \sum_\alpha \int \rho_{i\alpha}(\mathbf{r}')\omega_\lambda^{i\alpha}(\mathbf{r}-\mathbf{r}')\,\mathrm{d}\mathbf{r}'. \tag{7.25}$$

The general form of the functional derivatives required in the Euler–Lagrange equation is thus

$$\frac{\delta F}{\delta \rho_{i\alpha}(\mathbf{r})} = \int \sum_{\lambda} \frac{\partial f}{\partial n_\lambda}(\mathbf{r}')\omega_\lambda^{i\alpha}(\mathbf{r}'-\mathbf{r})\,\mathrm{d}\mathbf{r}'. \tag{7.26}$$

For spherically symmetric scalar weight functions, we find $\omega(\mathbf{r}) = \omega(-\mathbf{r})$, whereas for spherically symmetric vector weight functions, we find $\vec{\omega}(\mathbf{r}) = -\vec{\omega}(-\mathbf{r})$. Thus eq. (7.26) can be rewritten in terms of convolution integrals, as

$$\frac{\delta F}{\delta \rho_{i\alpha}(\mathbf{r})} = \int \sum_{\lambda}^{\text{scalar}} \frac{\partial f}{\partial n_\lambda}(\mathbf{r}')\omega_\lambda^{i\alpha}(\mathbf{r}-\mathbf{r}')\,\mathrm{d}\mathbf{r}' - \int \sum_{\lambda}^{\text{vector}} \frac{\partial f}{\partial \vec{n}_\lambda}(\mathbf{r}')\cdot\vec{\omega}_\lambda^{i\alpha}(\mathbf{r}-\mathbf{r}')\,\mathrm{d}\mathbf{r}'. \tag{7.27}$$

For a generic implementation, each Helmholtz energy contribution needs to provide a set of weight functions $\omega_\lambda^{i\alpha}$ and an expression for the Helmholtz energy density f as a function of the corresponding weighted densities. With the use of dual numbers, the partial derivatives needed in eq. (7.27) can be calculated exactly and automatically. In instances, where simplifications in the derivatives can be applied, the analytic derivatives can be implemented instead, to speed up the evaluation. Convolution integrals like the ones appearing in eqs. (7.21), (7.23), (7.25) and (7.27) can be solved efficiently using a fast Fourier transform[100].

7.3 gc-PC-SAFT Helmholtz energy functional

The framework presented in the last section requires the diameter $d_{i\alpha}$ of the segments and one or more expressions that constitute the residual Helmholtz energy functional $\hat{F}^{\text{res}}$. We use the group contribution version of the PC-SAFT equation of state[91] to provide these expressions. In this model, the segments are described with three necessary parameters, the size parameter $\sigma_{i\alpha}$, the energy parameter $\varepsilon_{i\alpha}$ and the length parameter $m_{i\alpha}$. As opposed to the homosegmented PC-SAFT equation of state, in which m characterizes the (noninteger) number of spherical segments forming a chain and is expected to be larger than or equal to 1, the values of $m_{i\alpha}$ are smaller than 1, which takes into account the fusing of spherical segments in the packing fraction. A component consisting of a single segment requires $m_{i1} = 1$ to be consistent with the homosegmented equation of state without adding an additional chain term. For associating segments, the number of association sites $N_{i\alpha}^A$ and $N_{i\alpha}^B$, the effective association volume parameter $\kappa_{i\alpha}^{AB}$ and the association energy $\varepsilon_{i\alpha}^{AB}$ have to be specified additionally.

The segment diameter $d_{i\alpha}$ needed in the calculation of $\omega_{\text{chain}}^{i\alpha\alpha'}(\mathbf{r})$, as well as for the other

contributions shown below, is defined as[75]

$$d_{i\alpha} = \sigma_{i\alpha}\left(1 - 0.12e^{-3\beta\varepsilon_{i\alpha}}\right). \tag{7.28}$$

Throughout this work we use single indices for pair potential parameters between like segments, that is, we write $\sigma_{i\alpha}$ instead of $\sigma_{i\alpha i\alpha}$.

Chain contribution

Based on eq. (7.12), the Helmholtz energy density contribution for the chain term reads

$$\beta\hat{f}^{\text{chain}} = -\frac{1}{2}\sum_{i}\sum_{\alpha}\sum_{\alpha'}\rho_{i\alpha}\ln y_{i\alpha\alpha'}. \tag{7.29}$$

The cavity correlation function is calculated from[76]

$$y_{i\alpha\alpha'} = \frac{1}{1-\zeta_3} + \frac{d_{i\alpha}d_{i\alpha'}}{d_{i\alpha}+d_{i\alpha'}}\frac{3\zeta_2}{(1-\zeta_3)^2} + \left(\frac{d_{i\alpha}d_{i\alpha'}}{d_{i\alpha}+d_{i\alpha'}}\right)^2\frac{2\zeta_2^2}{(1-\zeta_3)^3}. \tag{7.30}$$

The two weighted densities ζ_2 and ζ_3 are obtained using the corresponding weight functions $\omega^{i\alpha}_{\zeta_2} = \frac{m_{i\alpha}}{8d_{i\alpha}}\Theta(d_{i\alpha} - |\mathbf{r}|)$ and $\omega^{i\alpha}_{\zeta_3} = \frac{m_{i\alpha}}{8}\Theta(d_{i\alpha} - |\mathbf{r}|)$.

Hard sphere contribution

The hard sphere contribution models a fluid consisting of repulsive spheres of diameter $d_{i\alpha}$ using the White-Bear or modified fundamental measure theory[101,102]. The Helmholtz energy density is given by

$$\beta f^{\text{hs}} = -n_0\ln(1-n_3) + \frac{n_1n_2 - \vec{n}_1\cdot\vec{n}_2}{1-n_3} + \left(n_2^3 - 3n_2\vec{n}_2\cdot\vec{n}_2\right)\frac{n_3 + (1-n_3)^2\ln(1-n_3)}{36\pi n_3^2(1-n_3)^2}. \tag{7.31}$$

The fusion of the segments is accounted for by including the parameter $m_{i\alpha}$ in the weight functions for the four scalar weighted densities $\omega_3^{i\alpha}(\mathbf{r}) = m_{i\alpha}\Theta(d_{i\alpha}/2 - |\mathbf{r}|)$, $\omega_2^{i\alpha}(\mathbf{r}) = m_{i\alpha}\delta(d_{i\alpha}/2 - |\mathbf{r}|)$, $\omega_1^{i\alpha}(\mathbf{r}) = \omega_2^{i\alpha}(\mathbf{r})/2\pi d_{i\alpha}$ and $\omega_0^{i\alpha}(\mathbf{r}) = \omega_2^{i\alpha}(\mathbf{r})/\pi d_{i\alpha}^2$, and the two vector weighted densities $\vec{\omega}_2^{i\alpha}(\mathbf{r}) = m_{i\alpha}\frac{\mathbf{r}}{|\mathbf{r}|}\delta\left(d_{i\alpha}/2 - |\mathbf{r}|\right)$ and $\vec{\omega}_1^{i\alpha}(\mathbf{r}) = \vec{\omega}_2^{i\alpha}(\mathbf{r})/2\pi d_{i\alpha}$.

Dispersive attraction

The dispersive attraction is modeled using a weighted density approach. The Helmholtz energy density

$$\beta f^{\text{disp}} = -2\pi I_1(m,\eta)\sum_i\sum_j\sum_\alpha\sum_\beta m_{i\alpha}m_{j\beta}\bar{\rho}_{i\alpha}\bar{\rho}_{j\beta}\frac{\varepsilon_{i\alpha j\beta}}{k_BT}\sigma^3_{i\alpha j\beta} - \pi m C_1(m,\eta)I_2(m,\eta)\sum_i\sum_j\sum_\alpha\sum_\beta m_{i\alpha}m_{j\beta}\bar{\rho}_{i\alpha}\bar{\rho}_{j\beta}\left(\frac{\varepsilon_{i\alpha j\beta}}{k_BT}\right)^2\sigma^3_{i\alpha j\beta} \quad (7.32)$$

sums over all pairs of segments[76]. The expressions for I_1, I_2 and C_1 are taken directly from the original publication[75]. To evaluate them, the packing fraction η and an average chain length m are required. While the expression for the packing fraction in an inhomogeneous and heteronuclear system

$$\eta = \frac{\pi}{6}\sum_i\sum_\alpha m_{i\alpha}\bar{\rho}_{i\alpha}d^3_{i\alpha} \quad (7.33)$$

is straightforward, the average chain length is defined more arbitrarily, as

$$m = \frac{\sum_i\sum_\alpha \bar{\rho}_i m_{i\alpha}}{\sum_i \bar{\rho}_i} \quad \text{with} \quad \bar{\rho}_i = \sum_\alpha \frac{\bar{\rho}_{i\alpha}}{s_i} \quad (7.34)$$

with s_i the number of segments on molecule i. The weighted densities $\bar{\rho}_{i\alpha}$ are obtained using the weight functions $\omega^{i\alpha}_{\text{disp}} = \frac{\Theta(\psi d_{i\alpha}-|\mathbf{r}|)}{\frac{4}{3}\pi\psi^3 d^3_{i\alpha}}$ with $\psi = 1.5357$ as a model constant[92].

Association

For the association contribution, the model by Yu and Wu[103] is used. In contrast to the model by Segura et al.[93], which was used above to derive the expression for chain formation, it does not require additional evaluations of convolution integrals during the solution of the monomer fractions $\chi^A_{i\alpha}$. Instead, it uses the weighted densities $n^{i\alpha}_0$, $n^{i\alpha}_2$, n_3 and $\vec{n}^{i\alpha}_2$ from the fundamental measure theory for the hard-sphere contribution. The Helmholtz energy density reads

$$\beta f^{\text{assoc}} = \sum_i\sum_\alpha \frac{n^{i\alpha}_0}{m_{i\alpha}}\xi_{i\alpha}\sum_A N^A_{i\alpha}\left(\ln\chi^A_{i\alpha} - \frac{\chi^A_{i\alpha}}{2} + \frac{1}{2}\right) \quad (7.35)$$

with index A running over all kinds of association sites in the system. The fractions of nonbonded sites $\chi_{i\alpha}^{A}$ are determined by

$$\chi_{i\alpha}^{A} = \left(1 + \sum_{j} \sum_{\beta} \frac{n_0^{j\beta}}{m_{j\beta}} \xi_{j\beta} \sum_{B} N_{j\beta}^{B} \chi_{j\beta}^{B} \Delta_{i\alpha j\beta}^{AB} \right)^{-1} \tag{7.36}$$

and have to be solved iteratively at every grid point. A stable and fast algorithm was proposed by Michelsen[104]. Using the regular combining rules, the association strength $\Delta_{i\alpha j\beta}^{AB}$ is given by

$$\Delta_{i\alpha j\beta}^{AB} = \sqrt{\sigma_{i\alpha}^{3} \kappa_{i\alpha}^{AB} \sigma_{j\beta}^{3} \kappa_{j\beta}^{AB}} \left(e^{\frac{\beta}{2}\left(\varepsilon_{i\alpha}^{AB} + \varepsilon_{j\beta}^{AB}\right)} - 1 \right) y_{i\alpha j\beta}^{\text{assoc}}. \tag{7.37}$$

The cavity correlation function

$$y_{i\alpha j\beta}^{\text{assoc}} = \frac{1}{1-n_3} + \frac{d_{i\alpha} d_{j\beta}}{d_{i\alpha} + d_{j\beta}} \frac{n_2 \xi}{2(1-n_3)^2} + \left(\frac{d_{i\alpha} d_{j\beta}}{d_{i\alpha} + d_{j\beta}} \right)^2 \frac{n_2^2 \xi}{18(1-n_3)^3} \tag{7.38}$$

contains the factor ξ, which together with the factors $\xi_{i\alpha}$ in the Helmholtz energy density accounts for the inhomogeneity of the system. They are calculated using[103]

$$\xi_{i\alpha} = \frac{\vec{n}_2^{\,i\alpha} \cdot \vec{n}_2^{\,i\alpha}}{n_2^{i\alpha\,2}} \qquad \text{and} \qquad \xi = \frac{\vec{n}_2 \cdot \vec{n}_2}{n_2^2}. \tag{7.39}$$

7.4 Surfactant model

The class of surfactants, that this work aims to model are polyethylene glycol alkyl ethers. The chemical structure of these molecules is given by $HO{-}(CH_2{-}CH_2{-}O)_j{-}(CH_2)_{i-1}{-}CH_3$. To distinguish between the different molecules, the notation CiEj is introduced with i the number of carbon atoms in the alkyl tail and j the number of ethylene glycol segments. As shown in figure 7.1, we model these molecules by splitting each head group into two individual segments. All head segments are treated as equal, except for the outermost segment H_1 which contains the hydroxy group and is thus modeled using two association sites. Because this study is limited to linear chains, the tail groups are modeled as CH_2 and CH_3 segments. However, parameters for branched alkyl groups are also available in gc-PC-SAFT[91]. Figure 7.1 also shows the structures of water and octane, the two solvents used in this work. Water is modeled as a single segment with two association sites and octane consists of the same CH_2 and CH_3 groups as the tail of the surfactant.

The parameters for water were obtained from [the] previous study [in chapter 6], that

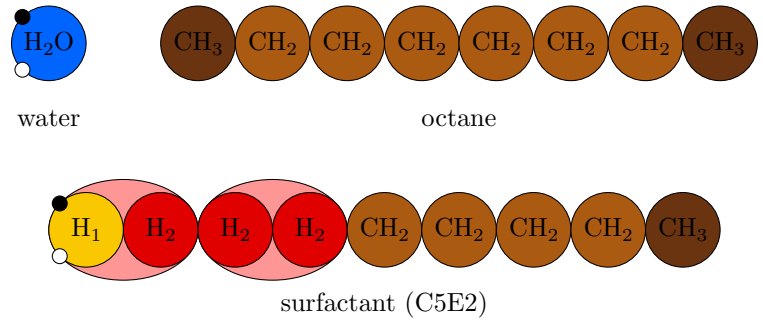

Figure 7.1: Surfactant and solvent models used in this work. Every ethylene glycol group is split into two segments. Water and the outermost head segment of the surfactant each possess two association sites.

Group	MW / g/mol	m	σ / Å	ε/k_B / K	scheme	κ^{AB}	ε^{AB}/k_B / K
H_2O	18.015	1.0	2.9375	272.03	2B	0.044480	3125.3
CH_3	15.035	0.77247	3.6937	181.49			
CH_2	14.027	0.79120	3.0207	157.23			
H_1	39.034	0.80136	3.4573	195.68	2B	0.044812	2771.3
H_2	22.027	0.80136	3.4573	195.68			

Table 7.1: Segment parameters used in this work. [The parameters for water are based on chapter 6 and those for CH_2 and CH_3 are used from literature[91].]

included surface tension data in the parameter estimation. The study does not clearly identify an optimal association scheme for water using PC-SAFT. The 2B[105] association scheme ($N^A = N^B = 1$) was selected because in the published parameter set $m = 1$ and thus, the chain contribution vanishes and the parameters can be used both in a heterosegmented and homosegmented context.

The parameters for CH_2 and CH_3 are taken from the original version of the gc-PC-SAFT equation of state[91]. The parameters of the head groups were determined by fitting them to experimental data for vapor pressures and liquid densities of small polyethylene glycol alkyl ethers. To reduce the number of degrees of freedom and thus to avoid overfitting, the parameters m, σ and ε of the head groups H_1 and H_2 were defined to be equal. The resulting surfactant parameters, together with the other segment parameters applied in this work are shown in table 7.1.

Figure 7.2a) shows results for the vapor pressures. With the exception of the smallest surfactant C1E1, the model gives a convincing agreement with the experiments. In figure 7.2b), the pure component surface tension of the same small surfactants is shown together with predictions from the gc-PC-SAFT functional. Without any additional parameters, the deviations from the experimental results are rather low.

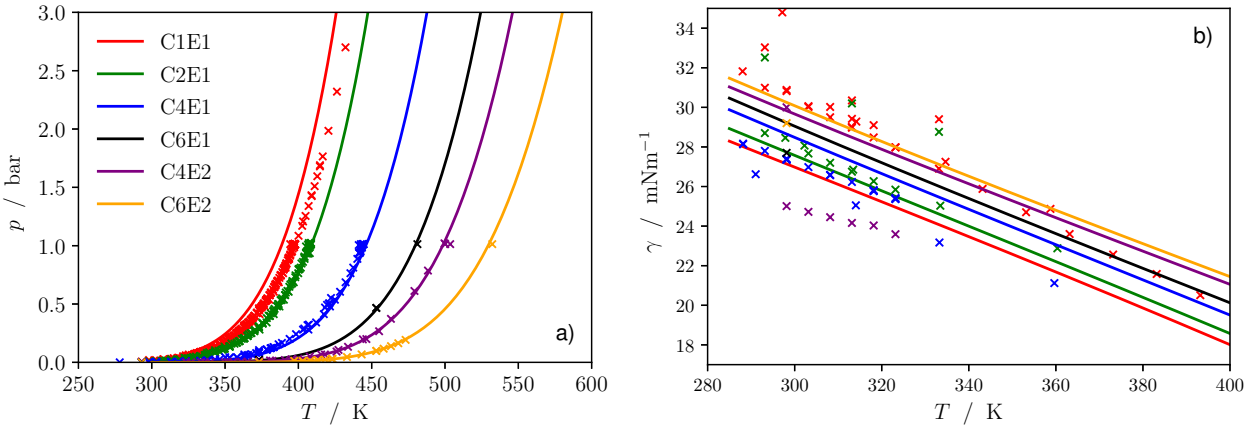

Figure 7.2: Vapor pressures (a) and Surface tensions (b) of the C1E1, C2E1, C4E1, C6E1, C4E2 and C6E2 surfactants. Comparison between the gc-PC-SAFT functional (lines) and experimental data[106] (symbols).

	H_2O	CH_3	CH_2	H_1	H_2
H_2O	-	0.20	0.20	0	-0.38
CH_3	0.20	-	0	0	0
CH_2	0.20	0	-	0	0
H_1	0	0	0	-	0
H_2	-0.38	0	0	0	-

Table 7.2: Binary $k_{i\alpha j\beta}$ parameters used in this work.

To model mixtures of water, surfactants and alkanes, binary interaction parameters are required. The parameters used in this work are shown in table 7.2. A significant positive $k_{i\alpha j\beta}$ parameter for the combinations H_2O/CH_2 and H_2O/CH_3 is required to describe the liquid–liquid behavior of water alkane mixtures. In most SAFT models it is difficult to accurately describe both the solubility of water in alkanes and vice versa. Because we are interested in interfacial properties, we use the liquid–liquid interfacial tension as a criterion instead.

Figure 7.3 shows the interfacial tension of binary mixtures containing water and different n-alkanes as a function of temperature. The calculations are conducted at $p = 1.5\,\text{bar}$ to avoid the destabilizing presence of a vapor phase in the strongly heteroazeotropic water/alkane systems, even though the experimental data is reported at ambient pressure. Because liquids are weakly compressible, we neglect the influence of the artificially elevated pressure on the interfacial tension. With a constant binary interaction parameter for H_2O and CH_2/CH_3, it is possible to obtain interfacial tensions in the same magnitude as the experimental results. To achieve a better temperature dependence, more degrees of freedoms (i.e. a temperature dependent $k_{i\alpha j\beta}$) would be necessary.

The model does not introduce association interactions representing the hydrogen bonds

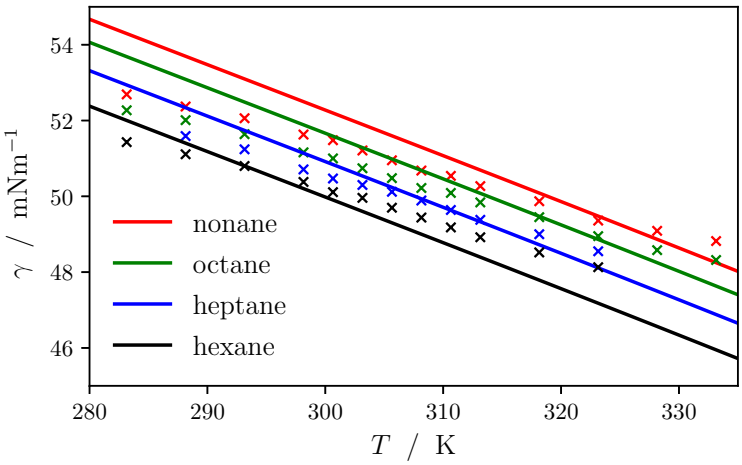

Figure 7.3: Liquid–liquid interfacial tension of binary systems consisting of n-alkanes and water at $p = 1.5\,\text{bar}$. Comparison between the gc-PC-SAFT functional (lines) and experimental data[107] (symbols).

between the ether oxygens of the head groups and water. Only the sole hydroxy group on the outer head segment is considered associating. To account for the full attractive interactions between water and the head groups, the binary interaction parameter $k_{\text{H}_2\text{O},\text{H}_2} = -0.38$ is introduced. Its value is chosen to capture the binary phase behavior of aqueous solutions of small surfactants. The resulting phase equilibria of the water/C2E1 system shown in figure 7.4 are close to experimental data and adequately model the azeotrope. For the longer C4E1 surfactant, the model predicts a liquid–liquid separation, that is not observed in the experiments. However, the phase behavior of water/C4E1 is peculiar as it shows a liquid–liquid separation with both a higher and a lower critical temperature in the range from 40 to 140 °C[108]. Capturing this behavior is a challenge, especially with the low number of degrees of freedom in a group contribution approach.

The model developed in this section is able to describe inhomogeneous systems containing water, alkanes, and one or more surfactants. In the following section, it is applied to calculate interfacial properties of water/surfactant and water/octane/surfactant systems.

7.5 Results and discussion

7.5.1 Vapor–liquid interfaces

The group contribution model derived in the last sections is able to predict the phase behavior and interfacial properties of aqueous solutions of arbitrarily long surfactants. Experimental data for these systems is sparse and mostly available for surfactants with a high number of

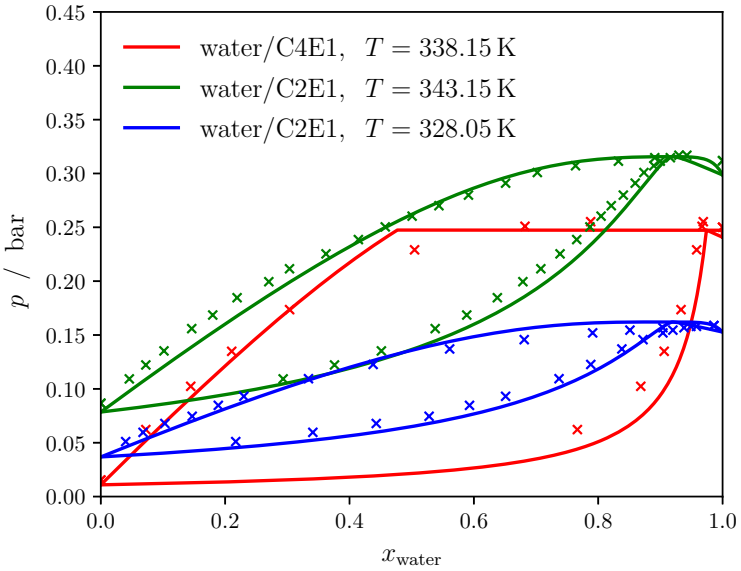

Figure 7.4: Phase equilibria of binary systems consisting of surfactants and water. Comparison between the gc-PC-SAFT functional (lines) and experimental data[108–110] (symbols).

head groups, for which the degree of extrapolation and thus the uncertainty of the gc-PC-SAFT model are high. The surface tension γ of the water/C10E4 system is measured by Eastoe et al.[111] and is compared to the model predictions in figure 7.5a). Despite the complexity of the system, the model captures the shape of the dependency of the surface tension on the liquid surfactant concentration $c_{\mathrm{surfactant}}$ well and underestimates the solubility of the surfactant molecules by only 1 order of magnitude. The experiments show the occurrence of a critical micelle concentration (cmc) beyond which the surface tension is not decreased any further due to the formation of micelles. This effect is not captured by the DFT approach, which is able to calculate surface tensions lower than the experimental minimum and even below zero. The negative surface tension is a clear sign for an unstable system that can only be calculated due to artificial constraints imposed by the planar geometry. However, even systems with small positive surface tensions can be expected to be unstable. To assess the stability of these systems, their energies need to be compared to different phases such as bilayers and micelles, an endeavor that, with significant additional computational effort, is possible with DFT[28] but out of the scope of this work.

Figure 7.5b) compares the interfacial adsorption $\Gamma_{\mathrm{surfactant}}$ obtained from the model with the corresponding experimental results. The adsorption of component i is defined as

$$\Gamma_i = \int_0^{z_0} \left(\rho_i(z) - \rho_i^{\mathrm{L}}\right) \mathrm{d}z + \int_{z_0}^{L} \left(\rho_i(z) - \rho_i^{\mathrm{V}}\right) \mathrm{d}z \tag{7.40}$$

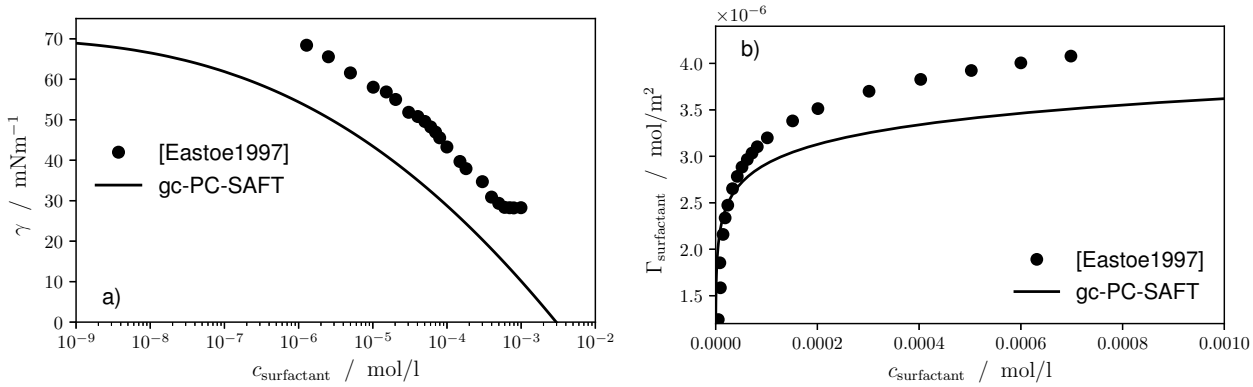

Figure 7.5: Surface tension (a) and interfacial adsorption (b) of the water/C10E4 mixture at $T = 298.15\,\text{K}$. Comparison between the gc-PC-SAFT functional (lines) and experimental data[111] (symbols).

with bulk densities in the vapor and liquid phases ρ_i^{V} and ρ_i^{L} and the length of the system L. In general, it depends on the dividing surface z_0. For this evaluation, the equimolar surface $z_{e,\text{H}_2\text{O}}$ of water

$$z_0 = z_{e,\text{H}_2\text{O}} = \int_0^L \frac{\rho_{\text{H}_2\text{O}}(z) - \rho_{\text{H}_2\text{O}}^{\text{V}}}{\rho_{\text{H}_2\text{O}}^{\text{L}} - \rho_{\text{H}_2\text{O}}^{\text{V}}}\,\text{d}z \tag{7.41}$$

was used. However, because the surfactant density is small in both the liquid and the vapor phases, in this specific system, the influence of the choice of the dividing surface on the value of the adsorption of the surfactant is miniscule. The model underestimates the amount of adsorbed surfactant molecules in the range close to the cmc but is again able to predict the qualitative behavior. We assess the results presented in figure 7.5 as satisfactory considering that the model parameters are not adjusted to the data presented within and progress to study the influence of the number of head groups on the behavior of the water/surfactant surface.

In figure 7.6, the surface tension of binary mixtures of water with surfactants containing (a) one (b) two and (c) three ethylene glycol groups is shown as a function of the liquid mole fraction of the surfactant. The temperature is $T = 298.15\,\text{K}$ and the calculation of surface tensions is carried out for concentrations up to the point at which the calculations become unstable due to the presence of a liquid–liquid phase separation. Increasing the length of the alkyl chain significantly reduces the amount of surfactant necessary to drastically lower the surface tension. This observation is consistent with the fact that there are no competing influences: increasing the length of the nonpolar tail reduces both the solubility of the surfactant in water and its vapor pressure. Therefore, the adsorption at the interface is

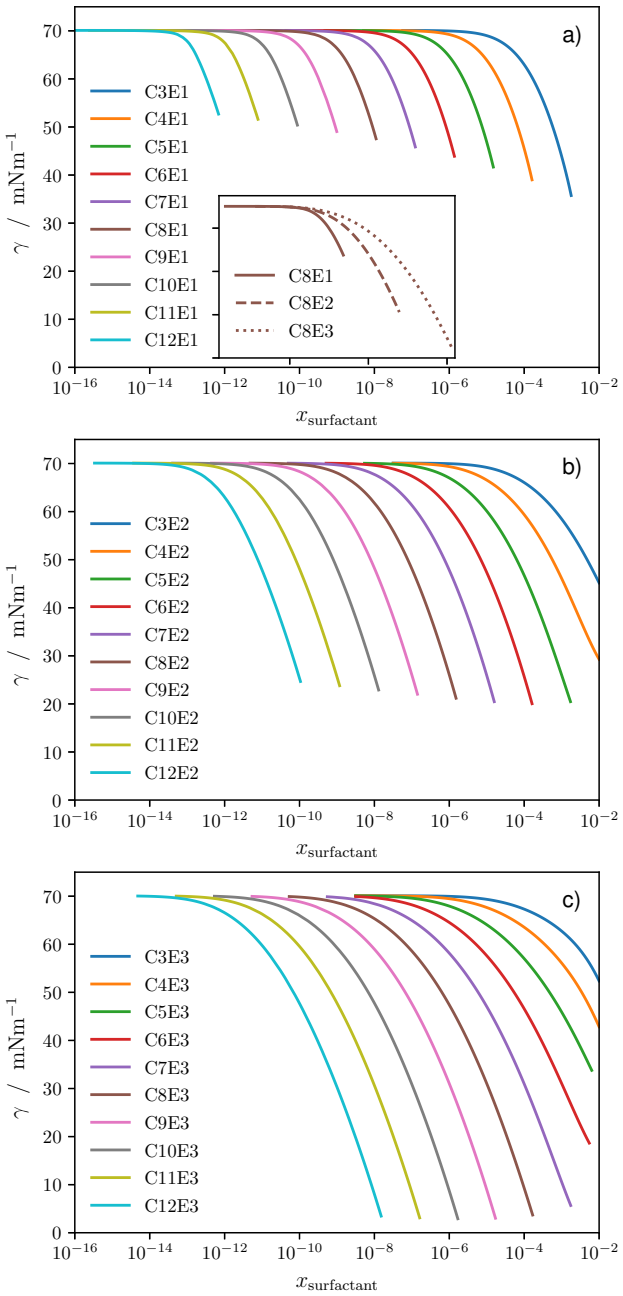

Figure 7.6: Surface tension of water/surfactant mixtures at $T = 298.15\,\mathrm{K}$ for surfactants with (a) one (b) two and (c) three ethylene glycol groups.

favored at smaller concentrations. However, for longer surfactants, the surface tension can not be reduced as much because the solubility of the surfactant is lower and the point at which a liquid–liquid separation is predicted is reached at higher surface tensions. Increasing the number of ethylene glycol groups, on the other hand, increases the solubility in water and thus, with a higher number of head groups, smaller surface tensions can be obtained. To facilitate the comparison between surfactants with different numbers of head groups

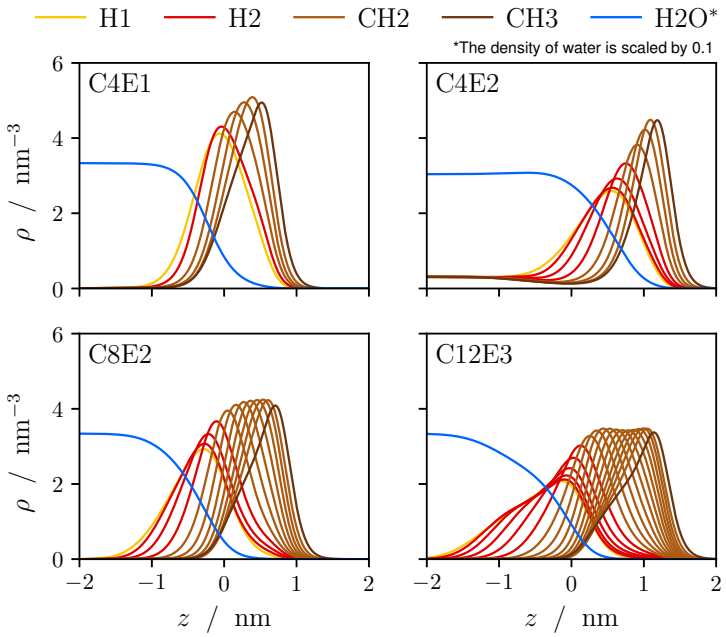

Figure 7.7: Interfacial density profiles of several water/surfactant mixtures at $T = 298.15\,\mathrm{K}$.

but an equal number of tail groups, the inset of figure 7.6a) shows the results for the C8Ex surfactants as a representative example. The solubility is increased significantly by adding head groups; therefore, the surface tension can be reduced further, but more surfactants are needed.

To gain insights into the structure of the surfactant molecules at the interface, figure 7.7 shows the density profiles of four selected systems. All profiles shown are taken at the highest stable concentration of the surfactants at $T = 298.15\,\mathrm{K}$. The local density of the surfactant segments at the interface is many orders of magnitude higher than the density in both the liquid and the vapor phase. Therefore, the model is able to capture the key property of surfactant molecules, the adsorption at interfaces. Due to the heterosegmented modeling approach, it can further be observed that in the interface the molecules are oriented with the polar head pointing to the liquid phase and the nonpolar tail groups toward the vapor phase. The densities of all surfactants with strongly varying lengths shown in figure 7.7 in the interface are similar and liquid like.

7.5.2 Liquid–liquid interfaces

We study the liquid–liquid interface of water/n-octane mixtures with varying amounts of surfactants. A feed state is defined by a given surfactant mole fraction $x^{\mathrm{feed}}_{\mathrm{surfactant}}$ and the ratio $\frac{x^{\mathrm{feed}}_{\mathrm{water}}}{x^{\mathrm{feed}}_{\mathrm{n-octane}}} = 1$. The phase equilibrium is then determined by a Tp-flash calculation at

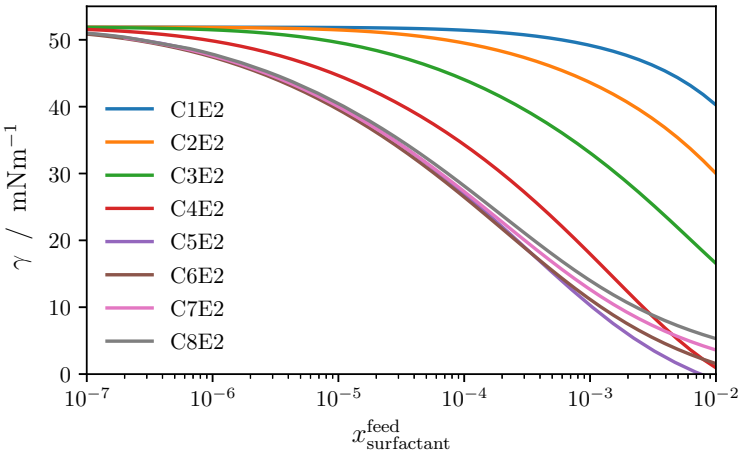

Figure 7.8: Interfacial tension of water/CxE2/octane mixtures at $T = 298.15\,\text{K}$ and $p = 1\,\text{bar}$.

$T = 298.15\,\text{K}$ and $p = 1\,\text{bar}$. A Tp-flash calculation considers bulk phases and does not account for an interface, so that in such a calculation $x^{\text{feed}}_{\text{surfactant}}$ is the total mole fraction of the surfactant dissolved in the bulk aqueous phase and the bulk hydrocarbon phase.

Figure 7.8 shows interfacial tensions γ as a function of the (bulk) feed mole fraction of the surfactant. Surfactant molecules with two ethylene glycol groups and a varying number of tail groups are compared. As opposed to the vapor–liquid surface, the results demonstrate that an optimal surfactant molecule can be identified. Beyond five tail groups the interfacial tension is not lowered any further by adding additional tail groups. This can be attributed to the higher solubility of the surfactant in the octane-rich phase.

This explanation is supported by the density profiles in figure 7.9. As expected, the surfactant head groups point towards the water-rich phase and the tail groups towards the octane-rich phase. For the C1E2 surfactant, the solubility in the water-rich phase is substantial and undesirably high if the goal is a modification of interfacial properties. By increasing the number of tail groups, the solubility in water decreases and the solubility in n-octane increases.

To obtain effective surfactants, it is therefore necessary to balance the polarities of the head groups and the tail groups. This is illustrated in figure 7.10 where the interfacial tension is again shown as a function of the surfactant feed concentration. The surfactants are chosen by starting with C4E1 and adding both a head and a tail group in each step. With this procedure, the effectiveness of the surfactants with respect to lowering the interfacial tension is increased with their size.

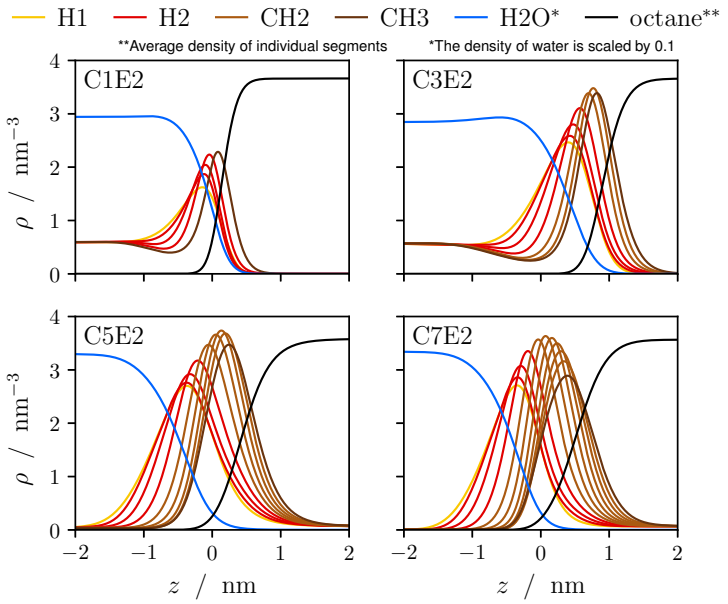

Figure 7.9: Interfacial density profiles of several water/surfactant/octane mixtures at $T = 298.15\,\mathrm{K}$, $p = 1\,\mathrm{bar}$ and $x^{\mathrm{feed}}_{\mathrm{surfactant}} = 0.01$.

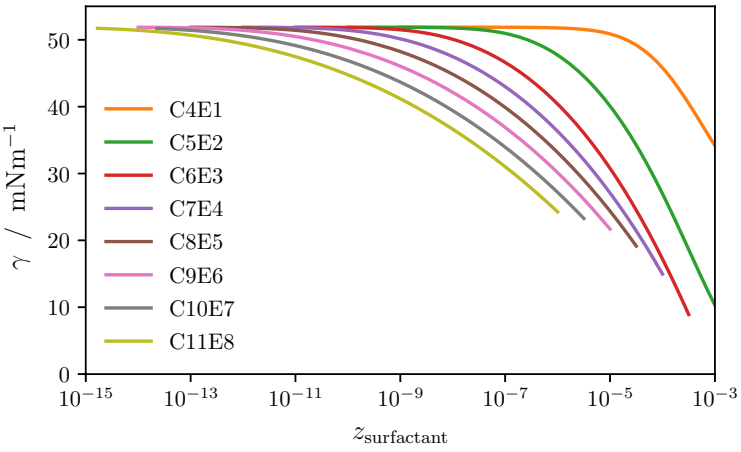

Figure 7.10: Interfacial tension of water/C(x+1)Ex/octane mixtures at $T = 298.15\,\mathrm{K}$ and $p = 1\,\mathrm{bar}$.

7.6 Conclusions

The heterosegmented density functional theory approach by Jain et al.[65] was revised and adapted to the group contribution PC-SAFT equation of state. The model was parametrized using small surfactants and then extrapolated to systems containing longer surfactant molecules. The calculations of density profiles and interfacial tensions show that the model is able to reproduce the strong adsorption of surfactant molecules in vapor–liquid and liquid–liquid interfaces. For vapor–liquid interfaces of water/surfactant systems, increasing the tail length

of the surfactant molecules reduces the amount of surfactant molecules necessary to influence the interface. Increasing the number of head groups, on the other hand, increases the solubility of the surfactant and thus reduces the values of the surface tension at the point where a liquid–liquid split occurs.

For liquid–liquid interfaces, the surfactant molecules need a low solubility in both the aqueous and the alkane-rich phases. This requires the number of head and tail groups to be balanced to obtain an effective surfactant.

A characteristic of surfactant systems beyond interfacial properties is the formation of micelles and other mesostructures. The theory developed in this work is not restricted to one-dimensional systems. Therefore, it is possible in a further step to calculate density profiles and free energies of micelles. Such calculations can be performed in a full three-dimensional geometry, or by exploiting symmetries in spherical or cylindrical coordinate systems.

References

[1] M. Sagir, M. Mushtaq, M. S. Tahir, M. B. Tahir, and A. R. Shaik. *Surfactants for Enhanced Oil Recovery Applications*. Springer Nature Switzerland, Cham, 2020. ISBN 978-3-030-18784-2. doi:10.1007/978-3-030-18785-9.

[2] D. Myers. *Surfactant science and technology*. John Wiley & Sons, Inc., Hoboken, N.J., 3rd edition, 2006. ISBN 978-0-471-68024-6.

[3] M. J. Rosen. *Surfactants and interfacial phenomena*. John Wiley & Sons, Inc., Hoboken, N.J., 3rd edition, 2004. ISBN 0-471-47818-0.

[4] S. Puvvada and D. Blankschtein. Molecular-thermodynamic approach to predict micellization, phase behavior and phase separation of micellar solutions. I. Application to nonionic surfactants. *The Journal of Chemical Physics*, **92**(6):3710–3724, 1990. doi:10.1063/1.457829.

[5] R. Nagarajan and E. Ruckenstein. Theory of surfactant self-assembly: a predictive molecular thermodynamic approach. *Langmuir*, **7**(12):2934–2969, 1991. doi:10.1021/la00060a012.

[6] Y. J. Nikas, S. Puvvada, and D. Blankschtein. Surface tensions of aqueous nonionic surfactant mixtures. *Langmuir*, **8**(11):2680–2689, 1992. doi:10.1021/la00047a018.

[7] B. C. Stephenson, K. Beers, and D. Blankschtein. Complementary Use of Simulations and Molecular-Thermodynamic Theory to Model Micellization. *Langmuir*, **22**(4):1500–1513, 2006. doi:10.1021/la052042c. PMID: 16460068.

[8] A. Khoshnood, B. Lukanov, and A. Firoozabadi. Temperature Effect on Micelle Formation: Molecular Thermodynamic Model Revisited. *Langmuir*, **32**(9):2175–2183, 2016.

doi:10.1021/acs.langmuir.6b00039. PMID: 26854650.

[9] V. Sresht, E. P. Lewandowski, D. Blankschtein, and A. Jusufi. Combined Molecular Dynamics Simulation–Molecular-Thermodynamic Theory Framework for Predicting Surface Tensions. *Langmuir*, **33**(33):8319–8329, 2017. doi:10.1021/acs.langmuir.7b01073. PMID: 28749139.

[10] J. C. Shelley and M. Y. Shelley. Computer simulation of surfactant solutions. *Current Opinion in Colloid & Interface Science*, **5**(1-2):101–110, 2000. doi:10.1016/S1359-0294(00)00042-X.

[11] S. Bandyopadhyay, M. Tarek, M. L. Lynch, and M. L. Klein. Molecular Dynamics Study of the Poly(oxyethylene) Surfactant C12E2 and Water. *Langmuir*, **16**(3):942–946, 2000. doi:10.1021/la9909493.

[12] H. Kuhn and H. Rehage. Molecular Dynamics Computer Simulations of Surfactant Monolayers: Monododecyl Pentaethylene Glycol at the Surface between Air and Water. *The Journal of Physical Chemistry B*, **103**(40):8493–8501, 1999. doi:10.1021/jp990595o.

[13] J.-B. Maillet, V. Lachet, and P. V. Coveney. Large scale molecular dynamics simulation of self-assembly processes in short and long chain cationic surfactants. *Physical Chemistry Chemical Physics*, **1**(23):5277–5290, 1999. doi:10.1039/a905216j.

[14] H. Chen and A. Z. Panagiotopoulos. Molecular Modeling of Surfactant Micellization Using Solvent-Accessible Surface Area. *Langmuir*, **35**(6):2443–2450, 2019. doi:10.1021/acs.langmuir.8b03440.

[15] C. P. Emborsky, Z. Feng, K. R. Cox, and W. G. Chapman. Recent advances in classical density functional theory for associating and polyatomic molecules. *Fluid Phase Equilibria*, **306**(1):15–30, 2011. doi:10.1016/j.fluid.2011.02.007.

[16] R. G. Larson, L. E. Scriven, and H. T. Davis. Monte Carlo simulation of model amphiphile-oil-water systems. *The Journal of Chemical Physics*, **83**(5):2411–2420, 1985. doi:10.1063/1.449286.

[17] R. G. Larson. Monte Carlo lattice simulation of amphiphilic systems in two and three dimensions. *The Journal of Chemical Physics*, **89**(3):1642–1650, 1988. doi:10.1063/1.455110.

[18] R. G. Larson. Self-assembly of surfactant liquid crystalline phases by Monte Carlo simulation. *The Journal of Chemical Physics*, **91**(4):2479–2488, 1989. doi:10.1063/1.457007.

[19] K. Esselink, P. Hilbers, N. van Os, B. Smit, and S. Karaborni. Molecular dynamics simulations of model oil/water/surfactant systems. *Colloids and Surfaces A: Physicochemical and Engineering Aspects*, **91**:155–167, 1994. doi:10.1016/0927-7757(94)02877-X.

[20] S. Karaborni, K. Esselink, P. A. J. Hilbers, B. Smit, J. Karthauser, N. M. van Os, and R. Zana. Simulating the Self-Assembly of Gemini (Dimeric) Surfactants. *Science*, **266**(5183):254–256, 1994. doi:10.1126/science.266.5183.254.

[21] P. B. Warren. Dissipative particle dynamics. *Current Opinion in Colloid & Interface Science*, **3**(6):620–624, 1998. doi:10.1016/S1359-0294(98)80089-7.

[22] S. Jury, P. Bladon, M. Cates, S. Krishna, M. Hagen, N. Ruddock, and P. Warren. Simulation of amphiphilic mesophases using dissipative particle dynamics. *Physical Chemistry Chemical Physics*, **1**(9):2051–2056, 1999. doi:10.1039/a809824g.

[23] H. S. Alasiri, A. S. Sultan, and W. G. Chapman. Effect of Surfactant Headgroup, Salts, and Temperature on Interfacial Properties: Dissipative Particle Dynamics and Experiment for the Water/Octane/Surfactant System. *Energy & Fuels*, **33**(7):6678–6688, 2019. doi:10.1021/acs.energyfuels.9b01740.

[24] B. M. Boghosian, P. V. Coveney, and A. N. Emerton. A Lattice-Gas Model of Microemulsions. *Proceedings of the Royal Society of London A*, **452**(1948):1221–1250, 1996. doi:10.1098/rspa.1996.0063.

[25] B. M. Boghosian, P. V. Coveney, and P. J. Love. A three-dimensional lattice-gas model for amphiphilic fluid dynamics. *Proceedings of the Royal Society of London. Series A: Mathematical, Physical and Engineering Sciences*, **456**(1998):1431–1454, 2000. doi:10.1098/rspa.2000.0570.

[26] V. V. Ginzburg, K. Chang, P. K. Jog, A. B. Argenton, and L. Rakesh. Modeling the interfacial tension in oil-water-nonionic surfactant mixtures using dissipative particle dynamics and self-consistent field theory. *Journal of Physical Chemistry B*, **115**(16):4654–4661, 2011. doi:10.1021/jp109234u.

[27] R. Evans. The nature of the liquid-vapour interface and other topics in the statistical mechanics of non-uniform, classical fluids. *Advances in Physics*, **28**(2):143–200, 1979. doi:10.1080/00018737900101365.

[28] L. Wang, A. Haghmoradi, J. Liu, S. Xi, G. J. Hirasaki, C. A. Miller, and W. G. Chapman. Modeling micelle formation and interfacial properties with iSAFT classical density functional theory. *Journal of Chemical Physics*, **146**(12):124705, 2017. doi:10.1063/1.4978503.

[29] T. Uneyama and M. Doi. Density Functional Theory for Block Copolymer Melts and Blends. *Macromolecules*, **38**(1):196–205, 2005. doi:10.1021/ma049385m.

[30] K. Chang and D. C. Morse. Diblock Copolymer Surfactants in Immiscible Homopolymer Blends: Swollen Micelles and Interfacial Tension. *Macromolecules*, **39**(22):7746–7756, 2006. doi:10.1021/ma060481s.

[31] K. Chang and D. C. Morse. Diblock Copolymer Surfactants in Immiscible Homopolymer Blends: Interfacial Bending Elasticity. *Macromolecules*, **39**(21):7397–7406, 2006. doi:10.1021/ma0604800.

[32] K. Chang, C. W. Macosko, and D. C. Morse. Ultralow Interfacial Tensions of Polymer/Polymer Interfaces with Diblock Copolymer Surfactants. *Macromolecules*, **40**(10):3819–3830, 2007.

doi:10.1021/ma062277a.

[33] C. P. Emborsky, K. R. Cox, and W. G. Chapman. Exploring parameter space effects on structure-property relationships of surfactants at liquid-liquid interfaces. *The Journal of Chemical Physics*, **135**(8):084708, 2011. doi:10.1063/1.3628452.

[34] J. Wu and Z. Li. Density-Functional Theory for Complex Fluids. *Annual Review of Physical Chemistry*, **58**(1):85–112, 2007. doi:10.1146/annurev.physchem.58.032806.104650.

[35] T. Uneyama and M. Doi. Calculation of the Micellar Structure of Polymer Surfactant on the Basis of the Density Functional Theory. *Macromolecules*, **38**(13):5817–5825, 2005. doi:10.1021/ma0507746.

[36] R. Evans. Density Functionals in the Theory of Nonuniform Fluids. In D. Henderson (editor), *Fundamentals of Inhomogeneous Fluids*, chapter 3. Marcel Dekker, Inc., New York, 1992. ISBN 0-8247-8711-0.

[37] M. Telo da Gama and K. Gubbins. Adsorption and orientation of amphiphilic molecules at a liquid-liquid interface. *Molecular Physics*, **59**(2):227–239, 1986. doi:10.1080/00268978600102031.

[38] G. Rosenthal and S. H. L. Klapp. Ordering of amphiphilic Janus particles at planar walls: A density functional study. *The Journal of Chemical Physics*, **134**(15):154707, 2011. doi:10.1063/1.3579453.

[39] C. Guerra, A. M. Somoza, and M. M. Telo da Gama. Asymmetric water-oil-amphiphile mixtures: Lamellar phases and droplet microemulsions. *The Journal of Chemical Physics*, **109**(3):1152–1161, 1998. doi:10.1063/1.476660.

[40] A. M. Somoza, E. Chacon, L. Mederos, and P. Tarazona. A model for membranes, vesicles and micelles in amphiphilic systems. *Journal of Physics: Condensed Matter*, **7**(29):5753–5776, 1995. doi:10.1088/0953-8984/7/29/005.

[41] E. Chacón, A. M. Somoza, and P. Tarazona. Elastic constants from a microscopic model of bilayer membrane. *The Journal of Chemical Physics*, **109**(6):2371–2379, 1998. doi:10.1063/1.476805.

[42] G. Rosenthal, K. E. Gubbins, and S. H. L. Klapp. Self-assembly of model amphiphilic Janus particles. *The Journal of Chemical Physics*, **136**(17):174901, 2012. doi:10.1063/1.4707954.

[43] G. Rosenthal and S. H. L. Klapp. Micelle and Bilayer Formation of Amphiphilic Janus Particles in a Slit-Pore. *International Journal of Molecular Sciences*, **13**(8):9431–9446, 2012. doi:10.3390/ijms13089431.

[44] M. Borówko, T. Pöschel, S. Sokołowski, and T. Staszewski. Janus Particles at Walls Modified with Tethered Chains. *The Journal of Physical Chemistry B*, **117**(4):1166–1175, 2013. doi:10.1021/jp3105979.

[45] O. Pizio, S. Sokołowski, and Z. Sokołowska. The structure and properties of a simple model mixture of amphiphilic molecules and ions at a solid surface. *The Journal of Chemical Physics*, **140**(17):174706, 2014. doi:10.1063/1.4873438.

[46] O. Pizio, W. Rżysko, S. Sokołowski, and Z. Sokołowska. Mixtures of ions and amphiphilic molecules in slit-like pores: A density functional approach. *The Journal of Chemical Physics*, **142**(16):164703, 2015. doi:10.1063/1.4918640.

[47] V. Talanquer and D. W. Oxtoby. Nucleation in molecular and dipolar fluids: Interaction site model. *The Journal of Chemical Physics*, **103**(9):3686–3695, 1995. doi:10.1063/1.470045.

[48] V. Talanquer and D. W. Oxtoby. A density-functional approach to nucleation in micellar solutions. *The Journal of Chemical Physics*, **113**(16):7013–7021, 2000. doi:10.1063/1.1288271.

[49] P. S. Christopher and D. W. Oxtoby. Density functional model of surfactant mesostructures. *The Journal of Chemical Physics*, **117**(20):9502–9509, 2002. doi:10.1063/1.1516785.

[50] M. Borówko, S. Sokołowski, and T. Staszewski. Amphiphilic Dimers at Liquid-Liquid Interfaces: A Density Functional Approach. *Journal of Physical Chemistry B*, **123**(27):5962–5972, 2019. doi:10.1021/acs.jpcb.9b04501.

[51] M. Schmidt and C. von Ferber. Amphiphilic hard body mixtures. *Physical Review E*, **64**(5):051115, 2001. doi:10.1103/PhysRevE.64.051115.

[52] J. M. Brader and M. Schmidt. Entropic interfaces in hard-core model amphiphilic mixtures. *Journal of Colloid and Interface Science*, **281**(2):495–502, 2005. doi:10.1016/j.jcis.2004.08.097.

[53] Y. Rosenfeld. Density functional theory of molecular fluids: Free-energy model for the inhomogeneous hard-body fluid. *Physical Review E*, **50**(5):R3318–R3321, 1994. doi:10.1103/PhysRevE.50.R3318.

[54] F. H. Stillinger. Variational model for micelle structure. *The Journal of Chemical Physics*, **78**(7):4654–4661, 1983. doi:10.1063/1.445310.

[55] S. D. Stoyanov, H. Rehage, and V. N. Paunov. Novel Surface Tension Isotherm for Surfactants Based on Local Density Functional Theory. *Physical Review Letters*, **91**(8):086102, 2003. doi:10.1103/PhysRevLett.91.086102.

[56] W. G. Chapman, G. Jackson, and K. E. Gubbins. Phase equilibria of associating fluids. *Molecular Physics*, **65**(5):1057–1079, 1988. doi:10.1080/00268978800101601.

[57] W. G. Chapman, K. E. Gubbins, G. Jackson, and M. Radosz. New Reference Equation of State for Associating Liquids. *Industrial & Engineering Chemistry Research*, **29**(8):1709–1721, 1990. doi:10.1021/ie00104a021.

[58] M. S. Wertheim. Fluids with Highly Directional Attractive Forces. I. Statistical Thermodynamics. *Journal of Statistical Physics*, **35**(1-2):19–34, 1984. doi:10.1007/BF01017362.

[59] M. S. Wertheim. Fluids with Highly Directional Attractive Forces. II. Thermodynamic Perturbation Theory and Integral Equations. *Journal of Statistical Physics*, **35**(1-2):35–47, 1984. doi:10.1007/BF01017363.

[60] M. S. Wertheim. Fluids with Highly Directional Attractive Forces. III. Multiple Attraction Sites. *Journal of Statistical Physics*, **42**(3-4):459–476, 1986. doi:10.1007/BF01127721.

[61] M. S. Wertheim. Fluids with Highly Directional Attractive Forces. IV. Equilibrium Polymerization. *Journal of Statistical Physics*, **42**(3-4):477–492, 1986. doi:10.1007/BF01127722.

[62] W. Zmpitas and J. Gross. Detailed pedagogical review and analysis of Wertheim's thermodynamic perturbation theory. *Fluid Phase Equilibria*, **428**:121 – 152, 2016. doi:http://dx.doi.org/10.1016/j.fluid.2016.07.033. Theo W. de Loos Festschrift.

[63] S. Tripathi and W. G. Chapman. Microstructure of inhomogeneous polyatomic mixtures from a density functional formalism for atomic mixtures. *The Journal of Chemical Physics*, **122**(9):094506, 2005. doi:10.1063/1.1853371.

[64] S. Tripathi and W. G. Chapman. Microstructure and Thermodynamics of Inhomogeneous Polymer Blends and Solutions. *Physical Review Letters*, **94**(8):087801, 2005. doi:10.1103/PhysRevLett.94.087801.

[65] S. Jain, A. Dominik, and W. G. Chapman. Modified interfacial statistical associating fluid theory: A perturbation density functional theory for inhomogeneous complex fluids. *The Journal of Chemical Physics*, **127**(24):244904, 2007. doi:10.1063/1.2806932.

[66] S. Xi, L. Wang, J. Liu, and W. Chapman. Thermodynamics, Microstructures, and Solubilization of Block Copolymer Micelles by Density Functional Theory. *Langmuir*, **35**(14):5081–5092, 2019. doi:10.1021/acs.langmuir.8b04336. PMID: 30855146.

[67] X. Mu, S. Xi, F. O. Alpak, and W. G. Chapman. Modified Density Gradient Theory for Surfactant Molecules Applied to Oil/Water Interfaces. *Industrial & Engineering Chemistry Research*, **57**(22):7643–7654, 2018. doi:10.1021/acs.iecr.8b00164.

[68] F. J. Blas and L. F. Vega. Thermodynamic behaviour of homonuclear and heteronuclear Lennard-Jones chains with association sites from simulation and theory. *Molecular Physics*, **92**(1):135–150, 1997. doi:10.1080/002689797170707.

[69] F. J. Blas and L. F. Vega. Prediction of Binary and Ternary Diagrams Using the Statistical Associating Fluid Theory (SAFT) Equation of State. *Industrial and Engineering Chemistry Research*, **37**:660–674, 1998. doi:10.1021/ie970449+.

[70] A. Galindo, L. A. Davies, A. Gil-Villegas, and G. Jackson. The thermodynamics of mixtures and the corresponding mixing rules in the SAFT-VR approach for potentials of variable range. *Molecular Physics*, **93**(2):241–252, 1998. doi:10.1080/002689798169249.

[71] A. Gil-Villegas, A. Galindo, P. J. Whitehead, S. J. Mills, G. Jackson, and A. N. Burgess. Statistical

associating fluid theory for chain molecules with attractive potentials of variable range. *The Journal of Chemical Physics*, **106**(10):4168–4186, 1997. doi:10.1063/1.473101.

[72] A. Lymperiadis, C. S. Adjiman, A. Galindo, and G. Jackson. A group contribution method for associating chain molecules based on the statistical associating fluid theory (SAFT-γ). *The Journal of Chemical Physics*, **127**(23):234903, 2007. doi:10.1063/1.2813894.

[73] V. Papaioannou, T. Lafitte, C. Avendaño, C. S. Adjiman, G. Jackson, E. A. Müller, and A. Galindo. Group contribution methodology based on the statistical associating fluid theory for heteronuclear molecules formed from Mie segments. *The Journal of Chemical Physics*, **140**(5):054107, 2014. doi:10.1063/1.4851455.

[74] J. Gross and G. Sadowski. Application of perturbation theory to a hard-chain reference fluid: an equation of state for square-well chains. *Fluid Phase Equilibria*, **168**(2):183–199, 2000. doi:10.1016/S0378-3812(00)00302-2.

[75] J. Gross and G. Sadowski. Perturbed-Chain SAFT: An Equation of State Based on a Perturbation Theory for Chain Molecules. *Industrial & Engineering Chemistry Research*, **40**(4):1244–1260, 2001. doi:10.1021/ie0003887.

[76] J. Gross, O. Spuhl, F. Tumakaka, and G. Sadowski. Modeling Copolymer Systems Using the Perturbed-Chain SAFT Equation of State. *Industrial & Engineering Chemistry Research*, **42**(6):1266–1274, 2003. doi:10.1021/ie020509y.

[77] J. Gross. An Equation-of-State Contribution for Polar Components: Quadrupolar Molecules. *AIChE Journal*, **51**(9):2556–2568, 2005. doi:10.1002/aic.10502.

[78] J. Gross and J. Vrabec. An Equation-of-State Contribution for Polar Components: Dipolar Molecules. *AIChE Journal*, **52**(3):1194–1204, 2006. doi:10.1002/aic.10683.

[79] J. Vrabec and J. Gross. Vapor-Liquid Equilibria Simulation and an Equation of State Contribution for Dipole-Quadrupole Interactions. *The Journal of Physical Chemistry B*, **112**(1):51–60, 2008. doi:10.1021/jp072619u.

[80] F. Tumakaka, J. Gross, and G. Sadowski. Thermodynamic modeling of complex systems using PC-SAFT. *Fluid Phase Equilibria*, **228-229**:89–98, 2005. doi:10.1016/j.fluid.2004.09.037.

[81] M. Lampe, M. Stavrou, H. M. Bücker, J. Gross, and A. Bardow. Simultaneous Optimization of Working Fluid and Process for Organic Rankine Cycles Using PC-SAFT. *Industrial & Engineering Chemistry Research*, **53**(21):8821–8830, 2014. doi:10.1021/ie5006542.

[82] P. V. Pontes, E. A. Crespo, M. A. Martins, L. P. Silva, C. M. Neves, G. J. Maximo, M. D. Hubinger, E. A. Batista, S. P. Pinho, J. A. Coutinho, G. Sadowski, and C. Held. Measurement and PC-SAFT modeling of solid-liquid equilibrium of deep eutectic solvents of quaternary ammonium chlorides and carboxylic acids. *Fluid Phase Equilibria*, **448**:69–80, 2017. doi:10.1016/j.fluid.2017.04.007.

[83] J. Gross. A density functional theory for vapor-liquid interfaces using the PCP-SAFT equation of

state. *The Journal of Chemical Physics*, **131**(20):204705, 2009. doi:10.1063/1.3263124.

[84] E. Sauer and J. Gross. Classical Density Functional Theory for Liquid-Fluid Interfaces and Confined Systems: A Functional for the Perturbed-Chain Polar Statistical Associating Fluid Theory Equation of State. *Industrial & Engineering Chemistry Research*, **56**(14):4119–4135, 2017. doi:10.1021/acs.iecr.6b04551.

[85] X. Tang and J. Gross. Density functional theory for calculating surface tensions with a simple renormalization formalism for the critical point. *The Journal of Supercritical Fluids*, **55**(2):735–742, 2010. doi:10.1016/j.supflu.2010.09.041.

[86] A. von Müller and K. Leonhard. Surface tension calculations by means of a PCP-SAFT-DFT formalism using equation of state parameters from quantum mechanics. *Fluid Phase Equilibria*, **356**:96–101, 2013. doi:10.1016/j.fluid.2013.07.005.

[87] C. Klink and J. Gross. A Density Functional Theory for Vapor-Liquid Interfaces of Mixtures Using the Perturbed-Chain Polar Statistical Associating Fluid Theory Equation of State. *Industrial & Engineering Chemistry Research*, **53**(14):6169–6178, 2014. doi:10.1021/ie4029895.

[88] C. Klink, B. Planková, and J. Gross. Density Functional Theory for Liquid-Liquid Interfaces of Mixtures Using the Perturbed-Chain Polar Statistical Associating Fluid Theory Equation of State. *Industrial & Engineering Chemistry Research*, **54**(16):4633–4642, 2015. doi:10.1021/acs.iecr.5b00445.

[89] E. Sauer, A. Terzis, M. Theiss, B. Weigand, and J. Gross. Prediction of Contact Angles and Density Profiles of Sessile Droplets Using Classical Density Functional Theory Based on the PCP-SAFT Equation of State. *Langmuir*, **34**(42):12519–12531, 2018. doi:10.1021/acs.langmuir.8b01985. PMID: 30247038.

[90] E. Sauer and J. Gross. Prediction of Adsorption Isotherms and Selectivities: Comparison between Classical Density Functional Theory Based on the Perturbed-Chain Statistical Associating Fluid Theory Equation of State and Ideal Adsorbed Solution Theory. *Langmuir*, **35**(36):11690–11701, 2019. doi:10.1021/acs.langmuir.9b02378. PMID: 31403314.

[91] E. Sauer, M. Stavrou, and J. Gross. Comparison between a Homo- and a Heterosegmented Group Contribution Approach Based on the Perturbed-Chain Polar Statistical Associating Fluid Theory Equation of State. *Industrial & Engineering Chemistry Research*, **53**(38):14854–14864, 2014. doi:10.1021/ie502203w.

[92] J. Mairhofer, B. Xiao, and J. Gross. A classical density functional theory for vapor-liquid interfaces consistent with the heterosegmented group-contribution perturbed-chain polar statistical associating fluid theory. *Fluid Phase Equilibria*, **472**:117 – 127, 2018. doi:https://doi.org/10.1016/j.fluid.2018.05.016.

[93] B. C. J. Segura, W. G. Chapman, and K. P. Shukla. Associating fluids with four bonding

sites against a hard wall: density functional theory. *Molecular Physics*, **90**(5):759–772, 1997. doi:10.1080/002689797172110.

[94] M. L. Michelsen and E. M. Hendriks. Physical properties from association models. *Fluid Phase Equilibria*, **180**(1):165 – 174, 2001. doi:https://doi.org/10.1016/S0378-3812(01)00344-2.

[95] Y. Zhang, A. Valiya Parambathu, and W. G. Chapman. Density functional study of dendrimer molecules in solvents of varying quality. *The Journal of Chemical Physics*, **149**(6):064904, 2018. doi:10.1063/1.5035423.

[96] Y. Rosenfeld. Free-energy model for the inhomogeneous hard-sphere fluid mixture and density-functional theory of freezing. *Physical Review Letters*, **63**:980–983, 1989. doi:10.1103/PhysRevLett.63.980.

[97] P. Tarazona. Free-energy density functional for hard spheres. *Physical Review A*, **31**:2672–2679, 1985. doi:10.1103/PhysRevA.31.2672.

[98] D. E. Sullivan. Van der Waals model of adsorption. *Physical Review B*, **20**:3991–4000, 1979. doi:10.1103/PhysRevB.20.3991.

[99] P. Tarazona and R. Evans. A simple density functional theory for inhomogeneous liquids. *Molecular Physics*, **52**(4):847–857, 1984. doi:10.1080/00268978400101601.

[100] R. Stierle, E. Sauer, J. Eller, M. Theiss, P. Rehner, P. Ackermann, and J. Gross. Guide to efficient solution of PC-SAFT classical density functional theory in various coordinate systems using fast fourier and similar transforms. *Fluid Phase Equilibria*, page 112306, 2019. doi:https://doi.org/10.1016/j.fluid.2019.112306.

[101] R. Roth, R. Evans, A. Lang, and G. Kahl. Fundamental measure theory for hard-sphere mixtures revisited: the White Bear version. *Journal of Physics: Condensed Matter*, **14**(46):12063, 2002. doi:10.1088/0953-8984/14/46/313.

[102] Y.-X. Yu and J. Wu. Structures of hard-sphere fluids from a modified fundamental-measure theory. *The Journal of Chemical Physics*, **117**(22):10156–10164, 2002. doi:10.1063/1.1520530.

[103] Y.-X. Yu and J. Wu. A fundamental-measure theory for inhomogeneous associating fluids. *The Journal of Chemical Physics*, **116**(16):7094–7103, 2002. doi:10.1063/1.1463435.

[104] M. L. Michelsen. Robust and efficient solution procedures for association models. *Industrial & engineering chemistry research*, **45**(25):8449–8453, 2006. doi:10.1021/ie060029x.

[105] S. H. Huang and M. Radosz. Equation of state for small, large, polydisperse, and associating molecules. *Industrial & Engineering Chemistry Research*, **29**(11):2284–2294, 1990. doi:10.1021/ie00107a014.

[106] Dortmund Data Bank. *www.ddbst.com*, 2020.

[107] S. Zeppieri, J. Rodríguez, and A. L. López de Ramos. Interfacial Tension of Alkane + Water Sys-

tems. *Journal of Chemical & Engineering Data*, **46**(5):1086–1088, 2001. doi:10.1021/je000245r.

[108] G. Scatchard and G. M. Wilson. Vapor-Liquid Equilibrium. XIII. The System Water-Butyl Glycol from 5 to 85°. *Journal of the American Chemical Society*, **86**(2):133–137, 1964. doi:10.1021/ja01056a004.

[109] M. Hirata and D. Hoshino. A study on vapor–liquid equilibria based on the theory of solution of groups model. *Asahi Garasu Kogyo Gijutsu Shoreikai Kenkyu Hokoku*, **41**:115–122, 1982.

[110] O. Chiavone-Filho, P. Proust, and P. Rasmussen. Vapor-liquid equilibria for glycol ether + water systems. *Journal of Chemical & Engineering Data*, **38**(1):128–131, 1993. doi:10.1021/je00009a031.

[111] J. Eastoe, J. S. Dalton, P. G. Rogueda, E. R. Crooks, A. R. Pitt, and E. A. Simister. Dynamic Surface Tensions of Nonionic Surfactant Solutions. *Journal of Colloid and Interface Science*, **188**(2):423–430, 1997. doi:https://doi.org/10.1006/jcis.1997.4778.

8 Conclusion

In the first part of this thesis, classical density functional theory (DFT) is used to model the interfacial properties of highly curved interfaces. From direct calculations of nanodroplets and -bubbles in spherical coordinates, the dependence of the surface tension on the curvature of the interface is shown to be well described by a second order polynomial. Based on this observation, a method is developed to calculate the coefficients of the polynomial from properties of a planar interface. This method reduces the dimensionality of the problem by one and eliminates the need for convolution integrals in spherical and cylindrical coordinate systems. The influence of the curvature on interfacial properties becomes relevant for the smallest of droplets, like critical clusters during nucleation processes. Correctly accounting for the curvature effect on the surface tension is one measure to increase the predictive capability of nucleation theories.

Further, predictive density gradient theory (pDGT) is introduced as a model with the appealing mathematical structure of a standard density gradient theory, but the predictive power originating from a DFT approach. In pDGT, the influence matrix, like the Helmholtz energy density, is calculated as a function of the local densities and temperature. The method is developed from DFT by a Taylor expansion of the full Helmholtz energy functional from DFT around a local density. This derivation implies limitations of pDGT in cases with steep density gradients. Indeed, for vapor-liquid systems, the deviation of surface tensions from pDGT compared to DFT results is highest at low temperatures, where the interfacial thickness is lowest. Also, any DGT is not able to model individual peaks in adsorption layers, that can be observed in molecular simulations and are well described by DFT. Therefore, the application is restricted to fluid-liquid interfaces. Because it can be written explicitly and therefore solved without iterating, the most advantageous application of pDGT is the prediction of surface tensions of pure components. This property of pDGT was exploited in a further study to assess the choice of PCP-SAFT parameters of water and alcohols. For water, a multitude of parametrizations have been published with different objective functions used for the regression. A common observation is that for water and other associating components, parametrizations that were obtained by fitting to phase equilibrium data are not able to reproduce experimental surface tension values. Therefore, a multiobjective optimization approach, in which different association models were compared, is employed. The two objectives in this case are bulk

phase equilibrium properties and surface tensions. The resulting pareto fronts give insight on what compromises between both objectives are attainable and can thus help assess strengths in different models.

The optimized water model is then used as a basis to study interfacial properties of water/surfactant and water/alkane/surfactant systems. Due to their amphiphilic character, the DFT approach has to be able to describe the polar heads and non-polar tails of the surfactant molecules individually. Therefore, the group contribution PC-SAFT equation of state is combined with a heteronuclear DFT approach. The model is parametrized using experimental data of small surfactants and is then used to predict properties of planar interfaces containing surfactants with additional head and tail groups. The model is able to capture the enrichment and the orientation of surfactant molecules in interfaces and predicts a steep decline in interfacial tensions at small bulk surfactant concentrations. The properties of surfactant systems are strongly influenced by the presence of structures like micelles. Therefore, the study could be extended by using DFT in spherical or cylindrical coordinates to calculate density profiles in micelles. Comparing free energies of different states then leads to a phase diagram prediction.

Appendices

A Supporting information to chapter 4

A.1 Additional results for Helfrich coefficients

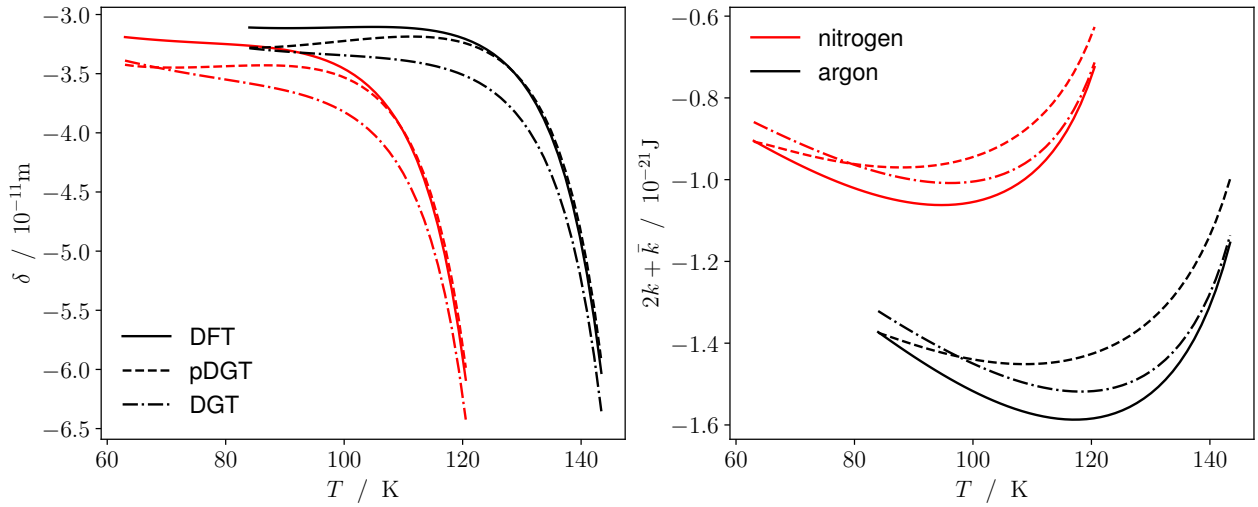

Figure A.1: Tolman length and spherical rigidity of argon and nitrogen.

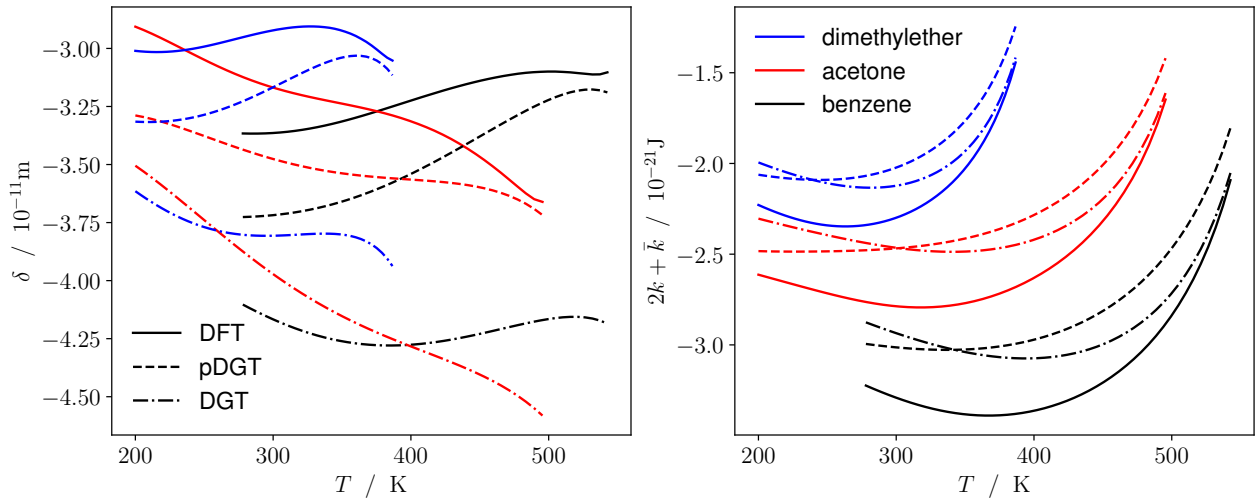

Figure A.2: Tolman length and spherical rigidity of the polar components benzene, acetone and dimethylether.

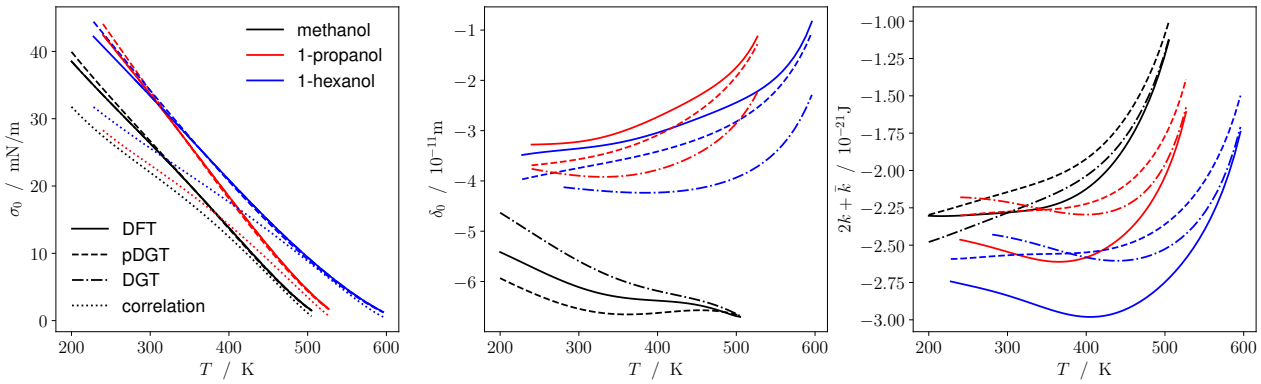

Figure A.3: Surface tension, Tolman length and spherical rigidity of three alkanols. Comparison between DFT, pDGT, DGT and empirical correlations[1]

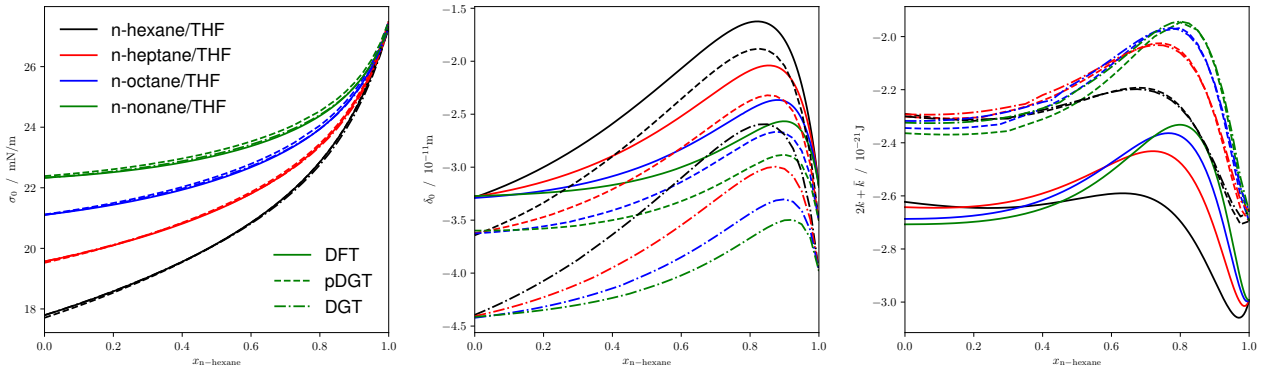

Figure A.4: Surface tension, Tolman length and spherical rigidity of the mixture of tetrahydrofuran with different n-alkanes at $T = 298.15\,\mathrm{K}$. Comparison between DFT, pDGT and DGT results.

A.2 Curvature expansion of convolution integrals

To obtain the curvature expansion of 3D convolution integrals, an explicit formula for them is required. A path to obtain those is the projection-slice theorem of the Fourier transform, that states that a slice along an axis through a multidimensional Fourier transform is equal to the Fourier transform of the projection on the same axis. The convolution integral can thus be written as

$$f \overset{3D}{\otimes} \omega = \mathscr{P}^{-1}\mathscr{F}^{-1}\left(\mathscr{F}\mathscr{P}(f)\mathscr{F}\mathscr{P}(\omega)\right) \tag{A.1}$$

where $\mathscr{P}(f)$ is the appropriate projection of f on one of the axes and $\mathscr{F}(f)$ the 1D Fourier transform along said axis.

A.2.1 Spherical coordinate system

If $f(r)$ or $\vec{f}(\mathbf{r}) = f_r(r)\vec{e}_r$ is spherically symmetric, the projection takes the simple form

$$\mathscr{P}(f(r))(z) = 2\pi \int_{|z|}^{\infty} f(r) r \,\mathrm{d}r \qquad \mathscr{P}(\vec{f}(r))(z) = 2\pi z \vec{e}_z \int_{|z|}^{\infty} f_r(r) \,\mathrm{d}r \tag{A.2}$$

and the corresponding inverse transforms are

$$\mathscr{P}^{-1}(F(z))(r) = -\frac{1}{2\pi r} \left.\frac{\mathrm{d}F(z)}{\mathrm{d}z}\right|_{z=r} \qquad \mathscr{P}^{-1}(\vec{F}(z))(r) = -\frac{1}{2\pi}\vec{e}_r \left.\frac{\mathrm{d}\frac{F_z(z)}{z}}{\mathrm{d}z}\right|_{z=r} \tag{A.3}$$

The convolution of a scalar function with a scalar weight function thus can be written as

$$\begin{aligned}
f \overset{3D}{\otimes} \omega &= -\frac{1}{2\pi r} \int \frac{\mathrm{d}}{\mathrm{d}z} \left(2\pi \int f(r') r' \Theta(r' - |z - z'|) \,\mathrm{d}r' \right)_{z=r} \omega(z') \,\mathrm{d}z' \\
&= -\frac{1}{r} \iint f(r') r' \delta(r' - |r - z'|)(-\mathrm{sign}(r - z'))\omega(z') \,\mathrm{d}z' \\
&= \frac{1}{r} \int f(|r - z'|)(r - z')\omega(z') \,\mathrm{d}z' \\
&= \int f(|r - z'|)\omega(z') \,\mathrm{d}z' - \frac{1}{r} \int f(|r - z'|) z' \omega(z') \,\mathrm{d}z' \\
&= f \otimes \omega - \frac{1}{r}(f \otimes (z\omega)) \\
&= f \otimes \omega - f \otimes (z\omega) \frac{1}{R} + z(f \otimes (z\omega)) \frac{1}{R^2} + \dots
\end{aligned} \tag{A.4}$$

Similar expressions can be derived for the convolution with a vector weight function

$$\begin{aligned}
f \overset{3D}{\otimes} \vec{\omega} &= -\frac{1}{2\pi}\vec{e}_r \int \frac{\mathrm{d}}{\mathrm{d}z} \left(\frac{1}{z} 2\pi \int f(r') r' \Theta(r' - |z - z'|) \,\mathrm{d}r' \right)_{z=r} \omega_z(z') \,\mathrm{d}z' \\
&= -\vec{e}_r \iint f(r') r' \left(\frac{-1}{r^2} \Theta(r' - |r - z'|) + \frac{1}{r} \delta(r' - |r - z'|)(-\mathrm{sign}(r - z')) \right) \mathrm{d}r' \omega_z(z') \,\mathrm{d}z' \\
&= \vec{e}_r \left(f \otimes \omega_z - \frac{1}{r}(f \otimes (z\omega_z)) + \frac{1}{r^2} \iint f(r') r' \omega_z(z') \Theta(z' - (r - r')) \,\mathrm{d}z' \,\mathrm{d}r' \right) \\
&= \vec{e}_r \left(f \otimes \omega_z - \frac{1}{r}(f \otimes (z\omega_z)) + \frac{1}{r^2}((rf) \otimes \hat{\omega}_z) \right) \\
&= \vec{e}_r \left(f \otimes \omega_z - \frac{1}{r}(f \otimes (z\omega_z - \hat{\omega}_z)) - \frac{1}{r^2}(f \otimes (z\hat{\omega}_z)) \right) \\
&= \vec{e}_r \left(f \otimes \omega_z - f \otimes (z\omega_z - \hat{\omega}_z) \frac{1}{R} + z(f \otimes (z\omega_z - \hat{\omega}_z)) \frac{1}{R^2} - f \otimes (z\hat{\omega}_z) \frac{1}{R^2} + \dots \right)
\end{aligned} \tag{A.5}$$

and the convolution of the inner product of a vector function and a vector weight function

$$\begin{aligned}
\vec{f} \overset{3D}{\otimes} \vec{\omega} &= \mathscr{P}^{-1}\mathscr{F}^{-1}\left(\mathscr{F}\mathscr{P}(\vec{f}) \cdot \mathscr{F}\mathscr{P}(\vec{\omega})\right) \\
&= -\frac{1}{2\pi r}\int \frac{\mathrm{d}}{\mathrm{d}z}\left(2\pi(z-z')\int f_r(r')\Theta(r'-|z-z'|)\,\mathrm{d}r'\right)_{z=r} \omega_z(z')\,\mathrm{d}z' \\
&= -\frac{1}{r}\iint f_r(r')\left(\Theta(r'-|r-z'|)+(r-z')\delta(r'-|r-z'|)(-\mathrm{sign}(r-z'))\right)\mathrm{d}r'\,\omega_z(z')\,\mathrm{d}z' \\
&= f_r \otimes \omega_z - \frac{1}{r} f_r \otimes (z\omega_z) - \frac{1}{r}\iint f_r(r')\omega_z(z')\Theta(z'-(r-r'))\,\mathrm{d}z'\,\mathrm{d}r' \\
&= f_r \otimes \omega_z - \frac{1}{r} f_r \otimes (z\omega_z + \tilde{\omega}) \\
&= f_r \otimes \omega_z - f_r \otimes (z\omega_z + \tilde{\omega})\frac{1}{R} + z\,(f_r \otimes (z\omega_z + \tilde{\omega}))\frac{1}{R^2} + \ldots
\end{aligned} \tag{A.6}$$

In the process, the weight function $\hat{\omega}_z$ was introduced as

$$\hat{\omega}_z(z) = \int_z^\infty \omega_z(z')\,\mathrm{d}z' \tag{A.7}$$

A.2.2 Cylindrical coordinate system

The same concept applied to a cylindrically symmetric function becomes significantly more strenuous. The projection in this case is commonly known as Abel transform

$$\mathscr{A}(f(r))(y) = 2\int_{|y|}^\infty \frac{f(r)r}{\sqrt{r^2-y^2}}\,\mathrm{d}r = -2\int_{|y|}^\infty f'(r)\sqrt{r^2-y^2}\,\mathrm{d}r \tag{A.8}$$

with the corresponding inverse transform

$$\mathscr{A}^{-1}(F(y))(r) = -\frac{1}{\pi}\int_r^\infty \frac{\mathrm{d}F}{\mathrm{d}y}\frac{1}{\sqrt{y^2-r^2}}\,\mathrm{d}y \tag{A.9}$$

The transformation can be extended to vector functions $\vec{f}(\mathbf{r}) = f_r(r)\vec{e}_r$

$$\mathscr{A}(\vec{f}(r))(y) = 2y\vec{e}_y\int_{|y|}^\infty f_r(r)\frac{1}{\sqrt{r^2-y^2}}\,\mathrm{d}r = -2y\vec{e}_y\int_{|y|}^\infty f_r'(r)\ln\left(\frac{\sqrt{r^2-y^2}+r}{|y|}\right)\mathrm{d}r \tag{A.10}$$

$$\mathscr{A}^{-1}(\vec{F}(y))(r) = -\frac{1}{\pi}\vec{e}_r \int_r^\infty \frac{\mathrm{d}\frac{F_y}{y}}{\mathrm{d}y} \frac{r}{\sqrt{y^2-r^2}}\,\mathrm{d}y \tag{A.11}$$

The convolution integrals do not simplify as nicely as they do in spherical coordinates.

$$\begin{aligned}
f \overset{3D}{\otimes} \omega &= \mathscr{A}^{-1}\mathscr{F}^{-1}(\mathscr{F}\mathscr{A}(f)\mathscr{F}\mathscr{P}(\omega)) \\
&= -\frac{1}{\pi}\int_r^\infty \int \frac{\mathrm{d}}{\mathrm{d}y}\left(-2\int_{y-y'}^\infty f'(r')\sqrt{r'^2-(y-y')^2}\,\mathrm{d}r'\right)\omega(y')\,\mathrm{d}y'\frac{1}{\sqrt{y^2-r^2}}\,\mathrm{d}y \\
&= -\frac{2}{\pi}\int_r^\infty \int \int_{y-y'}^\infty \frac{f'(r')(y-y')}{\sqrt{r'^2-(y-y')^2}}\,\mathrm{d}r'\omega(y')\,\mathrm{d}y'\frac{1}{\sqrt{y^2-r^2}}\,\mathrm{d}y \\
&= -\frac{2}{\pi}\int \int_{r-y'}^\infty \int_r^{r'+y'} \frac{(y-y')}{\sqrt{(r'^2-(y-y')^2)(y^2-r^2)}}\,\mathrm{d}y f'(r')\,\mathrm{d}r'\omega(y')\,\mathrm{d}y'
\end{aligned}$$

The innermost integral has to our knowledge no analytic solution. By doing the curvature expansion at this point during the derivation, however, we are at least able to obtain the solution as a series expansion.

$$\begin{aligned}
f \overset{3D}{\otimes} \omega &= -\int \int_{z-y'}^\infty \left(1-\frac{1}{2}y'\frac{1}{R}+\frac{1}{8}y'(3z+z')\frac{1}{R^2}+\ldots\right)f'(z')\,\mathrm{d}z'\omega(y')\,\mathrm{d}y' \\
&= f\otimes\omega - \frac{1}{2}f\otimes(z\omega)\frac{1}{R} - \frac{1}{8}\int\int_{z-y'}^\infty (3z+z')f'(z')\,\mathrm{d}z'y'\omega(y')\,\mathrm{d}y'\frac{1}{R^2}+\ldots \\
&= f\otimes\omega - \frac{1}{2}f\otimes(z\omega)\frac{1}{R} + \frac{1}{8}\left(\int(4z-y')f(z')y'\omega(y')\,\mathrm{d}y' + \int\int_{z-y'}^\infty f(z')y'\omega(y')\,\mathrm{d}z'\,\mathrm{d}y'\right)\frac{1}{R^2}+\ldots \\
&= f\otimes\omega - \frac{1}{2}f\otimes(z\omega)\frac{1}{R} + \frac{1}{2}z(f\otimes(z\omega))\frac{1}{R^2} - \frac{1}{8}f\otimes\left(z^2\omega-\tilde{\omega}\right)\frac{1}{R^2}+\ldots
\end{aligned}$$

The same procedure is used to obtain expressions for convolutions with vector weight functions

$$\begin{aligned}
f \overset{3D}{\otimes} \vec{\omega} &= \mathscr{A}^{-1}\mathscr{F}^{-1}(\mathscr{F}\mathscr{A}(f)\mathscr{F}\mathscr{P}(\vec{\omega})) \\
&= -\frac{1}{\pi}\vec{e}_r\int_r^\infty \int \frac{\mathrm{d}}{\mathrm{d}y}\frac{1}{y}\left(-2\int_{y-y'}^\infty f'(r')\sqrt{r'^2-(y-y')^2}\,\mathrm{d}r'\right)\omega_z(y')\,\mathrm{d}y'\frac{r}{\sqrt{y^2-r^2}}\,\mathrm{d}y \\
&= -\frac{2}{\pi}\vec{e}_r\int_r^\infty \int \int_{y-y'}^\infty f'(r')\left(\frac{1}{y^2}\sqrt{r'^2-(y-y')^2}+\frac{y-y'}{y\sqrt{r'^2-(y-y')^2}}\right)\mathrm{d}r'\omega_z(y')\,\mathrm{d}y'\frac{r}{\sqrt{y^2-r^2}}\,\mathrm{d}y
\end{aligned}$$

$$
\begin{aligned}
&= -\frac{2}{\pi}\vec{e}_r \int \int_{r-y'}^{\infty} \int_{r}^{r'+y'} \left(\frac{r\sqrt{r'^2-(y-y')^2}}{y^2\sqrt{y^2-r^2}} + \frac{r(y-y')}{y\sqrt{(r'^2-(y-y')^2)(y^2-r^2)}} \right) \mathrm{d}y f'(r')\,\mathrm{d}r'\omega_z(y')\,\mathrm{d}y' \\
&= -\frac{2}{\pi}\vec{e}_r \int \int_{r-y'}^{\infty} \int_{r}^{r'+y'} \frac{r(r'^2+y'(y-y'))}{y^2\sqrt{(r'^2-(y-y')^2)(y^2-r^2)}}\,\mathrm{d}y f'(r')\,\mathrm{d}r'\omega_z(y')\,\mathrm{d}y' \\
&= -\vec{e}_r \int \int_{z-y'}^{\infty} \left(1 - \frac{1}{2}(z-z')\frac{1}{R} + \frac{1}{16}(-3y'^2+9z^2-10zz'+z'^2)\frac{1}{R^2} + \ldots\right) f'(z')\,\mathrm{d}z'\omega_z(y')\,\mathrm{d}y' \\
&= \vec{e}_r \left(f \otimes \omega_z - \frac{1}{2} f \otimes (z\omega_z - \hat{\omega}_z)\frac{1}{R} + \frac{1}{2} z\,(f \otimes (z\omega_z - \hat{\omega}_z))\frac{1}{R^2} - \frac{1}{8} f \otimes \left(z\hat{\omega}_z + z^2\omega_z\right)\frac{1}{R^2} + \ldots \right)
\end{aligned}
$$

and the convolution of the inner product

$$
\begin{aligned}
\vec{f} \overset{3D}{\otimes} \vec{\omega} &= \mathscr{A}^{-1}\mathscr{F}^{-1}\left(\mathscr{F}\mathscr{A}(\vec{f}) \cdot \mathscr{F}\mathscr{P}(\vec{\omega})\right) \\
&= -\frac{1}{\pi}\int_{r}^{\infty} \int \frac{\mathrm{d}}{\mathrm{d}y} \left(-2(y-y') \int_{y-y'}^{\infty} f_r'(r') \ln\left(\frac{\sqrt{r'^2-(y-y')^2}+r'}{y-y'} \right) \mathrm{d}r' \right) \omega_z(y')\,\mathrm{d}y' \frac{1}{\sqrt{y^2-r^2}}\,\mathrm{d}y \\
&= -\frac{2}{\pi}\int_{r}^{\infty} \int \int_{y-y'}^{\infty} f_r'(r') \frac{r'}{\sqrt{r'^2-(y-y')^2}}\,\mathrm{d}r'\omega_z(y')\,\mathrm{d}y' \frac{1}{\sqrt{y^2-r^2}}\,\mathrm{d}y \\
&\quad -\frac{2}{\pi}\int_{r}^{\infty} \int \int_{y-y'}^{\infty} f_r(r') \frac{1}{\sqrt{r'^2-(y-y')^2}}\,\mathrm{d}r'\omega_z(y')\,\mathrm{d}y' \frac{1}{\sqrt{y^2-r^2}}\,\mathrm{d}y \\
&= -\frac{2}{\pi}\int \int_{r-y'}^{\infty} \int_{r}^{r'+y'} \frac{r'}{\sqrt{(r'^2-(y-y')^2)(y^2-r^2)}}\,\mathrm{d}y f_r'(r')\,\mathrm{d}r'\omega_z(y')\,\mathrm{d}y' \\
&\quad -\frac{2}{\pi}\int \int_{r-y'}^{\infty} \int_{r}^{r'+y'} \frac{1}{\sqrt{(r'^2-(y-y')^2)(y^2-r^2)}}\,\mathrm{d}y f_r(r')\,\mathrm{d}r'\omega_z(y')\,\mathrm{d}y' \\
&= -\int \int_{z-y'}^{\infty} \left(1 - \frac{1}{2}(z-z')\frac{1}{R} + \frac{1}{16}\left(y'^2+5z^2-2zz'-3z'^2\right)\frac{1}{R^2} + \ldots\right) f_r'(z')\,\mathrm{d}z'\omega_z(y')\,\mathrm{d}y' \\
&\quad -\int \int_{z-y'}^{\infty} \left(\frac{1}{R} - \frac{1}{2}(z+z')\frac{1}{R^2} + \ldots\right) f_r(z')\,\mathrm{d}z'\omega_z(y')\,\mathrm{d}y' \\
&= f_r \otimes \omega_z - \frac{1}{2} f_r \otimes (z\omega_z + \hat{\omega}_z)\frac{1}{R} + \frac{1}{2} z\,(f_r \otimes (z\omega_z + \hat{\omega}_z))\frac{1}{R^2} - \frac{1}{8}\left(f_r \otimes \left(z\hat{\omega}_z + z^2\omega_z\right)\right)\frac{1}{R^2} + \ldots
\end{aligned}
$$

The two geometries can be combined using the geometry factor g for the three cases

$$
f \overset{3D}{\otimes} \omega = f \otimes \omega - \frac{g}{2} f \otimes (z\omega)\frac{1}{R} + \frac{g}{2} z\,(f \otimes (z\omega))\frac{1}{R^2} + \frac{g(g-2)}{8} f \otimes \left(z^2\omega - \tilde{\omega}\right)\frac{1}{R^2} + \ldots \quad \text{(A.12)}
$$

$$f \overset{3D}{\otimes} \vec{\omega} = \vec{e}_r \left(f \otimes \omega_z - \frac{g}{2} f \otimes (z\omega_z - \hat{\omega}_z) \frac{1}{R} + \frac{g}{2} z \left(f \otimes (z\omega_z - \hat{\omega}_z) \right) \frac{1}{R^2} + \frac{g(g-2)}{8} f \otimes \left(z\hat{\omega}_z + z^2 \omega_z \right) \frac{1}{R^2} - \frac{g(g-1)}{2} f \otimes (z\hat{\omega}_z) + \dots \right) \quad \text{(A.13)}$$

$$\vec{f} \overset{3D}{\otimes} \vec{\omega} = f_r \otimes \omega_z - \frac{g}{2} f_r \otimes (z\omega_z + \hat{\omega}_z) \frac{1}{R} + \frac{g}{2} z \left(f_r \otimes (z\omega_z + \hat{\omega}_z) \right) \frac{1}{R^2} + \frac{g(g-2)}{8} \left(f_r \otimes \left(z\hat{\omega}_z + z^2 \omega_z \right) \right) \frac{1}{R^2} + \dots \quad \text{(A.14)}$$

A.3 Derivation of the second order expressions for the surface tension

The first term in the general expression for the second order correction to the surface tension

$$\int \left(f_2 - \boldsymbol{\rho}_2 \cdot \boldsymbol{\mu}_0 - \frac{1}{2} \boldsymbol{\rho}_1 \cdot \boldsymbol{\mu}_1 \right) \mathrm{d}z + g \int (f_1 - \boldsymbol{\rho}_1 \cdot \boldsymbol{\mu}_0) z \, \mathrm{d}z \quad \text{(A.15)}$$

can be rewritten using the curvature expansion of the Helmholtz energy density, the weighted densities and the Euler-Lagrange equation. The resulting sum over weighted densities can be split into a sum over scalar weighted densities

$$\begin{aligned} &\int \sum_{\alpha}^{\text{scal}} \Bigg(f_{\alpha 0} \left(\boldsymbol{\rho}_2 \otimes \boldsymbol{\omega}_\alpha - \frac{g}{2} \boldsymbol{\rho}_1 \otimes (z\boldsymbol{\omega}_\alpha) + \frac{g}{2} z \left(\boldsymbol{\rho}_0 \otimes (z\boldsymbol{\omega}_\alpha) \right) + \frac{g(g-2)}{8} \boldsymbol{\rho}_0 \otimes \tilde{\boldsymbol{\omega}}_\alpha \right) \\ &+ \frac{1}{2} f_{\alpha 1} \left(\boldsymbol{\rho}_1 \otimes \boldsymbol{\omega}_\alpha - \frac{g}{2} \boldsymbol{\rho}_0 \otimes (z\boldsymbol{\omega}_\alpha) \right) - \boldsymbol{\rho}_2 \cdot (f_{\alpha 0} \otimes \boldsymbol{\omega}_\alpha) \\ &- \frac{1}{2} \boldsymbol{\rho}_1 \cdot \left(f_{\alpha 1} \otimes \boldsymbol{\omega}_\alpha - \frac{g}{2} f_{\alpha 0} \otimes (z\boldsymbol{\omega}_\alpha) \right) \Bigg) \mathrm{d}z \\ &+ g \int \sum_{\alpha}^{\text{scal}} \left(f_{\alpha 0} (\boldsymbol{\rho}_1 \otimes \boldsymbol{\omega}_\alpha) - \frac{g}{2} f_{\alpha 0} (\boldsymbol{\rho}_0 \otimes (z\boldsymbol{\omega}_\alpha)) - \boldsymbol{\rho}_1 \cdot (f_{\alpha 0} \otimes \boldsymbol{\omega}_\alpha) \right) z \, \mathrm{d}z \end{aligned} \quad \text{(A.16)}$$

which simplifies to

$$\begin{aligned} &- \frac{g}{4} \int \sum_{\alpha}^{\text{scal}} \left(\boldsymbol{\rho}_1 \cdot (f_{\alpha 0} \otimes (z\boldsymbol{\omega}_\alpha)) + f_{\alpha 1} (\boldsymbol{\rho}_0 \otimes (z\boldsymbol{\omega}_\alpha)) \right) \mathrm{d}z \\ &+ \frac{g(g-2)}{8} \int \sum_{\alpha}^{\text{scal}} f_{\alpha 0} (\boldsymbol{\rho}_0 \otimes \tilde{\boldsymbol{\omega}}_\alpha) \, \mathrm{d}z - \frac{g(g-1)}{2} \int \sum_{\alpha}^{\text{scal}} f_{\alpha 0} (\boldsymbol{\rho}_0 \otimes (z\boldsymbol{\omega}_\alpha)) z \, \mathrm{d}z \end{aligned} \quad \text{(A.17)}$$

and vector weighted densities

$$\int \sum_{\alpha}^{\text{vec}} \Big(f_{\alpha 0} \Big(\boldsymbol{\rho}_2 \otimes \boldsymbol{\omega}_{\alpha z} - \frac{g}{2} \boldsymbol{\rho}_1 \otimes (z \boldsymbol{\omega}_{\alpha z} - \hat{\boldsymbol{\omega}}_{\alpha z}) + \frac{g}{2} z \, (\boldsymbol{\rho}_0 \otimes (z \boldsymbol{\omega}_{\alpha z} - \hat{\boldsymbol{\omega}}_{\alpha z})) \\ + \frac{g(g-2)}{8} \boldsymbol{\rho}_0 \otimes \left(z^2 \boldsymbol{\omega}_{\alpha z} \right) - \frac{g(3g-2)}{8} \boldsymbol{\rho}_0 \otimes (z \hat{\boldsymbol{\omega}}_{\alpha}) \Big) \\ + \frac{1}{2} f_{\alpha 1} \Big(\boldsymbol{\rho}_1 \otimes \boldsymbol{\omega}_{\alpha z} - \frac{g}{2} \boldsymbol{\rho}_0 \otimes (z \boldsymbol{\omega}_{\alpha z} - \hat{\boldsymbol{\omega}}_{\alpha z}) \Big) + \boldsymbol{\rho}_2 \cdot (f_{\alpha 0} \otimes \boldsymbol{\omega}_{\alpha z}) \\ + \frac{1}{2} \boldsymbol{\rho}_1 \cdot \Big(f_{\alpha 1} \otimes \boldsymbol{\omega}_{\alpha z} - \frac{g}{2} f_{\alpha 0} \otimes (z \boldsymbol{\omega}_{\alpha z} + \hat{\boldsymbol{\omega}}_{\alpha z}) \Big) \Big) \, \mathrm{d}z \\ + g \int \sum_{\alpha}^{\text{vec}} \Big(f_{\alpha 0} \, (\boldsymbol{\rho}_1 \otimes \boldsymbol{\omega}_{\alpha z}) - \frac{g}{2} f_{\alpha 0} \, (\boldsymbol{\rho}_0 \otimes (z \boldsymbol{\omega}_{\alpha z} - \hat{\boldsymbol{\omega}}_{\alpha z})) + \boldsymbol{\rho}_1 \cdot (f_{\alpha 0} \otimes \boldsymbol{\omega}_{\alpha z}) \Big) z \, \mathrm{d}z \tag{A.18}$$

which simplifies to

$$-\frac{g}{4} \int \sum_{\alpha}^{\text{vec}} (-\boldsymbol{\rho}_1 \cdot (f_{\alpha 0} \otimes (z \boldsymbol{\omega}_{\alpha z} + \hat{\boldsymbol{\omega}}_{\alpha z})) + f_{\alpha 1} \, (\boldsymbol{\rho}_0 \otimes (z \boldsymbol{\omega}_{\alpha z} - \hat{\boldsymbol{\omega}}_{\alpha z}))) \, \mathrm{d}z \\ + \frac{g(g-2)}{8} \int \sum_{\alpha}^{\text{vec}} f_{\alpha 0} \left(\boldsymbol{\rho}_0 \otimes \left(z^2 \boldsymbol{\omega}_{\alpha} \right) \right) \mathrm{d}z - \frac{g(3g-2)}{8} \int \sum_{\alpha}^{\text{vec}} f_{\alpha 0} \, (\boldsymbol{\rho}_0 \otimes (z \hat{\boldsymbol{\omega}}_{\alpha})) \, \mathrm{d}z \\ - \frac{g(g-1)}{2} \int \sum_{\alpha}^{\text{vec}} f_{\alpha 0} \, (\boldsymbol{\rho}_0 \otimes (z \boldsymbol{\omega}_{\alpha z} - \hat{\boldsymbol{\omega}}_{\alpha z})) \, z \, \mathrm{d}z \tag{A.19}$$

In these simplifications, the parity of the weight functions has to be taken into account as we find

$$\int f \, (g \otimes \omega) \, \mathrm{d}z = \int g \, (f \otimes \omega) \, \mathrm{d}z \times \begin{cases} 1 & \omega \text{ even} \\ -1 & \omega \text{ odd} \end{cases} \tag{A.20}$$

To simplify the results, the weight functions can be recombined as

$$\boldsymbol{\omega}_{\alpha}^{(1)} = \begin{cases} z \boldsymbol{\omega}_{\alpha} & \text{scalar} \\ z \boldsymbol{\omega}_{\alpha z} - \hat{\boldsymbol{\omega}}_{\alpha z} & \text{vector} \end{cases}, \qquad \boldsymbol{\omega}_{\alpha}^{(2)} = \begin{cases} z \boldsymbol{\omega}_{\alpha} & \text{scalar} \\ -z \boldsymbol{\omega}_{\alpha z} - \hat{\boldsymbol{\omega}}_{\alpha z} & \text{vector} \end{cases} \tag{A.21}$$

$$\boldsymbol{\omega}_{\alpha}^{(3)} = \begin{cases} \tilde{\boldsymbol{\omega}}_{\alpha} & \text{scalar} \\ z^2 \boldsymbol{\omega}_{\alpha z} + z \hat{\boldsymbol{\omega}}_{\alpha z} & \text{vector} \end{cases}, \qquad \boldsymbol{\omega}_{\alpha}^{(4)} = \begin{cases} \tilde{\boldsymbol{\omega}}_{\alpha} & \text{scalar} \\ z^2 \boldsymbol{\omega}_{\alpha z} - z \hat{\boldsymbol{\omega}}_{\alpha z} & \text{vector} \end{cases} \tag{A.22}$$

giving the final result for the second order contribution

$$\sigma_2 = \frac{g(g-1)}{2} \int \Delta \omega_0 z^2 \, \mathrm{d}z - \frac{g}{4} \int \sum_{\alpha} \left(\boldsymbol{\rho}_1 \cdot \left(f_{\alpha 0} \otimes \boldsymbol{\omega}_{\alpha}^{(2)} \right) + f_{\alpha 1} \left(\boldsymbol{\rho}_0 \otimes \boldsymbol{\omega}_{\alpha}^{(1)} \right) \right) \mathrm{d}z$$

$$-\frac{g(g-1)}{2}\int\sum_\alpha f_{\alpha 0}\left(\boldsymbol{\rho}_0\otimes\boldsymbol{\omega}_\alpha^{(1)}\right)z\,\mathrm{d}z+\frac{g(g-1)}{4}\int\sum_\alpha f_{\alpha 0}\left(\boldsymbol{\rho}_0\otimes\boldsymbol{\omega}_\alpha^{(4)}\right)\mathrm{d}z$$
$$-\frac{g^2}{8}\int\sum_\alpha f_{\alpha 0}\left(\boldsymbol{\rho}_0\otimes\boldsymbol{\omega}_\alpha^{(3)}\right)\mathrm{d}z-\frac{g}{2}\boldsymbol{\mu}_1\cdot\int\left(\boldsymbol{\rho}_0-\boldsymbol{\rho}_0^{\mathrm{bulk}}\right)z\,\mathrm{d}z-\boldsymbol{\mu}_2\cdot\boldsymbol{\Gamma}_0-\frac{1}{2}\boldsymbol{\mu}_1\cdot\boldsymbol{\Gamma}_1 \quad \text{(A.23)}$$

and thus the bending rigidity

$$k=2\sigma_2^c=-\frac{1}{4}\int\sum_\alpha\left(\boldsymbol{\rho}_1\cdot\left(f_{\alpha 0}\otimes\boldsymbol{\omega}_\alpha^{(2)}\right)+f_{\alpha 1}\left(\boldsymbol{\rho}_0\otimes\boldsymbol{\omega}_\alpha^{(1)}\right)\right)\mathrm{d}z-\frac{1}{4}\int\sum_\alpha f_{\alpha 0}\left(\boldsymbol{\rho}_0\otimes\boldsymbol{\omega}_\alpha^{(3)}\right)\mathrm{d}z$$
$$-\frac{1}{2}\boldsymbol{\mu}_1\cdot\int\left(\boldsymbol{\rho}_0-\boldsymbol{\rho}_0^{\mathrm{bulk}}\right)z\,\mathrm{d}z-2\boldsymbol{\mu}_2^c\cdot\boldsymbol{\Gamma}_0-\frac{1}{4}\boldsymbol{\mu}_1\cdot\boldsymbol{\Gamma}_1 \quad \text{(A.24)}$$

and the Gaussian rigidity

$$\bar{k}=\sigma_2^s-4\sigma_2^c=\int\Delta\omega_0 z^2\,\mathrm{d}z+\frac{1}{2}\int\sum_\alpha f_{\alpha 0}\left(\boldsymbol{\rho}_0\otimes\boldsymbol{\omega}_\alpha^{(4)}\right)\mathrm{d}z$$
$$-\int\sum_\alpha f_{\alpha 0}\left(\boldsymbol{\rho}_0\otimes\boldsymbol{\omega}_\alpha^{(1)}\right)z\,\mathrm{d}z+(4\boldsymbol{\mu}_2^c-\boldsymbol{\mu}_2^s)\cdot\boldsymbol{\Gamma}_0 \quad \text{(A.25)}$$

References

[1] A. Mulero, I. Cachadiña, and E. L. Sanjuán. Surface Tension of Alcohols. Data Selection and Recommended Correlations. *Journal of Physical and Chemical Reference Data*, **44**(3):033104, 2015. doi:10.1063/1.4927858.

B Supporting information to chapter 6

B.1 Derivation of the association contribution to the influence parameter in pDGT

B.1.1 Helmholtz energy functional

The association functional by Yu and Wu[1] written for the PCP-SAFT equation of state is given as

$$\Phi = \sum_i \frac{n_{0i}}{m_i}\xi_i \sum_{A_i} N_{A_i}\left(\ln \chi^{A_i} - \frac{\chi^{A_i}}{2} + \frac{1}{2}\right) \tag{B.1}$$

with the weighted densities n_{0i}, n_{2i}, n_3 and $\vec{n}_{2i}$ known from fundamental measure theory[2,3]. The fractions of unbounded sites χ^{A_i} can be calculated by solving the system of equations given by

$$\chi^{A_i} = \left(1 + \sum_j \frac{n_{0j}}{m_j}\xi_j \sum_{B_j} N_{B_j}\chi^{B_j}\Delta^{A_iB_j}\right)^{-1}. \tag{B.2}$$

The association volume $\Delta^{A_iB_j}$ is given by

$$\begin{aligned}\Delta^{A_iB_j} = \sigma_{ij}^3\kappa^{A_iB_j}&\left(\exp\left(\frac{\varepsilon^{A_iB_j}}{kT}\right)-1\right)\\ &\times\left(\frac{1}{1-n_3} + \left(\frac{d_id_j}{d_i+d_j}\right)\frac{n_2\xi}{2(1-n_3)^2} + \left(\frac{d_id_j}{d_i+d_j}\right)^2\frac{n_2^2\xi}{18(1-n_3)^3}\right)\end{aligned} \tag{B.3}$$

with d_i the usual PC-SAFT temperature dependent segment diameter

$$d_i = \sigma_{ii}\left(1 - 0.12\exp\left(-\frac{3\varepsilon_{ii}}{kT}\right)\right) \tag{B.4}$$

and the corrections due to the interface

$$\xi_i = 1 - \frac{\vec{n}_{2i}\cdot\vec{n}_{2i}}{n_{2i}^2} \qquad\qquad \xi = 1 - \frac{\vec{n}_2\cdot\vec{n}_2}{n_2^2}. \tag{B.5}$$

B.1.2 First partial derivatives of reduced Helmholtz energy density

To calculate the derivatives with respect to the weighted densities, the Q function proposed by Michelsen and Hendriks[4] is introduced.

$$Q = \sum_i \frac{n_{0i}}{m_i}\xi_i \sum_{A_i} N_{A_i}\left(\ln \chi^{A_i} - \chi^{A_i} + 1\right) - \frac{1}{2}\sum_{ij}\frac{n_{0i}}{m_i}\xi_i \frac{n_{0j}}{m_j}\xi_j \sum_{A_iB_j} N_{A_i}N_{B_j}\chi^{A_i}\chi^{B_j}\Delta^{A_iB_j} \tag{B.6}$$

The derivative of Q w.r.t. the fraction of unbounded sites χ^{A_i} is

$$\left(\frac{\partial Q}{\partial \chi^{A_i}}\right)_{n_\alpha} = \frac{n_{0i}}{m_i}\xi_i N_{A_i}\left(\frac{1}{\chi^{A_i}} - 1 - \sum_j \frac{n_{0j}}{m_j}\xi_j \sum_{B_j} N_{B_j}\chi^{B_j}\Delta^{A_iB_j}\right). \tag{B.7}$$

Therefore the solution of Eq. (B.2) is a stationary point of Q. The value of Q at the stationary point is exactly Φ, therefore the partial derivatives of Φ can be evaluated using

$$\left(\frac{\partial \Phi}{\partial n_\alpha}\right)_{n_{\beta\neq\alpha}} = \left(\frac{\partial Q}{\partial n_\alpha}\right)_{n_{\beta\neq\alpha},\chi^{A_i}} \tag{B.8}$$

and thereby avoiding the calculation of the partial derivatives of χ^{A_i}. A closed form for the influence parameter is only possible for a pure component. Here, we only consider components with two association sites A and B ($\Delta^{A_iB_j} = \Delta\delta_{AB}$). By introducing $\rho = \frac{n_0}{m}\xi$, Eq. (B.6) simplifies to

$$Q = \rho\left(N_A\left(\ln\chi^A - \chi^A + 1\right) + N_B\left(\ln\chi^B - \chi^B + 1\right)\right) - \rho^2 N_A N_B \chi^A \chi^B \Delta \tag{B.9}$$

The first partial derivatives of Φ with respect to $\boldsymbol{n} = \begin{pmatrix}\rho & \Delta\end{pmatrix}^\intercal$ can be calculated by

$$\Phi_{\boldsymbol{n}} = Q_{\boldsymbol{n}} = \begin{pmatrix} N_A \ln\chi^A + N_B \ln\chi^B \\ -\rho^2 N_A N_B \chi^A \chi^B \end{pmatrix} \tag{B.10}$$

where the partial derivatives of Q are evaluated at the stationary point.

B.1.3 Second partial derivatives of reduced Helmholtz energy density

For the second partial derivatives of Φ, all second partial derivatives of Q at the stationary point are required. The second partial derivatives of Q with respect to $\boldsymbol{\chi} = \begin{pmatrix}\chi^A & \chi^B\end{pmatrix}^\intercal$ are

$$Q_{\chi\chi} = \begin{pmatrix} -\frac{\rho N_A}{\chi^{A^2}} & -\rho^2 N_A N_B \Delta \\ -\rho^2 N_A N_B \Delta & -\frac{\rho N_B}{\chi^{B^2}} \end{pmatrix}, \tag{B.11}$$

the second partial derivatives of Q with respect to the variables $\boldsymbol{n} = \begin{pmatrix}\rho & \Delta\end{pmatrix}^\intercal$ are

$$Q_{\boldsymbol{nn}} = -2N_A N_B \chi^A \chi^B \begin{pmatrix}\Delta & \rho \\ \rho & 0\end{pmatrix} \tag{B.12}$$

and the second partial derivatives of Q with respect to $\boldsymbol{\chi}$ and $\boldsymbol{n}$ are

$$Q_{\boldsymbol{\chi n}} = -\rho N_A N_B \begin{pmatrix}\chi^B\Delta & \chi^B\rho \\ \chi^A\Delta & \chi^A\rho\end{pmatrix} = -\rho N_A N_B \begin{pmatrix}\chi^B \\ \chi^A\end{pmatrix}\begin{pmatrix}\Delta & \rho\end{pmatrix}. \tag{B.13}$$

The derivatives of Φ can be calculated via[4]

$$\Phi_{\boldsymbol{nn}} = Q_{\boldsymbol{nn}} - Q_{\boldsymbol{n\chi}} Q_{\boldsymbol{\chi\chi}}^{-1} Q_{\boldsymbol{\chi n}} \tag{B.14}$$

With the determinant of $Q_{\boldsymbol{\chi\chi}}$

$$d = \frac{\rho^2 N_A N_B}{\chi^{A2}\chi^{B2}} - \rho^4 N_A^2 N_B^2 \Delta^2 = \rho^2 N_A N_B \frac{1 - \rho^2 N_A N_B \chi^{A2}\chi^{B2}\Delta^2}{\chi^{A2}\chi^{B2}} \tag{B.15}$$

its inverse can be calculated as

$$Q_{\boldsymbol{\chi\chi}}^{-1} = \frac{1}{d}\begin{pmatrix}-\frac{\rho N_B}{\chi^{B2}} & \rho^2 N_A N_B \Delta \\ \rho^2 N_A N_B \Delta & -\frac{\rho N_A}{\chi^{A2}}\end{pmatrix} \tag{B.16}$$

The product $Q_{\boldsymbol{n\chi}} Q_{\boldsymbol{\chi\chi}}^{-1} Q_{\boldsymbol{\chi n}}$ simplifies to

$$\begin{aligned}
&Q_{\boldsymbol{n\chi}} Q_{\boldsymbol{\chi\chi}}^{-1} Q_{\boldsymbol{\chi n}} = \\
&\quad \frac{\rho^2 N_A^2 N_B^2}{d}\begin{pmatrix}\Delta \\ \rho\end{pmatrix}\begin{pmatrix}\chi^B & \chi^A\end{pmatrix}\begin{pmatrix}-\frac{\rho N_B}{\chi^{B2}} & \rho^2 N_A N_B \Delta \\ \rho^2 N_A N_B \Delta & -\frac{\rho N_A}{\chi^{A2}}\end{pmatrix}\begin{pmatrix}\chi^B \\ \chi^A\end{pmatrix}\begin{pmatrix}\Delta & \rho\end{pmatrix} \\
&\quad = \frac{N_A N_B \chi^{A2}\chi^{B2}}{\left(1 - \rho^2 N_A N_B \chi^{A2}\chi^{B2}\Delta^2\right)}\begin{pmatrix}\Delta \\ \rho\end{pmatrix}\left(-\rho N_B + 2\rho^2 N_A N_B \chi^A \chi^B \Delta - \rho N_A\right)\begin{pmatrix}\Delta & \rho\end{pmatrix} \\
&\quad = -\rho N_A N_B \chi^{A2}\chi^{B2}\frac{N_A + N_B - 2\rho N_A N_B \chi^A \chi^B \Delta}{1 - \rho^2 N_A N_B \chi^{A2}\chi^{B2}\Delta^2}\begin{pmatrix}\Delta^2 & \rho\Delta \\ \rho\Delta & \rho^2\end{pmatrix} \\
&\quad = -\rho N_A N_B \chi^{A2}\chi^{B2}\frac{N_A\chi^A + N_B\chi^B}{\chi^A + \chi^B - \chi^A\chi^B}\begin{pmatrix}\Delta^2 & \rho\Delta \\ \rho\Delta & \rho^2\end{pmatrix}
\end{aligned} \tag{B.17}$$

The second partial derivatives of Φ are thus

$$\begin{aligned}\Phi_{\rho\rho} &= -2N_AN_B\chi^A\chi^B\Delta + \rho N_AN_B\chi^{A^2}\chi^{B^2}\frac{N_A\chi^A+N_B\chi^B}{\chi^A+\chi^B-\chi^A\chi^B}\Delta^2 \\ &= -\frac{N_AN_B\chi^A\chi^B\Delta}{\chi^A+\chi^B-\chi^A\chi^B}\left(2\chi^A+2\chi^B-2\chi^A\chi^B-\rho N_A\chi^{A^2}\chi^B\Delta-\rho N_B\chi^A\chi^{B^2}\Delta\right) \\ &= -N_AN_B\chi^A\chi^B\Delta\frac{\chi^A+\chi^B}{\chi^A+\chi^B-\chi^A\chi^B} \qquad \text{(B.18)}\\ \Phi_{\rho\Delta} &= -2N_AN_B\chi^A\chi^B\rho + \rho N_AN_B\chi^{A^2}\chi^{B^2}\frac{N_A\chi^A+N_B\chi^B}{\chi^A+\chi^B-\chi^A\chi^B}\rho\Delta \\ &= -\frac{N_AN_B\chi^A\chi^B\rho}{\chi^A+\chi^B-\chi^A\chi^B}\left(2\chi^A+2\chi^B-2\chi^A\chi^B-\rho N_A\chi^{A^2}\chi^B\Delta-\rho N_B\chi^A\chi^{B^2}\Delta\right) \\ &= -N_AN_B\chi^A\chi^B\rho\frac{\chi^A+\chi^B}{\chi^A+\chi^B-\chi^A\chi^B} \qquad \text{(B.19)}\\ \Phi_{\Delta\Delta} &= N_AN_B\chi^{A^2}\chi^{B^2}\rho^3\frac{N_A\chi^A+N_B\chi^B}{\chi^A+\chi^B-\chi^A\chi^B} \qquad \text{(B.20)}\end{aligned}$$

B.1.4 Influence parameter

In the actual functional, ρ and Δ both depend on the weighted densities n_0, n_2, $\vec{n}_2$ and n_3 as

$$\rho = \frac{n_0}{m}\xi \qquad \text{(B.21)}$$

and

$$\Delta = k\left(\frac{1}{1-n_3}+\frac{dn_2\xi}{4(1-n_3)^2}+\frac{d^2n_2^2\xi}{72(1-n_3)^3}\right) \qquad \text{(B.22)}$$

with

$$\xi = 1-\frac{\vec{n}_2\cdot\vec{n}_2}{n_2^2}. \qquad \text{(B.23)}$$

The weight functions have the corresponding weight constants

$$\omega_0^0 = m \qquad \omega_0^2 = \frac{1}{24}md^2 \qquad \vec{\omega}_2^1 = \frac{1}{6}\pi md^3 \qquad \text{(B.24)}$$

$$\omega_2^0 = \pi md^2 \qquad \omega_2^2 = \frac{1}{24}\pi md^4 \qquad \text{(B.25)}$$

$$\omega_3^0 = \frac{\pi}{6}md^3 \qquad \omega_3^2 = \frac{1}{240}\pi md^5 \qquad \text{(B.26)}$$

With the partial derivatives of Φ, the influence parameter can be calculated as

$$c = -\sum_{\alpha\beta}\left(\Phi_{\boldsymbol{n}} \cdot \left(\frac{\partial^2 \boldsymbol{n}}{\partial n_\alpha \partial n_\beta}\right) + \left(\frac{\partial \boldsymbol{n}}{\partial n_\alpha}\right)^{\intercal} \Phi_{\boldsymbol{nn}} \left(\frac{\partial \boldsymbol{n}}{\partial n_\beta}\right)\right)\left(\omega_\alpha^0 \omega_\beta^2 + \omega_\alpha^2 \omega_\beta^0 - \omega_\alpha^1 \omega_\beta^1\right) \tag{B.27}$$

This calculation is elongated and error prone, but it can be automated in a symbolic math framework like sympy. The simplified result is

$$c = -\frac{d^2}{18\rho}\left(N_A \ln \chi^A + N_B \ln \chi^B\right) + N_A N_B \chi^A \chi^B d^2 k \left(f_1(\eta) - \frac{\chi^A + \chi^B}{\chi^A + \chi^B - \chi^A \chi^B} f_2(\eta)\right) \tag{B.28}$$

with

$$f_1(\eta) = \frac{16\eta^5 - 100\eta^4 + 227\eta^3 - 200\eta^2 + 30\eta}{180(2-\eta)(1-\eta)^5} \tag{B.29}$$

$$f_2(\eta) = \frac{2\eta^5 - 13\eta^4 + 20\eta^3 + 16\eta^2 - 32\eta - 20}{120(2-\eta)(1-\eta)^5} \tag{B.30}$$

B.1.5 Components with one type of association sites

If the molecules are modeled using on type of association site A ($\Rightarrow \quad \Delta^{A_i B_j} = \Delta$), the derivation has to be changed accordingly. The Q function simplifies to

$$Q = \rho N_A \left(\ln \chi^A - \chi^A + 1\right) - \frac{1}{2}\rho^2 N_A^2 \chi^{A2} \Delta. \tag{B.31}$$

The first derivatives of Φ are thus

$$\Phi_{\boldsymbol{n}} = Q_{\boldsymbol{n}} = \begin{pmatrix} N_A \ln \chi^A \\ -\frac{1}{2}\rho^2 N_A^2 \chi^{A2} \end{pmatrix}. \tag{B.32}$$

The second derivatives of Q are

$$Q_{\chi\chi} = \left(-\frac{\rho N_A}{\chi^{A2}} - \rho^2 N_A^2 \Delta\right) \tag{B.33}$$

$$Q_{\boldsymbol{nn}} = -N_A^2 \chi^{A2} \begin{pmatrix} \Delta & \rho \\ \rho & 0 \end{pmatrix} \tag{B.34}$$

$$Q_{\chi\boldsymbol{n}} = -\rho N_A^2 \chi^A \begin{pmatrix} \Delta & \rho \end{pmatrix}. \tag{B.35}$$

The product $Q_{n\chi}Q_{\chi\chi}^{-1}Q_{\chi n}$ simplifies to

$$\begin{aligned} Q_{n\chi}Q_{\chi\chi}^{-1}Q_{\chi n} &= \rho^2 N_A^4 \chi^{A2} \begin{pmatrix} \Delta \\ \rho \end{pmatrix} \frac{1}{-\frac{\rho N_A}{\chi^{A2}} - \rho^2 N_A^2 \Delta} \begin{pmatrix} \Delta & \rho \end{pmatrix} \\ &= -\frac{\rho N_A^3 \chi^{A4}}{2-\chi^A} \begin{pmatrix} \Delta^2 & \rho\Delta \\ \rho\Delta & \rho^2 \end{pmatrix} \end{aligned} \tag{B.36}$$

and the second derivatives of Φ are

$$\Phi_{\rho\rho} = -\frac{N_A^2 \chi^{A2} \Delta}{2-\chi^A} \qquad \Phi_{\rho\Delta} = -\frac{N_A^2 \chi^{A2} \rho}{2-\chi^A} \qquad \Phi_{\Delta\Delta} = \frac{N_A^3 \chi^{A4} \rho^3}{2-\chi^A} \tag{B.37}$$

Finally the influence parameter simplifies to

$$c = -\frac{d^2}{18\rho} N_A \ln \chi^A + \frac{1}{2} N_A^2 \chi^{A2} d^2 k \left(f_1(\eta) - \frac{2}{2-\chi^A} f_2(\eta) \right) \tag{B.38}$$

with $f_1(\eta)$ and $f_2(\eta)$ from above.

References

[1] Y.-X. Yu and J. Wu. A fundamental-measure theory for inhomogeneous associating fluids. *J. Chem. Phys.*, **116**(16):7094–7103, 2002. doi:10.1063/1.1463435.

[2] Y. Rosenfeld. Free-energy model for the inhomogeneous hard-sphere fluid mixture and density-functional theory of freezing. *Phys. Rev. Lett.*, **63**:980–983, 1989. doi:10.1103/PhysRevLett.63.980.

[3] R. Roth. Fundamental measure theory for hard-sphere mixtures: a review. *J. Phys.: Condens. Matter*, **22**(6):063102, 2010. doi:10.1088/0953-8984/22/6/063102.

[4] M. L. Michelsen and E. M. Hendriks. Physical properties from association models. *Fluid Phase Equilib.*, **180**(1):165 – 174, 2001. doi:https://doi.org/10.1016/S0378-3812(01)00344-2.

B.2 Full pareto results

This section contains the pareto plots for all components and all association schemes for the PC-SAFT equation of state and the PCP-SAFT equation of state (contatining a fitted dipole moment). As described in the main paper, the choice of weights is to some extent arbitrary and different for the different components. Therefore the weights used to obtain specific parameter sets are specified in the captions. The plots further show the surface tensions obtained with predictive density gradient theory and the phase envelopes in terms of vapor pressures and densities. The black crosses refer to the reference values as described in the main paper.

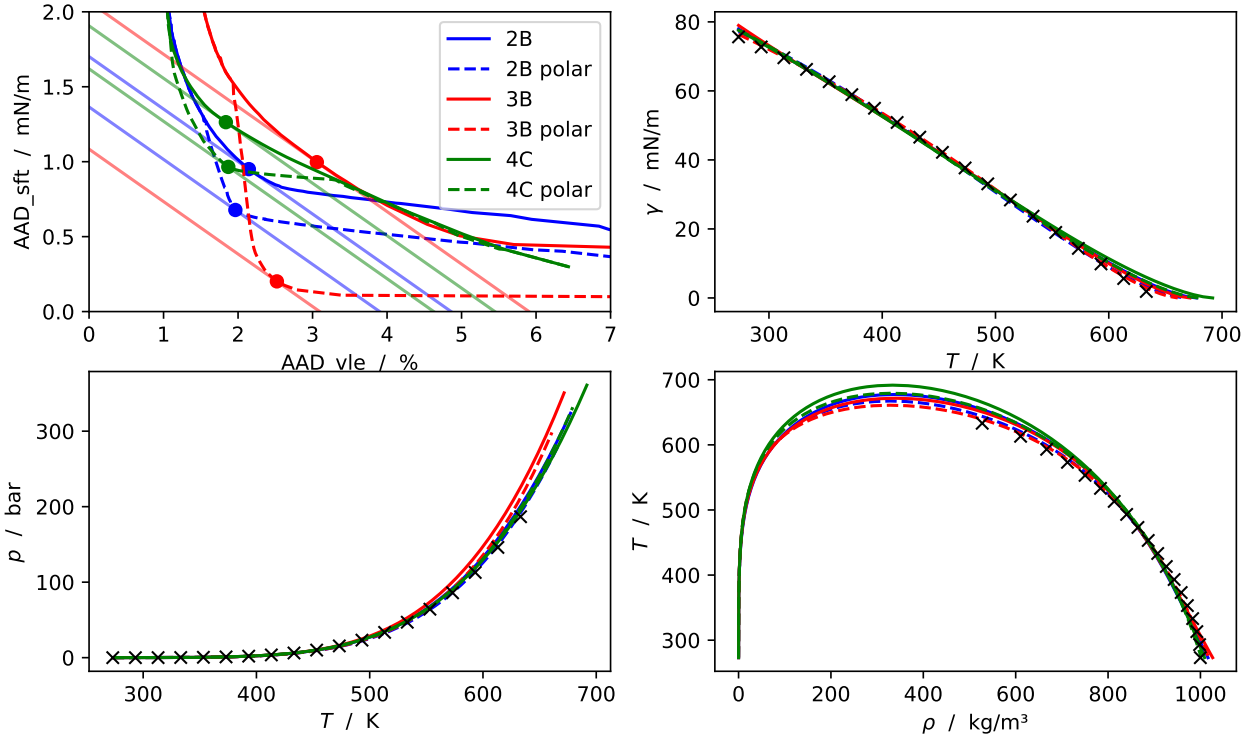

Figure B.1: water, $\mathrm{ref}_{\mathrm{vle}} = 2\,\%$, $\mathrm{ref}_{\mathrm{sft}} = 0.7\,\mathrm{mN\,m^{-1}}$

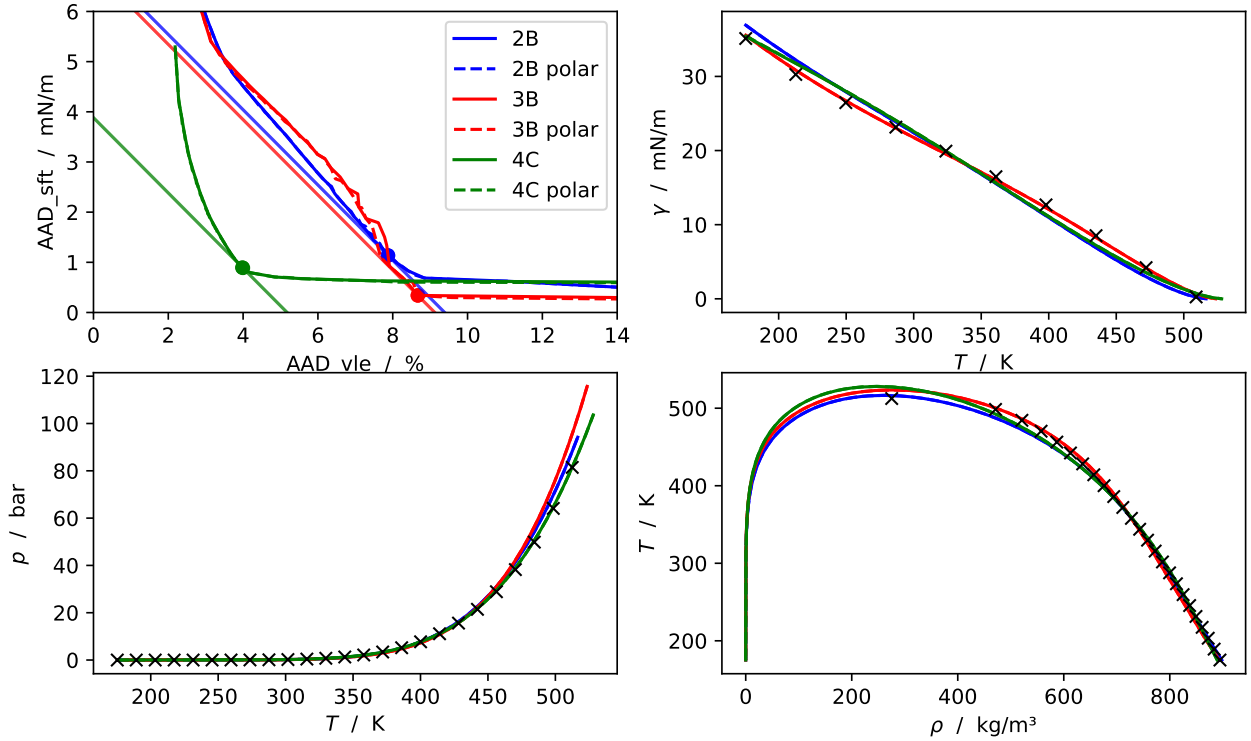

Figure B.2: methanol, $\mathrm{ref}_{\mathrm{vle}} = 2\,\%$, $\mathrm{ref}_{\mathrm{sft}} = 1.5\,\mathrm{mN\,m^{-1}}$

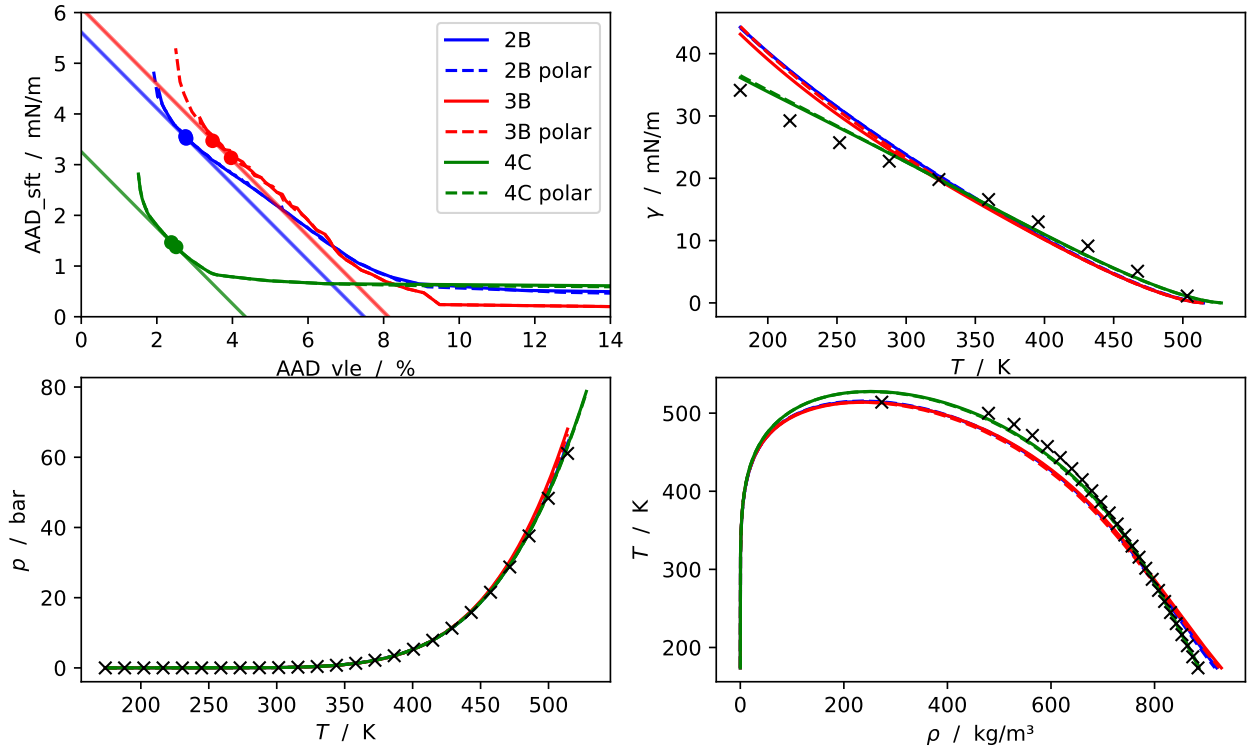

Figure B.3: ethanol, $\mathrm{ref}_{\mathrm{vle}} = 2\,\%$, $\mathrm{ref}_{\mathrm{sft}} = 1.5\,\mathrm{mN\,m^{-1}}$

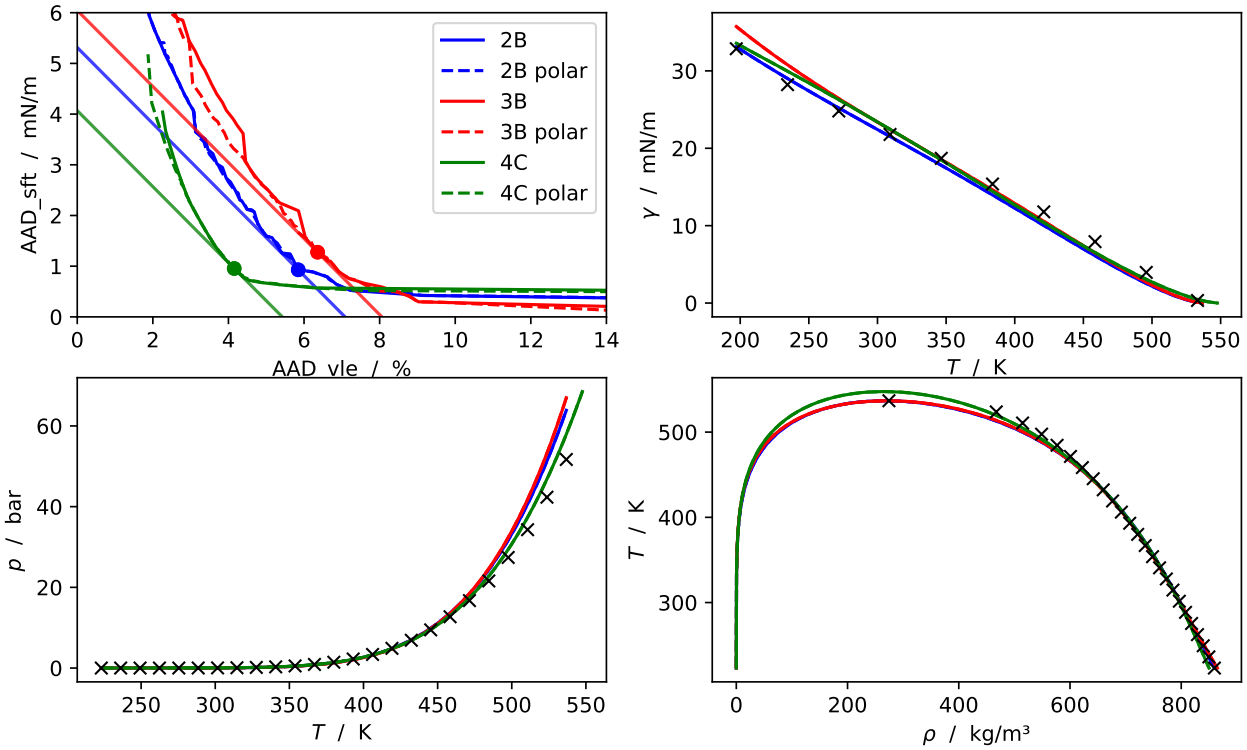

Figure B.4: 1-propanol, $\mathrm{ref}_{\mathrm{vle}} = 2\,\%$, $\mathrm{ref}_{\mathrm{sft}} = 1.5\,\mathrm{mN\,m^{-1}}$

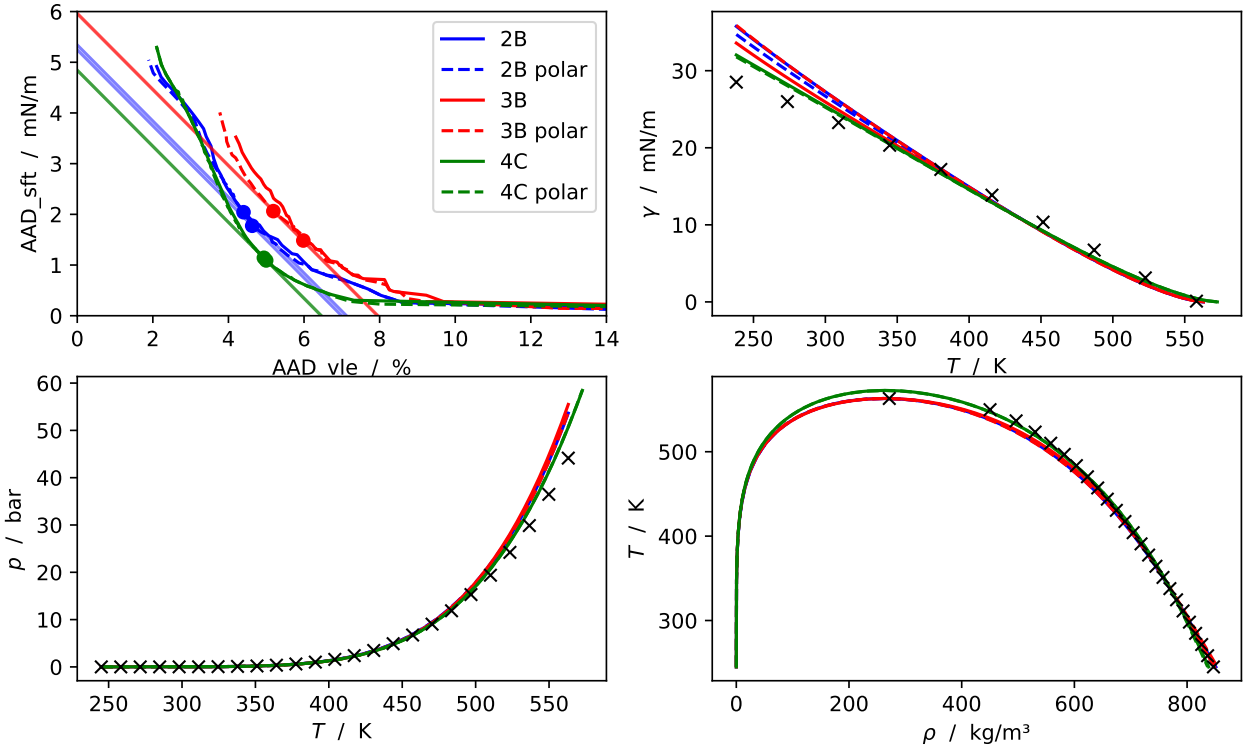

Figure B.5: 1-butanol, $\mathrm{ref}_{\mathrm{vle}} = 2\,\%$, $\mathrm{ref}_{\mathrm{sft}} = 1.5\,\mathrm{mN\,m^{-1}}$

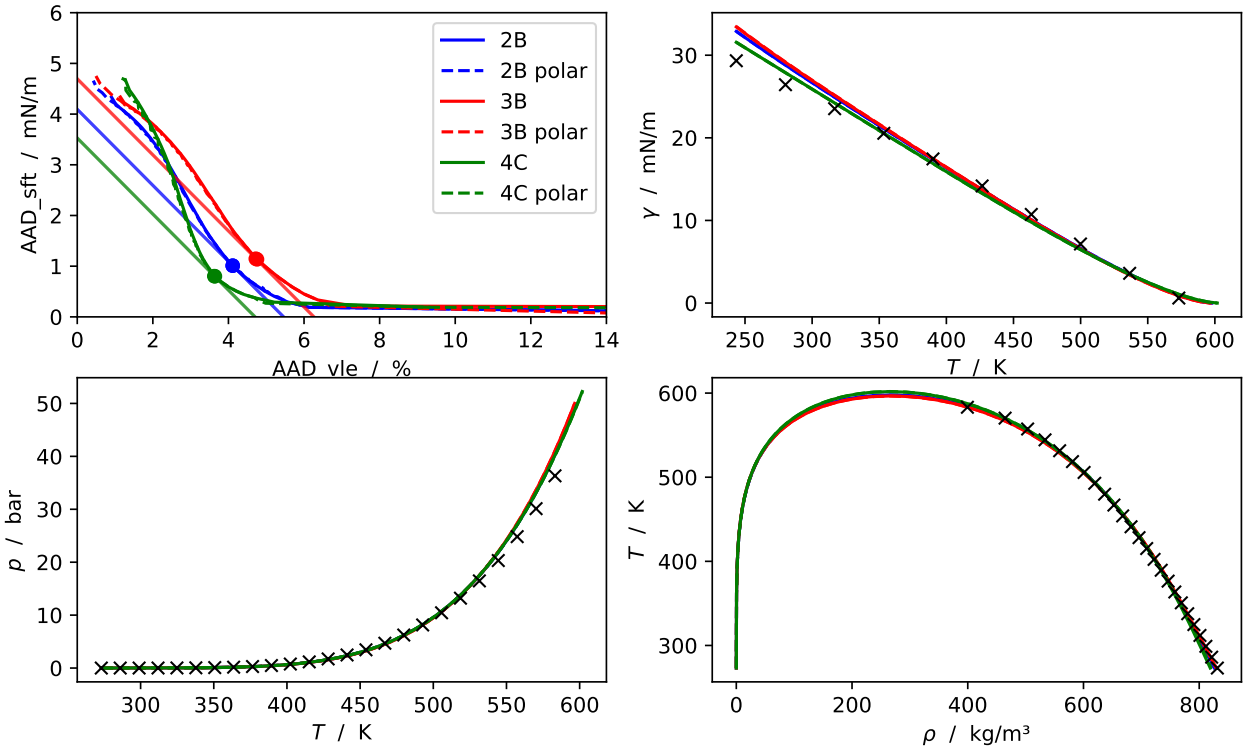

Figure B.6: 1-pentanol, $\mathrm{ref}_{\mathrm{vle}} = 2\,\%$, $\mathrm{ref}_{\mathrm{sft}} = 1.5\,\mathrm{mN\,m^{-1}}$

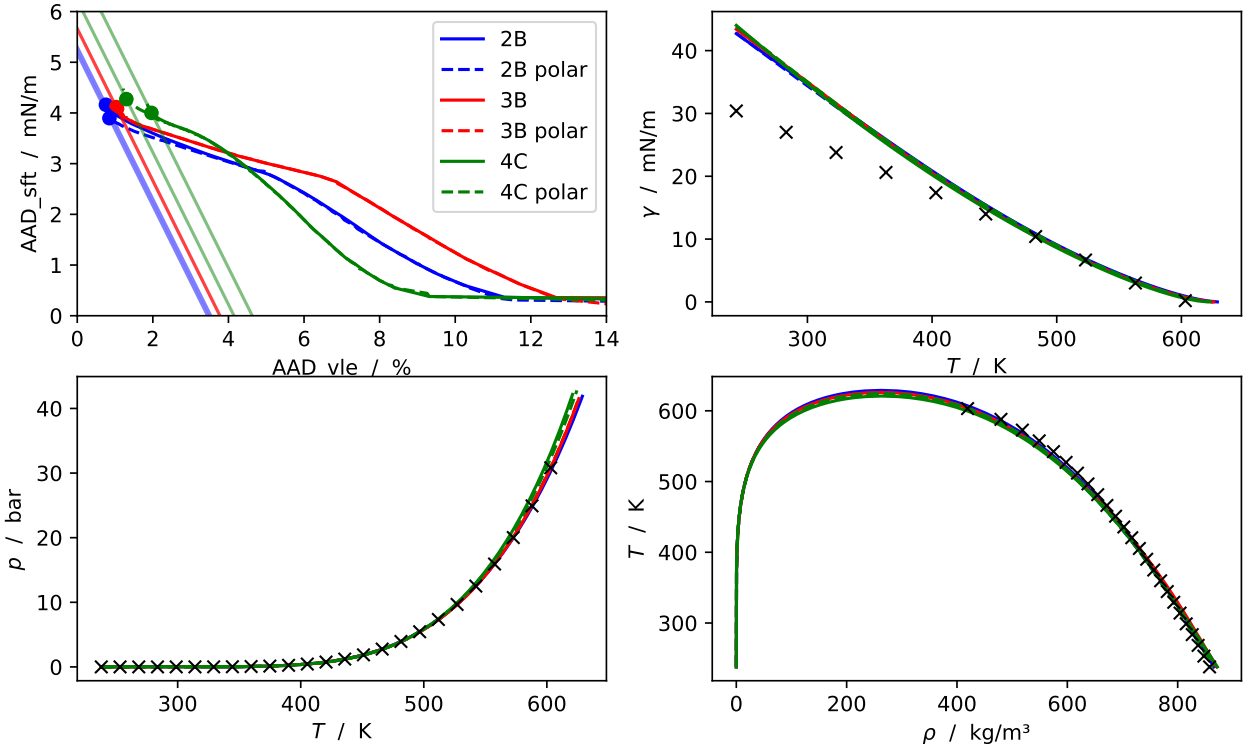

Figure B.7: 1-hexanol, $\mathrm{ref}_{\mathrm{vle}} = 2\,\%$, $\mathrm{ref}_{\mathrm{sft}} = 3\,\mathrm{mN\,m^{-1}}$

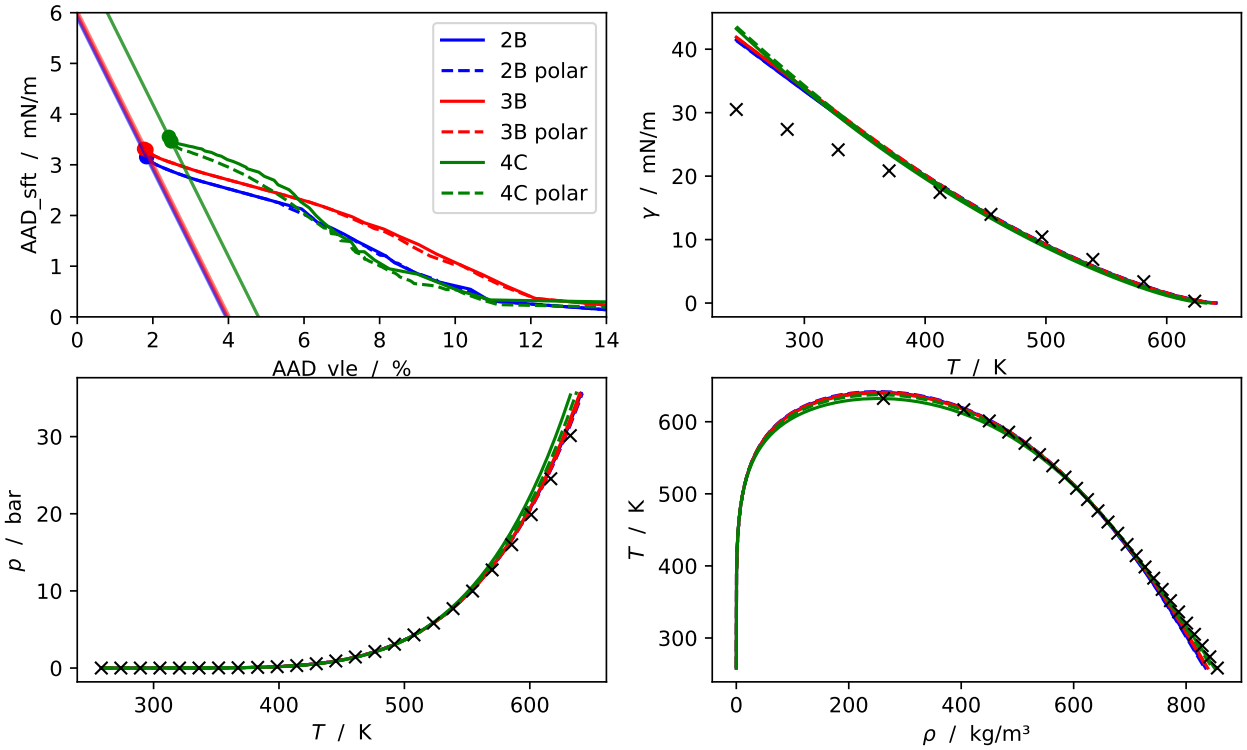

Figure B.8: 1-heptanol, $\mathrm{ref}_{\mathrm{vle}} = 2\,\%$, $\mathrm{ref}_{\mathrm{sft}} = 3\,\mathrm{mN\,m^{-1}}$

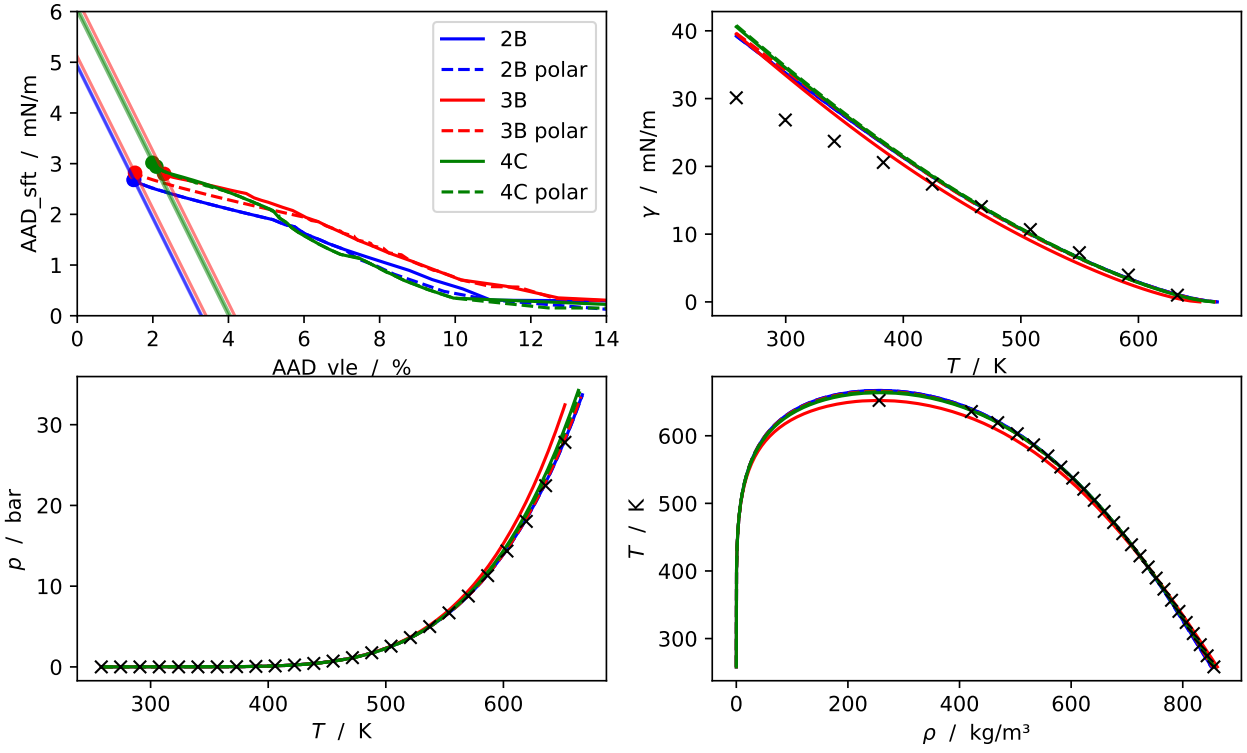

Figure B.9: 1-octanol, $\mathrm{ref}_{\mathrm{vle}} = 2\,\%$, $\mathrm{ref}_{\mathrm{sft}} = 3\,\mathrm{mN\,m^{-1}}$

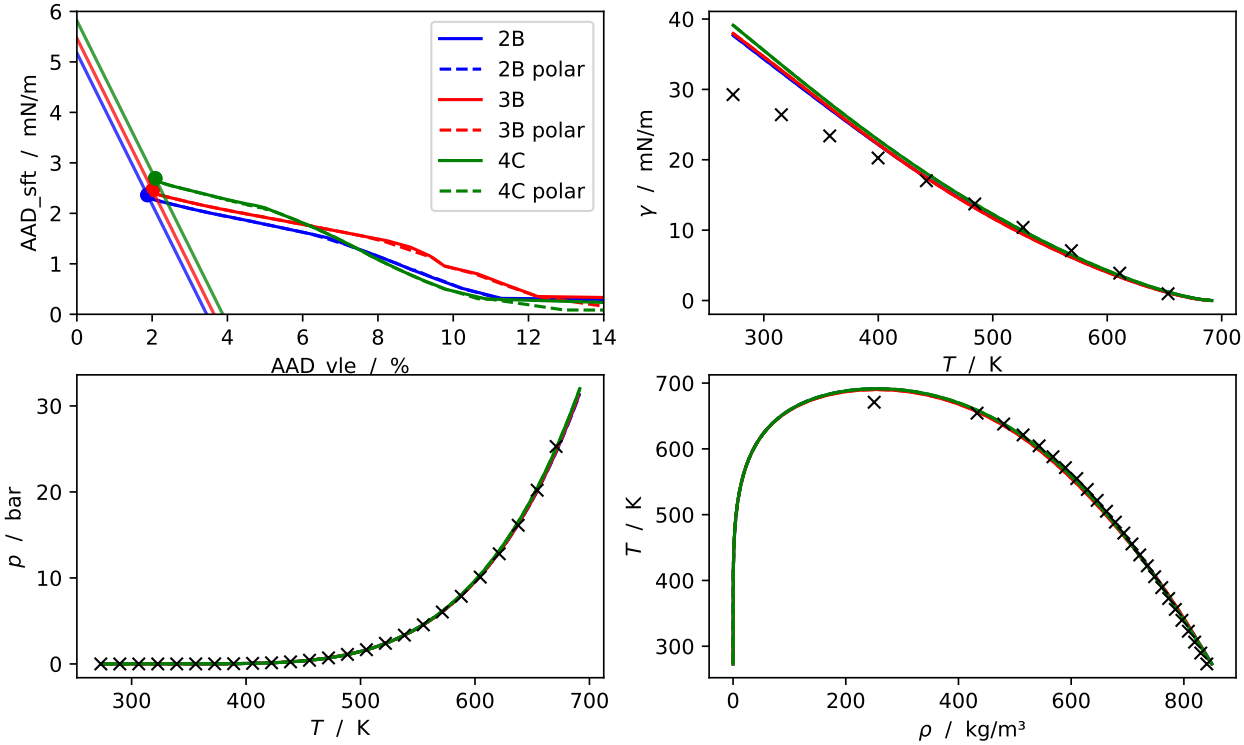

Figure B.10: 1-nonanol, $\mathrm{ref}_{\mathrm{vle}} = 2\,\%$, $\mathrm{ref}_{\mathrm{sft}} = 3\,\mathrm{mN\,m^{-1}}$

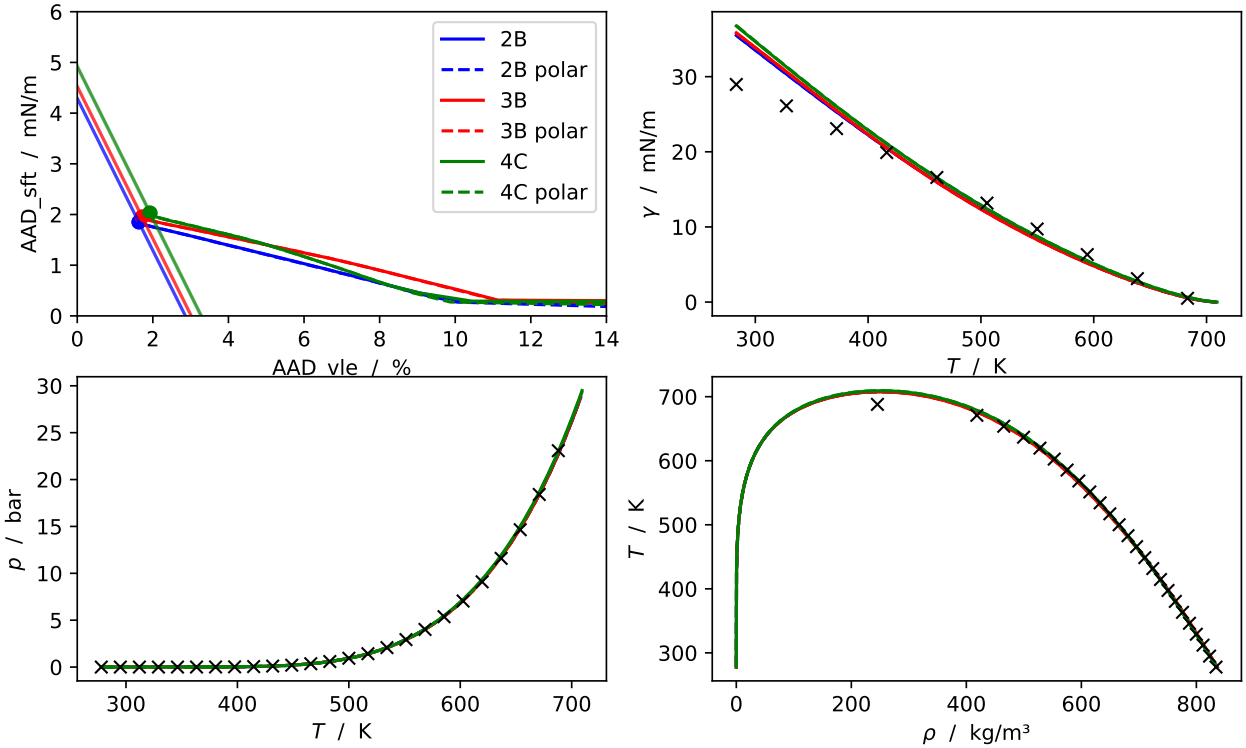

Figure B.11: 1-decanol, $\mathrm{ref}_{\mathrm{vle}} = 2\,\%$, $\mathrm{ref}_{\mathrm{sft}} = 3\,\mathrm{mN\,m^{-1}}$

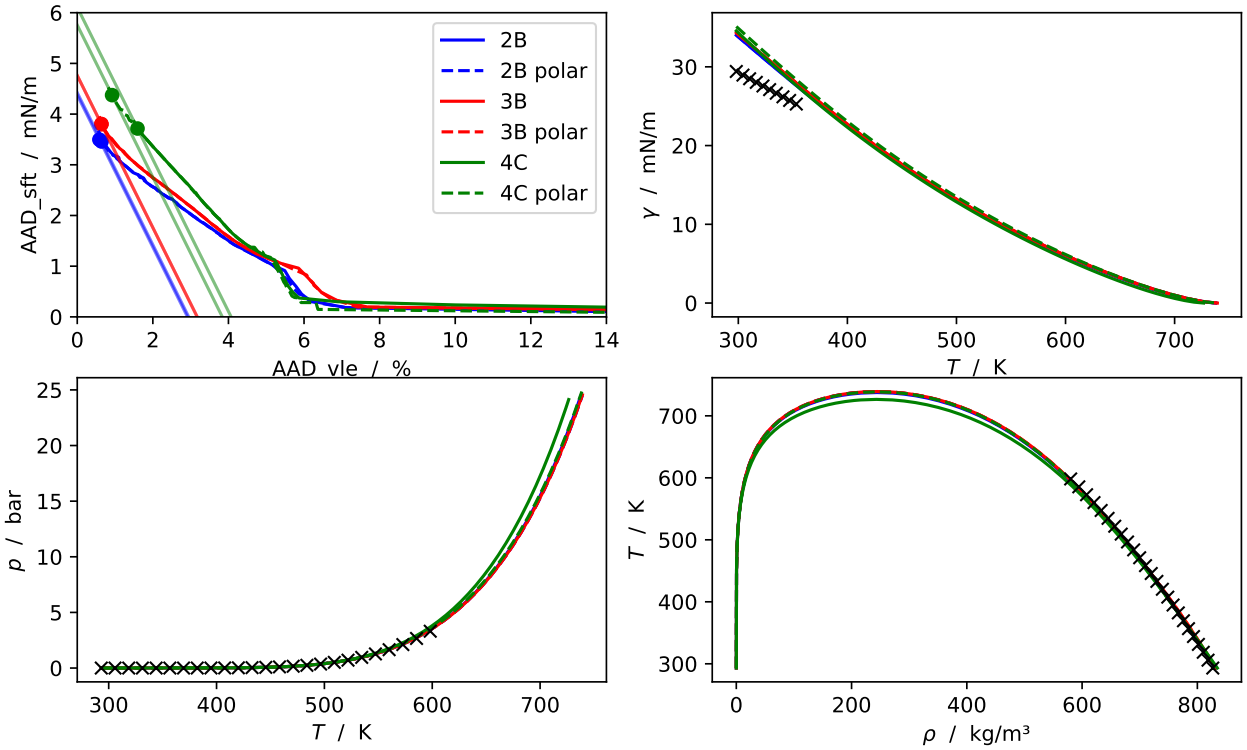

Figure B.12: 1-dodecanol, $\mathrm{ref}_{\mathrm{vle}} = 2\,\%$, $\mathrm{ref}_{\mathrm{sft}} = 3\,\mathrm{mN\,m^{-1}}$

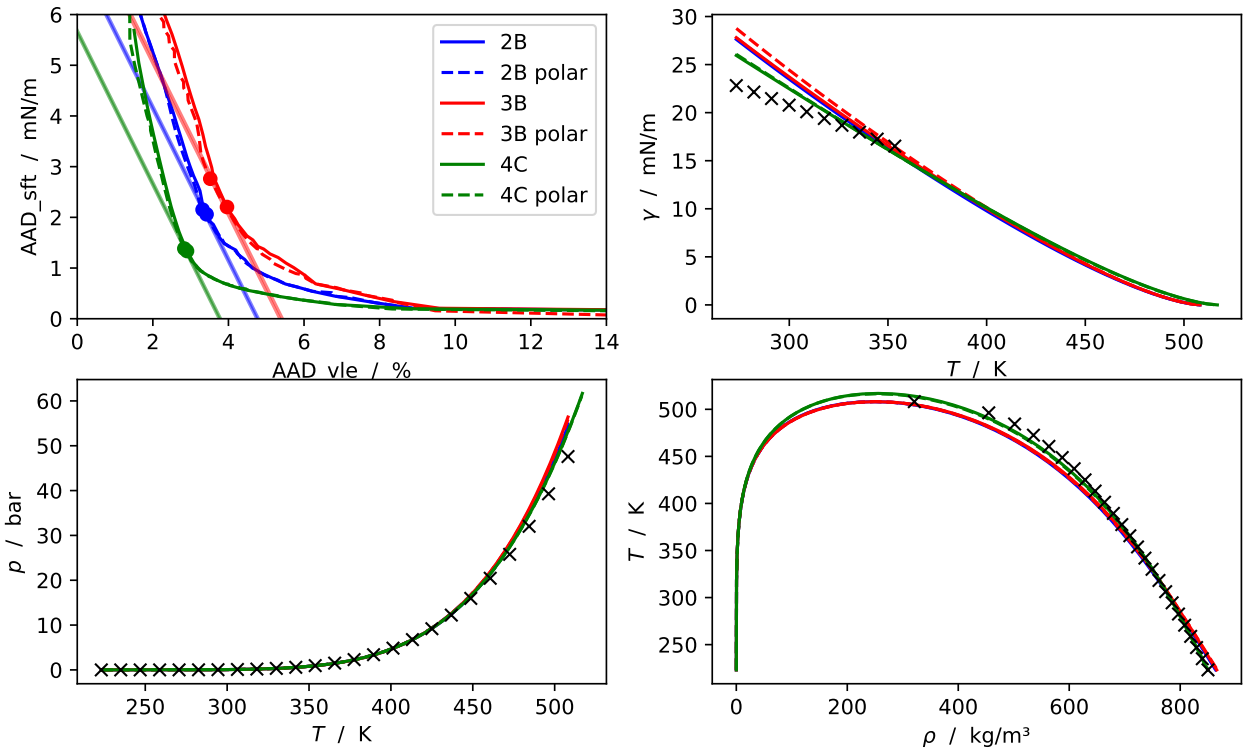

Figure B.13: 2-propanol, $\mathrm{ref}_{\mathrm{vle}} = 2\,\%$, $\mathrm{ref}_{\mathrm{sft}} = 3\,\mathrm{mN\,m^{-1}}$

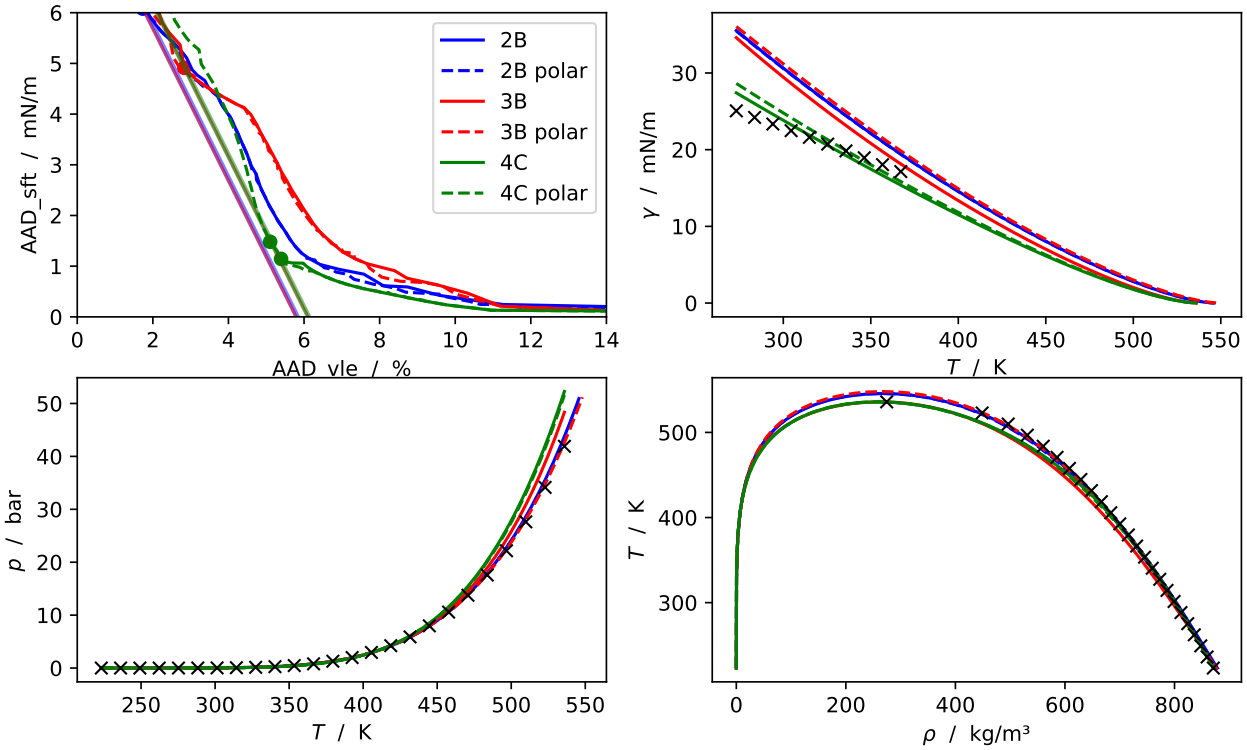

Figure B.14: 2-butanol, $\mathrm{ref}_{\mathrm{vle}} = 2\,\%$, $\mathrm{ref}_{\mathrm{sft}} = 3\,\mathrm{mN\,m^{-1}}$

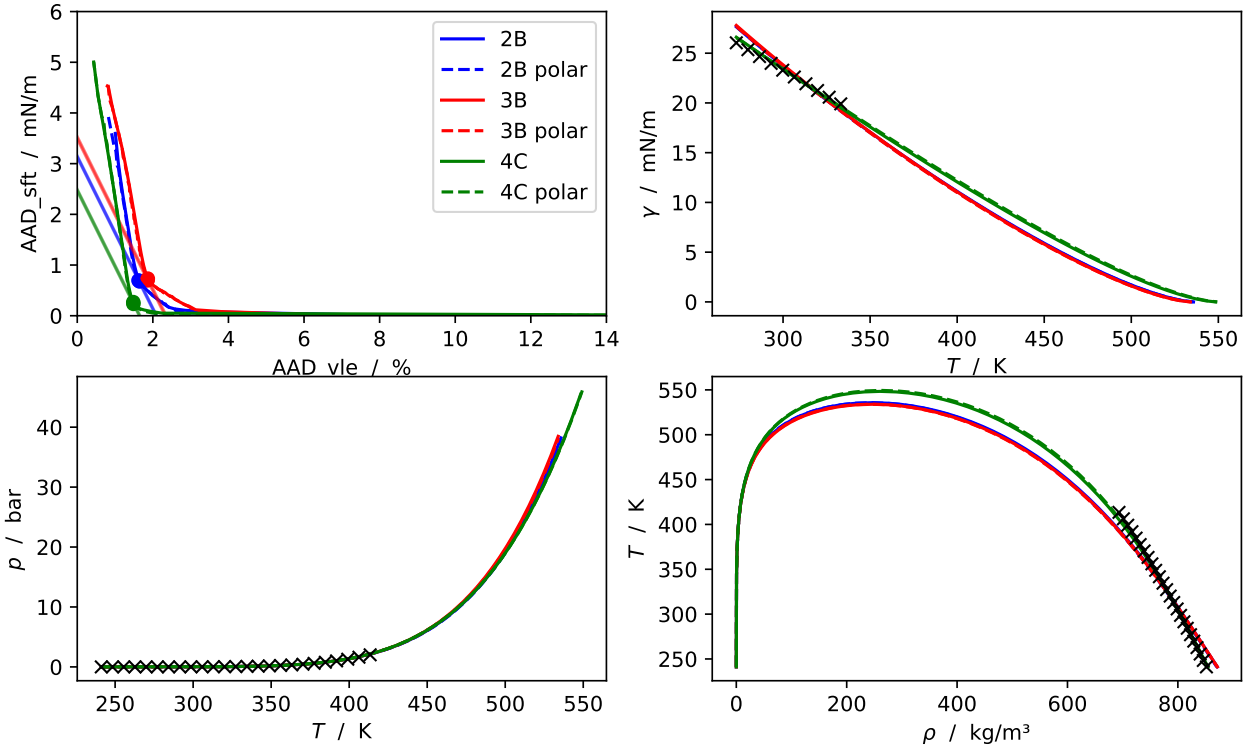

Figure B.15: 2-pentanol, $\mathrm{ref}_{\mathrm{vle}} = 2\,\%$, $\mathrm{ref}_{\mathrm{sft}} = 3\,\mathrm{mN\,m^{-1}}$

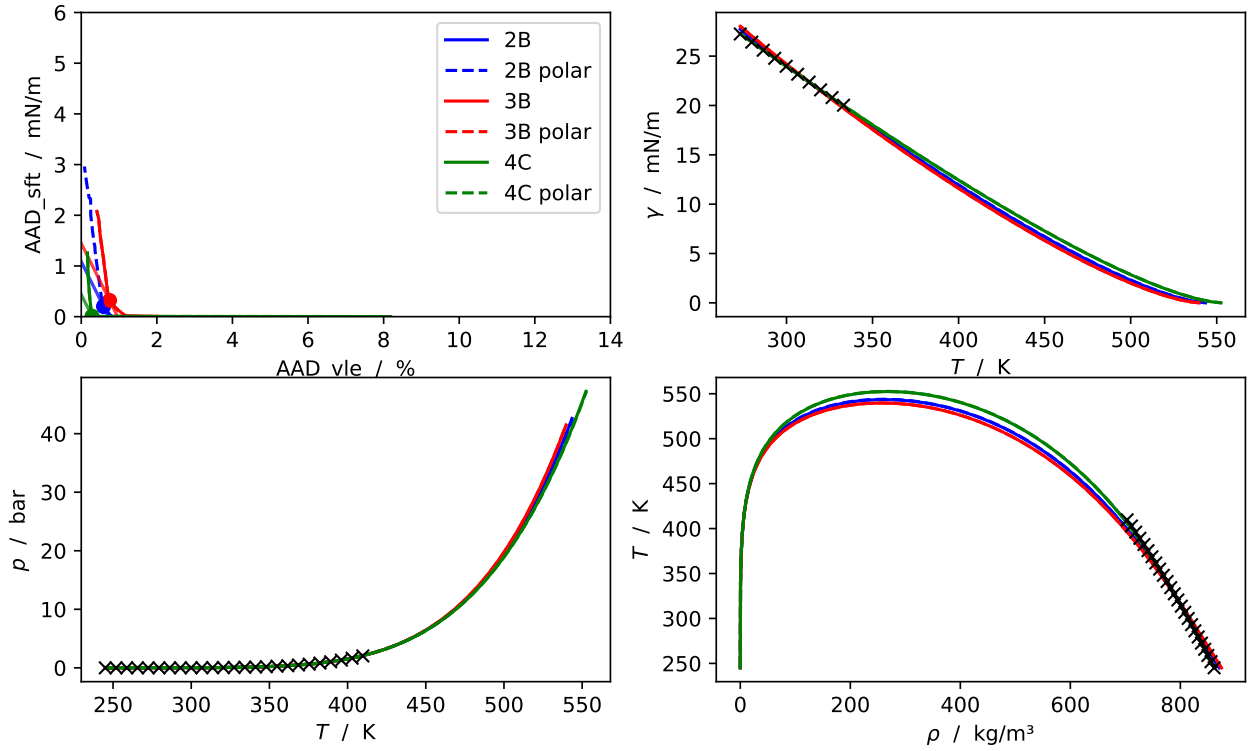

Figure B.16: 3-pentanol, $\mathrm{ref}_{\mathrm{vle}} = 2\,\%$, $\mathrm{ref}_{\mathrm{sft}} = 3\,\mathrm{mN\,m^{-1}}$

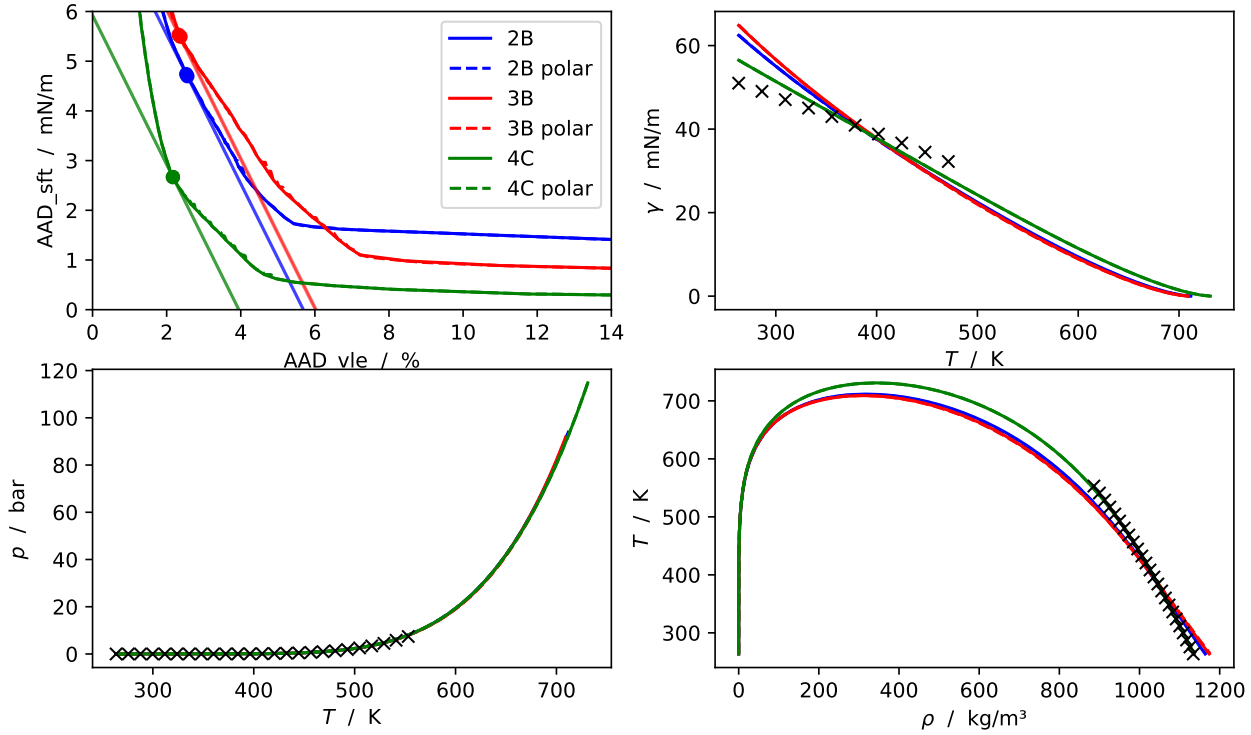

Figure B.17: 1,2-ethanediol, $\mathrm{ref}_{\mathrm{vle}} = 2\,\%$, $\mathrm{ref}_{\mathrm{sft}} = 3\,\mathrm{mN\,m^{-1}}$

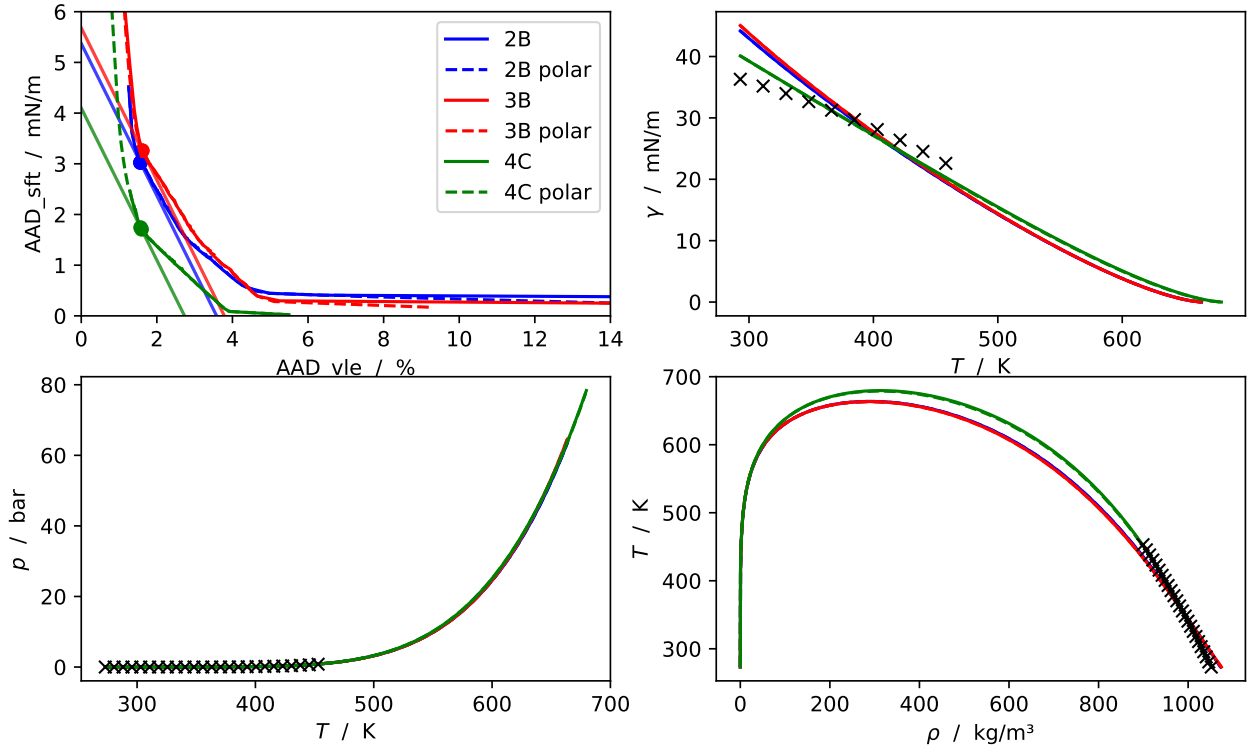

Figure B.18: 1,2-propanediol, $\mathrm{ref}_{\mathrm{vle}} = 2\,\%$, $\mathrm{ref}_{\mathrm{sft}} = 3\,\mathrm{mN\,m^{-1}}$

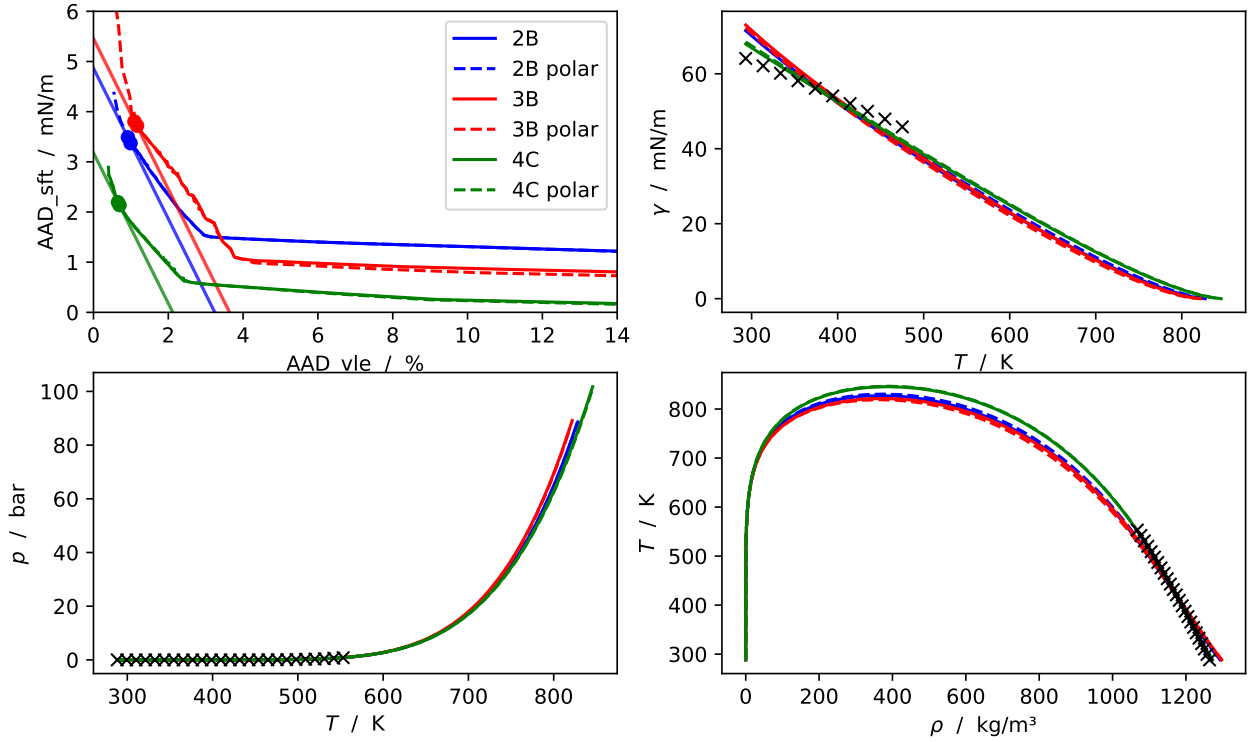

Figure B.19: glycerol, $\mathrm{ref}_{\mathrm{vle}} = 2\,\%$, $\mathrm{ref}_{\mathrm{sft}} = 3\,\mathrm{mN\,m^{-1}}$